

Genomic Analyses of Aleutian Disease Resilience in
American Mink

by

Guoyu Hu

Submitted in partial fulfillment of the requirements
for the degree of Doctor of Philosophy

at

Dalhousie University
Halifax, Nova Scotia
May 2024

© Copyright by Guoyu Hu, 2024

Table of Contents

<i>List of Tables</i>	<i>viii</i>
<i>List of Figures</i>	<i>xi</i>
<i>Abstract</i>	<i>xiii</i>
<i>List of Abbreviations and Symbols Used</i>	<i>xiv</i>
<i>Acknowledgement</i>	<i>xvii</i>
CHAPTER 1. Introduction	1
1.1 Introduction	1
1.2 Objectives.....	3
CHAPTER 2. Literature Review	5
2.1 American Mink Farming.....	5
2.2 Aleutian Disease in Mink.....	6
2.2.1 Aleutian Disease	6
2.2.2 Aleutian Disease Tests	8
2.2.3 Controlling Aleutian Disease	10
2.2.4 Aleutian Disease Resilience.....	11
2.3 Genetics of Aleutian Disease Resilience	12
2.3.1 Heritability	12
2.3.2 Genetic Correlation.....	13
2.4 Genomics of Aleutian Disease Resilience.....	14
2.4.1 Population Genomics	14
2.4.2 Selection Signatures.....	16
2.4.3 Genome-wide Association Studies	18

2.4.4	Genomic Selection	19
2.5	Conclusion.....	22
CHAPTER 3. Genetic and Phenotypic Correlations between Aleutian Disease Tests with Body Weight, Growth, and Feed Efficiency Traits in Mink.....24		
3.1	Introduction	24
3.2	Materials and Methods	27
3.2.1	Animals and Management	27
3.2.2	Aleutian Disease Tests	28
3.2.3	Body Weight Measurements and Growth Parameters	28
3.2.4	Feed Intake Measurement and Feed Efficiency	30
3.2.5	Feed-Intake-Related Traits.....	31
3.2.6	Statistical Analyses	32
3.3	Results and discussion.....	36
3.3.1	Descriptive Statistics.....	36
3.3.2	Random Maternal Genetic and Permanent Environmental Effects	36
3.3.3	Heritability and Repeatability Estimates.....	37
3.3.4	Correlations Between Aleutian Disease Tests and Body Weight.....	38
3.3.5	Correlations Between Aleutian Disease Tests and Growth.....	40
3.3.6	Correlations Between Aleutian Disease Tests and Feed Efficiency.....	42
3.3.7	Correlations Between Aleutian Disease Tests and Feed Intake	44
3.3.8	Aleutian Disease Resilience indicator traits.....	45
3.4	Conclusions	47
CHAPTER 4. Population Genomics of American Mink Using Genotypes Data58		
4.1	Introduction	58
4.2	Methods	62
4.2.1	Ethics Statement.....	62

4.2.2	Animals and Sampling	62
4.2.3	Sample Collection and Genotyping	62
4.2.4	Animals and SNP Quality Control	63
4.2.5	Population Genetic Parameters, Linkage Disequilibrium, and Effective Population Size	63
4.2.6	Genetic Distances and Genetic Diversity	64
4.2.7	Genetic Structure and Admixture Patterns	65
4.3	Results	65
4.3.1	Population Genetic Parameters, Linkage Disequilibrium and Effective Population Size	65
4.3.2	Genetic Distances and Genetic Diversity	67
4.3.3	Genetic Structure and Admixture Patterns	68
4.4	Discussion	70
4.5	Conclusions	78
<i>CHAPTER 5. Identifying Selection Signatures for Immune Response and Resilience to Aleutian Disease in Mink Using Genotype Data</i>		91
5.1	Introduction	91
5.2	Materials and Methods	94
5.2.1	Animals and Sampling	94
5.2.2	Aleutian Disease Tests	95
5.2.3	Growth and Feed Efficiency Measurement	95
5.2.4	Pelt Quality Evaluation	96
5.2.5	Female Reproductive Performance Measurement	97
5.2.6	Animal Grouping	97
5.2.7	Sample Collection and Genotyping	98
5.2.8	Animals and SNP Quality Control	98

5.2.9	Methods for Detection of Selection Signatures	99
5.2.10	Gene Annotation, Gene Ontology, and Functional Analysis	100
5.3	Results	101
5.3.1	Selection Signatures for Immune Response Trait	101
5.3.2	Selection Signatures for General Resilience and Female Reproductive Performance Traits	103
5.3.3	Common Genes Among Studied Traits and KEGG Pathways	105
5.4	Discussion	106
5.4.1	Immune Responses	107
5.4.2	General Resilience	110
5.4.3	Female Reproductive Performance	111
5.4.4	Common Genes and Ontology Terms Among All Three Traits	113
5.5	Conclusion	114
<i>CHAPTER 6. Genome-wide Association Studies for Immune Response and Resilience to Aleutian Disease in Mink.....</i>		133
6.1	Introduction	133
6.2	Materials and Methods	135
6.2.1	Ethics approval	135
6.2.2	Animals and Phenotypes	135
6.2.3	Sample Collection and Genotyping	137
6.2.4	Estimation of Breeding Values and De-regressed Breeding Values	137
6.2.5	Animals and SNP Quality Control	138
6.2.6	Genome-Wide Association Studies	138
6.2.7	Gene Annotation, Gene Ontology, and Functional Analysis	139
6.3	Results	140
6.3.1	Summary Information of Phenotype Data and Genotype Data	140

6.3.2	Genome-wide Association Studies	141
6.3.3	Gene Annotation and Gene Ontology of Significant SNPs	142
6.4	Discussion	143
6.4.1	Candidate Genes for ELISA-G	144
6.4.2	Candidate Genes for IAT	146
6.4.3	Candidate Genes for DOF	147
6.4.4	Overrepresentations of Candidate Genes for ELISA-G.....	147
6.5	Conclusion.....	149
<i>CHAPTER 7. Genomic Prediction of Immune Response and Resilience to Aleutian Disease in Mink.....</i>		159
7.1	Introduction	159
7.2	Materials and Methods	161
7.2.1	Ethics Approval.....	161
7.2.2	Animals and Phenotypes.....	161
7.2.3	Tongue Sample Collection and Genotyping	163
7.2.4	Animals and SNP Quality Control.....	164
7.2.5	Statistical Methods for Genetic and Genomic Predictions	164
7.2.6	Cross-Validation and Model Comparison.....	167
7.3	Results	168
7.3.1	Descriptive Statistics.....	168
7.3.2	Estimation of Genetic Parameters.....	168
7.3.3	Prediction Abilities, Accuracies, and Bias	169
7.4	Discussions.....	170
7.5	Conclusion.....	176
<i>CHAPTER 8. General Discussion and Conclusion</i>		181
8.1	Summary and general discussion	181

8.1.1	Genetic Parameters	182
8.1.2	Population Genomics	183
8.1.3	Selection Signatures	184
8.1.4	Genome-wide Association Studies	185
8.1.5	Genomic Prediction	186
8.1.6	Conclusion	187
8.1.7	General Recommendations and Future Directions	188
	REFERENCES	190
	<i>APPENDIX 1. List of Publications and Conference Presentations (as of March 1, 2024)</i>	<i>232</i>
	<i>APPENDIX 2. Description of Electronic Supplements.....</i>	<i>234</i>
	<i>SUPPLEMENTARY MATERIAL</i>	<i>235</i>
	Supplementary dataset 1	236
	Supplementary dataset 2.....	236
	Supplementary dataset 3.....	236
	Supplementary dataset 4.....	236

List of Tables

Table 3.1 Significance of fixed and random effects included in the models for analysis of Aleutian disease tests, growth, feed efficiency, and feed intake traits in mink.....	49
Table 3.2 Descriptive statistics for Aleutian disease tests, growth, feed efficiency, and feed intake traits in mink.	51
Table 3.3 Estimates of variance components and genetic parameters with their standard errors (SE) for Aleutian disease tests, growth, feed efficiency, and feed intake traits in mink.	53
Table 3.4 Estimates of phenotypic correlations with their standard errors between Aleutian disease tests with feed efficiency, growth, and feed intake traits in mink.	55
Table 3.5 Estimates of genetic correlations with their standard errors between Aleutian disease tests with feed efficiency, growth, and feed intake traits in mink.	56
Table 4.1 Average minor allele frequency (MAF), observed heterozygosity, and nucleotide diversity for five color types of American mink in CCFAR, whole CCFAR population, and whole MFF population.	80
Table 4.2 Summary of the average and standard deviation of r^2 between adjacent SNPs on all chromosomes of five color types of American mink in CCFAR, whole CCFAR population, and whole MFF population.....	81
Table 4.3 Estimation of Nei's genetic distance (upper diagonal) and Weir and Cockerham's F_{st} (lower diagonal) between various color types of American mink.....	82
Table 4.4 Analysis of molecular variance (AMOVA) in various color types of American mink.	82
Table 5.1 The number of individuals from different color types of each subgroup in different Aleutian disease tests and the final dataset for detecting selection signatures for immune response to Aleutian mink disease virus infection in American mink.	116

Table 5.2 The number of individuals with positive counterimmunoelectrophoresis test results in each subgroup of feed conversion ratio, Kleiber ratio, live pelt quality, general resilience performance, and female reproductive performance traits.	116
Table 5.3 Immune response related genes annotated from the selection signatures detected from different color types.....	117
Table 5.4 Significant (q-value<0.05) biological processes detected from overrepresentation tests of candidate genes from the whole studied population and different color types of mink for immune response trait.	118
Table 5.5 Significant (q-value<0.05) cellular components and molecular functions detected from overrepresentation tests of candidate genes from the whole studied population and different color types of mink for immune response trait.	120
Table 5.6 Significant (q-value<0.05) biological processes, cellular components, and molecular functions detected from overrepresentation tests of candidate genes for general resilience and female reproductive performance traits.	122
Table 5.7 Significantly (q-value<0.05) presented Kyoto Encyclopaedia of Genes and Genomes (KEGG) pathways of genes detected from signatures selection analyses of the immune response, general resilience, and female reproductive performance traits.....	124
Table 6.1 Descriptive statistics of four studied traits.....	150
Table 6.2 Summary information of significant (q<0.01) SNPs for enzyme-linked immunosorbent assay test, iodine agglutination test, and off-feed days traits.	151
Table 6.3 Significant (q<0.01) SNPs and genes annotated from the significant SNPs for enzyme-linked immunosorbent assay test, iodine agglutination test, and off-feed days traits.....	152
Table 6.4 Significant (false discovery rate adjusted p-value<0.05) functional enrichment of candidate genes detected from enzyme-linked immunosorbent assay test trait.	154
Table 7.1 Number of animals in the training and validation populations.....	178
Table 7.2 Descriptive statistics of five studied traits.	178

Table 7.3 Estimates of variance components and heritabilities with their standard errors (SE) for all studied traits using traditional best linear unbiased prediction model and full dataset.....	178
Table 7.4 Estimates of variance components and heritabilities with their standard errors (SE) for all studied traits from three different prediction models using validation dataset.....	179
Table 7.5 The prediction abilities and accuracies and their SE for all studied traits from three different prediction models using validation dataset.	180
Table 7.6 Regression coefficient and their standard errors of adjusted phenotypes on the predicted breeding value (EBV or GEBV) from three different prediction models using validation dataset for all studied traits.	180
Supplementary dataset 1. Significant SNPs detected as candidate selection signatures for immune response trait by each method, and the genes annotated from these candidate selection signatures from Chapter 5.....	236
Supplementary dataset 2. The genes annotated from the detected significant SNPs for immune response, general resilience, and female reproductive performance traits, and the common genes among the three studied traits from Chapter 5.	236
Supplementary dataset 3. The significant SNPs detected as candidate selection signatures for general resilience and female reproductive performance trait by each method, and the genes annotated from these candidate selection signatures from Chapter 5.....	236
Supplementary dataset 4. The dataset of significant SNPs detected from the GWAS analyses, and the genes annotated from these significant SNPs for all three studied traits in Chapter 6.....	236

List of Figures

Figure 3.1 The distribution of Aleutian disease tests..	57
Figure 4.1 Linkage disequilibrium measured by r^2 plotted as a function of inter-market distance (kb)	83
Figure 4.2 Estimated effective population sizes for various color types of American mink from 5 to 250 generations ago.	84
Figure 4.3 Unrooted consensus tree showing the genetic relationships among the six color types using the unweighted pair group method and the unbiased Nei's genetic distance.	85
Figure 4.4 The scatterplots of discriminant analysis of principal components	86
Figure 4.5 The number of individuals from various color types in 40 assigned clusters inferred by discriminant analysis of principal components.	87
Figure 4.6 The probability of membership of each sample in the 40 assigned clusters inferred by discriminant analysis of principal components.	88
Figure 4.7 ADMIXTURE analyses of six color types American mink with cross-validation error plot for K - values from 2 to 75.	89
Figure 4.8 Admixture pattern of six color types American mink at $K = 2, 3, 4, 6, 40,$ and 75.	90
Figure 5.1 Genome-wide distribution of selection signatures for immune response trait detected by F_{st} (Z-transformed), nucleotide diversity ($\theta\pi$ ratio), and XP-EHH across all autosomes in the whole population (All) and different color types (Black, Demi, Mahogany, and Pastel) individuals.	125
Figure 5.2 The overlapped selection signatures detected in the whole population (All) and different color types (Black, Demi, Mahogany, and Pastel) individuals among pairwise fixation index (F_{st} , top 5%), nucleotide diversity ($\theta\pi$, top 5%), and cross-population extended haplotype homozygosity (XP-EHH, $-\log(p\text{-value}) > 2$) tests for immune response trait.	126
Figure 5.3 The Venn diagram shows the genes overlapping among the whole population (All) and different color types (Black, Demi, Mahogany, and Pastel) for immune response trait.	127

Figure 5.4 The pie charts of functional classifications (including biology process, cellular component, and molecular function) of candidate genes under selection pressure in the whole population (All) and different color types (Black, Demi, Mahogany, and Pastel) individuals for immune response trait.	128
Figure 5.5 Genome-wide distribution of selection signatures for general resilience and reproductive performance traits detected by F_{st} (Z-transformed), nucleotide diversity ($\theta\pi$ ratio), and XP-EHH across all autosomes from the whole population	129
Figure 5.6 The overlapped selection signatures detected from the whole population individuals among pairwise fixation index (F_{st} , top 5%), nucleotide diversity ($\theta\pi$, top 5%), and cross-population extended haplotype homozygosity (XP-EHH, $-\log(p\text{-value}) > 2$) tests for general resilience and reproductive performance traits.	130
Figure 5.7 The pie charts of functional classifications (including biology process, cellular component, and molecular function) of candidate genes under selection pressure in the whole population individuals for general resilience and female reproductive performance traits.....	131
Figure 5.8 The overlapped genes among immune response, general resilience, and female reproductive performance traits.....	132
Figure 6.1 Frequency distribution histogram for AMDV-G based enzyme-linked immunosorbent assay test (ELISA-G), Iodine agglutination test (IAT), proportion of off-feed days (DOF), and Variation in daily feed intake (Varf).	155
Figure 6.2 The filtered SNP density distributions on Nvison chromosomes.	156
Figure 6.3 Manhattan plots and Quantile-Quantile plots for four studied traits.	157
Figure 6.4 The pie charts of functional classifications (molecular function, cellular component, and biology process) of candidate genes related to significant ($q < 0.05$) SNPs for AMDV-G based enzyme-linked immunosorbent assay test (ELISA-G), iodine agglutination test (IAT), and the proportion of off-feed days (IAT).	158
Supplementary Figure 1. Optimization α -score graph.	235
Supplementary Figure 2. Population genetic clustering results based on the Bayesian Information Criterion (BIC) in relation to the number of clusters identified by the find.cluster function in DAPC analysis.....	235

Abstract

Aleutian disease (AD) causes severe health issues and results in substantial economic losses for the mink industry. The ineffectiveness of vaccination, medication, and culling strategies in controlling AD has compelled mink farmers to select AD-resilient mink. However, as expounded in Chapter 2 of this thesis, the absence of a comprehensive understanding of the genetic/genomic architecture of AD resilience hinders breeders from incorporating this innovative trait into their breeding programs. Thus, this thesis aimed to provide a comprehensive view of the genetic and genomic architecture of AD resilience and explore the potential utilization of genomic information in the selection process for AD resilience. Genetic correlations elucidated in Chapter 3 delineated the genetic relationships among various AD tests and other AD-resilient traits. The outcomes emphasized the antigen-based enzyme-linked immunosorbent assay test as the most reliable and practical indicator trait for selecting AD-resilient mink among all AD tests. Chapter 4 delved into the genetic structure of farmed mink, utilizing phenotypes from the first Axiom Affymetrix Mink 70K single nucleotide polymorphism (SNP) panel. The updated population genomics information from Chapter 4 directed the genomic analyses throughout this thesis. Selection signatures (Chapter 5) and genome-wide association studies (GWAS, Chapter 6) were performed to explore the genomic architecture of AD resilience. The detected SNPs provided an opportunity for improving the resilience of mink to AD using marker-assisted selection or genomic selection in mink, and the identified genes and biological pathways contributed to a deeper understanding of the genomic architecture underlying the immune response and resilience of mink to AD. Chapter 7 examined various genomic prediction methods to assess their feasibility and determine the optimal strategy for leveraging genomic information to augment genetic gains for AD resilience in mink. The most suitable prediction approach was recommended for each AD-resilient trait based on prediction accuracies and biases of different methods for each trait. In conclusion, the studies conducted in this thesis not only offer practical insights and recommendations for the prospective implementation of genetic/genomic selection for AD resilience but also advance our comprehension of the genomic architecture and biological pathways associated with AD resilience in mink.

List of Abbreviations and Symbols Used

AD	Aleutian Disease
ADFI	Average Daily Feed Intake
ADG	Average Daily Gain
AIP	Age At the Inflection Point
AMDV	Aleutian Mink Disease Virus
AMOVA	Analysis of Molecular Variance
BIC	Bayesian Information Criterion
BLUP	Best Linear Unbiased Prediction
BP	Biological Process
BW	Body Weight
CBL	Black Color Type in Canadian Centre for Fur Animal Research
CC	Cellular Component
CCFAR	Canadian Centre for Fur Animal Research
CDE	Demi Color Type in Canadian Centre for Fur Animal Research
CIEP	Counterimmunoelectrophoresis
CMA	Mahogany Color Type in Canadian Centre for Fur Animal Research
CPA	Pastel Color Type in Canadian Centre for fur Animal Research
CST	Stardust Color Type in Canadian Centre for Fur Animal Research
CV	Coefficient of Variation
DEBV	De-Regressed Estimated Breeding Value
DFI	Daily Feed Intake
DOF	Proportion of Off-Feed Days Based on Feed Intake
EBV	Estimated Breeding Values
XP-EHH	Cross-Population Extended Haplotype Homozygosity
ELISA	Enzyme-Linked Immunosorbent Assay
ELISA-G	<i>In Vitro</i> Cultured Aleutian Mink Disease Virus Antigen-Based Enzyme-Linked Immunosorbent Assay Test
ELISA-P	Capsid Protein of Aleutian Mink Disease Virus-Based Enzyme-Linked Immunosorbent Assay Test

FCR	Feed Conversion Ratio
FDR	False Discovery Rate
FRP	Female Reproductive Performance
Fst	Fixation Index
GBLUP	Genomic Best Linear Unbiased Prediction
GBS	Genotyping-By-Sequencing
GEBV	Genomic Estimated Breeding Values
GO	Gene Ontology
GRP	General Resilience
GWAS	Genome-wide Association Studies
h^2	Heritability
HW	Body Weight at Harvest
IAT	Iodine Agglutination Test
IRE	Immune Response
k	Maturation Rate
KEGG	Kyoto Encyclopedia of Genes and Genomes
KR	Kleiber Ratio
LD	Linkage Disequilibrium
m	Inflection Parameter
MAF	Average Minor Allele Frequency
MBL	Black Color Type in Millbank Fur Farm
MF	Molecular Function
MFF	Millbank Fur Farm
N_e	Effective Population Sizes
NA	Not Applicable
NS	Not Significant
NT	Not Tested
PCA	Principal Component Analysis
r	Repeatability
QUA	Overall Pelt Quality
RFI	Residual Feed Intake

RG	Residual Gain
RIG	Residual Intake and Gain
SD	Standard Deviation
SE	Standard Error
SSGBLUP	Single-Step Genomic Best Linear Unbiased Prediction
SNP	Single Nucleotide Polymorphism
VarF	Day-To-Day Variation in Feed Intake
WGS	Whole Genome Sequencing
WIP	Weight At the Inflection Point

Acknowledgement

First of all, I would like to sincerely express my deep appreciation to my supervisor, Dr. Younes Miar, for his enormous guidance, support, and encouragement throughout this study. I appreciate every moment that Dr. Miar spent with me to help with my study, thanks to him for always standing by my side during my ups and downs. His continuous guidance and feedback are the key to the successful completion of this project.

I appreciate Dr. Duy Ngoc Do and Dr. Pourya Davoudi for their valuable and constructive comments, suggestions, and criticisms. I am also grateful to my supervisory committee members, Dr. Alyson Kelvin and Dr. Ghader Manafiazar, for all the help and valuable suggestions on this thesis. My experiments would not be able to conduct without the help from the Canadian Centre for Fur Animal Research and Millbank Fur Farm staff.

Thanks to Natural Sciences and Engineering Research Council (NSERC), Mitacs, Digital research alliance of Canada, Canada Mink Breeders Association, Nova Scotia Mink Breeders Association, and Mink Veterinary Consulting and Research Service Ltd. for financial support of my thesis, and Dr. Miar for providing funding so that I have this opportunity to study on this project.

I am very grateful to my lovely Canadian family, Dr. Robert Livingston and Marilyn Livingston, for making me feel like I am at home in Canada. I would like to thank my Chinese family, Yaunhua Rao, Guoqiang Hu, Shuangying Yu, and Yuanlin Rao, for their unconditional support and love throughout my study and all the guidance and encouragement. Last but not least, my great gratitude to my girlfriend, Mohan Zhou, for her help, company, and support. I also want to thank everyone who helped me with my study and life in Canada.

CHAPTER 1. Introduction

1.1 Introduction

Aleutian disease (AD) in mink, which is caused by the Aleutian mink disease virus (AMDV), is one of the most severe health issues for mink farming and imposes tremendous financial losses to the mink industry (Henson *et al.* 1962; Porter *et al.* 1982; Farid & Ferns 2011; Reichert & Kostro 2014; Wiggans *et al.* 2017). Several common disease-controlling approaches, including vaccination, medicine, and culling strategy, have been attempted to control AD, but failed. Thus, mink farmers attempt to control AD by selecting AD-resilient mink based on AD tests and/or AD-resilient indicator traits, such as growth, pelt quality, and reproductive performance (Knuutila *et al.* 2009; Farid & Ferns 2011; Farid & Rupasinghe 2016; Farid & Ferns 2017; Farid *et al.* 2018). Mink farmers have conducted the phenotypic selection of AD-resilient mink, but the comprehensive genetic background and architecture of AD resilience have not been explored, which has become an obstacle for mink breeders to apply genetic/genomic selection for AD resilience in mink.

A comprehensive understanding of genetic and phenotypic parameters associated with traits of interest is essential for implementing genetic selection (Toghiani 2012). Nevertheless, there is a scarcity of research focusing on the genetic parameters of AD tests and their correlations with other indicator traits related to AD resilience. Thus, Chapter 3 of this thesis delved deeper into the assessment of genetic and phenotypic connections between AD tests and other AD resilience traits such as body weight, growth, and feed efficiency (Hu *et al.* 2022).

Comprehending the genetic structure of the target population is imperative for conducting genomic investigations and formulating genomic selection programs (Groeneveld *et al.*

2010; Wellmann & Bennewitz 2019). Previous studies have scrutinized the population genomics of mink in Canada through the utilization of genotyping-by-sequencing (GBS) (Karimi *et al.* 2020) and whole-genome sequencing data (WGS) (Karimi *et al.* 2021b). Nevertheless, no research has explored the genetic structure of domestically farmed mink with diverse color variations using chromosome-based genotype data. Thus, Chapter 4 in this thesis endeavored to address this gap by employing genotype information derived from the Axiom Affymetrix Mink 70K single nucleotide polymorphism (SNP) panel with the aim of investigating the population structure of farm-raised American mink in Canada.

Selection signatures and genome-wide association studies (GWAS) are the two popular methods for exploring the genetic architecture of the traits of interest (Saravanan *et al.* 2020; Uffelmann *et al.* 2021). Selection signatures investigation enables the identification of specific loci influenced by selective pressures, revealing genes linked to the studied traits (Kreitman 2000; Qanbari & Simianer 2014; Ma *et al.* 2015). Notably, prior research by Karimi *et al.* (2021a) exclusively delved into selection signatures associated with AD using GBS data in black color mink under a disease challenge model. However, there is a gap in using genotype information to detect selection signatures concerning AD resilience in mink reared in an AD-positive environment. Thus, the Chapter 5 in this thesis applied the genotypes and phenotypes from mink raised in an AD-positive farm to detect the selection signatures related to immune response, general response, and female reproductive performance to AD. This study facilitated the identification of genes and biological pathways associated with AD resilience. On the other hand, GWAS serves as another valuable method for identifying genes and biological pathways linked to complex traits (Sharma *et al.* 2015). There is no GWAS pertaining to AD resilience in the existing

literature. Therefore, Chapter 6 utilized phenotypic data (immune responses and feed-intake-related traits) and genotypic information from mink raised in an AD-positive farm to conduct GWAS to pinpoint SNPs and genes associated with immune response and the resilient ability of mink to AD.

Genomic selection has the potential to enhance the genetic improvement of the target trait by reducing the generation interval and enhancing selection accuracy (Goddard & Hayes 2007; Meuwissen *et al.* 2013; Miar *et al.* 2015; Meuwissen *et al.* 2016). The advent of highly dense SNP marker panels has facilitated the adoption of genomic selection across various major farm animal species (Misztal *et al.* 2021). The development of the first Axiom Affymetrix Mink 70K SNP panel provides an opportunity to apply genomic selection approaches to facilitate the selection of AD-resilient mink. Nonetheless, there have been no previous genomic prediction studies related to AD resilience in mink. Thus, Chapter 7 in this thesis used several genomic prediction methods, including genomic best linear unbiased prediction (GBLUP) and single-step GBLUP (ssGBLUP) methods, to carry out the inaugural prediction of genomic breeding values for indicator traits associated with AD resilience in mink.

1.2 Objectives

The overall goal of this thesis was to understand the genomic architecture of AD resilience and provide the most feasible and effective selection approach to improve the resilience of American mink to AD. As a result, the potential outcomes from this research would help mink farmers effectively reduce the adverse influences of AD.

The specific objectives included:

- 1) To estimate the phenotypic and genetic relationships between AD tests and other important traits (e.g., feed efficiency, body growth, and feed-intake-related traits).
- 2) To investigate the population genomics of American mink using genotypes derived from the first 70K SNP panel for mink.
- 3) To detect the significant genomic regions, SNPs, quantitative trait loci, genes, and pathways underlying AD resilience using genomic data through GWAS and signatures of selection studies.
- 4) To evaluate the performance of different genomic prediction methods for AD resilience traits.

CHAPTER 2. Literature Review

2.1 American Mink Farming

American mink belongs to the weasel family and is a primarily carnivorous mammal and semiaquatic species native to North America (García *et al.* 2010). American mink is one of the major sources for the fur industries because of its high quality and various colours (Tamlin *et al.* 2009). The production cycle of farming mink includes four main seasons:

1) conditioning and breeding season (December to March), where mink farmers focus on adjusting the feed to provide the mink with good conditions for breeding in March.

2) whelping and weaning season (April-June), where dams will give birth at the end of April or early May (5-6 kits on average), and the kits will be weaned at the end of June (approximately 6-8 weeks old).

3) growth and furring season (July-October), mink will be fed *ad-lib* to fulfill their growth potential in the barn. The mink will start furring in August, and their body growth will be completed in September, which is approximately 20 weeks after they were born (Sørensen *et al.* 2003; Do & Miar 2020).

4) grading and harvesting (November-December), where farmers determine which mink will be pelted or kept as breeding stock for future season based on physical evaluation of mink. After pelting, the dried pelts are shipped to the auction houses for sale (Moller & Sorensen 2003).

From 2014 to 2018, mink farms in Canada produced about 2.7 million pelts per year, and Nova Scotia was the largest mink pelt producer and contributed approximately 54% of

these produced pelts. The trade of 13.4 million mink pelts in these five-year periods contributed \$482 million to the Canadian economy (Statistics Canada 2018a, 2018b). However, the market downturn and the COVID-19 pandemic caused the mink industry to face serious challenges. In Canada, from 2015 to 2020, the number of mink farms dramatically dropped from 213 to 63, decreasing mink production from approximately three million to about one million per year (Statistics Canada 2022). However, the mink industry seems to be on the upturn based on fur auction reports in recent years, as market demand and fur prices showed an upward tendency (Oaten 2021; sagafurs 2022). Thus, with the smaller number of mink farms in Canada, improving the efficiency (e.g., improved disease resilience, feed efficiency, reproduction performance, and pelt quality) of mink farming in Canada through genetic/genomic selection programs could help to meet the rising market demand, help mink farmers obtain more economic benefits from the rising pelt prices, and increase the competitiveness of mink farmed in Canada in the international market.

2.2 Aleutian Disease in Mink

2.2.1 Aleutian Disease

Aleutian disease (AD) is a chronic and persistent viral infection caused by the Aleutian mink disease virus (AMDV). As one of the most severe health issues in the mink farming, AD brings tremendous financial losses to the mink industry and has made it difficult for mink farmers to maintain their farming. In Nova Scotia, AD causes multi-million-dollar losses to the mink industry (Rupasinghe & Farid 2017). In Denmark, AD was estimated to cause approximately 10 million USD in economic losses to the mink industry annually. In

Finland, the financial losses caused by AD were more than 2 million euros (Knuutila *et al.* 2009).

AMDV is a non-enveloped single-stranded DNA virus in the parvovirus family (genus *Amdoparvovirus*, species *Carnivore amdoparvovirus1*). The AMDV genome spans approximately 4.8 kilobases and encompasses two structural proteins along with three non-structural proteins (NS1, NS2, and NS3). Notably, the NS1 gene holds significance due to its pivotal involvement in viral replication, exhibiting notable genetic variability across distinct strains (Gottschalck *et al.* 1994; Best *et al.* 2003; Huang *et al.* 2014). AMDV infection causes significant pathology, including glomerulonephritis, plasmacytosis, hypergammaglobulinemia, and arteritis to the infected mink (Porter *et al.* 1969; Cho & Ingram 1973; Porter *et al.* 1973). Macrophages are considered to be the primary locations for the replication of the virus (Porter *et al.* 1972). Consequently, the virus becomes concentrated in organs abundant with macrophages, such as lymph nodes, spleen, and bone marrow (Bloom *et al.* 1994). One of the significant manifestations of AMDV infection is plasma cell proliferation, known as plasmacytosis, which is the symbol of AD (Bloom *et al.* 1994). Plasma cells, specialized white blood cells responsible for antibody production and storage, signify the occurrence of a humoral immune response to an antigen when present in tissues (Minges Wols 2015). The infection with AMDV also alters the blood protein profile of mink. Infected mink exhibit a gradual increase in serum gamma-globulin levels throughout the infection (Bloom *et al.* 1994). While the specific proportion of anti-AMDV antibodies within the elevated gamma-globulins remains unknown, it is evident that AMDV is responsible for the excessive production of immunoglobulins (Tabel & Ingram 1970). The cellular immune response of mink to AMDV infection has not been

precisely delineated. Best and Bloom (2006) indicated that although the level of CD4+ (helper) T cells remains at normal levels during the infection period, the number of CD8+ (cytotoxic) T cells rises. Upon recognition of their antigen and subsequent activation, CD8+ T cells engage in the elimination of infected or malignant cells. Furthermore, CD8+ T cells may contribute to an exaggerated immune response, leading to immunopathology or immune-mediated damage (Schäfer & Zerneck 2020; Aichele *et al.* 2022). AMDV infection also causes adverse effects on female reproductive performance, such as small litter size, fetal death, and abortion. Infection of dams with AMDV before pregnancy decreased the number of kits, and infection with AMDV in mid-pregnancy caused fetal death or abortion (Henson *et al.* 1962; Reichert & Kostro 2014). Additionally, small body size due to chronic progressive weight loss (Porter *et al.* 1982), low feed intake (inappetence) (Eklund *et al.* 1968; Jensen *et al.* 2016b), and poor pelt quality characterized by hair depigmentation (Farid & Ferns 2011) are also adverse outcomes caused by AD. Together, these clinical features on AMDV infection in farmed mink directly reduce the financial income of mink farmers. Thus, an effective, practical, and reliable management strategy is needed to reduce the adverse effects caused by AD.

2.2.2 Aleutian Disease Tests

Counterimmunoelectrophoresis (CIEP) and enzyme-linked immunosorbent assay (ELISA) are two common diagnosing tests for AD. CIEP could diagnose AMDV by testing mink for anti-AMDV antibodies (Farid *et al.* 2015). CIEP is highly specific to AMDV and has been widely used for routine detection of AMDV antibodies (Cho & Ingram 1972). Mink farms in Europe and North America widely applied CIEP-based culling strategies. The ELISA tests currently are the most common method for routine screening of AD (Ma *et al.* 2016).

ELISA diagnoses AD based on recombinant virus-like particles for identifying the AMDV antibodies in mink sera and quantifying the concentrations of antibodies in the samples (Knuutila *et al.* 2009). Depending on the geographical locations, two main ELISA systems are commonly employed in the mink farms. The first system is the capsid protein of AMDV-based ELISA (ELISA-P) (Knuutila *et al.* 2009), which is commonly used in the Netherlands and Finland (Farid & Rupasinghe 2016), and the second system is *in vitro* cultured AMDV antigen-based ELISA (ELISA-G) (Aasted & Cohn 1982), that is generally used in Denmark and USA (Farid & Rupasinghe 2016). In Denmark, ELISA has been approved by the Danish authorities for diagnosing AD in mink (Dam-Tuxen *et al.* 2014). The agreement between ELISA and CIEP results were assessed in previous studies CIEP has been established as the reference standard in AD diagnostics owing to its high specificity and cost-effectiveness (Aasted & Bloom 1983; Andersson & Wallgren 2013). Andersson and Wallgren (2013) reported that ELISA-P demonstrates sensitivity and specificity comparable to CIEP, while ELISA-G exhibits lower sensitivity in comparison to CIEP. Farid and Segervall (2014) observed moderate concordance between ELISA-P classifications and anti-AMDV antibody titers determined by CIEP. Another study indicated that ELISA-G displayed higher sensitivity but lower specificity than CIEP (Dam-Tuxen *et al.* 2014). In the absence of any other practical measuring method, despite lacking validation for antibody quantification (Farid & Segervall 2014), ELISA is recommended as an alternative to CIEP for ranking mink based on anti-AMDV antibody titers (Andersson & Wallgren 2013; Farid & Segervall 2014).

The Iodine agglutination test (IAT) is a method for quickly but roughly diagnosing AD. The IAT is a non-AD-specific test used to diagnose AD by detecting unhealthy animals

with high amounts of serum gamma globulin, as AD is characterized in mink by marked hypergammaglobulinemia (Henson *et al.* 1962; Williams *et al.* 1965; Henson *et al.* 1976). The IAT test has been used as a simple field procedure to detect mink infected with AMDV by several ranches in North America and the Netherlands (Gunnarsson 2001).

2.2.3 Controlling Aleutian Disease

Several methods, including vaccination, medicine, and culling strategy, have been attempted to control AD, but these methods have been largely ineffective. No effective vaccine has been created against AMDV at this point. Several previous studies that attempted to produce an effective vaccine against AMDV ended with failure (Porter *et al.* 1972; Aasted *et al.* 1998; Castelruiz *et al.* 2005; Markarian & Abrahamyan 2021), including formalin-inactivated AMDV vaccine (Porter *et al.* 1972). Several studies created partially effective protection, such as vaccinating mink AMDV capsid proteins (Aasted *et al.* 1998), and NS1 AMDV gene (Castelruiz *et al.* 2005). No effective treatment has been created for AD so far. While the immunosuppressive drug Cyclophosphamide can provide temporary protection against gross and microscopic lesions of AD in mink, its usage is accompanied by adverse effects such as necrosis and depletion of lymphoid tissues (Cheema *et al.* 1972). Culling mink with positive results of AD tests has been applied as the primary method to prevent/control AD (Cho & Greenfield 1978). CIEP and IAT were commonly used in the culling strategy, but the attempts to eradicate AMDV using these methods failed in mink farms (Themudo *et al.* 2011; Farid *et al.* 2012). Iceland is the only country which believed that successfully eradicated the AMDV virus in farmed mink over a 12-year period using CIEP between 1984 and 1996 (Gunnarsson 2001). Despite CIEP being utilized for viral eradication in Nova Scotia and Denmark since the mid-1970s, the AMDV virus persists in

these regions (Themudo *et al.* 2011; Farid *et al.* 2012). The failure of test-and-removal strategies can be attributed to various factors, including the variability of the virus genome, biosecurity lapses, the presence of infected wild animals in the natural environment, and the persistence of the virus on farms (Farid *et al.* 2012). Consequently, AD remains an enduring and challenging issue for the mink industry (Gunnarsson 2001; Christensen *et al.* 2011; Themudo *et al.* 2011). Thus, the suggestion of selecting mink resilient to AD is proposed as a potential solution to mitigate the adverse effects caused by the disease effectively (Hu *et al.* 2020).

2.2.4 Aleutian Disease Resilience

Disease resilience is the ability of animals to minimize the adverse effects caused by disruptions and to maintain their production performance under pathogen exposure (Albers *et al.* 1987; Bisset & Morris 1996). Several AD-related traits have been treated as AD resilience indicator traits. AD has been determined to be an immune complex disease because the antibodies specifically generated against AMDV demonstrate an inability to neutralize the virus effectively. Instead, these antibodies form complexes with the infectious virus, leading to detrimental effects on the mink's glomerular and arterial systems, as documented in previous research (Porter *et al.* 1969; Cho & Ingram 1973; Porter *et al.* 1973; Stolze & Kaaden 1987). Consequently, the severity of AD infection is positively correlated with the elevated production levels of anti-AMDV antibodies (Porter *et al.* 1972; Kanno *et al.* 1993; Bloom *et al.* 1994; Aasted *et al.* 1998; Bloom *et al.* 2001). Additionally, AD infection has been observed to negatively impact various traits, including body weight growth (Porter *et al.* 1982), feed intake (Elzhov *et al.* 2016; Jensen *et al.* 2016b), pelt quality (Farid & Ferns 2011), and female reproductive performance (Henson

et al. 1962; Reichert & Kostro 2014). Thus, anti-AMDV antibody level, growth, feed efficiency, and female reproductive performance were suggested as AD-resilience indicator traits in previous studies (Hu *et al.* 2021; Hu *et al.* 2022).

Phenotypic selection for mink resilient to AD has been implemented in major mink pelt-producing regions. In Nova Scotia, several farms identified AD-resilient mink by evaluating production traits and IAT results (Farid & Ferns 2017). Some AD-positive mink farms in North America and Europe employ the ELISA test results to select AD-resilient mink (Knuutila *et al.* 2009; Farid & Rupasinghe 2016; Farid *et al.* 2018). Despite some mink farms opting for the AD-specific test (ELISA) or non-AD-specific test (IAT) to choose AD-resilient mink, the practicality of utilizing AD tests as genetic selection indicators for AD resilience remains unvalidated. Simultaneously, the limited understanding of the genetic and genomic architecture associated with AD resilience poses a barrier for mink breeders to incorporate this novel trait into their breeding programs.

2.3 Genetics of Aleutian Disease Resilience

2.3.1 Heritability

The assessment of heritabilities and genetic correlations among traits of interest constitutes crucial genetic population parameters for animal breeding programs (Miar *et al.* 2014a; Miar *et al.* 2014b; Karimi *et al.* 2018). Narrow sense heritability denotes the proportion of phenotypic variance in a trait attributable to genetic factors, signifying the strength of the correlation between phenotypes and breeding values (Visscher *et al.* 2008). High heritability in a trait indicates that a substantial portion of its variation in the population results from genetic differences, making the phenotype a reliable indicator of genetic merit or breeding value (Falconer & Mackay 1996; Getabalew *et al.* 2019). Consequently,

heritability estimation is an indispensable indicator for artificial selection programs, influencing the accuracy of breeding value estimation from phenotypic information and the formulation of breeding strategies. Heritabilities of AD tests were rarely estimated. Notably, the heritabilities of AD tests have been infrequently appraised, with estimated values ranging from 0.39 to 0.61 for ELISA tests and from 0.11 to 0.58 for CIEP (Farid *et al.* 2018; Farid 2020; Hu *et al.* 2021). The heritability of IAT was only estimated to be 0.26 by Hu *et al.* (2021).

2.3.2 Genetic Correlation

The genetic correlation elucidates the relationship between the breeding values of two traits, illustrating the impact of selecting one trait on the response of other traits (Searle 1961). The AD can cause adverse influences on reproductive performance (Henson *et al.* 1962; Reichert & Kostro 2014), growth (Kowalczyk *et al.* 2019), feed intake (Eklund *et al.* 1968; Jensen *et al.* 2016a), and pelt quality (Farid & Ferns 2011), which are key traits in mink industry and could be treated as AD-resilient traits. Thus, it is imperative to assess the genetic correlations between AD tests and AD-resilient traits such as growth, feed efficiency, reproduction, fur quality, and pelt size. This evaluation is crucial for discerning potential adverse influences from the selection of AD tests on AD-resilient traits and determining the feasibility of employing AD tests as reliable indicators for selecting resilient mink. The genetic correlations between AD tests with pelt quality, female reproductive performance, the extent of anemia, and harvest length in mink have been explored by Hu *et al.* (2021). In Hu *et al.* study (2021), ELISA-G was suggested as the most suitable indicator trait among all AD tests for genetic selection of AD-resilient mink in AD endemic ranches due to its moderate heritability (0.39) and repeatability (0.58) and

significant ($P < 0.05$) negative genetic correlations with reproductive performance traits (from -0.41 to -0.49), packed-cell volume (-0.53), and harvest length (-0.45). A comprehensive view of the genetic and phenotypic correlations between target traits and other important traits are important for genetic selection. However, the genetic correlations between AD tests and other AD resilience traits (e.g., growth, feed efficiency, and feed-intake-related traits) have not been investigated.

2.4 Genomics of Aleutian Disease Resilience

2.4.1 Population Genomics

To establish an effective genomic selection program for domestic animals, it is imperative to comprehend the genetic structure of the target population (Groeneveld *et al.* 2010; Wellmann & Bennewitz 2019). Population genomics investigates the impact of evolutionary processes and selection on genomic and population variations, concurrently examining numerous loci and genome regions (Black *et al.* 2001; Luikart *et al.* 2003). The genetic structure of target populations is usually revealed by exploring domestication history, genetic diversity, genetic relationships, and genetic patterns of the studied populations. Two crucial parameters for revealing the genetic structure of the target population are linkage disequilibrium (LD) and effective population sizes (N_e). The LD is defined as the non-random association of alleles at two or more loci (Slatkin 2008). Various factors such as genetic drift, selection, epistatic combinations, population structure, and admixture between distinct populations could lead to LD between unlinked markers (Pfaff *et al.* 2001; Ardlie *et al.* 2002; Qanbari 2020). The magnitude of LD is employed to determine the optimal marker density for genome-wide mapping studies (Goddard & Hayes 2009), and both genomic selection and genome-wide association studies (GWAS)

depend on the presence of LD between markers and functional variants (Bush & Moore 2012; Hay & Rekaya 2018). In the meantime, the extent of LD between unlinked loci can be utilized to estimate the recent and past N_e (Hill 1981; Waples & Do 2010). The N_e is used to measure the rate of inbreeding and loss of genetic diversity and quantify the extent of variability in a population and the effectiveness of selection relative to drift (Charlesworth 2009; Ryman *et al.* 2019). A population is prone to the loss of genetic variation when the N_e of this population is estimated to be small. Genetic diversity is a measurement that quantifies the magnitude of genetic variability within a population and is a fundamental source of biodiversity (Hughes *et al.* 2008; Ellegren & Galtier 2016). The understanding of genetic diversity in the target population is the foundation for successful and sustainable breeding programs, providing the raw material needed for adaptation, resilience, and improvement of the target population (Notter 1999; Ollivier 2009). American mink of different color types show different performance for some traits, such as susceptibility to AD (Ellis 1996) and reproductive performance (Kidd *et al.* 2009). Thus, investigating the genetic structure of American mink of various color types could also help explain variation in performance for traits of economic interest.

The population genomics information of farm and feral American mink were investigated using information from diverse molecular markers, such as microsatellite, mitochondrial DNA, and single nucleotide polymorphism (SNP) markers. Microsatellite loci were employed to assess the genetic structures of feral American mink captured in Japan (Yukari *et al.* 2010), Sweden (Zalewski *et al.* 2016), and Spain (Lecis *et al.* 2008). The genomic data obtained from mitochondrial DNA and microsatellite loci were utilized to comprehend the genetic structure of introduced American mink in southern Chile (Mora *et al.* 2018).

The population genetic structure of farm and feral American mink in Poland and Denmark was explored using genotypes obtained from 194 SNPs derived from the restriction-site associated DNA sequencing method (Thirstrup *et al.* 2015). Additionally, an investigation into the LD and N_e of black American mink in Canada was conducted, leveraging data from 13,321 SNPs detected through the genotyping-by-sequencing (GBS) approach on 46 scaffolds from 285 individuals (Karimi *et al.* 2020). Furthermore, the genetic structure of American mink in Canada was probed by randomly selecting 100,000 SNPs through whole-genome sequencing (WGS) across 51 scaffolds from 100 farm mink (Karimi *et al.* 2021b). Notably, there is a gap in research pertaining to the genetic structure of farmed American mink with diverse color types, utilizing a relatively substantial sample size (approximately 3,000) and genotypic data from a medium-density SNP panel. However, no study has investigated the genetic structure of farm mink with various color types using genotypic data from a medium-density SNP panel.

2.4.2 Selection Signatures

Selection signatures refer to the reduction, elimination or change in the genetic variation surrounding specific genomic regions that have undergone selection pressure (Nielsen 2005; Jensen *et al.* 2016a). The regional changes/reduction in genetic variation upstream and downstream of the selected beneficial mutation could be triggered by the rapid fixation of that mutation after several generations (Nielsen 2005; Jensen *et al.* 2016a). The identification of these selection signatures is one of the main interests of animal geneticists due to its potential to uncover genes or advantageous mutations that confer benefits to particular livestock populations (Zhao *et al.* 2015).

The advancements in next-generation sequencing technologies, high-density SNP arrays, and bioinformatics tools have significantly enhanced the detection of selection signatures in livestock species (Bertolini *et al.* 2018). Notably, studies employing selection signatures have pinpointed genes linked to disease resistance/susceptibility in cattle (Li *et al.* 2020; Saravanan *et al.* 2021). For instance, Xu *et al.* (Xu *et al.* 2020) conducted a selection signature study identifying genes associated with swine susceptibility to respiratory disease. For AD in American mink, the GBS data and five AD-related phenotypes (antibody titer, mortality, AD symptoms in the kidneys, and virus clearance at two different times) from 225 experimental black mink, which were intranasally inoculated AMDV, were applied to detect the selection signatures associated with the response of mink to AD infection (Karimi *et al.* 2021a), and a total of 99 genomic regions, which harboured 63 genes, were identified. These 63 genes were mostly related to immune response, liver development, and reproduction (Karimi *et al.* 2021a). Phenotypic selection for mink resilient to AD based on AD-resilient traits (e.g., production traits, IAT results, and ELISA results) has been implemented in several mink farms in North America (Farid & Rupasinghe 2016; Farid & Ferns 2017; Farid *et al.* 2018) and Europe (Knuuttila *et al.* 2009), but the study of selection signatures focusing on the response of mink to AD have not been conducted using genotype data in conjunction with AD-resilience indicator traits (e.g., growth, feed efficiency, pelt quality, and reproduction) for mink reared in AD-positive commercial farms.

The development of the first medium-density (70K) SNP panel for mink (Do *et al.* 2024) makes it feasible to conduct a selection signatures study in mink using genotypes. Using a medium-density SNP panel for selection signatures offers a balanced approach by

providing sufficient resolution to detect selection signatures without the high costs and computational demands of WGS or high-density SNP panels. It allows for more efficient data processing and analysis compared to WGS or high-density SNP panels, while offering better detection power and accuracy than low-density SNP panels. This balance makes it a cost-effective and practical choice for large-scale studies aiming to identify genomic variations linked to selection pressures (Mancini *et al.* 2014; Brito *et al.* 2017; Persichilli *et al.* 2023; Sarviaho *et al.* 2024).

2.4.3 Genome-wide Association Studies

Disease traits typically manifest as quantitative traits characterized by intricate genetic structures (VanRaden 2008; Leach *et al.* 2010; Thompson-Crispi *et al.* 2014; Hu *et al.* 2020; Doeschl-Wilson *et al.* 2021). In the context of disease investigation, genomic studies concentrate on pinpointing genetic variations that correlate with host responses to the disease and seek to unveil associations between genotype and phenotype by scrutinizing thousands to millions of genetic variants across the genomes of numerous individuals (Tam *et al.* 2019). The GWAS uses phenotypic information and sequence/genotypic variations to detect gene(s) associated with the target trait (Hirschhorn & Daly 2005). In such analyses, subjects undergo whole-genome sequencing or genotyping for a specific set of genetic markers, contingent upon the species and the accessibility of sequence data or genotyping panel. Markers exhibiting statistically significant variations in minor allele frequencies among individual phenotypes are regarded as indicators of association. The SNPs and potential genes identified through GWAS contribute to an enhanced comprehension of the genetic framework and biological mechanisms governing hosts' responses to diseases.

The GWAS has been regarded as the ideal method for identifying genes associated with various phenotypes and biological pathways of complex traits (Sharma *et al.* 2015). Since its inception in humans (Klein *et al.* 2005), GWAS has gained widespread application in the domain of complex disease genetics, leading to the identification of numerous genetic variants associated with complex diseases in humans (refer to the GWAS catalog: <https://www.ebi.ac.uk/gwas/home>). In recent years, advancements in next-generation sequencing technologies, high-density SNP arrays, and bioinformatics tools have enhanced the popularity of GWAS in the identification of genetic variants and genes linked to immune response and disease resilience traits in livestock. For instance, in swine, GWAS has revealed several SNPs and genes correlated with resilience to porcine reproductive and respiratory syndrome (Boddicker *et al.* 2014; Yang *et al.* 2016; Hickmann *et al.* 2021), *Mycoplasma hyopneumoniae* (Uemoto *et al.* 2021), and polymicrobial disease (Cheng *et al.* 2022). In cattle, GWAS studies have identified multiple SNPs and genes associated with resilience to paratuberculosis (Alonso-Hearn *et al.* 2022) and Johne's disease (Alpay *et al.* 2014; Mallikarjunappa *et al.* 2020). In poultry, Psifidi *et al.* (Psifidi *et al.* 2016) conducted GWAS to find the SNPs and genes associated with the immune response to four infectious diseases (infectious bursal disease, Marek's disease, fowl typhoid, and fowl cholera) and resistance to *Eimeria* and cestode parasitism. However, no GWAS on mink immune response to AD and AD-resilience indicator traits had been conducted using genotype data.

2.4.4 Genomic Selection

Genomic selection aims to estimate the breeding values using the genomic diversity captured by extensive markers distributed across the genome, all without requiring knowledge of the specific gene locations (Goddard & Hayes 2007). Genomic selection

operates under the assumption that all markers could be associated with a gene influencing a specific trait. It focuses on estimating the effects of these markers rather than statistically testing their significance. The process involves phenotyping for the trait and genotyping individuals in a reference population to assess SNP effects. Subsequently, selection candidates undergo genotyping, and their genotypic information is integrated with the previously estimated effects to derive genomic estimated breeding values for the selection candidates. The advent of dense panels of SNP markers has facilitated the widespread application of genomic selection in major farm animal species (Misztal *et al.* 2021). This implementation serves to expedite genetic trends by enhancing selection accuracy and diminishing generation intervals. The augmented accuracy in selection is particularly crucial for traits characterized by low heritabilities, where traditional selection processes tend to be sluggish (Misztal *et al.* 2021). Compared with the traditional pedigree-based genetic selection, genomic selection, which uses a genomic information-based relationship matrix that provides more accurate relationship coefficients among individuals, is believed to increase the accuracy of estimated breeding values (Goddard 2009; Atefi *et al.* 2018; Budhlakoti *et al.* 2022).

The heritabilities of traits associated with diseases typically exhibit a low-to-moderate range. Consequently, the utilization of genomic selection is recommended to enhance these disease-related traits (Bishop & Woolliams 2014; Iheshiulor *et al.* 2017). Notably, studies employing genomic selection to enhance resistance to porcine reproductive and respiratory syndrome in pigs have been undertaken (Serão *et al.* 2016; Waide *et al.* 2018). The common methods used to conduct genomic prediction studies are genomic best linear unbiased prediction (GBLUP), single-step GBLUP (ssGBLUP), and several Bayesian approaches.

Machine learning methods have also been applied to genomic predictions in recent years. The GBLUP is a multi-step method that uses genomic information to predict genomic breeding values (VanRaden 2008; Hayes *et al.* 2009). The GBLUP process encompasses three key steps: 1) constructing a comprehensive response variable summarizing all available phenotypic information for genotyped animals, 2) utilizing genomic prediction to link the response variable to marker information, and 3) integrating genomic predictions with parental average estimated breeding values (Christensen *et al.* 2012). In comparison to GBLUP, ssGBLUP is a more streamlined single-step methodology that combines pedigree, phenotypic, and genomic information for the genetic evaluation of all breeding individuals in a unified model (Misztal *et al.* 2013). Meanwhile, the ssGBLUP was found to be simple, fast, and accurate (Misztal *et al.* 2013; Cardoso *et al.* 2015; Silva *et al.* 2016). Bayesian genomic prediction approaches (Bayes A, B, C, etc.) involve nonlinear methods typically implemented in genomic prediction using the Markov Chain Monte Carlo algorithm (Iheshiulor *et al.* 2017). In recent years, machine learning methods have also been utilized in genomic predictions (An *et al.* 2021). Several previous studies applied machine learning methods, including random forests, gradient boosting machine, and extreme gradient boosting, in genomic prediction for economically important traits in livestock species, such as milk yield in Holstein cattle (Long *et al.* 2011) and body weight in Brahman cattle (Li *et al.* 2018). With the development of dense panels of SNP markers, genomic selection has been widely adopted in major farm animal species (Misztal *et al.* 2021). The chromosome-level genome assembly by Karimi *et al.* (Karimi *et al.* 2022) and the development of the first Axiom Affymetrix Mink 70K SNP panel for American mink (Do *et al.* 2024) have facilitated the feasibility of genomic prediction studies for AD

resilience in mink. However, no genomic prediction studies have been conducted for AD resilience in mink.

2.5 Conclusion

AD causes major health concerns and economic losses to the global mink industry. The ineffectiveness of vaccination, medicine, and culling strategy in controlling AD has urged mink farmers to select AD-resilient mink. However, the lack of comprehensive knowledge of the genetic/genomic architecture of AD resilience prevents breeders from integrating this novel trait into their breeding programs. A comprehensive view of genetic parameters for target traits is necessary for conducting genetic selection. However, studies related to the genetic parameters of AD-resilient traits are rare. Thus, further research in estimating the genetic parameters of AD-resilient traits and the genetic correlations among AD-resilient traits is needed. The development of the first Axiom Affymetrix Mink 70K SNP panel makes genomic studies for AD resilience in mink feasible. Understanding the population genomics of the target population is essential to conducting genomic studies and developing genomic selection programs. However, no investigation has been made into the genetic structure of farmed mink with various color types using chromosome-based genotype data. Therefore, investigating the population genomics of farm mink using genotypic information from the first medium-density SNP panel for mink is needed prior to conducting further genomic studies on AD resilience. Selection signatures and GWAS are popular methods for investigating the genomic architecture of traits of interest. However, none of these approaches have been applied in studying the genomic architecture underlying AD resilience. Thus, conducting selection signatures and GWAS would provide a great opportunity to better understand the genomic architecture underlying mink's

resilience to AD and shed light on the underlying biological mechanisms involved. Genomic selection is believed to expedite genetic trends through heightened selection accuracy and decreased generation intervals. This heightened accuracy is especially crucial for traits with low heritabilities, where traditional selection processes are sluggish. Disease-related traits, such as AD resilience traits, typically exhibit low-to-moderate heritabilities, underscoring the potential of genomic selection to improve these traits. However, no genomic prediction studies have been conducted for AD resilience in mink. Hence, performing genomic prediction studies on AD-resilient traits presents an avenue to assess the viability of genomic selection for enhancing mink resilience against AD.

CHAPTER 3. Genetic and Phenotypic Correlations between Aleutian Disease Tests with Body Weight, Growth, and Feed Efficiency Traits in Mink¹

3.1 Introduction

As one of the most severe diseases in mink farming, Aleutian disease (AD) brings tremendous financial losses to the mink industry and has made it difficult for mink farmers to maintain their farming. Aleutian disease is caused by the Aleutian mink disease virus (AMDV). AMDV is a non-enveloped single-stranded DNA virus in parvovirus family (genus *Amdoparvovirus*, species *Carnivore amdoparvovirus 1*). AMDV infection causes significant pathology, including hypergammaglobulinemia, glomerulonephritis, plasmacytosis, and arteritis to the infected mink (Porter *et al.* 1969; Cho & Ingram 1973; Porter *et al.* 1973). AMDV infection also causes adverse effects on female reproductive performance for example small litter size, fetal death, and abortion (Henson *et al.* 1962; Reichert & Kostro 2014). Additionally, small body size due to such as chronic progressive weight loss (Porter *et al.* 1982), low feed intake (inappetence) (Eklund *et al.* 1968; Jensen *et al.* 2016b), and poor pelt quality characterized by hair depigmentation (Farid & Ferns 2011) are also adverse outcomes. Together, these clinical features on AMDV infection in farmed mink directly reduce the financial income of mink farmers. Therefore, an effective, practical, and reliable approach is urgently needed by the mink farmers to minimize the

¹ A version of this chapter has been published in Journal of Animal Science by Hu et al. 2022. Genetic and phenotypic correlations between Aleutian disease tests with body weight, growth, and feed efficiency traits in mink. 100(12), skac346. doi: <https://doi.org/10.1093/jas/skac346>

adverse effects of AD. Unfortunately, vaccination and recovery from natural infection have not been identified as viable strategies of protection due to antibody disease enhancement. Specifically antibodies elicited toward the Aleutian mink disease virus are not capable of neutralizing the virus and instead the infectious virus forms complexes with pre-existing antibody complexes leading to lesions in the glomerulus and arteries of the mink host (Porter *et al.* 1969; Cho & Ingram 1973; Porter *et al.* 1973; Stolze & Kaaden 1987).

Several methods have been attempted to control AD for farmed mink, however, at this time control measures have not been successful. No effective vaccine or medicine has been developed with the ability to protect against infection without inducing vaccine enhanced disease (Liu *et al.* 2017; Farid *et al.* 2018). Culling mink after testing positive for AD has been the primary method to control AD, however, culling does not successfully prevent future outbreaks (Gunnarsson 2001; Christensen *et al.* 2011; Themudo *et al.* 2011; Farid *et al.* 2012). Feeding mink, which were challenged with AMDV, with dietary kelp (*Ascophylum nodosum*) supplementation showed some benefits to the survival rate of adult mink and litter size, but the effects were not significant compared to the control group (Farid *et al.* 2020). In recent years, the selection of AD-resilient individuals based on AD tests is suggested as a potential solution to cope with the adverse effects caused by AD effectively (Farid *et al.* 2018; Hu *et al.* 2020).

Several AD tests have been applied in the phenotypic selection of AD-resilient mink in a number of mink-producing areas, but the feasibility of employing AD tests in the genetic selection of AD-resilient mink has not been evaluated. Several mink farms in the province of Nova Scotia in Canada select for AD-resilient mink based on the productive performance and iodine agglutination test (IAT, measuring gamma globulin level) results (Farid & Ferns

2017). Some AD positive mink farms in North America and Europe (Knuutila *et al.* 2009; Farid & Rupasinghe 2016; Farid *et al.* 2018) have selected AD-resilient mink based on enzyme-linked immunosorbent assay tests (ELISA, measuring anti-AMDV antibody level). Although some mink farmers use AD tests in the phenotypic selection of AD-resilient mink, the feasibility of this approach has not been explored due to the lack of comprehensive genetic background knowledge of AD tests.

An effective genetic selection program requires a comprehensive study of genetic and phenotypic parameters for traits of interest (Toghiani 2012). Studies of the genetic parameter of AD tests and their correlations with AD-resilient or other economically important traits are rare. However, Hu *et al.* (2021) estimated heritabilities (\pm SE) for AMDV antigen-based ELISA (ELISA-G), AMDV capsid protein-based ELISA (ELISA-P), counterimmunoelectrophoresis (CIEP), and IAT of 0.39 ± 0.06 , 0.61 ± 0.07 , 0.11 ± 0.07 , and 0.26 ± 0.05 , respectively. The genetic and phenotypic correlations between AD tests with pelt quality, reproductive performance, packed-cell volume, and harvest length were also estimated by (Hu *et al.* 2021), and ELISA-G was suggested as a good indicator trait for selecting AD-resilient mink. A comprehensive view of the genetic and phenotypic correlations between target traits and other important traits are important for genetic selection. Here in this thesis chapter, we further investigated the genetic and phenotypic correlations between AD tests and other economically important or AD-resilient traits to provide a more comprehensive view of the genetic and phenotypic correlations between AD tests and other economically important traits in mink. The overall objective of this thesis chapter was to estimate the genetic and phenotypic correlations between AD tests with body weights at different ages, growth parameters obtained from the Richards growth

model (Do & Miar 2020), different measurements of feed efficiency, and feed-intake-related traits

3.2 Materials and Methods

This study was approved by the Dalhousie University Animal Care and Use Committee (certification#: 2018-009 and 2019-012). All the mink were raised based on the Code of Practice for the Care and Handling of Farmed Mink guidelines from the Canada Mink Breeders Association (Turner P *et al.* 2013).

3.2.1 Animals and Management

Animals in this study were raised under standard farming conditions at the Canadian Centre for Fur Animal Research (CCFAR) at Dalhousie University, Faculty of Agriculture (Truro, Nova Scotia, Canada) from 2013 to 2021. All mink had *ad libitum* access to food and water. The annual mink production cycle in CCFAR contains four periods: 1) conditioning and breeding season (December-March), where mink farmers adjust the feed to provide the mink with good conditions for breeding in March; 2) whelping and weaning season (April-June), where females will give birth at the end of April or early May, and the kits will be weaned at the end of June; 3) growth and furring season (July-October), animals will be fed ad-lib to fulfill their growth potential; and 4) grading and harvesting (November-December), where farmers determine which mink will be pelted or kept as breeding stock for future season. An AD outbreak on CCFAR was identified in 2013. The source of this outbreak was not determined. AMDV-contaminated feed as well as contact with wild animals carrying AMDV have been considered as the most likely causes. Meanwhile, no persistent breeding program was employed in CCFAR during the study years (2013 to 2021). The total of 2,488 mink (males = 832 and females = 1,656) used in this study were

the progeny of 444 sires and 852 dams. Pedigree information of 17 generations comprising 24,864 individuals was used.

3.2.2 Aleutian Disease Tests

All AD tests were conducted using established protocols described by Hu et al. (2021). Briefly, blood samples of the studied mink (n=2,352) were collected using the toenail clipping approach at two different periods: 1) in mid-November of 2013, 2014, 2018, and 2019 before selecting breeders; and 2) in mid-February of 2013, 2014, 2017, 2018, 2019, 2020, and 2021 before mating. Both ELISA-G and ELISA-P systems were employed to quantify the anti-AMDV antibodies in the serum. The ELISA-G test was conducted at Middleton Veterinary Services (Nova Scotia, Canada), and the test results included eight categories from 0 (low) to 7 (high), with 1-point increments. The ELISA-P tests were conducted at Nederlandse Federatie van Edelpelsdierenhouders (Wijchen, Netherlands), and the test results included nine categories from 0 (low) to 8 (high), with 1-point increments. The CIEP tests were conducted at the Animal Health Laboratory at the University of Guelph (Guelph, Canada) to detect the existence of anti-AMDV antibodies in the blood samples, and the results were recorded as 0 (negative) and 1 (positive). The IAT tests were conducted at CCFAR to measure the serum gamma globulin level in the serum, and the results were scored into four categories from 0 (low) to 4 (high).

3.2.3 Body Weight Measurements and Growth Parameters

A total of 1,088 mink born in 2018 and 2019 were randomly selected for collecting body weight (BW) data. All BW data were collected using established protocols described by Do et al. (2021). Briefly, selected mink were weighed at birth, which happens between the end of April and early May, and at weaning around the end of June (about seven weeks of

age). After weaning, each selected mink was raised in a single cage and weighed every three weeks from 13 to 28 weeks after birth. Thus, the BW traits included BW at week 13 (BW13), week 16 (BW16), week 19 (BW19), week 22 (BW22), week 25 (BW25), and week 28 (BW28). The BW of mink at harvest (HW) was measured at two different times. The HW of mink, which were not selected as breeders, were measured at harvest days in December 2018 and 2019. Additionally, HW of sires that completed their breeding tasks and dams that mated but failed to become pregnant were measured at harvest days in February 2019 and 2020.

Growth parameters were derived from the Richards growth model (Richards & Kavanagh 1945). This model was suggested previously to be the most suitable model to describe the growth of mink (Liu *et al.* 2011; Do & Miar 2020). The `minpack.lm` packages (Elzhov *et al.* 2016) in R software (R Development Core Team 2011) was used to fit individual BW records into the following Richards growth model, as described by Do *et al.* (2021):

$$BW_t = \frac{\alpha}{(1 - \beta \times e^{-kt})^{1/m}},$$

where BW_t is the BW (kg) at age t (weeks), α is the asymptotic weight (kg), β is the parameter characterizing the first part of growth before the inflection point, k is the maturation rate, and m is the inflection parameter.

The parameters, α , m , and k , derived from Richards model were then used to calculate the age at the inflection point (AIP) and the weight at the inflection point (WIP) as follows:

$$AIP = \frac{\alpha}{(m + 1)^{1/m}},$$

$$WIP = \frac{-\ln(m/\beta)}{k}$$

3.2.4 Feed Intake Measurement and Feed Efficiency

The feed intake data were collected from August 1st to November 14th in 2018 and 2019 at CCFAR using the established protocols described by Davoudi et al. (2022). Briefly, 1,088 mink had both feed intake and growth traits data. Mink were housed individually in single cages, and feed was distributed to each pen every day. The amounts of feed allocated to mink were regulated based on the leftover records to avoid unnecessary feed waste and meet the mink's appetite. The difference between the amount of feed leftover and feed provided was recorded as daily feed intake (DFI). The average of the DFI records during the feeding trial was used as the average daily feed intake (ADFI).

Feed efficiency traits were calculated using both feed intake and growth data. The BW13 was treated as the initial BW, and the BW on the last day of the feeding trial was treated as the final BW. The following equation was used to calculate the average daily gain (ADG):

$$ADG = \frac{Final\ BW - Initial\ BW}{Number\ of\ days\ on\ the\ test},$$

For calculating the feed conversion ratio (FCR), the following equation was used:

$$FCR = \frac{ADFI}{ADG},$$

The Mid-test metabolic BW ($BW^{0.75}$) and Kleiber ratio (KR) were calculated using the following equations, respectively:

$$BW^{0.75} = \left(\frac{Initial\ BW + Final\ BW}{2} \right)^{0.75},$$

$$KR = \frac{ADG}{BW^{0.75}}$$

The linear regression model used to estimate the residual feed intake (RFI) was:

$$ADFI = \beta_0 + \beta_1 ADG + \beta_2 BW^{0.75} + \varepsilon,$$

where β_0 is the equation intercept, β_1 is the partial regression coefficient of ADG, β_2 is the partial regression coefficient of $BW^{0.75}$, and ε is RFI.

Residual gain (RG) was estimated using the following linear regression model:

$$ADG = \beta_0 + \beta_1 ADFI + \beta_2 BW^{0.75} + \varepsilon,$$

where β_0 is the equation intercept, β_1 is the partial regression coefficient of ADFI, β_2 is the partial regression coefficient of $BW^{0.75}$, and ε is RG.

The following equation (Berry & Crowley 2012) was used to derive the residual intake and gain (RIG):

$$RIG = \left(-1 \times \left(\frac{RFI_i}{RFI_{sd}} \right) \right) + \left(\frac{RG_i}{RG_{sd}} \right),$$

where RFI_i is the RFI for individual i , RFI_{sd} is the standard deviation of RFI for all animals, RG_i is the residual gain for animal i , and RG_{sd} is the standard deviation of RG for all animals.

3.2.5 Feed-Intake-Related Traits

Two feed intake traits, the day-to-day variation in feed intake (VarF) and the proportion of off-feed days based on feed intake (DOF), were derived from the DFI data available for each mink using the method described by Putz et al. (2019). The VarF was measured based on the root mean square error of within-individual regression of DFI on day using ordinary least squares linear regression. The off-feed days were identified using a 5% quantile regression of DFI on age across all mink. The negative residuals below the regression line were treated as off-feed days for each mink. The DOF was calculated as the proportion of off-feed days to the total recorded days of DFI.

3.2.6 Statistical Analyses

A univariate animal model was used to estimate the variance components of random additive genetic, permanent environmental, and maternal genetic effects for individual traits using ASReml 4.1 software (Gilmour *et al.* 2018). The model was as follows:

$$\mathbf{y} = \mathbf{X}\mathbf{b} + \mathbf{Z}\mathbf{a} + \mathbf{W}\mathbf{pe} + \mathbf{G}\mathbf{m} + \mathbf{e},$$

where \mathbf{y} is the vector of phenotypes; \mathbf{X} is the incidence matrix relating phenotypes to fixed effects; \mathbf{b} is the vector of fixed effects; \mathbf{Z} is the incidence matrix relating phenotypes to random additive genetic effects; \mathbf{a} is the vector of random additive genetic effects, with $\mathbf{a} \sim N(0, \mathbf{A}\sigma_a^2)$, where \mathbf{A} is the numerator relationship matrix, and σ_a^2 is the additive genetic variance; \mathbf{W} is the incidence matrix relating phenotypes to random permanent environmental effects; \mathbf{pe} is the vector of random permanent environmental effects, with $\mathbf{pe} \sim N(0, \mathbf{I}\sigma_{pe}^2)$, where \mathbf{I} is an identity matrix, and σ_{pe}^2 is the permanent environmental variance; \mathbf{G} is the incidence matrix relating phenotypes to random maternal genetic effects; \mathbf{m} is the vector of random maternal genetic effects, with $\mathbf{m} \sim N(0, \mathbf{A}\sigma_m^2)$, where σ_m^2 is the maternal genetic variance; and \mathbf{e} is the vector of residual effects, with $\mathbf{e} \sim N(0, \mathbf{I}\sigma_e^2)$, where σ_e^2 is the residual variance.

The significance of fixed effects and covariates was tested using Wald statistics in the REML procedure of ASReml 4.1 (Gilmour *et al.* 2018), and only significant ($P < 0.05$) effects were kept in the mixed model analyses for each trait (Table 3.1). The fixed effects of sex and color type were tested for all studied traits. The fixed effect of AD test year (2013 to 2021), which described the year that the animals were tested for AD, was tested for AD test traits. The fixed effect of row-by-year, which described the location of cages (six rows) where mink were raised in 2018 and 2019, was tested for feed efficiency and

feed intake traits. The fixed effects of dam age (1 to 3 years old), which described the age of the animals' dams when they were born, and birth year (2018 and 2019), which described the year that the animals were born, were tested for growth traits. Blood collection age (in days) obtained for AD tests was only tested for AD traits. The age at harvest (in days) was tested for harvest weight only. The age at the end of feeding trial (in days) was tested for both feed efficiency and feed intake traits.

The following likelihood ratio tests, which compares the full model and the reduced model, was used to test the significance of the random maternal genetic and permanent environmental effects:

$$-2(\log L_{reduced\ model} - \log L_{full\ model}) \\ \sim \chi^2_{df\ (full\ model) - df\ (reduced\ model)},$$

where $\log L$ and df are log-likelihood and degrees of freedom. The random maternal genetic effect was tested for all studied traits. The random permanent environmental effect was only tested for AD tests because only AD tests had repeated records in different years.

To estimate the genetic and phenotypic correlations between traits, the bivariate models were conducted using ASReml 4.1 software (Gilmour *et al.* 2018). Relevant significant fixed and random effects were included in bivariate analyses for each trait (Table 3.1). The following bivariate model was used to analyze the traits:

$$\begin{bmatrix} \mathbf{y}_1 \\ \mathbf{y}_2 \end{bmatrix} = \begin{bmatrix} \mathbf{X}_1 & 0 \\ 0 & \mathbf{X}_2 \end{bmatrix} \begin{bmatrix} \mathbf{b}_1 \\ \mathbf{b}_2 \end{bmatrix} + \begin{bmatrix} \mathbf{Z}_{a1} & 0 \\ 0 & \mathbf{Z}_{a2} \end{bmatrix} \begin{bmatrix} \mathbf{a}_1 \\ \mathbf{a}_2 \end{bmatrix} + \begin{bmatrix} \mathbf{Z}_{pe1} & 0 \\ 0 & \mathbf{Z}_{pe2} \end{bmatrix} \begin{bmatrix} \mathbf{pe}_1 \\ \mathbf{pe}_2 \end{bmatrix} + \begin{bmatrix} \mathbf{Z}_{m1} & 0 \\ 0 & \mathbf{Z}_{m2} \end{bmatrix} \begin{bmatrix} \mathbf{m}_1 \\ \mathbf{m}_2 \end{bmatrix} + \begin{bmatrix} \mathbf{e}_1 \\ \mathbf{e}_2 \end{bmatrix},$$

where subscript numbers 1 and 2 refer to trait 1 and 2; \mathbf{y} is the vector of phenotypes; \mathbf{X} is the incidence matrix relating phenotypes to fixed effects; \mathbf{b} is the vector of fixed effects; \mathbf{Z}_a is the incidence matrix relating phenotypes to random additive genetic effects; \mathbf{a} is the vector of random additive genetic effects; \mathbf{Z}_{pe} is the incidence matrix relating phenotypes

to random permanent environmental effects; pe is the vector of random permanent environmental effects; Z_m is the incidence matrix relating phenotypes to random maternal genetic effects; m is the vector of random maternal genetic effects; and e is the vector of residual effects. The assumptions for the bivariate random effects were:

$$\begin{aligned} \begin{bmatrix} a_1 \\ a_2 \end{bmatrix} &\sim MVN \left(0, A \otimes \begin{bmatrix} \sigma_{a1}^2 & \sigma_{a1a2} \\ \sigma_{a1a2} & \sigma_{a2}^2 \end{bmatrix} \right), \\ \begin{bmatrix} pe_1 \\ pe_2 \end{bmatrix} &\sim MVN \left(0, I \otimes \begin{bmatrix} \sigma_{pe1}^2 & \sigma_{pe1pe2} \\ \sigma_{pe1pe2} & \sigma_{pe2}^2 \end{bmatrix} \right), \\ \begin{bmatrix} m_1 \\ m_2 \end{bmatrix} &\sim MVN \left(0, A \otimes \begin{bmatrix} \sigma_{m1}^2 & \sigma_{m1m2} \\ \sigma_{m1m2} & \sigma_{m2}^2 \end{bmatrix} \right), \text{ and} \\ \begin{bmatrix} e_1 \\ e_2 \end{bmatrix} &\sim MVN \left(0, I \otimes \begin{bmatrix} \sigma_{e1}^2 & \sigma_{e1e2} \\ \sigma_{e1e2} & \sigma_{e2}^2 \end{bmatrix} \right), \end{aligned}$$

where subscript numbers 1 and 2 refer to traits 1 and 2; A is the numerator relationship matrix; I is an identity matrix; σ_a^2 is the variance of random additive genetic effects; σ_{a1a2} is the covariance between random additive genetics effects for traits 1 and 2; σ_{pe}^2 is the variance of random permanent environmental effects; σ_{pe1pe2} is the covariance between random permanent environmental effects for traits 1 and 2; σ_m^2 is the variance of random maternal genetic effects; σ_{m1m2} is the covariance between random maternal genetic effects for traits 1 and 2; σ_e^2 is the variance of random residual effects; and σ_{e1e2} is the covariance between residual effects for traits 1 and 2.

Random additive genetic effects were included in the final model for all traits. Random permanent environmental effect was only significant ($P < 0.05$) for ELISA-G and IAT (Table 3.1). Random maternal genetic effect was included in the final models for all studied traits

except for IAT, DOF, and VarF, because the random maternal genetic effects were not significant ($P>0.05$) for these traits (Table 3.1).

Phenotypic variances were calculated as $\sigma_p^2 = \sigma_a^2 + \sigma_e^2$ for DOF and VarF, as $\sigma_p^2 = \sigma_a^2 + \sigma_m^2 + \sigma_e^2$ for ELISA-P, CIEP, all growth traits, and all feed efficiency traits, as $\sigma_p^2 = \sigma_a^2 + \sigma_{pe}^2 + \sigma_e^2$ for IAT, and as $\sigma_p^2 = \sigma_a^2 + \sigma_{pe}^2 + \sigma_m^2 + \sigma_e^2$ for ELISA-G. Heritability (h^2) was calculated as follows:

$$h^2 = \frac{\sigma_a^2}{\sigma_p^2},$$

Repeatability (r) was defined as follows:

$$r^2 = \frac{\sigma_a^2 + \sigma_{pe}^2}{\sigma_p^2}$$

Phenotypic and genetic correlations among traits were calculated based on bivariate models' (co)variance components.

In this study, the binary trait of CIEP was analyzed as a continuous trait, which was not theoretically optimal as the suitable methodology was the threshold model (Gianola 1982). The generalized linear mixed models (GLMM) procedures with animal model in ASReml (Gilmour *et al.* 2018) were initially used to analyze the CIEP trait, but this method failed to estimate the variances caused by random additive genetic effects. The GLMM procedure with sire model was suggested as more appropriate method to run threshold model on the user guide of ASReml (Southey & Gilmour 2021). However, the sire model was not practical for mink breeding because the current breeding procedure in mink had more focused on dams than sires. In the meantime, several other studies also treated binary traits as continuous traits when they estimated genetic parameters for disease-related traits (Farid

et al. 2018; Gunia *et al.* 2018). Thus, CIEP was treated and analyzed as continuous trait in this study.

3.3 Results and discussion

3.3.1 Descriptive Statistics

The number of records, mean, standard deviation (SD), range, and coefficient of variation (CV) for each trait are presented in Table 3.2. Among all studied traits, ELISA-G (n=2,896) and IAT (n=2,236) had the most data records because CCFAR started recording these traits from 2013 while the other traits were measured after 2018. Compared with the previous study (Hu *et al.* 2021), we collected 537 more records of ELISA-G and 531 records of IAT in 2021. The lowest number of records was for HW (844) because this trait was only recorded after 2018. The CVs of ELISA-G (125%) and IAT (150.75%) were 12.33% larger and 12.41% lower than our previous study (Hu *et al.*, 2021), respectively, which may be due to more records being used in this study. The CVs for BW traits at different ages increased with animal age and ranged from 23.39 to 31.28%. Except for growth parameter (m), the CVs of growth parameters were less than 42%, which ranged from 16.88% to 41.67%. The CVs ranged from 28.60% to 45.67% for feed efficiency traits. In addition, the distributions of all four AD test traits are presented in Figure 3.1.

3.3.2 Random Maternal Genetic and Permanent Environmental Effects

Estimates of variance components and genetic parameters for all studied traits are presented in Table 3.3. Among AD tests, the random maternal genetic effect was significant ($P < 0.05$) for ELISA-G, ELISA-P, and CIEP (Table 3.1). In mink, the trans-placental transmission of AMDV was detected (Broll & Alexandersen 1996), and thus, the significance of maternal genetic effect on AD-specific tests is expected. The random

permanent environmental effect was significant ($P < 0.05$) for ELISA-G and IAT (Table 3.1). This was not the case for the latter in the previous study (Hu *et al.* 2021), which might be due to the larger sample size and more repeated IAT records on the same individuals in the current study.

3.3.3 Heritability and Repeatability Estimates

Heritability estimates (\pm SE) for all studied traits are presented in Table 3.3. The estimated heritabilities (\pm SE) of ELISA-G (0.26 ± 0.05) and IAT (0.20 ± 0.04) in the current study were lower than the estimates reported in the previous study (Hu *et al.* 2021) of 0.39 ± 0.06 for ELISA-G and 0.26 ± 0.05 for IAT. The larger sample size, more complete pedigree information, and more phenotypic records in this study lead to different models and variance components than the previous study (Hu *et al.* 2021), resulting in different estimates of heritabilities for these traits. The heritabilities of BW, growth parameters (Do *et al.* 2021), and feed efficiency traits (Davoudi *et al.* 2022) were previously reported in mink. The estimated heritabilities of BW traits (ranging from 0.23 ± 0.13 to 0.35 ± 0.11) and growth parameters (ranging from 0.17 ± 0.08 to 0.39 ± 0.11) in this study were moderate and lower than the estimates reported by Do *et al.* (2021). This might be due to the use of numerator relationship matrix for random maternal genetic effects in this study, compared with the identity matrix used by Do *et al.* (2021). The heritabilities of feed efficiency traits were estimated to be moderate and ranged from 0.20 ± 0.10 to 0.24 ± 0.11 , which were similar to the estimates by Davoudi *et al.* (2022). The estimated heritabilities (\pm SE) were 0.14 ± 0.05 for DOF and 0.15 ± 0.06 for VarF, indicating the presence of small additive genetic effects for both traits. The DOF and VarF traits were new traits in mink research, and thus, no previous estimates were available for comparison. The estimated heritabilities

of VarF and DOF in swine ranged from 0.08 to 0.21 and from 0.10 to 0.15, respectively, which were similar to our results for mink (Putz *et al.* 2019; Cheng *et al.* 2020; Cheng *et al.* 2021).

The repeatability (\pm SE) of IAT was estimated to be 0.41 ± 0.04 (Table 3.3). Repeatability indicates the tendency of animals to maintain their performance for a certain trait over time. The moderate repeatability of IAT indicated that mink with a low IAT score would likely remain low in subsequent tests. Most farmed commercial mink will only be kept in a barn for less than nine months if they are not selected as breeders for the next season. Thus, instead of routine tests of IAT, which could cause extra stress on farmed mink, one-time IAT test result would be reliable in making selection decisions.

3.3.4 Correlations Between Aleutian Disease Tests and Body Weight

The phenotypic and genetic correlations between AD tests and body weight traits are presented in Tables 3.4 and 3.5, respectively. Both ELISA-G and ELISA-P showed significant ($P<0.05$) low negative phenotypic correlations with BW22, BW25, BW28, and HW (ranging from -0.08 ± 0.04 to -0.15 ± 0.04). All the phenotypic correlations were not significant ($P>0.05$) between BWs at different ages and ELISA and CIEP tests, and the phenotypic correlations were slightly decreased from week 13 to week 28, which indicated that the influence caused by AD on individual BW were not getting severer with the increase of age. In the meantime, the absolute genetic correlations between AD tests and BWs at 13, 16, 19, and 22 weeks were all larger than their corresponding phenotypic correlations. The IAT showed significant ($P<0.05$) low phenotypic correlations with BW13, BW16, BW28, and HW (ranged from -0.11 ± 0.04 to 0.08 ± 0.03). Although a significant loss of body weight was observed in AD-infected mink (Eklund *et al.* 1968), it

is still unknown to what extent AD influences the BW of infected mink. Among all AD tests, only IAT showed significant ($P < 0.05$) moderate positive genetic correlation (0.45 ± 0.23) with BW16 and negative moderate genetic correlation (-0.47 ± 0.12) with HW. These estimates indicated that the selection of mink with lower IAT scores could decrease the BW of mink at 16 weeks of age but increase the BW of mink at harvest. No AD-specific tests (ELISA-G, ELISA-P, and CIEP) showed significant ($P < 0.05$) genetic correlations with body weight traits. These non-significant ($P > 0.05$) genetic correlations indicated that selecting for a low ELISA test score or negative CIEP would not influence body weight traits. Although all the genetic correlations between BWs at different ages and AD tests were not significant, but all AD tests showed the highest absolute genetic correlations with BW at 16 weeks of age compared with BWs at other ages, which indicated BW at week 16 might be the best BW indicator trait to select for favorable AD test results indirectly. Therefore, mink farmers could select mink with low anti-AMDV antibody levels based on ELISA or CIEP tests without adverse consequences on body weight.

This study is the first study to estimate the phenotypic and genetic correlations between AD tests and body weight traits; thus, no estimates were available in the literature for direct comparison. The genetic correlations between disease traits and body weight traits were estimated in other livestock species. For example, in feedlot cattle, the bovine respiratory disease had a low genetic correlation (0.04) with hot carcass weight (Snowder *et al.* 2007). In dairy cattle, the genetic correlations between infectious diseases (e.g., endotoxemia, enteritis, foot rot, mastitis, metritis, pneumonia) and BW at different days in milk production ranged from -0.05 to -0.81 (Frigo *et al.* 2010). In sheep, the genetic correlations between body weight and fecal egg count (used to measure the resistance to *nematode*

parasites) were low-to-moderate negative ranging from -0.18 to -0.26 (Eady *et al.* 1998). In chicken, the antibody response against Newcastle disease virus vaccine was estimated to have low genetic correlations (range from -0.04 to -0.08) with BW at 8, 12, 16, and 20 weeks of age (Lwelamira *et al.* 2009).

3.3.5 Correlations Between Aleutian Disease Tests and Growth

The phenotypic and genetic correlations between AD tests and growth traits are shown in Tables 3.4 and 3.5, respectively. IAT showed significant ($P < 0.05$) low negative phenotypic correlation (-0.14 ± 0.04) and non-significant ($P > 0.05$) negative genetic correlation (-0.24 ± 0.18) with ADG. These results revealed that higher serum gamma globulin level decreases the average daily weight gain of mink, which could be mainly due to the environmental effects. The IAT is a non-AD-specific test and is designed to diagnose AD by detecting hypergammaglobulinemia, which could be caused by other environmental factors such as stress, temperature, and other diseases (Delves & Roitt 1998); thus, the phenotypic correlation between IAT and ADG mainly could be attributed to the environmental effects. Among all AD test traits, only ELISA-G showed significant ($P < 0.05$) moderate negative phenotypic (-0.32 ± 0.03) and genetic (-0.37 ± 0.16) correlations with ADG. This indicated that selection for a low ELISA-G score would increase the ADG. Meanwhile, ADG could be applied as a low-stress and economic indicator to indirectly select mink with low ELISA-G scores. The non-significant ($P > 0.05$) genetic correlations between ADG with ELISA-P, CIEP, and IAT indicated that the selection of mink with low ELISA-P, IAT, or negative CIEP results would not cause significant influences on mink growth. The genetic correlation between AD and ADG was not estimated in previous research in mink. The genetic correlations between disease traits and ADG were widely

estimated in other livestock species, and the genetic correlations were usually low or not significant, which were in agreement with our results. For example, several studies reported that cattle with bovine respiratory disease generally had lower ADG than healthy individuals (Bateman *et al.* 1990; Gardner *et al.* 1999; Snowden *et al.* 2006), but the genetic correlations were not significant (Snowden *et al.* 2007). In addition, the parasite burden traits in cattle, including tick infestation, gastrointestinal nematodes infection, and *Eimeria spp.* infection, were estimated to have low genetic correlations (from -0.22 to 0.12) with ADG (Biegelmeyer *et al.* 2015; Ribeiro *et al.* 2021). In swine, several studies reported that lung lesions caused by *Mycoplasma pneumonia* could significantly reduce ADG (Okada *et al.* 1999; Wilson *et al.* 2012) and had a low (0.002) genetic correlation with ADG (Okamura *et al.* 2016). In sheep, the ewe fecal egg counts, which were used to assess the severity of *Teladorsagia circumcincta* and *Haemonchus contortus* infection, was estimated to have a low genetic correlation (-0.15) with ADG (Bouix *et al.* 1998).

Both ELISA-G and ELISA-P showed significant ($P < 0.05$) moderate positive genetic correlations (0.38 ± 0.19 and 0.36 ± 0.18 , respectively) with parameter k , which indicated that selection of mink with lower anti-AMDV antibody levels could decrease the maturation rate of mink. The smaller magnitude of the k parameter will lead to later mature growth (Do *et al.* 2021). The relationship between later mature growth and other economically important traits (such as fur size, fur quality, and reproduction) has not been studied, but mink with lower k tends to have larger mature body weight, and thus may lead to larger harvest length (Do *et al.* 2021). The previous study (Hu *et al.*, 2021) estimated significant ($P < 0.05$) moderate negative phenotypic (-0.30 ± 0.06) and genetic (-0.45 ± 0.16) correlations between ELISA-G and harvest length. Therefore, the significant positive

correlations between ELISA tests and the k growth parameter could be treated as favorable correlations, but further investigation is needed. Although most of the genetic correlations between growth parameters and AD tests were not significant, the absolute genetic correlations between AD tests with k , m , and WIP were larger than their corresponding absolute phenotypic correlations. Both ELISA-G and ELISA-P showed significant ($P < 0.05$) low negative phenotypic correlations with α (-0.07 ± 0.03 and -0.10 ± 0.04 , respectively), but non-significant ($P > 0.05$) genetic correlations with α (-0.01 ± 0.22 and 0.02 ± 0.22 , respectively). These estimates revealed that higher anti-AMDV antibody level might decrease the mature body weight of mink, which could be mainly due to non-genetic effects. Although it has been observed that higher immune response could cause adverse influences on growth in livestock, the underlying mechanism is still unclear (Doeschl-Wilson *et al.* 2009; van der Most *et al.* 2011; Hu *et al.* 2020). Energy allocation could be one of the reasons leading to the unfavorable relationship between animal growth and immune response because the resources spent on immune response were no longer available for growth and other energy-consuming processes, such as locomotion and thermoregulation (van der Most *et al.* 2011).

3.3.6 Correlations Between Aleutian Disease Tests and Feed Efficiency

Phenotypic and genetic correlations between AD tests and feed efficiency traits are shown in Tables 3.4 and 3.5, respectively. The phenotypic correlations between AD tests and feed efficiency traits were either low (ranged from -0.15 ± 0.04 to 0.09 ± 0.04) or not significant ($P > 0.05$). None of the AD test traits showed a significant ($P < 0.05$) genetic correlation with feed efficiency traits. Although CIEP did not show significant genetic correlations with any feed efficiency traits (DFI, FCR, RFI, RG, and RIG), their magnitudes were very close or

consistent (ranged from 0.19 ± 0.43 to 0.23 ± 0.48). The genetic correlation between AD and feed efficiency was not estimated in previous studies in mink for direct comparison. The genetic correlations between disease and feed efficiency traits were rarely estimated, even in the main livestock species. In poultry, the ratio of the weight of right ventricle to the total ventricles, which is used to measure the ascites syndrome, was estimated to have low negative genetic correlations (-0.17 to -0.19) with feed intake between 23 and 48 days of age and residual feed intake (Pakdel *et al.* 2005). Meanwhile, a moderate positive (0.38) genetic correlation between total ventricles and feed efficiency, which was defined as the ratio between body weight gain and feed intake during the experiment, was also detected (Pakdel *et al.* 2005). In swine, osteochondrosis lesions were estimated to have low-to-moderate genetic correlations with FCR, ranging from -0.23 to 0.40 (Kadarmideen *et al.* 2004). In cattle, the mastitis incidence in Danish Friesian cattle was estimated to have a significant ($P < 0.05$) low negative genetic correlation (-0.15) with feed efficiency, and the mastitis incidence in Danish Jersey cattle was estimated to have a significant ($P < 0.05$) high negative genetic correlation (-0.79) with feed efficiency (Wassmuth *et al.* 2000). In addition, ketosis incidence in Danish Jersey cattle was estimated to have a significant ($P < 0.05$) moderate negative genetic correlation (-0.37) with feed efficiency (Wassmuth *et al.* 2000). The non-significant ($P > 0.05$) genetic correlations between AD tests and feed efficiency traits indicated that the selection of mink with favorable AD test results (low ELISA and IAT score and negative CIEP) would not cause a significant influence on the feed efficiency of mink. Feed is the largest cost, up to 70% of the total, in mink farming (Berg & Lohi 1992; Sørensen *et al.* 2003), and AD is the most severe disease that causes tremendous economic losses to mink farmers. Together, these two can significantly influence the

financial return for mink farmers. The genetic correlations between AD test and feed efficiency estimated in this study indicated that mink breeders could select mink with higher feed efficiency and AD resilience simultaneously through genetic selection without adverse influences on farmers' profitability. This would significantly contribute to producing efficient mink, which are resilient to AD and feed efficient, to minimize the economic losses caused by AD, reduce environmental impacts from mink production, and improve mink profitability.

3.3.7 Correlations Between Aleutian Disease Tests and Feed Intake

Phenotypic and genetic correlations between AD tests and feed intake traits derived from DFI data are shown in Tables 3.4 and 3.5, respectively. Among all AD tests, only IAT showed a significant ($P < 0.05$) low positive phenotypic (0.08 ± 0.04) correlation with DOF. The ELISA-P showed a significant ($P < 0.05$) moderate positive genetic correlation (0.42 ± 0.17) with DOF, and IAT showed a significant ($P < 0.05$) high positive genetic correlation (0.73 ± 0.16) with DOF. These estimates indicated that selection of mink with lower ELISA-P or IAT scores could reduce the off-feed days, and thus reduce the adverse influences caused by AD on mink appetite in AD positive farms. No significant phenotypic or genetic correlations between AD tests and VarF were estimated, indicating the selection of AD tests on mink would not cause significant influences on the consistency of feed intake.

Except for this study, the genetic correlations between disease traits with DOF and VarF have only been estimated in swine because they are novel resilient traits recently used in swine (Putz *et al.* 2019). DOF was estimated to have moderate-to-high genetic correlations with the number of health treatments (range from 0.50 to 0.85) and mortality (0.30 to 0.80).

The VarF was estimated to have moderate-to-high genetic correlations with the number of health treatments (range from -0.30 to 0.60) and mortality (0.37 to 0.85) in a natural disease challenge swine farm (Putz *et al.* 2019; Cheng *et al.* 2020).

3.3.8 Aleutian Disease Resilience indicator traits

In recent years, numerous studies have suggested that selection of resilience should be used as a practical method to cope with diseases in livestock industries (Berghof *et al.* 2019a; Harlizius *et al.* 2020; Hu *et al.* 2020; Iung *et al.* 2020; Knap & Doeschl-Wilson 2020). Resilience is defined as an animal's ability to maintain its performance under pathogen exposure (Albers *et al.* 1987; Bisset & Morris 1996). A reliable and practical disease resilience indicator trait genetically correlated with health traits is essential for the genetic selection of healthy animals (Mulder & Rashidi 2017; Berghof *et al.* 2019a). Body weight, growth, and feed intake traits have been suggested as indicators for specific disease resilience traits or general resilience traits in farm animals (Colditz & Hine 2016; Berghof *et al.* 2019a). For example, in layer chickens, the standardized body weight deviations were suggested as general resilience traits (Berghof *et al.* 2019b). In swine, growth rate was suggested as a disease resilience trait for porcine reproductive and respiratory syndrome (Hess *et al.* 2018; Knap & Doeschl-Wilson 2020), and traits derived from feed intake data were suggested as general disease resilience traits (Putz *et al.* 2019; Cheng *et al.* 2020; Cheng *et al.* 2021). In mink, AD has been reported to cause adverse influences on body weight, growth, and appetite (Eklund *et al.* 1968; Porter *et al.* 1982; Jensen *et al.* 2016b); thus, the studied traits of BW, growth, feed efficiency, and feed intake traits, could be treated as AD resilience traits in the AD positive farms.

Among all AD tests, ELISA-G may be the most practical and reliable test to be employed as an indicator for selecting AD-resilient mink. The CIEP did not show any significant genetic correlations with other AD resilience traits in this study, and together with its low heritability (0.09 ± 0.07), it may not be a good indicator for AD resilience. Due to the low test price and easy test procedure of IAT, together with assessing the production traits, has been used by mink farms to select for AD-resilience in North America (Farid & Ferns 2011). Although IAT was estimated to have moderate heritability (0.20 ± 0.04) and repeatability (0.41 ± 0.04) and showed significant favorable moderate genetic correlations with ELISA tests (Hu *et al.* 2021), DOF (0.73 ± 0.16), and HW(-0.47 ± 0.20), the potential adverse effects on pelt nap length (the length of the guard hair protruding from the underwool) caused by selecting for lower IAT scores cannot be ignored (Hu *et al.* 2021). Therefore, IAT may not be the best indicator trait for selecting AD-resilient mink. Although ELISA-P showed the highest heritability (0.59 ± 0.07) among all AD test traits with significant favorable genetic correlations with k and DOF, the unknown repeatability may require mink farmers to have multiple ELISA-P tests on the same individual, which would increase the expense of AD tests. Meanwhile, compared with ELISA-G, ELISA-P did not show significant ($P<0.05$) favorable genetic correlations with female reproductive performance traits, which are important AD resilient traits (Hu *et al.* 2021). Thus, further investigation is required before using ELISA-P in selecting AD-resilient mink. The ELISA-G was estimated to have moderate heritability (0.26 ± 0.05) and high repeatability (0.52 ± 0.04), indicating that the one-time ELISA-G test could be a reliable indicator for selecting mink with low anti-AMDV antibody level to reduce the formation of infectious virus-antibody complexes. Meanwhile, ELISA-G showed significant ($P<0.05$) favorable

genetic correlations with ADG and k growth parameter and non-significant ($P>0.05$) genetic correlations with other growth parameters, BW, feed efficiency, DOF, and VarF. All these estimated genetic parameters for ELISA-G indicated that selection of mink with lower AMDV-G ELISA could improve the average daily gain and bring benefits to mature weight without causing adverse influences on body weight, feed efficiency, off-feed days, and consistency of feed intake. Meanwhile, the previous study (Hu *et al.* 2021) showed that selection for low ELISA-G test results could also increase both female reproductive performance traits and harvest length and decrease the extent of anemia without influencing pelt quality in AD positive farms. Therefore, ELISA-G could be the most practical and reliable indicator in genetic selection for selecting AD-resilient mink in AD positive mink farms compared to other AD tests.

3.4 Conclusions

Finding a practical solution to control AD is one of the top priorities for the mink industry due to the tremendous financial losses caused by AD. Genetic selection for AD-resilient mink would provide a great opportunity to reduce the adverse influences caused by AD in mink farming. This research was a further supplement and exploration of the potential of AD tests in genetic selection of AD-resilient mink by involving more economically important or AD-resilient traits, thus providing a more reliable and comprehensive view of employing AD tests in AD-resilient mink selection. The estimated genetic parameters for AD tests in this thesis chapter further demonstrated that ELISA-G was the most reliable and practical indicator trait among all AD tests that could be applied in the genetic selection of AD-resilient mink. However, unlike genetic studies on other main livestock species such as cattle, swine, and poultry, which usually had larger sample sizes due to the longer data

collection histories, wider data collection ranges, and more complete data-sharing systems, the sample size used in this study was relatively smaller. Thus, further studies with larger sample sizes and more populations/farms are required to validate the current findings. In addition, future genomic studies, such as genome-wide association studies, linkage map and quantitative trait loci fine mapping, could be applied to better understand the biological mechanisms behind the correlations between AD tests and AD-resilient or other economically important traits in mink. In the absence of any other AD-resilient-related indicator trait, ELISA-G could be applied as the most useful and practical indicator trait to select AD-resilient mink in AD positive farms.

Table 3.1 Significance of fixed and random effects included in the models for analysis of Aleutian disease tests, growth, feed efficiency, and feed intake traits in mink.

Traits ¹	Factors						Covariates			Random effects	
	Sex	Color type	AD test year	Row-by-year	Dam age	Birth year	Blood test age	Harvest age	Feeding trial end age	Maternal genetic	Permanent environmental
ELISA-G	*	NS	*	-	-	-	NS	-	-	*	*
ELISA-P	NS	NS	NS	-	-	-	NS	-	-	*	NS
CIEP	*	NS	NS	-	-	-	*	-	-	*	NS
IAT	NS	NS	*	-	-	-	NS	-	-	NS	*
BW13	*	NS	-	-	NS	*	-	-	-	*	-
BW16	*	NS	-	-	NS	*	-	-	-	*	-
BW19	*	NS	-	-	NS	NS	-	-	-	*	-
BW22	*	NS	-	-	NS	NS	-	-	-	*	-
BW25	*	NS	-	-	NS	*	-	-	-	*	-
BW28	*	NS	-	-	NS	*	-	-	-	*	-
HW	*	*	-	-	NS	*	-	NS	-	*	-
ADG	*	NS	-	NS	-	-	-	-	*	*	-
α	*	NS	-	-	NS	NS	-	-	-	*	-
k	NS	NS	-	-	NS	*	-	-	-	*	-
m	NS	NS	-	-	NS	*	-	-	-	*	-
AIP	*	NS	-	-	NS	*	-	-	-	*	-
WIP	*	NS	-	-	NS	NS	-	-	-	*	-
DFI	*	NS	-	*	-	-	-	-	NS	*	-
FCR	*	NS	-	*	-	-	-	-	*	*	-
RFI	*	NS	-	*	-	-	-	-	NS	*	-
RG	NS	NS	-	NS	-	-	-	-	*	*	-
RIG	*	NS	-	*	-	-	-	-	*	*	-
KR	*	NS	-	*	-	-	-	-	*	*	-

Table 3.1 Continuous.

Traits ¹	Factors						Covariates			Random effects	
	Sex	Color type	AD test year	Row-by-year	Dam age	Birth year	Blood test age	Harvest age	Feeding trial end age	Maternal genetic	Permanent environmental
DOF	NS	NS	-	*	-	-	-	-	*	NS	-
VarF	*	NS	-	*	-	-	-	-	*	NS	-

¹ELISA-G = AMDV-G based enzyme-linked immunosorbent assay test; ELISA-P = VP2 based enzyme-linked immunosorbent assay test; CIEP = Counterimmunoelectrophoresis test; IAT = Iodine agglutination test; BW (13 to 28) = Body weight at corresponding measurement week (13 to 28); HW = Body weight at harvest; ADG = Average daily gain; α = Asymptotic weight in kg; k = Second part of growth curve, in which growth rate decreases until the animal reaches the asymptotic or mature weight (α); m = shape parameter determining the position of curve inflection point; AIP = age at the inflection point; WIP = weight at the inflection point; DFI = Daily feed intake; FCR = Feed conversion ratio; RFI = Residual feed intake; RG = Residual gain; RIG = Residual intake and gain; KR = Kleiber ratio; DOF = the proportion of off-feed days; VarF = Variation in daily feed intake.

* = significant (P<0.05)

NS = not significant (P>0.05)

- = not tested

Table 3.2 Descriptive statistics for Aleutian disease tests, growth, feed efficiency, and feed intake traits in mink.

Traits ¹	Number of records	Mean	SD	Range	CV (%)
ELISA-G	2896	1.92	2.40	0 to 7	125.00
ELISA-P	1152	2.14	2.16	0 to 8	100.93
CIEP	1127	0.82	0.38	0 to 1	46.34
IAT	2236	0.67	1.01	0 to 4	150.75
BW13 (kg)	1059	1.24	0.29	0.64 to 1.95	23.39
BW16 (kg)	1056	1.54	0.41	0.66 to 2.53	26.62
BW19 (kg)	1051	1.77	0.53	0.75 to 3.03	29.94
BW22 (kg)	1046	1.99	0.60	0.96 to 3.4	30.15
BW25 (kg)	1032	2.07	0.63	0.93 to 3.75	30.43
BW28 (kg)	1026	2.11	0.66	1.00 to 3.86	31.28
HW (kg)	844	2.09	0.64	0.94 to 3.94	30.62
ADG (g/day)	1046	8.32	3.80	1.27 to 19.67	45.67
α (kg)	1029	2.18	0.70	0.99 to 4.62	32.11
k	1025	0.24	0.10	0.01 to 0.85	41.67
m	1020	0.64	0.84	0.17×10^{-5} to 4.79	131.25
AIP (week)	1018	10.90	1.84	6.40 to 17.72	16.88
WIP (kg)	1024	0.97	0.35	0.13 to 2.20	36.08
DFI (g/day)	1079	224.90	57.68	89.84 to 366.89	25.65
FCR	1038	31.07	11.34	11.04 to 78.28	36.50
RFI (g/day)	1044	-0.06	36.63	-86.57 to 169.42	-
RG (g/day)	1042	0.01	1.37	-5.77 to 5.34	-
RIG (g/day)	1043	-0.01	1.52	-5.61 to 5.08	-
KR	1046	5.42	1.55	1.15 to 9.73	28.60
DOF	1074	0.06	0.08	0.00 to 0.65	152.73

Table 3.2 Continuous.

Traits ¹	Number of records	Mean	SD	Range	CV (%)
VarF	1074	48.31	11.49	27.37 to 98.88	23.78

¹ELISA-G = AMDV-G based enzyme-linked immunosorbent assay test; ELISA-P = VP2 based enzyme-linked immunosorbent assay test; CIEP = Counterimmunoelectrophoresis test; IAT = Iodine agglutination test; BW (13 to 28) = Body weight at corresponding measurement week (13 to 28); HW = Body weight at harvest; ADG = Average daily gain; α = Asymptotic weight in kg; k = Second part of growth curve, in which growth rate decreases until the animal reaches the asymptotic or mature weight (α); m = shape parameter determining the position of curve inflection point; AIP = age at the inflection point; WIP = weight at the inflection point; DFI = Daily feed intake; FCR = Feed conversion ratio; RFI = Residual feed intake; RG = Residual gain; RIG = Residual intake and gain; KR = Kleiber ratio; DOF = the proportion of off-feed days; VarF = Variation in daily feed intake; SD = Standard deviation; CV = Coefficient of variation.

Table 3.3 Estimates of variance components and genetic parameters with their standard errors (SE) for Aleutian disease tests, growth, feed efficiency, and feed intake traits in mink.

Traits ¹	Variance components				Genetic parameters			
	$\sigma_a^2 \pm SE$	$\sigma_m^2 \pm SE$	$\sigma_{pe}^2 \pm SE$	$\sigma_e^2 \pm SE$	$h^2 \pm SE$	$c_d^2 \pm SE$	$c_{pe}^2 \pm SE$	$r \pm SE$
ELISA-G	1.148±0.245	0.585±0.141	1.137±0.168	1.501±0.088	0.26±0.05	0.13±0.03	0.26±0.40	0.52±0.04
ELISA-P	2.950±0.473	0.402±0.204	NS	1.599±0.075	0.59±0.07	0.08±0.04	NA	NA
CIEP	0.014±0.010	0.020±0.007	NS	0.114±0.008	0.09±0.07	0.14±0.04	NA	NA
IAT	0.199±0.044	NS	0.210±0.051	0.597±0.041	0.20±0.04	NA	0.21±0.51	0.41±0.04
BW13	0.004±0.002	0.006±0.001	-	0.008±0.001	0.23±0.13	0.35±0.07	NA	NA
BW16	0.008±0.004	0.007±0.002	-	0.017±0.002	0.26±0.12	0.23±0.06	NA	NA
BW19	0.015±0.006	0.008±0.003	-	0.025±0.003	0.31±0.11	0.17±0.05	NA	NA
BW22	0.024±0.008	0.009±0.003	-	0.036±0.005	0.35±0.11	0.13±0.05	NA	NA
BW25	0.021±0.009	0.010±0.004	-	0.039±0.005	0.30±0.11	0.15±0.05	NA	NA
BW28	0.019±0.009	0.013±0.004	-	0.044±0.005	0.25±0.11	0.17±0.05	NA	NA
HW	0.013±0.007	0.008±0.004	-	0.062±0.005	0.15±0.09	0.10±0.05	NA	NA
ADG	0.998±0.434	0.610±0.212	NS	2.645±0.261	0.24±0.10	0.14±0.05	NA	NA
α	0.016±0.008	0.015±0.005	-	0.066±0.005	0.17±0.08	0.15±0.05	NA	NA
k	0.003±0.001	0.001±0.001	-	0.007±0.001	0.25±0.10	0.10±0.05	NA	NA
m	0.277±0.094	0.071±0.036	-	0.387±0.053	0.38±0.11	0.10±0.05	NA	NA
AIP	1.107±0.356	0.550±0.164	-	1.186±0.191	0.39±0.11	0.19±0.06	NA	NA
WIP	0.019±0.006	0.010±0.003	-	0.019±0.003	0.39±0.11	0.22±0.06	NA	NA
DFI	160.835±75.157	115.647±37.186	-	419.822±44.426	0.23±0.10	0.17±0.05	NA	NA
FCR	13.207±6.506	6.534±3.111	NS	46.522±4.117	0.20±0.10	0.10±0.05	NA	-
RFI	101.495±43.006	44.271±20.687	NS	314.588±27.766	0.22±0.09	0.10±0.04	NA	-
RG	0.374±0.184	0.378±0.100	-	0.966±0.106	0.22±0.10	0.22±0.06	NA	NA
RIG	0.375±0.178	0.311±0.092	-	0.905±0.102	0.24±0.11	0.20±0.06	NA	NA
KR	0.222±0.116	0.197±0.060	-	0.675±0.069	0.20±0.10	0.18±0.05	NA	NA

Table 3.3 Continuous.

Traits ¹	Variance components				Genetic parameters			
	$\sigma_a^2 \pm SE$	$\sigma_m^2 \pm SE$	$\sigma_{pe}^2 \pm SE$	$\sigma_e^2 \pm SE$	$h^2 \pm SE$	$c_d^2 \pm SE$	$c_{pe}^2 \pm SE$	$r \pm SE$
DOF	0.0009 ± 0.0003	NS	–	0.0054 ± 0.0003	0.14±0.05	NA	NA	NA
VarF	8.865 ± 3.532	NS	–	51.352 ± 3.453	0.15±0.06	NA	NA	NA

¹ELISA-G = AMDV-G based enzyme-linked immunosorbent assay test; ELISA-P = VP2 based enzyme-linked immunosorbent assay test; CIEP = Counterimmunoelectrophoresis test; IAT = Iodine agglutination test; BW (13 to 28) = Body weight at corresponding measurement week (13 to 28); HW = Body weight at harvest; ADG = Average daily gain; α = Asymptotic weight in kg; k = Second part of growth curve, in which growth rate decreases until the animal reaches the asymptotic or mature weight (α); m = shape parameter determining the position of curve inflection point; AIP = age at the inflection point; WIP = weight at the inflection point; DFI = Daily feed intake; FCR = Feed conversion ratio; RFI = Residual feed intake; RG = Residual gain; RIG = Residual intake and gain; KR = Kleiber ratio; DOF = the proportion of off-feed days; VarF = Variation in daily feed intake.

σ_a^2 = additive genetic variance; σ_m^2 = maternal genetic variance; σ_{pe}^2 = permanent environmental variance; σ_e^2 = residual variance.

H^2 = heritability from univariate models; c_d^2 = proportion of phenotypic variance explained by maternal genetic effects; c_{pe}^2 = proportion of phenotypic variance explained by permanent environmental effects; r = repeatability

NS = not significant (P>0.05)

NA = not applicable

- = not tested

Table 3.4 Estimates of phenotypic correlations with their standard errors between Aleutian disease tests with feed efficiency, growth, and feed intake traits in mink.

Traits ¹	ELISA-G	ELISA-P	CIEP	IAT
BW13	-0.05±0.04	-0.03±0.04	-0.04±0.04	0.08±0.03*
BW16	-0.06±0.04	-0.04±0.04	-0.05±0.04	0.07±0.03*
BW19	-0.07±0.04	-0.06±0.04	-0.05±0.04	0.01±0.04
BW22	-0.08±0.04*	-0.08±0.04*	-0.06±0.04	-0.02±0.04
BW25	-0.08±0.04*	-0.11±0.04*	-0.07±0.04	-0.04±0.04
BW28	-0.11±0.04*	-0.15±0.04*	-0.07±0.04	-0.07±0.03*
HW	-0.12±0.04*	-0.14±0.04*	-0.03±0.04	-0.11±0.04*
ADG	-0.32±0.03*	-0.15±0.04*	-0.04±0.04	-0.14±0.04*
α	-0.07±0.03*	-0.10±0.04*	-0.04±0.04	-0.08±0.03*
k	0.10±0.04*	0.15±0.04*	0.01±0.04	0.13±0.03*
m	0.05±0.04	0.09±0.04*	-0.02±0.04	0.06±0.04
AIP	-0.04±0.04	-0.01±0.04	-0.03±0.04	0.02±0.04
WIP	0.01±0.04	-0.01±0.04	-0.04±0.04	0.03±0.04
DFI	-0.08±0.04*	-0.14±0.04*	-0.05±0.04	-0.03±0.04
FCR	0.09±0.04*	0.09±0.04*	0.03±0.04	0.10±0.04*
RFI	0.02±0.03	-0.02±0.04	0.01±0.04	0.03±0.04
RG	-0.05±0.04	-0.07±0.04	0.03±0.04	-0.13±0.04*
RIG	-0.04±0.04	-0.05±0.04	0.03±0.04	-0.11±0.04*
KR	-0.10±0.04*	-0.14±0.04*	-0.02±0.04	-0.15±0.04*
DOF	0.02±0.03	0.07±0.04	-0.05±0.03	0.08±0.04*
VarF	0.01±0.03	0.06±0.04	-0.04±0.03	-0.01±0.03

¹ELISA-G = AMDV-G based enzyme-linked immunosorbent assay test; ELISA-P = VP2 based enzyme-linked immunosorbent assay test; CIEP = Counterimmunoelectrophoresis test; IAT = Iodine agglutination test; BW (13 to 28) = Body weight at corresponding measurement week (13 to 28); HW = Body weight at harvest; ADG = Average daily gain; α = Asymptotic weight in kg; k = Second part of growth curve, in which growth rate decreases until the animal reaches the asymptotic or mature weight (α); m = shape parameter determining the position of curve inflection point; AIP = age at the inflection point; WIP = weight at the inflection point; DFI = Daily feed intake; FCR = Feed conversion ratio; RFI = Residual feed intake; RG = Residual gain; RIG = Residual intake and gain; KR = Kleiber ratio; DOF = the proportion of off-feed days; VarF = Variation in daily feed intake. * = significant (P<0.05).

Table 3.5 Estimates of genetic correlations with their standard errors between Aleutian disease tests with feed efficiency, growth, and feed intake traits in mink.

Traits ¹	ELISA-G	ELISA-P	CIEP	IAT
BW13	0.16±0.20	0.19±0.23	-0.17±0.42	0.42±0.27
BW16	0.23±0.20	0.21±0.22	-0.35±0.37	0.45±0.23*
BW19	0.14±0.18	0.13±0.18	-0.19±0.35	0.21±0.19
BW22	0.09±0.17	0.09±0.18	-0.14±0.34	0.14±0.18
BW25	-0.01±0.18	-0.02±0.19	-0.30±0.32	0.01±0.18
BW28	-0.06±0.19	-0.16±0.19	0.21±0.46	-0.01±0.20
HW	0.37±0.26	0.01±0.22	0.49±0.48	-0.47±0.20*
ADG	-0.37±0.16*	-0.15±0.20	-0.02±0.40	-0.24±0.18
α	-0.01±0.22	0.02±0.22	0.14±0.45	0.02±0.22
k	0.38±0.19*	0.36±0.18*	-0.35±0.40	0.26±0.19
m	0.12±0.17	0.11±0.16	-0.63±0.35	0.15±0.17
AIP	-0.01±0.16	0.03±0.17	-0.58±0.32	0.05±0.16
WIP	0.15±0.17	0.05±0.17	-0.51±0.31	0.25±0.17
DFI	-0.13±0.20	0.08±0.22	0.21±0.45	-0.01±0.21
FCR	0.15±0.25	0.09±0.22	0.23±0.48	0.03±0.21
RFI	-0.04±0.22	-0.05±0.20	0.21±0.41	0.02±0.20
RG	0.23±0.22	-0.11±0.22	0.21±0.42	-0.17±0.21
RIG	0.20±0.21	-0.08±0.22	0.19±0.43	-0.16±0.21
KR	-0.02±0.02	-0.21±0.22	0.02±0.48	-0.19±0.20
DOF	0.22±0.19	0.42±0.17*	-0.02±0.22	0.73±0.16*
VarF	0.04±0.19	0.19±0.18	-0.12±0.23	0.09±0.21

¹ELISA-G = AMDV-G based enzyme-linked immunosorbent assay test; ELISA-P = VP2 based enzyme-linked immunosorbent assay test; CIEP = Counterimmunoelectrophoresis test; IAT = Iodine agglutination test; BW (13 to 28) = Body weight at corresponding measurement week (13 to 28); HW = Body weight at harvest; ADG = Average daily gain; α = Asymptotic weight in kg; k = Second part of growth curve, in which growth rate decreases until the animal reaches the asymptotic or mature weight (α); m = shape parameter determining the position of curve inflection point; AIP = age at the inflection point; WIP = weight at the inflection point; DFI = Daily feed intake; FCR = Feed conversion ratio; RFI = Residual feed intake; RG = Residual gain; RIG = Residual intake and gain; KR = Kleiber ratio; DOF = the proportion of off-feed days; VarF = Variation in daily feed intake. * = significant (P<0.05).

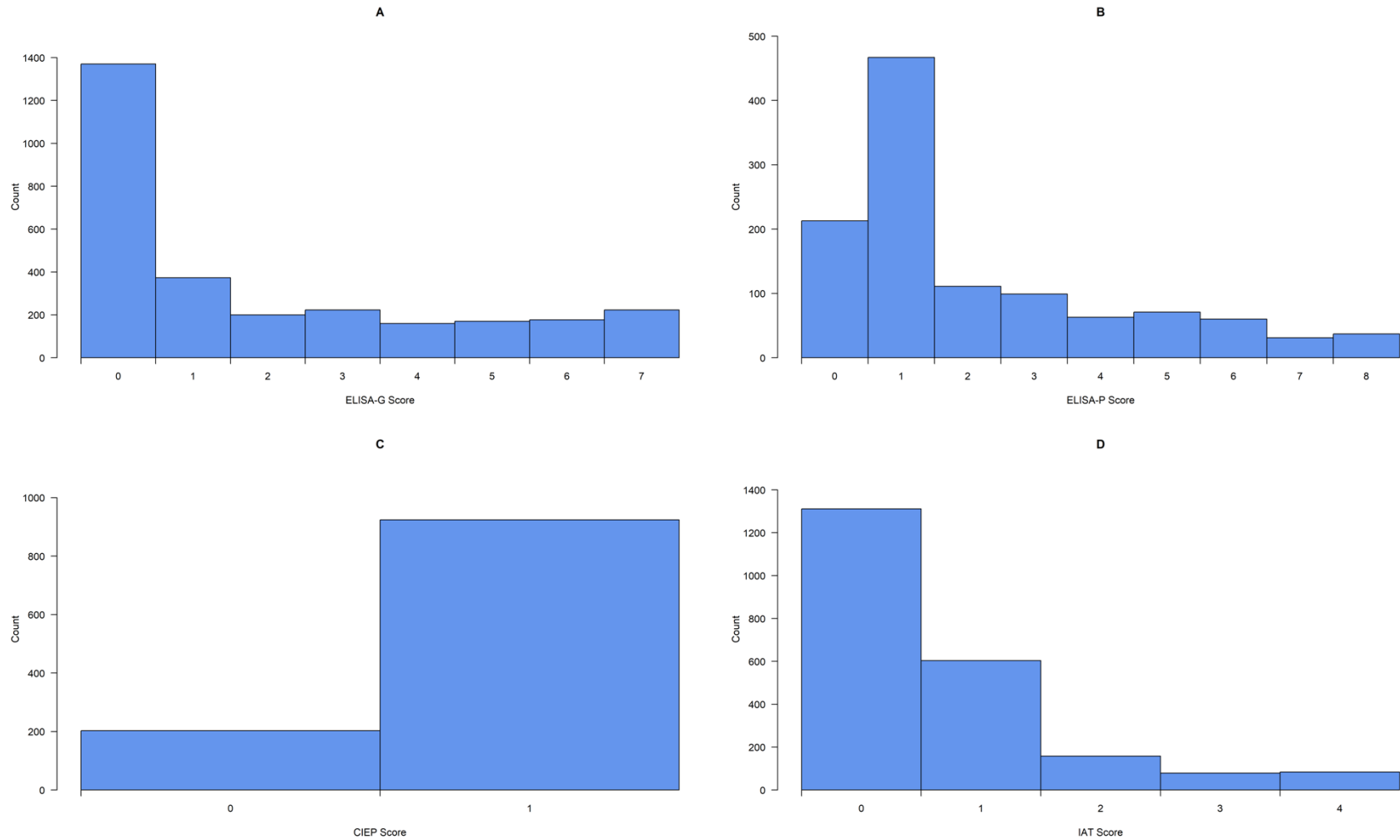


Figure 3.1 The distribution of Aleutian disease tests. (A) VP2 based enzyme-linked immunosorbent assay test; (B) AMDV-G based enzyme-linked immunosorbent assay test; (C) Counterimmunoelectrophoresis test; (D) Iodine agglutination test.

CHAPTER 4. Population Genomics of American Mink Using Genotypes Data¹

4.1 Introduction

American mink (*Neogale vison*) is a semiaquatic and carnivorous mammal that belongs to the weasel (*Mustelidae*) family (García *et al.* 2010). It is native to North America but has been farmed in many countries and used as one of the primary fur sources for fur industries worldwide due to its high-quality fur and various colors (Anistoroaei *et al.* 2009; Tamlin *et al.* 2009; Thirstrup *et al.* 2015; Zhang *et al.* 2021a). With the COVID-19 (coronavirus disease from 2019) pandemic and the market downturn, the mink industry faces serious challenges. In Canada, from 2015 to 2020, the number of mink farms dropped from 213 to 63, decreasing mink production from three million to one million per year (Statistics_Canada 2022). However, the mink industry appears to be on the upturn, as market demand and fur prices have increased, based on fur auction reports in recent years (Oaten 2021; sagafurs 2022). With a smaller number of mink farms, improving the efficiency (e.g., improved disease resilience, feed efficiency, reproduction performance, and pelt quality) of mink farms through advanced genomic selection programs could help to meet the rising market demand and help mink farmers obtain more economic benefits from the rising pelt prices. Genomic selection has been applied in the main livestock species, such as dairy cattle (Wiggans *et al.* 2017), swine (Miar *et al.* 2015; Knol *et al.*

¹ A version of this chapter has been published in *Frontiers in Genetics* by Hu *et al.* 2023. Population genomics of American mink using genotype data. 14:1175408. doi: <https://doi.org/10.3389/fgene.2023.1175408>

2016), and poultry (Wolc *et al.* 2016), to improve genetic merit, but this breeding strategy has not been utilized in the mink industry to date.

To develop an efficient genomic selection program in domestic animals, understanding the genetic structure of the target population is essential (Groeneveld *et al.* 2010; Wellmann & Bennewitz 2019). American mink of different color types show different performance for some traits. For example, it has been known that light-colored mink are more susceptible to the Aleutian mink disease virus than dark color types (Ellis 1996). Meanwhile, better reproductive performance was observed in brown color mink compared with the other color types (Kidd *et al.* 2009). Thus, investigating the genetic structure of American mink of various color types could also help explain variation in performance for traits of economic interest. The genetic structure of target populations is usually revealed by exploring domestication history, genetic diversity, genetic relationship, and genetic pattern of the populations. Linkage disequilibrium (LD) and effective population sizes (N_e) are two important parameters for revealing genetic structure of target population. The LD is defined as the non-random association of alleles at two or more loci (Slatkin 2008). Genetic drift, selection, epistatic combinations, population structure, and admixture between distinct populations are all potential causes leading to LD between unlinked markers (Pfaff *et al.* 2001; Ardlie *et al.* 2002; Qanbari 2020). The magnitude of LD is used to determine the appropriate density of markers for genome-wide mapping studies (Goddard & Hayes 2009), and both genomic selection and genome-wide association studies (GWAS) depend on the presence of LD between markers and functional variants (Bush & Moore 2012; Hay & Rekaya 2018). In the meantime, the extent of LD between unlinked loci can be utilized to estimate the recent and past N_e (Hill 1981; Waples & Do 2010). The N_e is used to

measure the rate of inbreeding and loss of genetic diversity and quantify the extent of variability in a population and the effectiveness of selection relative to drift (Charlesworth 2009; Ryman *et al.* 2019). Analysis of molecular variance (AMOVA) is another popular method of detecting population differentiation (Excoffier *et al.* 1992). The AMOVA can explain the genetic variation patterns of studied populations by quantifying the contribution of various population structure levels using marker data from different genotypes (Fitzpatrick 2009). In addition to AMOVA, discriminant analysis of principal components (DAPC) (Jombart *et al.* 2010) and ADMIXTURE (Alexander *et al.* 2009) are also common analyses used to assess the genetic structure of a population using molecular marker information. In brief, DAPC is a multivariate method that can identify and describe clusters of individuals which are genetically related (Jombart *et al.* 2010; Deperi *et al.* 2018; Thia 2022), and ADMIXTURE can infer the number of ancestral populations that generated the current population and the proportions of individual genomes derived from each ancestral population (Alexander *et al.* 2009; Alexander & Lange 2011; Liu *et al.* 2020a).

The genetic structures of farm and feral American mink were previously studied using information from different molecular markers, including microsatellite, mitochondrial DNA, and single nucleotide polymorphism (SNP) markers. Microsatellite loci were used to investigate the genetic structures of wild-caught American mink in Japan (Yukari *et al.* 2010), Sweden (Zalewski *et al.* 2016), and Spain (Lecis *et al.* 2008). The information from mitochondrial DNA and 11 microsatellite loci were applied to understand the genetic structure of introduced American mink in southern Chile (Mora *et al.* 2018). Genotypes obtained from 194 SNPs, generated from the restriction-site associated DNA sequencing method, were used to investigate the population genetic structure of farm and feral

American mink in Poland and Denmark (Thirstrup *et al.* 2015). Data containing 13,321 SNPs, which were detected using the genotyping-by-sequencing (GBS) approach on 46 scaffolds from 285 black American mink, were used to investigate LD and N_e of black American mink in Canada (Karimi *et al.* 2020). Moreover, 100,000 SNPs, which were randomly selected through whole-genome sequencing (WGS) across 51 scaffolds from 100 farm mink, were used to investigate the genetic structure of American mink in Canada (Karimi *et al.* 2021b). However, there is no study investigating the genetic structure of farmed American mink with various color types using a relatively large sample size (about 3,000) with genotypic data from a medium-density SNP panel.

Investigation of the genetic structure of American mink using genotypic data from a medium-density SNP panel will benefit the future use of this genotyping panel for use in genomic selection, as well as other genomic studies, such as quantitative trait locus mapping, identification of signatures of selection, and GWAS. Meanwhile, one critical factor affecting the accuracy of estimating population genetic diversity parameters is the sample size (Bashalkhanov *et al.* 2009). The sample size in the previous studies, which investigated the genetic structure of American mink, were all less than 300 individuals (Lecis *et al.* 2008; Yukari *et al.* 2010; Thirstrup *et al.* 2015; Zalewski *et al.* 2016; Mora *et al.* 2018; Karimi *et al.* 2020; Karimi *et al.* 2021b). Small sample sizes could lead to significant errors in determining allelic richness and therefore influence the accuracy of the estimators of genetic diversity in populations (Bashalkhanov *et al.* 2009). Thus, the main purpose of this thesis chapter was to use genotypic data from the first medium-density 70K SNP panel for American mink with a larger sample size to 1) investigate the LD pattern and N_e of farm American mink in Canada, 2) explore the genetic distance and genetic

diversity among various color types of American mink, and 3) reveal the genetic structure and admixture pattern of farm American mink in Canada.

4.2 Methods

4.2.1 Ethics Statement

This study was approved by the Dalhousie University Animal Care and Use Committee (certification#: 2018-009 and 2019-012). All the mink were raised based on the Code of Practice for the Care and Handling of Farmed Mink guidelines from the Canada Mink Breeders Association (Turner P *et al.* 2013).

4.2.2 Animals and Sampling

The individuals used in this study were from two farms, including the Canadian Center for Fur Animal Research (CCFAR, n=1,411) at Dalhousie University, Faculty of Agriculture (Nova Scotia, Canada) and Millbank Fur Farm (MFF, n=1,562) at Rockwood (Ontario, Canada). Mink from CCFAR included five color types: black (CBL, n = 177), demi (CDE, n = 542), mahogany (CMA, n = 527), pastel (CPA, n=152), and stardust (CST, n = 13). The colors of the studied mink were identified and assigned to them at their weaning age by experienced technicians at CCFAR. All individuals from MFF were Black color type (MBL, n = 1,562). There was no migration of mink between the two farms. There was no regular mating system on both farms, and breeders were selected based on their phenotypic performances without considering the color types.

4.2.3 Sample Collection and Genotyping

DNA extraction was performed on tongue tissue from animals using the Dneasy Blood and Tissue Kit (Qiagen, Hilden, Germany), according to the manufacturer's instructions. The quantity and quality of DNA were measured with a NanoDrop ND-1000 spectrophotometer

(NanoDrop Technologies Inc., Wilmington, DE). The 260/280 nm readings for all samples ranged from 1.8 to 2.0. All samples were diluted to a final concentration of 500 ng, checked for DNA quality, and finally genotyped by Axiom Affymetrix Mink 70K panel (Neogen, Lincoln, Nebraska, USA) (Do *et al.* 2024).

4.2.4 Animals and SNP Quality Control

Prior to analyses of the genotyping data, animals and SNPs were excluded from the dataset based on the following criteria using PLINK software (Purcell *et al.* 2007): SNPs having a minor allele frequency lower than 1%, a call rate lower than 90%, an excess of heterozygosity higher than 15%, and Mendelian error frequency larger than 5%, SNPs that were out of Hardy-Weinberg equilibrium with very low probability (1×10^{-5}), and individuals with a call rate lower than 90%. Overall, 2,973 genotyped animals with 24,161 SNPs remained for the following analyses.

4.2.5 Population Genetic Parameters, Linkage Disequilibrium, and Effective Population Size

The average minor allele frequency (MAF) and observed heterozygosity were estimated for each color type and whole CCFAR population using SNP1101 software (Sargolzaei 2014). The nucleotide diversity was conducted for each SNP and color type and whole CCFAR population based on the method proposed by Nei and Li (1979) using VCFtools software (Danecek *et al.* 2011).

Linkage disequilibrium (r) was measured as proposed by Hill and Robertson (1968) and calculated according to the following equation using SNP1101 software (Sargolzaei 2014):

$$r_{ij} = \frac{(P_{ij} - P_i \cdot P_j)^2}{P_i \cdot (1 - P_i) \cdot P_j \cdot (1 - P_j)}$$

in which P_{ij} is the frequency of the two-marker haplotype (I = allele I at locus 1; j = allele j at locus 2), and P_i and P_j are the frequencies of allele I at locus 1 and allele j at locus 2, respectively (Badke *et al.* 2012).

The LD was calculated in four distance sets with different bin sizes, which included 100 kb with a bin size of 10 kb, 500 kb with a bin size of 50 kb, 1,000 kb with a bin size of 100 kb, and 10 Mb with a bin size of 1,000 kb. The average r^2 of each bin was plotted against the median size of the bin to show the trend of LD with the increases in genome distances. Effective population sizes for various color types were estimated using SNP1101 software (Sargolzaei 2014) by the following equation (Sved 1971):

$$Ne = \left(\frac{1}{4c}\right)\left(\frac{1}{r^2} - 1\right)$$

in which Ne is the effective population size; c is the marker distance in Morgans. Additionally, past effective population size at generation T was calculated by the approximation $T = \frac{1}{2c}$ (Hayes *et al.* 2003). Effective population size was calculated for 1, 5, 10, 20, 50, 100, 200, and 250 generations ago.

4.2.6 Genetic Distances and Genetic Diversity

Pairwise genetic distances were calculated using Nei's (Nei 1972) method (standard genetic distance method) under the 'StAMPP' package of R (Pembleton *et al.* 2013). Additionally, a dendrogram of genetic distance among all color types was produced through the unweighted pair group method with the arithmetic mean method in the "poppr" R package (Kamvar *et al.* 2014) based on Nei's distance (Nei 1972). The pairwise F_{st} was calculated based on Weir and Cockerham's procedures (Weir & Cockerham 1984) using the 'StAMPP' package of R (Pembleton *et al.* 2013). The Nei's genetic distances matrix of the six color types was also used to construct the phylogenetic trees using the unweighted

pair group method in the “poppr” R package (Kamvar *et al.* 2014). In addition, AMOVA (Excoffier *et al.* 1992) was performed using ade4 implemented in the “poppr” R package (Kamvar *et al.* 2014) to determine the partition of genetic diversity among samples at different hierarchical levels.

4.2.7 Genetic Structure and Admixture Patterns

Population structure was analyzed by the discriminant analysis of principal components (DAPC) method using the “adegenet” package of R (Jombart *et al.* 2010). The number of clusters in the population was defined by using the *find.clusters* function under the “adegenet” package. This function implements a clustering procedure used in DAPC by running successive K-means with an increasing number of clusters (K) after transforming data using a principal component analysis (PCA). The most suitable number of clusters has the lowest associated Bayesian Information Criterion (BIC). An α -score optimization was used to determine the number of principal components to retain. Additionally, an unsupervised analysis in ADMIXTURE version 1.3.0 (Alexander *et al.* 2009) was applied to further assessing the potential admixture among the various color types. Five-fold cross-validation (CV) procedure was performed, and the CV scores were used to determine the best K value.

4.3 Results

4.3.1 Population Genetic Parameters, Linkage Disequilibrium and Effective Population Size

The MAF, observed heterozygosity, and nucleotide diversity for each SNP, color type and whole CCFAR population are present in Table 4.1. The average MAF ranged from 0.212 (mahogany) to 0.246 (stardust). The lowest level of observed heterozygosity (30.6%) was

observed in mahogany color type of CCFAR, whereas the stardust color type of CCFAR had the highest percentage of observed heterozygosity (34.9%). The overall nucleotide diversity ranged from 0.283 (stardust) to 0.307 (demi). Considering the whole CCFAR population individuals, the MAF was 0.216, the observed heterozygosity was 30.576%, and the overall nucleotide diversity was 0.307 (Table 4.1).

The average r^2 between adjacent SNPs on all chromosomes for six color types of American mink and the whole CCFAR American mink population are presented in Table 4.2. The average r^2 between adjacent SNPs among various color types ranged from 0.373 ± 0.402 (CPA) to 0.406 ± 0.408 (MBL). Compared with the MFF population (MBL), the average r^2 between adjacent SNPs for the whole CCFAR population (0.399 ± 0.404) was lower (Table 4.2). The LD decay measured by r^2 with different inter-marker distances (up to 100 kb, 500 kb, 1000 kb, and 10 Mb) and consecutive bins (10 kb, 50 kb, 100 kb, and 1 Mb) in six color types mink is presented in Figure 1. Within the 1000 kb inter-marker distance range, MBL and CST showed the two highest average r^2 among all color types at the same inter-marker distance, while CDE and CPA had the two lowest average r^2 among all color types. CDE reached an average $r^2 < 0.2$ with the shortest inter-marker distance (around 325 kb) among all color types, while CST reached an average $r^2 < 0.2$ with the longest inter-marker distance (around 850 kb) among all color types. Both CMA and CPA reached an average $r^2 < 0.2$ at the inter-marker distance of approximately 350 kb. CBL and MBL reached an average $r^2 < 0.2$ at the inter-marker distance of approximately 475 kb and 650 kb, respectively. The average r^2 of the whole CCFAR population was < 0.2 at the inter-marker distance of 350 kb. The most rapid LD decays for all color types were observed when the

average inter-marker distances increased from 50 to 150 kb, and CDE had the most rapid reduction of LD in this interval (Figure 4.1).

The N_e was evaluated based on LD estimates (r^2) from five to 250 generations ago, and the estimates of N_e are shown in Figure 2. In general, all the color types showed a marked decrease over generations. The recent N_e , five generations ago, of CBL, CDE, CMA, CPA, CST, and MBL was 58, 76, 80, 60, 24, and 91, respectively. For the whole CCFAR population, the N_e was 76 at five generations ago. The maximum N_e was observed 250 generations ago for all color types, where CDE had the highest N_e of 384 and CST had the lowest N_e of 276. CDE had the highest N_e , and CST had the lowest N_e from 50 to 250 generations ago. However, in more recent generations, from five to ten generations ago, MBL was observed to have the highest N_e , and CST was found to have the lowest N_e . The decline of N_e was more rapid from 5 to 50 generations ago for all color types in CCFAR and from 5 to 100 generations ago for the MFF population. In the meantime, in more recent generations (5 to 50 generations ago), the N_e of the CCFAR population decreased more rapidly than the MFF population (Figure 4.2).

4.3.2 Genetic Distances and Genetic Diversity

Weir and Cockerham's F_{st} and Nei's genetic distances among six color types are shown in Table 4.3. None of the F_{st} values between the two color types were larger than 0.1, and none of the Nei's genetic distances between the two color types were larger than 0.06. The lowest F_{st} (0.006) and Nei's genetic distance (0.003) were found between CMA and CDE. The CPA and CST showed the highest F_{st} (0.096) and Nei's genetic distance (0.053). To examine the genetic relationship among various color types, a phylogenetic tree was also constructed using the unweighted pair group method and Nei's genetic distance (Figure

4.3). The phylogenetic tree revealed two main clusters, with CST in one cluster and CDE, CPA, CMA, CBL, and MBL in the second cluster. Meanwhile, CDE and CMA were assigned to the subgroup with the least genetic distance.

The results from AMOVA for various color types are shown in Table 4.4. The differentiation within color types represented the highest proportion of total molecular variation in the populations (91.6%). The variation among color types was significant ($p < 0.05$) but only represented 4.1% of the total molecular variation in the populations. The variation among farms was estimated to represent 4.3% of the total molecular variation in the populations but was not significant ($p > 0.05$).

4.3.3 Genetic Structure and Admixture Patterns

A total of 123 principal components were retained for DAPC analysis based on the result of the α -score optimization analysis (Supplementary Figure 1). Sequential K-means clustering and the BIC indicated an optimum of 40 clusters in the studied populations (Supplementary Figure 2), and the DAPC showed 40 clusters in Figure 4.4. Figures 4.4(a) and 4.4(b) present the scatterplots of the first two linear discriminants and the first three linear discriminants for all samples, respectively. Figure 4.4(c) shows the distribution of various color types of mink in these 40 clusters in the scatterplot of the first two linear discriminants. The number of individuals from different color types in each cluster is shown in Figure 4.5. Eighteen clusters concentrated on the left side of the y-axis, and most MBL individuals were grouped into those clusters (Figures 4.4a and 4.4c). Twenty-two clusters spread on the right side of the y-axis, and most of the CCFAR individuals were grouped into these clusters (Figures 4.4a and 4.4c). Compared with the clusters on the right side of the y-axis, where most of the CCFAR individuals were located, the clusters on the

left side of the y-axis, where most of the MFF individuals were located, were more concentrated in a smaller area and more overlapped with each other. The three-dimensional scatterplot separated the clusters located on the right side of the y-axis of the DAPC scatterplot of the first two linear discriminants more widely but not the clusters located on the left side of the y-axis (Figure 4.4b). MBL individuals were classified into 28 clusters and were the dominant color type in 18 of those clusters. Individuals in CDE, CPA, CMA, CST, and CBL color types were classified into 28, 15, 31, 6, and 16 clusters, respectively, and were not the dominant color type in those clusters (Figure 4.5). Additionally, the individual posterior membership probabilities to different clusters are presented in Figure 4.6. All the color types were largely admixed with several different clusters.

A model-based maximum likelihood approach was used to infer population structure at different K levels (Figures 4.7 and 4.8). The CV error was markedly reduced with each increase in K until K = 4. Hereafter, the CV error gradually decreased with an increasing K, but the differences in CV error between adjacent Ks were less and less. The lowest CV was found when K=75 within the range of K values that we tested (Figure 4.7). The ADMIXTURE runs for K = 2, 3, 4, 6, 40, and 75 are shown in Figure 4.8. The results indicated that the most likely partition was for K = 3, based on visual inspection of the admixture plots. The ideal method to define the number of K should be based on the CV error, but the CV error in this study kept decreasing with increased K (Figure 4.7). Visual inspection of admixture plots was used to define the best K according to the other studies (Mujibi *et al.* 2018; Lal *et al.* 2021). At K = 2, a clear distinctness between MBL and CPA was found. The rest of the color types were admixed with two clusters. At K = 3, the study populations showed a relatively distinguishable distinctness between CCFAR and MFF

populations. Most MFF individuals were assigned to one cluster (average 85.26% on ancestry fractions), and the other two clusters were dominant in the CCFAR population. The CBL (average of 77.51% on ancestry fractions) and CPA (average of 79.13% on ancestry fractions) became distinct clusters within the CCFAR population and the two main genetic compositions in the CCFAR population. In the meantime, CDE and CMA were admixed with the three clusters and seemed to share a similar admixture pattern. When $K = 4$ and 6 , except for the CPA color type, where one cluster seemed like the dominant cluster in this color type, all other color types were admixed with at least two clusters. In the meantime, the CCFAR population showed a higher level of admixture than the MFF population. When $K = 40$ and 75 , no obvious distinction in ADMIXTURE among various color types was found, and all color types were admixed with several clusters (Figure 4.8).

4.4 Discussion

The average r^2 between adjacent SNPs on all chromosomes for various color types were in the range of 0.373 to 0.406. The estimated average r^2 between adjacent SNPs was higher than the estimates from previous studies (Karimi *et al.* 2020; Karimi *et al.* 2021b). The average r^2 was estimated to be 0.30 using 13,321 SNPs extracted from 99 scaffolds with GBS data (Karimi *et al.* 2020). The average r^2 was estimated to range from 0.280 to 0.366 for various color types using 100,000 SNPs extracted from 51 scaffolds with the WGS data (Karimi *et al.* 2021b). The different SNP marker densities, sample sizes, data resources, using incomplete scaffold-based vs. complete chromosome-based reference genomes, and population structures among the studies are the potential causes leading to these discrepancies. The $r^2 > 0.2$ is considered the minimum threshold value for genomic selection to achieve an accuracy of > 0.85 (Meuwissen *et al.* 2001; Hayes *et al.* 2009;

Samorè & Fontanesi 2016). In the current study, the average r^2 of CCFAR and MFF populations decreased to <0.2 when the inter-marker interval reached larger than 350 kb and 650 kb, respectively. These estimates indicated that the minimum marker density for conducting genomic selection at acceptable accuracy for the CCFAR population is about 7,700 SNPs (2.68 Gb/350 kb, where 2.68 Gb (Karimi *et al.* 2022) is the size of American mink genome assembly) and about 4,200 SNPs (2.68 Gb/650 kb) for the MFF population. For GWAS, $r^2 > 0.3$ is commonly used as the ideal threshold LD to obtain sufficient power and accuracy (Ardlie *et al.* 2002; Wang *et al.* 2018; Wu *et al.* 2019; Zhang *et al.* 2021b). The r^2 was estimated to be more than 0.3 when the marker distances were less than 125 kb and 225 kb for CCFAR and MFF populations, respectively, which indicated approximate 22,000 (2.68 Gb/125 kb) and 12,000 (2.68 Gb/225kb) SNPs are necessary to conduct GWAS in CCFAR and MFF populations, respectively. It has been noted that more markers are needed to perform adequate genomic studies in admixed populations (Toosi *et al.* 2010; Thomasen *et al.* 2013; Brito *et al.* 2015; Karimi *et al.* 2021b). Thus, the higher level of admixture in the CCFAR population may be the reason for the required higher marker density for conducting genomic selection in this population compared to the MFF population. Using GBS data, Karimi *et al.* (2020) suggested the density of 60,000 SNPs and 120,000 SNPs, which were all higher than the estimates in the current study, are required for conducting genomic selection and GWAS in black American mink, respectively. Karimi *et al.* (2021b) suggested a larger number of SNPs to conduct genomic selection (120,000 for CCFAR and 24,000 for MFF) and GWAS (240,000 for both farms) by using WGS data of 100 American mink from the same population. The different estimates of r^2 between the current study and previous studies (Karimi *et al.* 2020; Karimi

et al. 2021b) are the causes for the different suggested marker densities of conducting genomic selection and GWAS in American mink.

In this study, the N_e at five generations ago was estimated to be 76 and 91 for CCFAR and MFF populations, respectively. In Spain, the N_e of American mink in six locations ranged from 7.2 to 34.8 using information from ten polymorphic microsatellite loci (Lecis *et al.* 2008). On Swedish coasts, depending on the geographical location of the sampling, the N_e of American mink was estimated to be from 17.5 to 70.8 using genotypes from 21 microsatellite markers (Zalewski *et al.* 2016). The N_e at five generations ago was estimated to be 116 for black American mink, which was also higher than the estimates in this study, using SNP data obtained from the GBS data (Karimi *et al.*, 2020). Compared with this study, Karimi *et al.* (2021b) estimated a higher N_e at five generations ago (99) for CCFAR and a lower N_e at five generations ago (50) for MFF using SNP information extracted from the WGS data of 100 mink. The estimates of the current study indicated that the N_e declined more rapidly from 5 to 50 generations ago for the CCFAR and from 5 to 100 generations ago for the MFF population, which coincided with the time when the farms were established. The CCFAR was established about 40 years ago (1984), and the MFF was founded over 90 years ago (1930). These trends were different from those estimated by using WGS data (Karimi *et al.* 2021b) and GBS data (Karimi *et al.* 2020), where the decline of N_e was more rapid between 150 and 200 generations ago. The different estimations of LD patterns among studies are the cause leading to the different N_e estimates. The N_e of the CCFAR population decreased more rapidly than the MFF population in more recent generations (5 to 50 generations ago). This may be related to different breeding

managements and strategies, population genetic backgrounds, and populations sizes (MFF has larger population size than CCFAR) in these two farms.

Both F_{st} (less than 0.1) and Nei's genetic distances (less than 0.06) among various color types were low, which indicated the low genetic differentiation among various color types. This was in agreement with the AMOVA results, where the variation within color types explained 91.6% of total molecular variation, while the variation among color types only explained 4.1% of the total molecular variation in the populations. Compared with other color types, CST had the farthest genetic distances (Nei's genetic distance values) with CDE, CPA, CMA, and MBL color types. This was in agreement with the result from the phylogenetic tree, which separated CST into a separate cluster from other color types. The F_{st} and Nei's genetic distances among various color types were estimated in the range of 0.015 to 0.124 and 0.013 to 0.065, respectively, using WGS data (Karimi *et al.* 2021b). They were all slightly higher than the estimates from this study (F_{st} ranged from 0.006 to 0.096, and Nei's genetic distance ranged from 0.003 to 0.053). The overall F_{st} among seven color types of American mink from 14 different geographical locations in Poland and Denmark was estimated to be 0.08 by Thirstrup *et al.* (2015) using information from 194 SNPs generated from the restriction-site associated DNA sequencing data, which was also higher than the overall F_{st} (0.041) among six color types in the study. In southern Chile, the F_{st} among 153 mink obtained from 12 locations were estimated to be in the range from 0.017 and 0.364, which was also higher than the estimates in this study (0.006 to 0.096), using genotypic data from 11 polymorphic microsatellite loci (Mora *et al.* 2018).

The mink of the six color types were differentiated into 40 clusters using multivariate DAPC analysis in this study. Individuals within the same color type were divided into

clusters ranging from six to 31 (Figures 4.5 and 4.6), which indicated the existence of genetic differentiation among mink within the same color. These results were in agreement with the result from AMOVA (Table 4.4), where the variation within color types represented the majority of the total molecular variation in the populations, and the high level of nucleotide diversity within each color type (Table 4.1). In the meantime, 97% (1,526 individuals) of MBL individuals and 97% (1,378 individuals) of CCFAR individuals were grouped into the clusters located on the left and right side of the y-axis of the DAPC scatterplot of the first two linear discriminants (Figure 4.4c), respectively. These results indicated that the DAPC analysis was able to separate CCFAR and MFF populations by the first linear discriminant (explained 41.23% of the variance). However, DAPC analysis was not able to further differentiate the clusters within a farm as the clusters on the same side of the y-axis of the DAPC scatterplots were overlapped, and the distances between clusters were minimal (Figure 4.4). This may be caused by high gene flow and admixture events in recent generations of the studied populations because there was no regular mating system on both farms, and animals were mostly selected based on their phenotypic performances without considering their color types. Additionally, the clusters, where most of the CCFAR individuals were located, were more dispersed in a wider area and less overlapped with each other on the DAPC scatterplots compared with the clusters, where most of the MFF individuals were located (Figure 4.4), indicating CCFAR population may have a higher level of admixture than MFF population. These results were in agreement with the admixture patterns we observed when $K = 2, 3, 4,$ and 6 , where the CCFAR population showed a higher level of admixture than the MFF population (Figure 4.8). This may be related to the introduction of breeders from different farms within after the Aleutian

disease outbreak in CCFAR in 2013 (the generation interval is one year in CCFAR), as multiple breeder sources may result in higher levels of admixture (Verhoeven *et al.* 2011; Parker *et al.* 2017; Karaman *et al.* 2021). Most of the mink in the barn were dead or culled at that time when Aleutian disease occurred. Thus, within three years of the disease outbreak, about 150 mink (120 dams and 30 sires) from six farms were introduced and used as breeders in the breeding season at CCFAR, which might lead to a higher admixture level in the population compared with the MFF population. The populations (CCFAR and MFF) were clustered into only three groups in DAPC analysis using WGS data from 100 individuals (Karimi *et al.* 2021b). Compared to the DAPC results from this study, the MFF population was not clearly differentiated from the CCFAR population, and individuals within the same color tended to be grouped in the same cluster instead of several different clusters. The marker densities (100k vs. 24k) and sample sizes (100 vs. 2,973) are the possible reasons leading to the differences. The DAPC analysis differentiated 205 American mink in three different areas of Sweden into five clusters using the genotypic data from 21 microsatellites (Zalewski *et al.* 2016). The five clusters clearly differentiated the individuals from different study areas, indicating that geographical distribution was one of the critical factors in differentiating American mink. In our study, the geographical distribution might also play an important role in differentiating mink from two populations because the CCFAR and MFF populations were clearly separated by the first linear discriminant in the DAPC scatterplot (Figure 4.4).

In this study, three ancestral genetic groups were considered to delineate the studied populations' genetic structure based on the change of CV error against K and visual inspection of the admixture plots. The change in CV error against K (Figure 4.7) indicated

that the improvement in model fitness started to decrease between $K = 3$ and $K = 5$, suggesting that $K = 3$ may be the best cluster number that describes the studied populations. Compared to the admixture plots when $K = 2, 4, 6, 40,$ and 75 , the admixture plot when $K = 3$ seemed to describe the genetic structure of studied populations better. Similar to the DAPC results, when $K = 3$, a distinguishable distinctness between CCFAR and MFF populations was observed in the admixture plot, which further illustrated geographical distribution as a critical factor in differentiating American mink. The CCFAR population showed a higher level of admixture than the MFF population, which might be caused by the use of breeders from multiple sources in CCFAR (Introduced breeders from six different farms after the Aleutian disease outbreak) and a relatively single breeder source in MFF. Meanwhile, MBL and CBL were clearly identified with a distinct ancestral population suggesting that these two black color types derive from different ancestral populations and color type might not be a reliable indicator to differentiate American mink. Within the CCFAR population, CBL and CPA had their own clusters, and CDE, CMA, and CST showed noticeable admixtures of these two clusters. Many color types in American mink are exclusively line-bred because many color types are recessive to the standard brown color type, and the rest are blended (Shackelford 1948; Joergensen 1985; Nes *et al.* 1988). For example, mahogany is achieved by breeding the black and standard brown color types (Joergensen 1985). This could explain the admixture patterns of CMA and CDE in this study since these are visually very close color types, and CPA is one of the dominant brown color types. In the meantime, CDE and CMA seemed to share a similar admixture pattern, which indicated these two color types might share a similar genetic structure. Several results from this study also supported the point that CDE and CMA had a similar

genetic structure: 1) CDE and CMA showed the closest genetic distance (lowest Nei's and F_{st} values) among all color types (Table 4.3); 2) the phylogenetic tree grouped CDE and CMA into the same subgroup (Figure 4.3); 3) CDE and CMA showed a similar trend in LD and N_e decay (Figures 4.1 and 4.2); and 4) most of CDE and CMA individuals appeared in the same clusters generated from DAPC analysis (Figure 4.5). These results further illustrated the color type may not be a reliable indicator to differentiate American mink populations. The admixture patterns from this study are similar to the estimated admixture patterns of American mink in Canada in previous studies. The admixture patterns of farmed and wild American mink in Ontario, Canada, were investigated by Kidd *et al.* (2009) using the data from 10 microsatellite loci. In their studied farm populations, mink in black and pastel color types had their own groups, and mink in mahogany color type were mixed with several groups (Kidd *et al.* 2009), which were in the same patterns as this study. The admixture patterns of the current studied populations were also investigated in the small sample size using WGS data (Karimi *et al.* 2021b). Similar to the results from this study, when $K = 3$, individuals in black and pastel color types had their own groups, and individuals in demi and mahogany color types were mixed with those three groups (Karimi *et al.* 2021b).

Genetic structure and admixture pattern analyses conducted in this study did not detect clear genetic distinctions among the mink of various color types. Two potential reasons could lead to these results. The studied individuals were sampled from only two farms, which might make the samples not the ideal sample structures to reveal the population structures. Thus, future studies should consider including animals of various color types from wild and more geographically distributed farms. In the meantime, it has been noted

that a larger number of markers may be needed to resolve population genomics studies when the genetic distance (F_{st}) between the populations is low (Patterson *et al.* 2006). Thus, future studies could impute the SNP genotypes to WGS to obtain larger marker density to further investigate the genetic structure and admixture pattern of the studied populations.

4.5 Conclusions

In this thesis chapter, 2,973 animals from two farms and their genotypes obtained from the first developed medium-density SNP panel for American mink were used to investigate their LD patterns and genetic structure in various color types. The estimated LD patterns suggested that 7,700 and 4,200 SNPs are the minimum marker densities to conduct genomic selection programs in CCFAR and MFF populations, respectively. The results from genetic distances and diversity analyses indicated genetic differentiation among various color types was low, and most of the genetic variation occurred within color types rather than between color types. Three ancestral genetic compositions were considered the most appropriate number of ancestral genetic compositions to delineate the populations' genetic structure. The black (both CCFAR and MFF) and pastel color types seemed to have their own ancestral clusters, and demi, mahogany, and stardust were admixed with the three ancestral genetic compositions. Additionally, mink in demi and mahogany color types seemed to have a similar admixture pattern, but further study is needed. The genetic structure and admixture pattern of mink of various color types and within the same color type were not clearly identified in this study. Thus, future studies with samples from wider geographically distributed locations and higher marker density are needed to differentiate the mink within the same color type.

This thesis chapter provided useful information for conducting genomic evaluations in the mink industry using genotypes from the medium-density SNP panel. The mink industry faces several challenges caused by the Covid-19 pandemic, industry downturn, and decreasing market demand. Improving production efficiency through advanced genomic approaches could help the mink industry meet these challenges. The LD patterns and genetic structures obtained from the first SNP panel for American mink would provide the essential information to implement the SNP panel in genomic studies of American mink.

Table 4.1 Average minor allele frequency (MAF), observed heterozygosity, and nucleotide diversity for five color types of American mink in CCFAR, whole CCFAR population, and whole MFF population.

Color type	Number of individuals	Average MAF	Observed heterozygosity (%)	Average nucleotide diversity
CBL ¹	177	0.220	31.821	0.297
CDE ²	542	0.216	31.029	0.307
CMA ³	527	0.212	30.594	0.303
CPA ⁴	152	0.236	32.644	0.294
CST ⁵	13	0.246	34.947	0.283
CCFAR ⁶	1,411	0.216	30.576	0.307
MBL ⁷	1,562	0.226	31.938	0.288

∞ ¹ black color type mink in the Canadian Center for Fur Animal Research (CCFAR); ² demi color type mink in CCFAR; ³ mahogany color type mink in CCFAR, ⁴ pastel color type mink in CCFAR; ⁵ stardust color type mink in CCFAR; ⁶ all mink in CCFAR; ⁷ black color type mink in Millbank Fur Farm.

Table 4.2 Summary of the average and standard deviation of r^2 between adjacent SNPs on all chromosomes of five color types of American mink in CCFAR, whole CCFAR population, and whole MFF population.

Chr ¹	CCFAR ²	CBL ³	CDE ⁴	CMA ⁵	CPA ⁶	CST ⁷	MBL ⁸
	Average $r^2 \pm SD$						
1	0.444±0.451	0.403±0.445	0.425±0.447	0.415±0.445	0.415±0.441	0.408± 0.438	0.419±0.451
2	0.412±0.446	0.379±0.443	0.395±0.440	0.399±0.441	0.387±0.435	0.369± 0.424	0.392±0.445
3	0.354±0.440	0.336±0.431	0.339±0.433	0.340±0.434	0.335±0.425	0.346± 0.420	0.341±0.429
4	0.404±0.447	0.396±0.449	0.385±0.443	0.384±0.442	0.367±0.434	0.400± 0.440	0.406±0.450
5	0.369±0.365	0.368±0.369	0.346±0.364	0.356±0.365	0.336±0.366	0.368± 0.378	0.388±0.379
6	0.432±0.453	0.391±0.445	0.418±0.448	0.415±0.449	0.404±0.442	0.372± 0.430	0.422±0.447
7	0.396±0.377	0.393±0.381	0.380±0.378	0.381±0.377	0.375±0.380	0.396± 0.383	0.407±0.385
8	0.428±0.378	0.425±0.388	0.412±0.381	0.423±0.382	0.403±0.386	0.382± 0.389	0.449±0.392
9	0.345±0.351	0.357±0.360	0.334±0.351	0.342±0.355	0.331±0.355	0.361± 0.371	0.357±0.362
10	0.269±0.397	0.268±0.399	0.261±0.390	0.248±0.385	0.263±0.384	0.285± 0.387	0.277±0.404
11	0.558±0.386	0.557±0.399	0.531±0.393	0.540±0.391	0.502±0.406	0.533± 0.432	0.597±0.397
12	0.504±0.377	0.519±0.394	0.470±0.378	0.499±0.387	0.438±0.387	0.490± 0.419	0.545±0.397
13	0.384±0.382	0.397±0.386	0.364±0.380	0.376±0.381	0.368±0.381	0.416± 0.396	0.427±0.396
14	0.293±0.401	0.291±0.402	0.266±0.390	0.285±0.393	0.293±0.399	0.340± 0.421	0.258±0.372
Mean	0.399±0.404	0.391±0.407	0.380±0.401	0.386±0.402	0.373±0.402	0.390± 0.409	0.406±0.408

¹ chromosome; ² all mink from the Canadian Center for Fur Animal Research (CCFAR); ³ black color type mink in CCFAR; ⁴ demi color type mink in CCFAR; ⁵ mahogany color type mink in CCFAR, ⁶ pastel color type mink in CCFAR; ⁷ stardust color type mink in CCFAR; ⁸ black color type mink in Millbank Fur Farm.

r^2 = Linkage disequilibrium; SD = Standard deviation.

Table 4.3 Estimation of Nei's genetic distance (upper diagonal) and Weir and Cockerham's Fst (lower diagonal) between various color types of American mink.

	CDE ¹	CPA ²	CMA ³	CST ⁴	CBL ⁵	MBL ⁶
CDE	0	0.012	0.003	0.027	0.010	0.018
CPA	0.024	0	0.021	0.053	0.033	0.037
CMA	0.006	0.044	0	0.023	0.005	0.012
CST	0.042	0.096	0.033	0	0.018	0.035
CBL	0.021	0.068	0.010	0.024	0	0.015
MBL	0.040	0.081	0.028	0.063	0.035	0

¹ demi color type mink in the Canadian Center for Fur Animal Research (CCFAR); ² pastel color type mink in CCFAR; ³ mahogany color type mink in CCFAR; ⁴ stardust color type mink in CCFAR; ⁵ black color type mink in CCFAR; ⁶ black color type mink in Millbank Fur Farm.

82

Table 4.4 Analysis of molecular variance (AMOVA) in various color types of American mink.

Source of Variation	Degrees of Freedom	Sum of Squares	Mean Squared Deviations	Variance Components	Percentage of Variation
Among farms	1	10.720	10.720	0.004	4.291
Among color types	4	4.425	1.106	0.004*	4.067
Within color types	2,967	279.795	0.094	0.094*	91.642
Total	2,972	294.940	11.920	0.102	100

* p<0.05.

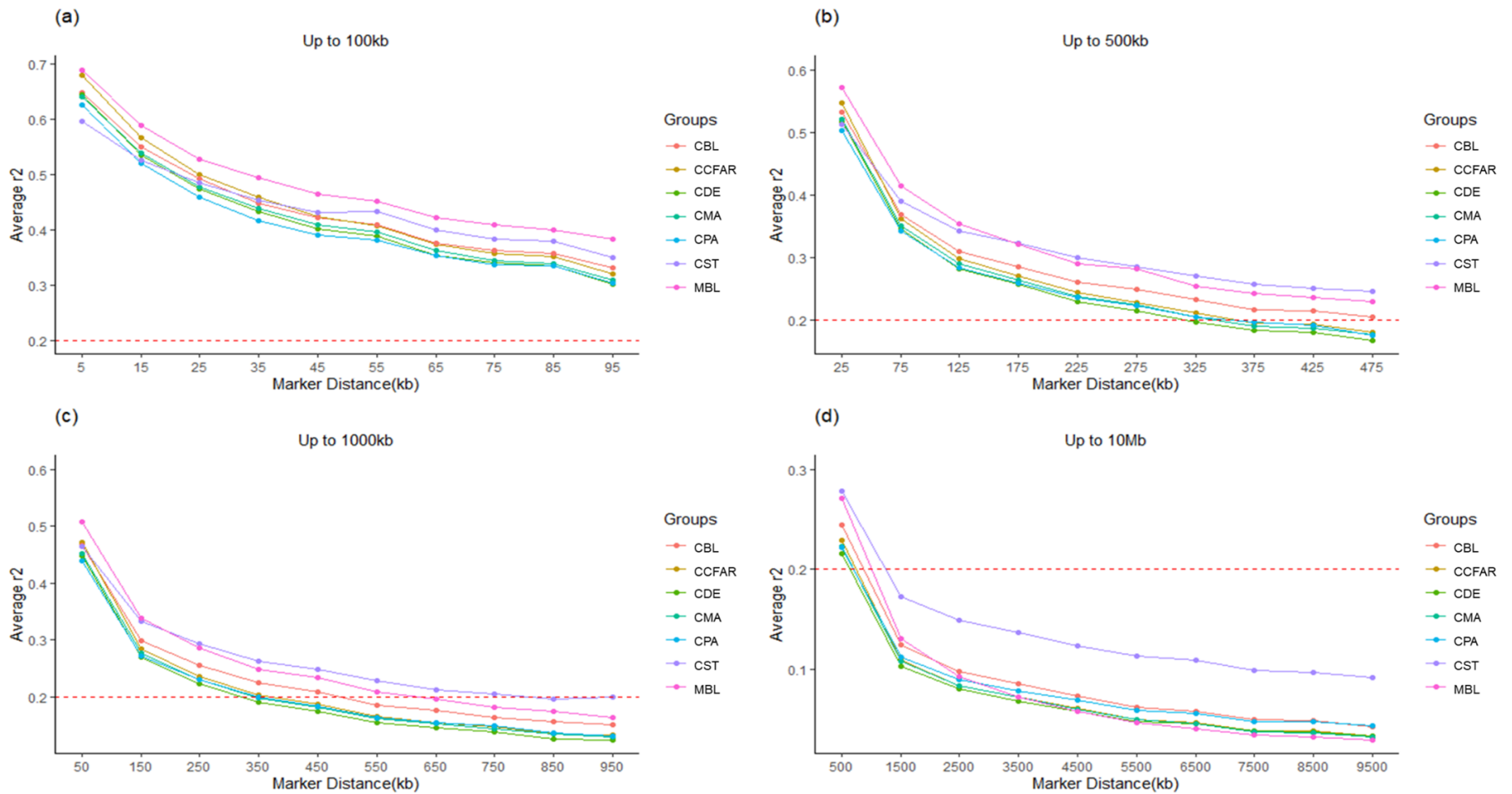


Figure 4.1 Linkage disequilibrium measured by r^2 plotted as a function of inter-market distance (kb). (a) from 0 up to 100 kb using consecutive 10 kb bins, (b) up to 500 kb using consecutive 50 kb bins, (c) up to 1000 kb using consecutive 100 kb bins, and (d) up to 10 Mb using consecutive 1000 kb bins. CCFAR = all mink from the Canadian Center for Fur Animal Research (CCFAR). MBL= black color type mink in Millbank Fur Farm; CBL, CDE, CMA, CPA, and CST are black, demi, mahogany, pastel, and stardust color type mink in CCFAR, respectively.

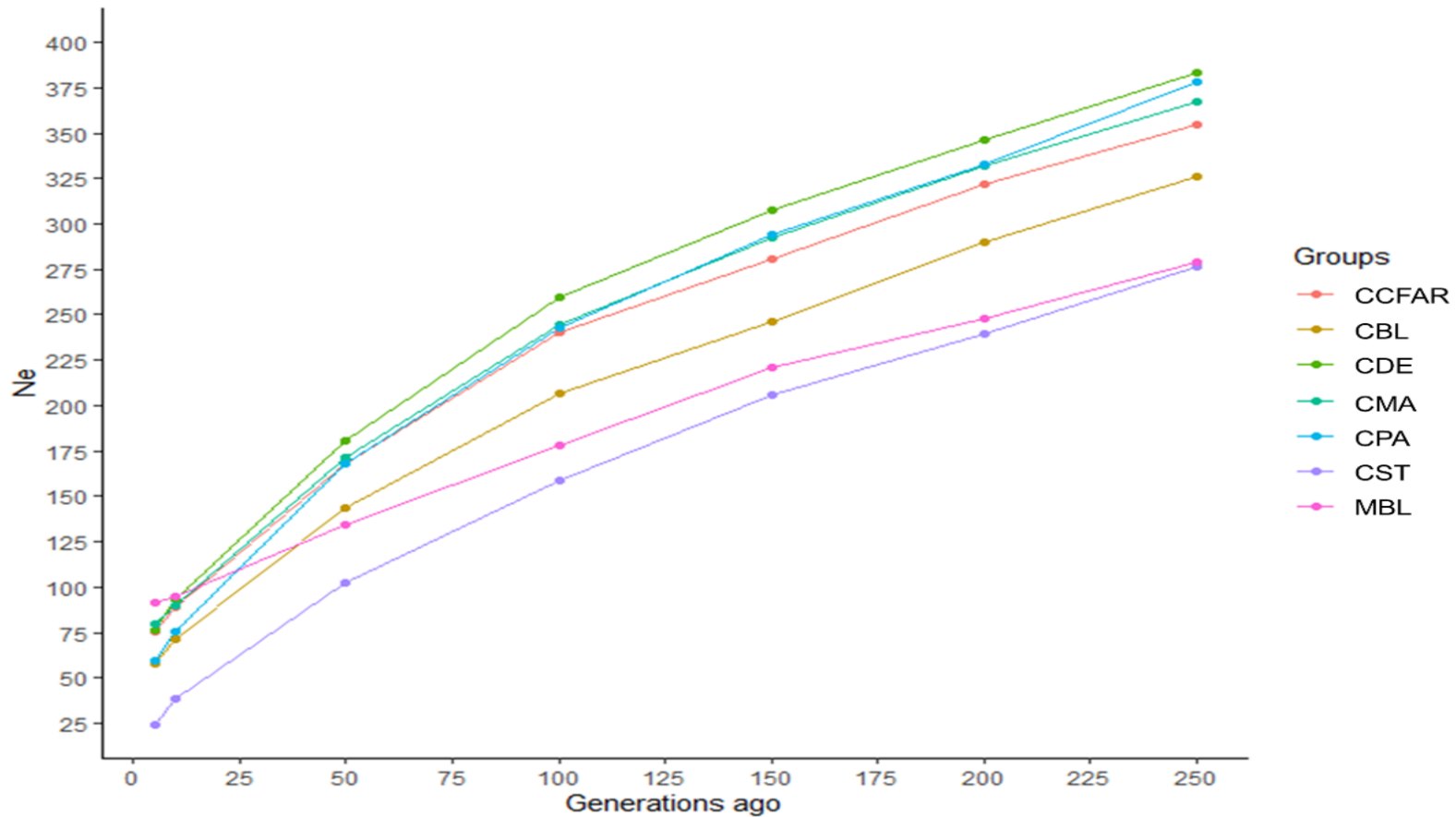


Figure 4.2 Estimated effective population sizes for various color types of American mink from 5 to 250 generations ago. CCFAR = all mink from the Canadian Center for Fur Animal Research (CCFAR). MBL= black color type mink in Millbank Fur Farm; CBL, CDE, CMA, CPA, and CST are black, demi, mahogany, pastel, and stardust color type mink in CCFAR, respectively.

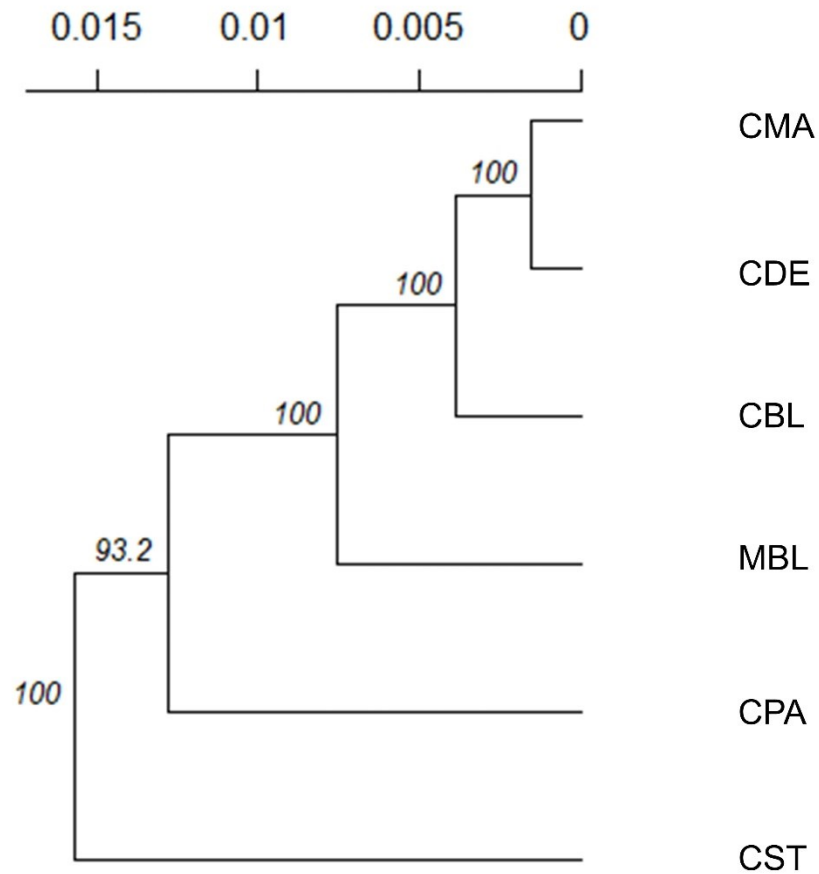


Figure 4.3 Unrooted consensus tree showing the genetic relationships among the six color types using the unweighted pair group method and the unbiased Nei's genetic distance. The values at the nodes are the percentages of bootstrap values from 1,000 replications of resampling. The x-axis represents the genetic distances between color types. MBL= black color type mink in Millbank Fur Farm; CBL, CDE, CMA, CPA, and CST are black, demi, mahogany, pastel, and stardust color type mink in the Canadian Center for Fur Animal Research, respectively.

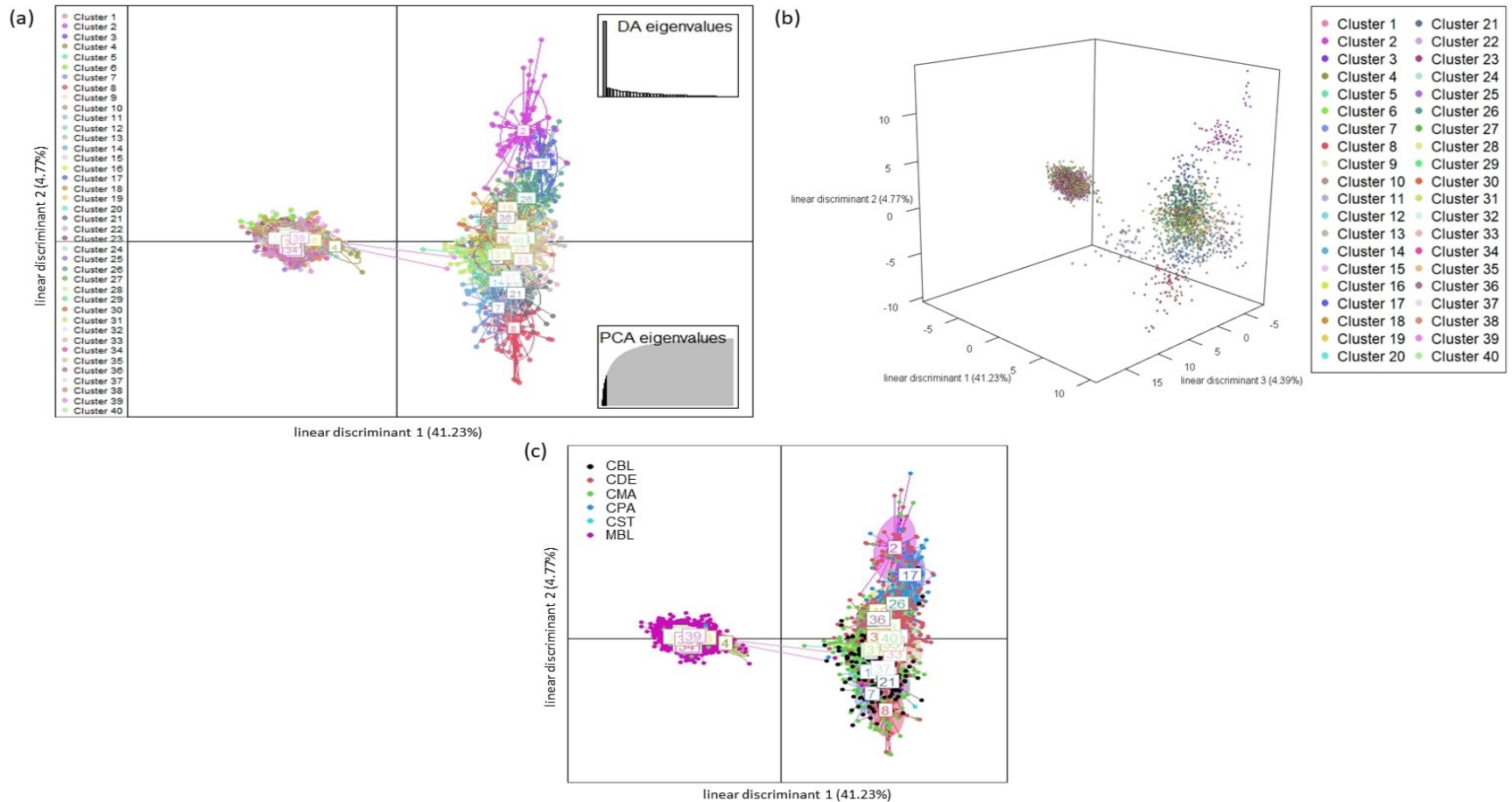


Figure 4.4 The scatterplots of discriminant analysis of principal components. Each ellipse represents a cluster, and each dot represents an individual. Different clusters are separated by colors. MBL= black color type mink in Millbank Fur Farm; CBL, CDE, CMA, CPA, and CST are black, demi, mahogany, pastel, and stardust color type mink in CCFAR, respectively. a) The scatterplot of the first two linear discriminants (x and y-axis, respectively), which explained 41.23 and 4.77% of the variation, respectively. Individual dot is a given color based on which cluster the individual is grouped to; b) The 3D scatterplot of the first three linear discriminants (x, y, and z-axis, respectively), which explained 41.23, 4.77, and 4.39% of the variation, respectively. Individual dot is a given color based on which cluster the individual is grouped to; and c) Scatterplot of the first two linear discriminants (x and y-axis, respectively). Different clusters are separated by colors and inertia ellipses labeled with a number. Individual dot is a given a color based on the individual color type.

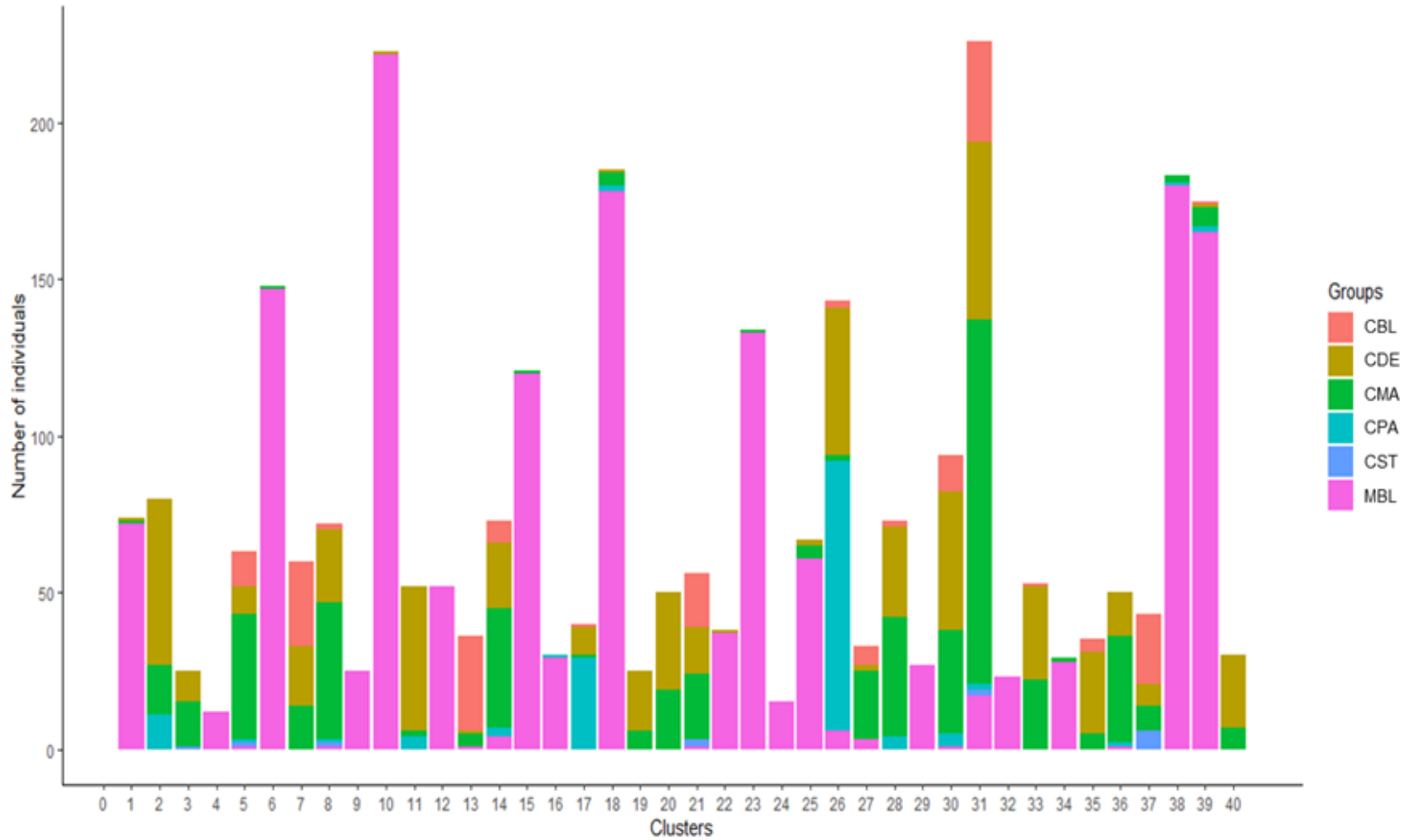


Figure 4.5 The number of individuals from various color types in 40 assigned clusters inferred by discriminant analysis of principal components. MBL= black color type mink in Millbank Fur Farm; CBL, CDE, CMA, CPA, and CST are black, demi, mahogany, pastel, and stardust color type mink in the Canadian Center for Fur Animal Research, respectively.

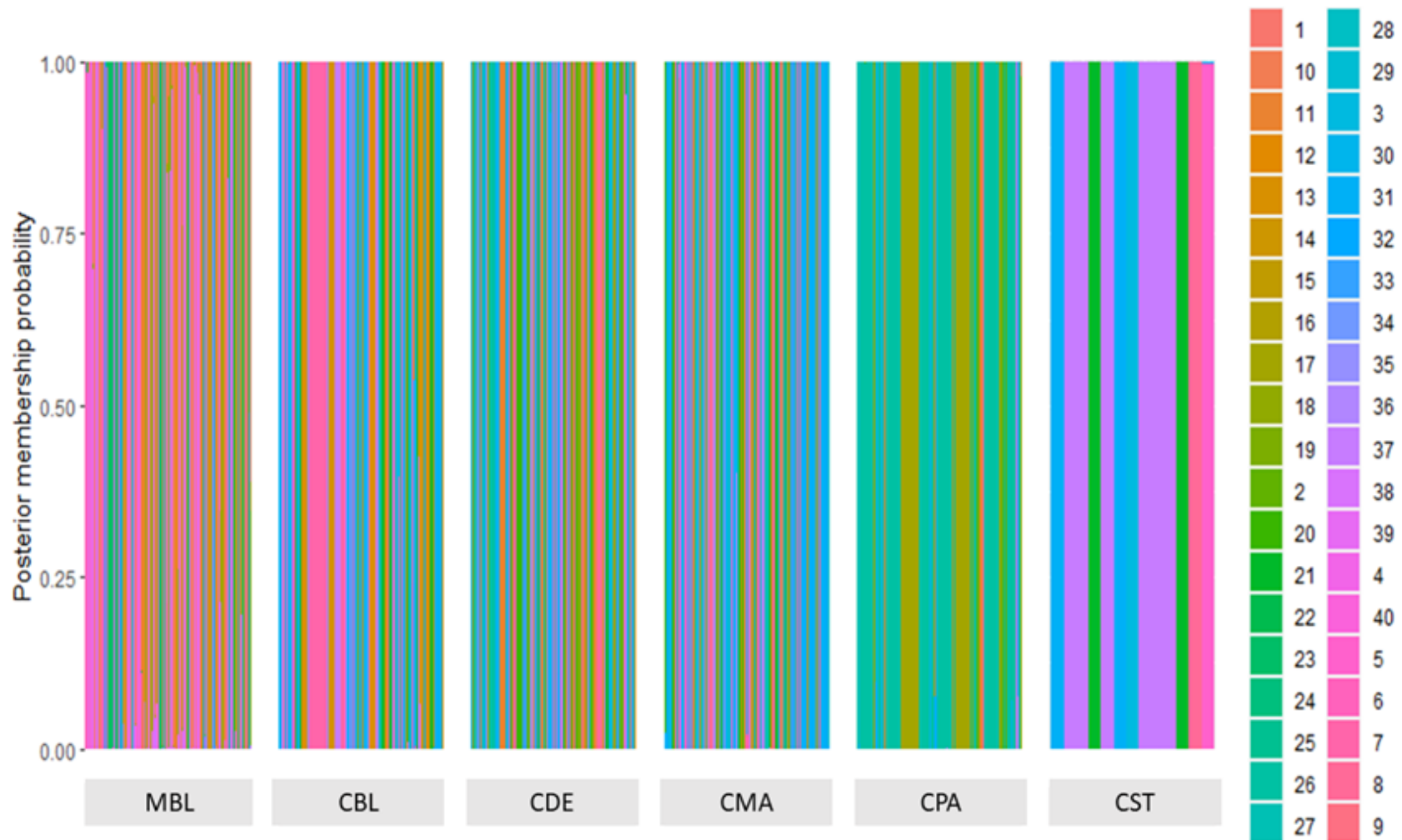


Figure 4.6 The probability of membership of each sample in the 40 assigned clusters inferred by discriminant analysis of principal components. MBL= black color type mink in Millbank Fur Farm; CBL, CDE, CMA, CPA, and CST are black, demi, mahogany, pastel, and stardust color type mink in the Canadian Center for Fur Animal Research, respectively.

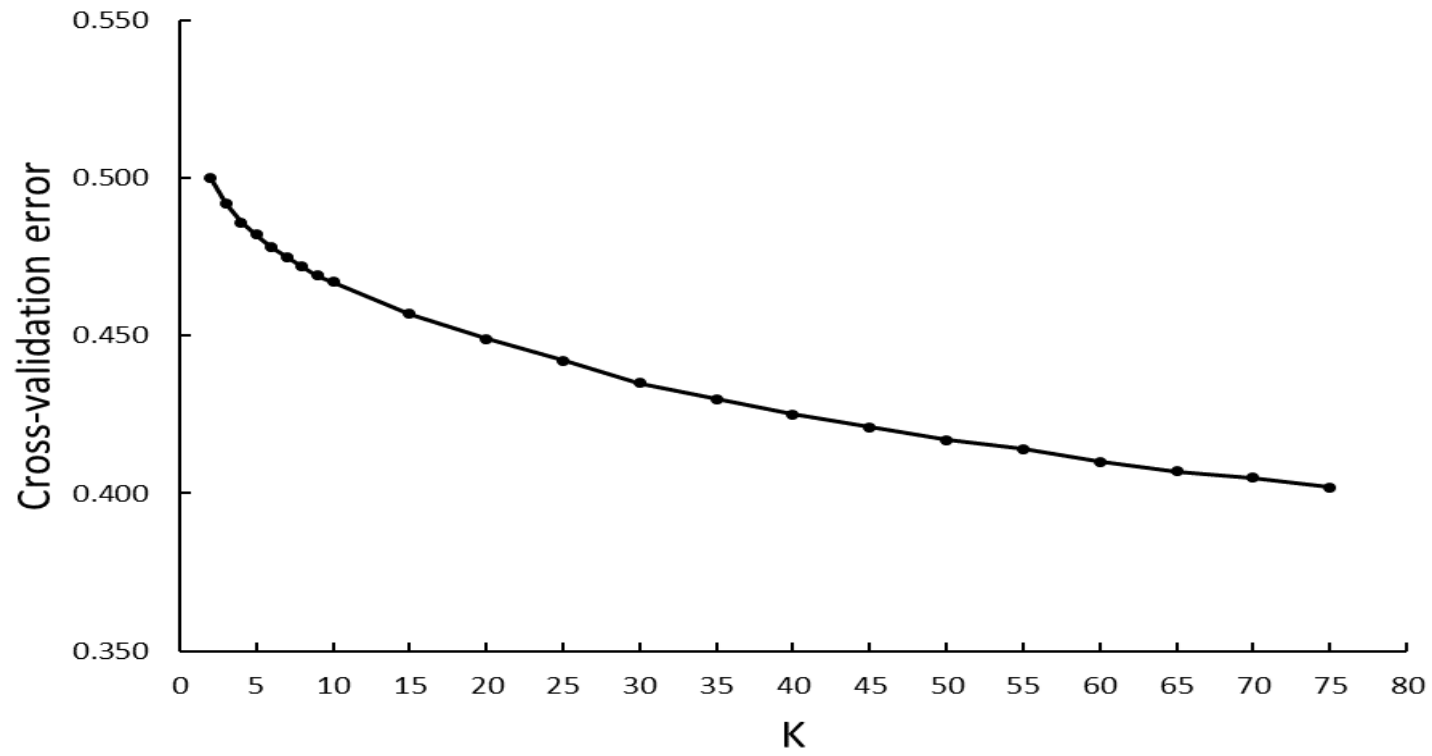


Figure 4.7 ADMIXTURE analyses of six color types American mink with cross-validation error plot for K-values from 2 to 75.

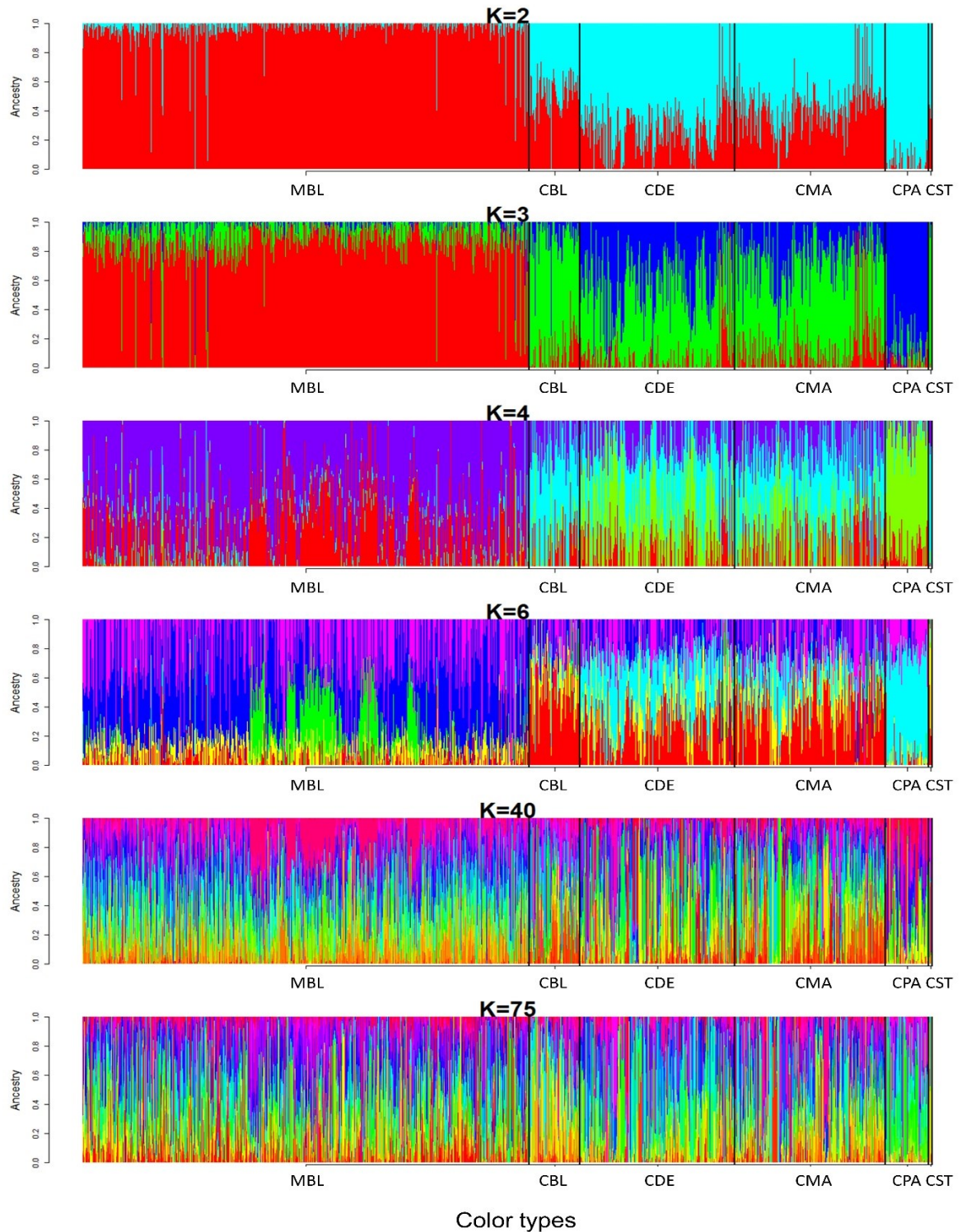


Figure 4.8 Admixture pattern of six color types American mink at $K = 2, 3, 4, 6, 40,$ and 75 . MBL= black color type mink at Millbank Fur Farm; CBL, CDE, CMA, CPA, and CST are black, demi, mahogany, pastel, and stardust color type mink in the Canadian Center for Fur Animal Research, respectively.

CHAPTER 5. Identifying Selection Signatures for Immune Response and Resilience to Aleutian Disease in Mink Using Genotype Data¹

5.1 Introduction

Aleutian disease (AD) is one of the most severe diseases in mink farming, leading to significant financial losses to the mink industry due to its adverse influences on several economically important traits. This disease is caused by the Aleutian mink disease virus (AMDV) and has been determined to be an immune complex disease. Specific antibodies produced against AMDV fail to neutralize the virus and instead form complexes with the infectious virus, resulting in damage to the mink's glomerular and arterial systems (Porter *et al.* 1969; Cho & Ingram 1973; Porter *et al.* 1973; Stolze & Kaaden 1987). Thus, the higher the levels of anti-AMDV antibodies produced, the more severe the infection caused by AD (Porter *et al.* 1972; Kanno *et al.* 1993; Bloom *et al.* 1994; Aasted *et al.* 1998; Bloom *et al.* 2001). Meanwhile, AD infection was also found to cause adverse influences on body weight growth (Porter *et al.* 1982), feed intake (Elzhov *et al.* 2016; Jensen *et al.* 2016b), pelt quality (Farid & Ferns 2011), and female reproductive performance (Henson *et al.* 1962; Reichert & Kostro 2014). Thus, anti-AMDV antibody level, growth, feed efficiency, and female reproductive performance were suggested as AD-resilience indicator traits in previous studies (Hu *et al.* 2021; Hu *et al.* 2022). Several methods, including vaccination,

¹ A version of this Chapter will be submitted to the *Frontiers in Genetics* by Hu *et al.* 2024. Identifying Selection Signatures for Immune Response and Resilience to Aleutian Disease in Mink Using Genotype Data.

medicine, and culling strategy, have been attempted to control AD, but these measures have been largely ineffective. Consequently, mink farmers have resorted to select AD-resilient mink based on AD tests and/or mink performance in AD-resilience indicator traits, such as body size, pelt quality, and reproductive performance to manage populations in the presence of AD. Several mink farms in the Canadian province of Nova Scotia select AD-resilient mink using the iodine agglutination test and assessments of the productive performance (Farid & Ferns 2017). Similarly, Some AD-positive mink farms in North America and Europe have applied enzyme-linked immunosorbent assay tests (ELISA) to select AD-resilient mink (Knuuttila *et al.* 2009; Farid & Rupasinghe 2016; Farid *et al.* 2018).

Selection could cause changes in the patterns of genetic variation among selected loci and linked neutral loci. These patterns are termed selection signatures, and they can be used to identify loci subject to the selection (Kreitman 2000; Qanbari & Simianer 2014; Ma *et al.* 2015). Therefore, identifying the signatures would be helpful for detecting genes and biological processes related to AD resilience. Characterizing the genomic regions associated with mink response to AD could aid in the development of breeding programs focus on improving AD-resilience in mink farms. Several statistical methods have been proposed for detecting selection signatures in livestock. The pairwise fixation index (F_{st}) (Weir & Cockerham 1984), nucleotide diversity ($\theta\pi$) (Nei & Li 1979), and cross-population extended haplotype homozygosity (XP-EHH) (Sabeti *et al.* 2007) are the three methods commonly used to detect selection signatures, where the F_{st} and $\theta\pi$ are based on the genetic diversity and genetic differentiation, and XP-EHH is based on the frequency of extended haplotypes between two subpopulations.

Advancements in next-generation sequencing technologies, high-density single nucleotide polymorphism (SNP) arrays, and bioinformatics tools, have now significantly improved the detection of selection signatures in livestock species (Bertolini *et al.* 2018). For example, studies using selection signatures have identified several genes associated with disease resistance/susceptibility in cattle (Li *et al.* 2020; Saravanan *et al.* 2021). Xu *et al.* (Xu *et al.* 2020) conducted a signature of selection study and detected several genes related to susceptibility of swine to respiratory disease. For AD in American mink, Karimi *et al.* (2021a) detected 99 genomic regions associated with the response to AD infection using genotyping by sequencing (GBS) data and five phenotypes (anti-AMDV antibody titer, mortality, AD symptoms in the kidneys, and virus clearance at two different times) from 225 experimental black American mink that were inoculated with AMDV. These regions encompassed 63 genes involved in immune response, liver development, and reproduction (Karimi *et al.* 2021a). However, signature of selection study focusing on the response of mink to AD had not been conducted using genotype data in conjunction with AD-resilience indicator traits (e.g., growth, feed efficiency, pelt quality, and reproduction) for mink reared in an AD-positive commercial farms. It has been reported that mink with darker color types seem to be more resilient to AMDV than lighter color types (Ellis 1996). A signature of selection study is a potential approach to study the performances of different color types of mink against AD infection. Therefore, the objectives of this thesis chapter were to use genotype data and different color types of American mink to 1) detect the selection signatures associated with immune response, general resilience, and female reproductive performance resilience to AD; 2) identify the genes related to immune response, general resilience, and female reproductive performance resilience to AD; and 3) investigate

whether mink of different color types exhibit distinct respond to AD, and exploring potential differences in AD resilience mechanisms among color variations.

5.2 Materials and Methods

This study was approved by the Dalhousie University Animal Care and Use Committee (certification#: 2018-009 and 2019-012). All the mink were farmed following the Code of Practice for the Care and Handling of Farmed Mink guidelines from the Canada Mink Breeders Association (Turner P *et al.* 2013).

5.2.1 Animals and Sampling

All the individuals (n=1,411) studied in this research were from the Canadian Centre for Fur Animal Research (CCFAR) at Dalhousie University, Faculty of Agriculture (Truro, Nova Scotia, Canada) from 2013 to 2021. In 2013, an outbreak of AD occurred at CCFAR, resulting in most of the mink were dead or culled in the barn. The exact source of outbreak was not determined definitively, but it was suspected that AMDV-contaminated feed and contact with wild animals carrying AMDV were the most likely causes. Thus, within three years of the disease outbreak, about 150 mink (120 dams and 30 sires) from six AD-positive farms in Nova Scotia (Canada), which were believed to be resilient to AD and have been phenotypically selected for AD-resilient mink for many years, were introduced and used as breeders at CCFAR. AD was first identified in the province of Nova Scotia in Canada in 1941 (Agriculture and Marketing of Nova Scotia Government 1998), and many mink farms in the province started selecting for AD-resilient mink based on specific AD-resilient traits (Farid & Ferns 2017). The studied mink included five different color types: black (n = 177), demi (n = 542), mahogany (n = 527), pastel (n = 152), and stardust (n = 13). The

color type of each individual was identified by experienced technicians at CCFAR at weaning.

5.2.2 Aleutian Disease Tests

Counterimmunoelectrophoresis (CIEP) and antigen-based enzyme-linked immunosorbent assay tests (ELISA-G) were used to measure the immune response of studied mink to AD virus exposure. The tests were conducted using established protocols described by Hu *et al.* (2021). In brief, blood samples of the studied mink were collected in mid-November before selecting breeders and in mid-February before mating from 2013 to 2021. The blood samples were sent to the Animal Health Laboratory at the University of Guelph (Ontario, Canada) and Middleton Veterinary Services (Nova Scotia, Canada) for CIEP and ELISA-G tests, respectively. The CIEP tests were used to detect the existence of anti-AMDV antibodies, and the results were recorded as 0 (negative: none or extremely low antibody level detected) or 1 (positive: detectable antibody level). The ELISA-G tests were applied to measure amounts of antibodies against AMDV using optical density, and the test results included eight categories with 1-point increments from 0 (none or extremely low level of antibody) to 7 (extremely high antibody level).

5.2.3 Growth and Feed Efficiency Measurement

Kleiber ratio (KR) and feed conversion ratio (FCR) were used to measure the growth and feed efficiency of the studied mink, respectively. The body weights of studied individuals were collected using the established protocols described by Do *et al.* (2021). Briefly, the body weight (BW) of the mink were measured at both birth and weaning (around six weeks after birth) and every three weeks from 13 to 28 weeks after birth. The average daily gain

(ADG) and Mid-test metabolic BW ($BW^{0.75}$) were calculated by the following equations, respectively:

$$ADG = \frac{Final\ BW - Initial\ BW}{Number\ of\ days\ on\ the\ test},$$

$$BW^{0.75} = \left(\frac{Initial\ BW + Final\ BW}{2} \right)^{0.75},$$

where *final BW* was the BW on the last day of the feeding trial, and *initial BW* was the BW at 13 weeks of age. The Kleiber ratio (KR) was calculated using the following equation:

$$KR = \frac{ADG}{BW^{0.75}}.$$

The feed intake data of the studied mink were collected using the established protocols described by Davoudi *et al.* (2022). Briefly, mink were raised individually in separate cages, and feed was distributed daily to cages. The daily feed intake (DFI) of each mink was measured by calculating the difference between the amount of feed left over and the feed provided. The individual DFI records obtained during the experiment were averaged to obtain the individual average daily feed intake (ADFI). The FCR was calculated using the following equation:

$$FCR = \frac{ADFI}{ADG}.$$

5.2.4 Pelt Quality Evaluation

Live grading of overall pelt quality (QUA) was performed to measure the qualities of the mink pelt when they were alive. The gradings were conducted based on the North American

Fur Auctions live animal grading procedure by a skilled technician. The gradings focused on checking the color consistency, fur roughness, and overall gloss. The QUA was scored into three categories from 1 (poor) to 3 (best).

5.2.5 Female Reproductive Performance Measurement

Female reproductive performance was measured and recorded by the technicians in CCFAR during each annual reproduction cycle from 2006 to 2021. In this study, the number of newborn kits that survived 24 hours after birth was used to quantify the reproduction performance of dams under AMDV exposure.

5.2.6 Animal Grouping

Studied individuals were grouped into pairwise subgroups based on their immune response, general resilience, and female reproduction performance. Studied individuals with both CIEP and ELISA-G test results were grouped into low or high immune response subgroups based on their CIEP and ELISA-G test results. Individuals with zero ELISA-G scores and negative CIEP results were grouped into low immune response subgroups, and individuals with 5-7 ELISA-G scores and positive CIEP results were grouped into high immune response subgroup (Table 5.1). In this study, we not only grouped the entire populations of individuals into low or high immune response subgroups but also the individuals within the same color type, which included black, demi, mahogany, and pastel color types (Table 5.1). For resilience indicator traits, two methods were used to group CIEP-positive individuals into pairwise groups (Table 5.2). Studied individuals with positive CIEP results that had BW, feed intake, and pelt quality records, were grouped into resilient or susceptible subgroups. The CIEP-positive individuals, which had bottom 20% FCR (14.38 to 22.49), top 20% KR (7.14 to 9.17), and score 3 (high pelt quality) for QUA were grouped into the

resilient subgroup, and the CIEP positive individuals, which had top 20% FCR (41.46 to 72.28), bottom 20% KR (2.19 to 4.41), and score 1 (low pelt quality) for QUA, were grouped into the susceptible subgroup (Table 5.2). In the meantime, studied CIEP-positive dams, that had records for the number of newborn kits that survived 24 hours after birth, were grouped into low or high female reproductive performance subgroups. The CIEP-positive dams with less than four newborn kits that survived 24 hours after birth were grouped into the low reproductive performance subgroup, and the CIEP-positive dams that had more than nine newborn kits that survived 24 hours after birth were grouped into the high reproductive performance subgroup (Table 5.2).

5.2.7 Sample Collection and Genotyping

Tongue tissues from studied individuals were collected before pelting. DNeasy Blood and Tissue Kit (Qiagen, Hilden, Germany) was used to extract the DNA from the tongue tissue based on the manufacturer's instructions. NanoDrop ND-1000 spectrophotometer (NanoDrop Technologies Inc., Wilmington, DE) was applied to measure the quantity and quality of extracted DNA samples. The 260/280 nm readings for all samples ranged from 1.7 to 2.0. All samples had a final concentration of 20 ng, and finally were genotyped by an Axiom Affymetrix Mink 70K SNP panel (Neogen, Lincoln, Nebraska, USA) (Do *et al.* 2024).

5.2.8 Animals and SNP Quality Control

PLINK (Purcell *et al.* 2007) was used to conduct animal and SNP data quality control. SNPs that had minor allele frequency lower than 1%, call rate lower than 90%, excess of heterozygosity higher than 15%, Mendelian error frequency larger than 5%, and were out of Hardy-Weinberg equilibrium with very low probability (1×10^{-5}), were excluded from

the analyses. Meanwhile, mink, that had a call rate lower than 90%, were also removed from the dataset. After the quality control, 26,406 SNPs and 1,411 animals remained for further analyses.

5.2.9 Methods for Detection of Selection Signatures

Three methods, including pairwise fixation index (F_{st}) (Weir & Cockerham 1984), nucleotide diversity ($\theta\pi$) (Nei & Li 1979), and cross-population extended haplotype homozygosity (XP-EHH) (Sabeti *et al.* 2007), were performed to detect the selection signatures. The F_{st} and $\theta\pi$ methods directly utilize the SNP genotype, while the XP-EHH method uses phased data. The F_{st} analysis was conducted for each SNP based on the method proposed by Weir and Cockerham (1984) using VCFtools software (Danecek *et al.* 2011). The Z-transformation was performed using the *scale* function in the R program (Team 2022) to normalize the F_{st} values. All negative F_{st} values were set to zero. The F_{st} values of all SNPs were ranked, and the SNPs with the top 5% F_{st} values were considered candidate selection signatures. The $\theta\pi$ analysis was conducted for each SNP based on the method proposed by Nei and Li (1979) using VCFtools software (Danecek *et al.* 2011). The $\theta\pi$ ratios were computed as $\theta\pi(\text{subgroup1})/\theta\pi(\text{subgroup2})$ for all pairs of groups and were then log₂-transformed ($\log_2(\theta\pi \text{ ratios})$). The SNPs with the top 5% $\theta\pi$ ratio values were considered candidate selection signatures. The XP-EHH approach was calculated for each SNP using Selscan software (Torres *et al.* 2018). The missing genotypes were removed using VCFtools software (Danecek *et al.* 2011), and the genotypes were phased using Beagle software (Browning *et al.* 2018) because Selscan software can only handle the phased genotypes without missing genotypes. The original obtained XP-EHH values were normalized using the *norm* function within the Selscan software. Then, the *pnorm*

function in the R program was applied to calculate the p-values of the normalized XP-EHH values. The p-values of the normalized XP-EHH values were log-transformed, and the SNPs with $-\log(\text{p-value})$ more than two were considered as candidate selection signatures. Only the SNPs detected as candidate selection signatures by at least two methods were used for gene annotation, gene ontology, and functional analyses.

5.2.10 Gene Annotation, Gene Ontology, and Functional Analysis

The potential selection regions were defined by extending 350 kb both upstream and downstream of the candidate selection signatures. The regions were defined based on the previous study that suggested that linkage disequilibrium ($r^2 < 0.2$) in the current studied American mink population did not exceed 350 kb (Hu *et al.* 2023). The gene annotation was conducted using the Bedtools software (Quinlan 2014) referring to the genome assembly of *Neogale vison* (Karimi *et al.* 2022). The gene ontology (GO) terms, including biological process (GO:BP), cellular component (GO:CC), and molecular function (GO:MF), were assigned to annotated genes using PANTHER 14.1 (Thomas *et al.* 2003). The overrepresentation tests of annotated genes were conducted using Fisher's exact test and adjusted by the false discovery rate (FDR) correction, and the terms with FDR adjusted p-value (q-value) < 0.05 were considered as the overrepresented terms. Meanwhile, the Kyoto Encyclopedia of Genes and Genomes (KEGG) pathway analyses were conducted using the clusterProfiler package (Yu *et al.* 2012) in the R program with FDR control.

5.3 Results

5.3.1 Selection Signatures for Immune Response Trait

The genome-wide distribution of selection signatures associated with the immune response trait was assessed using F_{st} , $\theta\pi$ ratio, and XP-EHH. The results are presented in Figure 5.1, displaying the distribution across all autosomal chromosomes. Additionally, Figure 5.2 illustrates the selection signatures that overlap across the three methods. Supplementary dataset 1 presents the SNPs (chromosome number and location on the chromosome) detected as candidate selection signatures by each method, and the SNPs detected as candidate selection signatures by at least two methods. When considering the entire population of individuals, a total of 619 SNPs were detected as candidate selection signatures by at least two methods. Notably, 33 SNPs were detected by all three methods, and were considered as strongly selected candidates for immune response trait (Figure 5.2). Furthermore, when analyzing individuals within specific color types, 444, 512, 385, and 335 were detected as candidate selection signatures by at least two methods for black, demi, mahogany, and pastel color type mink, respectively. In addition, 57, 31, 32, and 45 SNPs were detected by all three methods for black, demi, mahogany, and pastel color type mink, respectively, highlighting strong selection signature candidates specific to the immune response trait within each color type (Figure 5.2).

The candidate genes annotated from the selection signatures for immune response trait in the whole population and different color types are listed in Supplementary dataset 1. Figure 5.3 shows the overlapped annotated candidate genes among the whole population and different color types for immune response trait. A total of 1,611 candidate genes were annotated from the selection signatures detected from the whole population (Figure 5.3 and

Supplementary dataset 2). For black, demi, mahogany, and pastel color type individuals, 1,355, 1,645, 1,436, and 1,042 candidate genes were annotated, respectively (Figure 5.3). Among the candidate genes annotated from the whole population and different color types, many genes were found to be associated with the AD-characterized phenotypes, including immune system process, growth, pigmentation (except for the black color type), reproduction, and response to stimulus (Supplementary dataset 2, Figure 5.3 and 5.4). Table 5.3 provides a list of genes specifically related to immune response trait for all color types. However, no common gene was detected among all color types for immune response trait (Figure 5.3).

Figure 5.4 presents the functional classifications of candidate genes related to the immune response trait. The genes annotated from the whole population, black, demi, mahogany, and pastel color type individuals were classified into 17, 18, 17, 20, and 18 GO:BP categories, respectively, where the top four biological processes were cellular process, metabolic process, biological regulation, and response to stimulus in all cases (Figure 5.4). The cellular anatomical entity and protein-containing complex were the two cellular components detected from the whole population and all color types. Regarding the GO:MF classifications, both analyses for whole population individuals and black color type individuals detected 11 GO:MF, while analyses for demi, mahogany, and pastel color type individuals detected 12 GO:MF. The top four GO:MF categories for the whole population and all color types were binding, catalytic activity, transcription regulator activity, and molecular transducer activity (Figure 5.4).

Table 5.4 (GO:BP) and Table 5.5 (GO:CC and GO:MF) present the overrepresentations of candidate genes related to the immune response trait. A total of 27, 18, 50, 26, and 18

significant (q -value <0.05) overrepresented GO enrichment terms were detected from the whole population, black, demi, mahogany, and pastel color type individuals, respectively (Tables 5.4 and 5.5). Among all detected significant (q -value <0.05) overrepresented GO enrichment terms, some of them were commonly detected in the whole population and all color types (Tables 5.4 and 5.5), including two GO:BP (detection of chemical stimulus involved in sensory perception of smell (GO:0050911) and sensory perception of smell (GO:0007608)), three GO:CC (cytoplasm (GO:0005737), intracellular anatomical structure (GO:0005622), and organelle (GO:0043226)), and one molecular function (olfactory receptor activity (GO:0004984)). While some were only detected in a certain color type of mink or the entire population. For example, the biological process of adaptive immune response (GO:0002250) and system development (GO:0048731) were only detected for the whole population. Several metabolize-related GO:BP (e.g., heterocycle metabolic process (GO:0046483), macromolecule metabolic process (GO:0043170), and nitrogen compound metabolic process (GO:0006807)) and several GO:CC (e.g., envelope (GO:0031975), protein-containing complex (GO:0032991), and synapse (GO:0045202)) were only detected in demi color type mink. Two unique GO:MF, catalytic activity (GO:0003824) and hydrolase activity (GO:0016787), were only detected in mahogany color type mink.

5.3.2 Selection Signatures for General Resilience and Female Reproductive Performance Traits

The genome-wide distribution of selection signatures detected by F_{st} , $\theta\pi$ ratio, and XP-EHH for general resilience and female reproductive performance traits across all 14 chromosomes are presented in Figure 5.5, and the overlapped selection signatures are presented in Figure 5.6. Supplementary dataset 3 presents the SNPs detected as candidate

selection signatures by each method and the SNPs detected as candidate selection signatures by at least two methods. For general resilience trait, 569 SNPs were detected as candidate selection signatures by at least two methods, and 57 SNPs were detected as candidate selection signatures by all three methods (Figure 5.6). For female reproductive performance trait, 526 SNPs were detected as candidate selection signatures by at least two methods, and 16 SNPs were detected as candidate selection signatures by all three methods (Figure 5.6).

The candidate genes annotated from the candidate selection signatures for general resilience and female reproductive performance traits are listed in Supplementary dataset 3, and the functional classifications of candidate genes are shown in Figure 5.7. A total of 1,933 genes were annotated from the selection signatures for general resilience trait (Supplementary dataset 2). Several annotated genes were related to AD resilient traits, including growth, immune system process, pigmentation, and reproduction. The functional classifications of the annotated genes resulted in 18 GO:BP, two GO:CC, and 11 GO:MF. The annotation of selection signatures related to the female reproductive performance trait resulted in a total of 1,538 genes (Supplementary dataset 2). Except for ten genes related to reproduction, several other genes were related to some AD-resilience indicator traits, including growth, immune system process, and pigmentation. The annotated genes were classified into 18 GO:BP, two GO:CC, and 11 GO:MF.

The overrepresentations of candidate genes related to the general resilience and female reproductive performance traits are presented in Table 5.6. For general resilience trait, nine significant ($q\text{-value}<0.05$) overrepresented GO:BP were detected that were involved primarily in development, cellular process, and sensory perception of smell. In the

meantime, nine GO:CC (mostly related to organelle) and three GO:MF (related to olfactory receptor activity or binding) were significant ($q\text{-value}<0.05$) in the overrepresentation tests of candidate genes related to the general resilience. The overrepresentation tests of candidate genes from female reproductive performance traits resulted in ten significant ($q\text{-value}<0.05$) overrepresented GO:BP (mostly related to development and detection of stimulus), six significant overrepresented GO:CC (mostly related organelle), and four significant overrepresented GO:MF (related to olfactory receptor activity or binding).

5.3.3 Common Genes Among Studied Traits and KEGG Pathways

The overlapped genes among immune response, general resilience, and female reproductive performance traits are presented in Figure 5.8. In brief, 1,347, 1,680, and 1,277 unique genes were annotated from the selection signatures related to immune response, general resilience, and female reproductive performance traits, respectively. Sixteen genes, including *ARHGAP19* (chr2: 209,800,177-209,812,754 bp), *COL14A1* (chr4: 19,536,084-19,755,397 bp), *DEPTOR* (chr4: 19,803,040-19,933,557 bp), *EXOSC1* (chr2: 209,917,603-209,928,479 bp), *FAM135B* (chr4: 4,922,384-4,961,329 bp), *FRAT1* (chr2: 209,829,018-209,831,565 bp), *FRAT2* (chr2: 209,839,939-209,842,216 bp), *LOC122905718* (chr4: 5,215,903-5,216,010 bp), *MMS19* (chr2: 209,938,058-209,971,536 bp), *MRPL13* (chr4: 19,501,767-19,518,965 bp), *PGAMI* (chr2: 209,910,223-209,917,518 bp), *PTCHD4* (chr1: 94,047,590-94,230,349 bp), *RRP12* (chr2: 209,866,295-209,895,940 bp), *TBX18* (chr1: 44,912,005-44,922,875 bp), *UBTD1* (chr2: 209,972,082-210,024,677 bp), and *ZDHHC16* (chr2: 209,928,631-209,937,825 bp), were detected from all three studied traits.

The significant ($q < 0.05$) KEGG pathways of candidate genes from immune response, general resilience, and female reproductive performance traits are listed in Table 5.7. For immune response trait, only one significant ($q < 0.05$) pathway, the longevity regulating pathway, was detected. For female reproductive performance trait, one significant ($q < 0.05$) pathway, the mitogen-activated protein kinase (MAPK) signaling pathway, was detected. No significant ($q < 0.05$) KEGG pathway was detected for general resilience trait.

5.4 Discussion

The failure to control AD by culling strategy, immunoprophylaxis, and medical treatment resulted in the selection of AD-resilient mink based on the diagnostic tests or individual production performances. Although the phenotypic selection of AD-resilient mink is conducted in many AD-positive mink farms, the genomic architecture of AD resilience is still unclear, which might influence the effectiveness of selecting AD-resilient mink. In this study, genotypes from Axiom Affymetrix Mink 70K panel and three common methods (Fst, $\theta\pi$, and XP-EHH) were applied to detect the selection signatures related to immune response, general resilience, and female reproductive performance of farmed American mink under AMDV exposure. In brief, 1,611, 1,933, and 1,538 genes were annotated from the 619, 569, and 526 selection signatures detected from immune response, general resilience, and female reproductive performance traits, respectively. Although more than a thousand genes have been annotated as potential candidates for these traits, many genes, such as the identified *LOC122904335*, *LOC122905665*, and *LOC122904336* genes, were novel genes of unknown function in mink; thus, the discussions were focused on the genes with available information in the existing literature. Functional enrichment analyses revealed that some annotated genes might play an important role in the immune system

process, growth, reproduction, pigmentation, and sensory perception and detection of smell.

5.4.1 Immune Responses

A total of 1,611 genes were detected to be related to the immune response trait by considering the whole population (Supplementary dataset 2). Some of these annotated genes were found to be related to the immune system process (Figure 5.4, Tables 5.4 and 5.5). A total of 23 genes, including *CCL26*, *CD28*, *CGAS*, *DEF6*, *EPOR*, *FAS*, *FYB1*, *GGT1*, *HIC2*, *IL16*, *JAK3*, *MEIS1*, *MFAP3*, *PATZ1*, *RUNX2*, *SHFL*, *SIGLEC15*, *THEMIS*, *TNFRSF21*, *TOX*, *TREM2*, *YES1*, and *ZNF572*, were related to immune system process, which might have important roles in immune-mediated responses to AMDV infection. Three genes, including *TNFRSF21* (chr1: 93,535,621-93,549,929 bp), *CCL26* (chr4: 10,918,021-10,922,028 bp), and *TREM2* (chr1: 87,946,316-87,950,960 bp), are related to inflammatory processes (Stubbs *et al.* 2010; Santer *et al.* 2012; Liu *et al.* 2020b). This may be due to several inflammations, which include interstitial nephritis, myocarditis, hepatitis, splenitis, meningoencephalitis, pneumonia, glomerulonephritis, and arteritis, caused by AD infection (Jepsen *et al.* 2009). Four genes, *SIGLEC15* (chr3:151,209,875-151,221,497 bp), *JAK3* (chr6: 213,007,629-213,025,411 bp), *DEF6* (chr1: 117,504,375-117,525,807 bp), and *FAS* (chr2: 164,464,382-164,489,036 bp), were found to be related to autoimmune disorders in humans (Hsu *et al.* 2012; García-Bermúdez *et al.* 2015; Serwas *et al.* 2019; Läubli & Varki 2020); and AD is defined as an immune complex-mediated disorder disease in mink (Bloom *et al.* 1988). Three genes, *IL16* (chr13: 150,353,853-150,448,017 bp), *THEMIS* (chr1: 73,061,569-73,141,431 bp), and *CD28* (chr3: 15,437,373-15,465,940 bp), were found to be related to T-cell proliferation (June *et al.* 1987; Wilson *et al.* 2004; Fu *et*

al. 2009), and the *TOX* (chr4: 75,470,800-75,728,160 bp) gene was detected to be a crucial transcription factor involved in the exhaustion of CD8⁺ T cells (Seo *et al.* 2019). The detections of those genes might be related to the proliferation of CD8⁺ T cells after AD infection, as CD8⁺ T cells were found to double in numbers during the development of AD (Aasted 1989). The *EPOR* (chr6: 216,150,503-216,156,409 bp) gene was discovered to be associated with the production of red blood cells, and severe anemia was observed in AD-infected mink few months after infection (McGuire *et al.* 1979). The *FYB1* (chr1: 286,138,312-286,169,159 bp) gene was found to be related to thrombocytopenia (Levin *et al.* 2015), which is one of the typical symptoms of AD infection (Gordon *et al.* 1967). The *CGAS* (chr1: 114,736,330-114,760,223 bp) gene was related to the production of the type I interferons and activation of inflammasomes (Wang *et al.* 2017; Decout *et al.* 2021); and the increase of the number of type I interferons was observed in the host during AD infection (Jensen *et al.* 2003). In the meantime, the overrepresentation tests on the annotated genes detected one significant ($q < 0.05$) GO:BP, adaptive immune response (GO:0002250), related to immune response, where eight genes (*IL12B*, *TNFRSF21*, *TAP1*, *JAK3*, *TAP2*, *C7*, *THEMIS*, and *C6*) were involved.

The immune-response-related genes detected in this study were different from the genes detected by a previous study (Karimi *et al.* 2021a). Seven genes, including *TRAF3IP2*, *WDR7*, *SWAP70*, *TNFRSF11A*, *CBFB*, *IGF2R*, and *GPR65*, were detected and related to the immune system process by Karimi *et al.* (2021a), and none of these genes were detected in the current study. Several potential reasons could lead to these discrepancies: 1) the use of different types of genomic data (GBS in their study vs. genotypes in this study), 2) the uses of different grouping methods, where kidney lesions levels and virus loads were also

considered in grouping animals in their study in addition to antibody titer; 3) the different ways the animal contracted AMDV (intranasal inoculation in their study vs. natural exposure in this study); and 4) the color types of studied mink (only black in their study vs. multiple colors in this study).

A total of 20, 26, 19, and 9 genes were found to be related to the immune response in black, demi, mahogany, and pastel color type, respectively (Table 5.3). Most of the genes detected from a single-color type were unique from the rest of color types. For black, demi, and mahogany color types, there were few genes in common between the two color types, but no common gene was detected among all of them. For pastel, eight of nine detected genes (only *TNFRSF1B* gene was common with black color type) were unique from the rest of three darker color types, which might indicate pastel color type mink has different immune responses to AD infection compared with the other three darker color types of mink. This could be a potential reason to explain the previous finding by Ellis (Ellis 1996), where the mink with lighter color types were observed to be more susceptible to the AMDV than darker mink.

The KEGG pathway analyses of annotated genes from the whole population or different color types detected only one significant pathway, the longevity regulation pathway in mahogany color type mink. The relationship between longevity and immune response is complex. On the one hand, a strong and well-functioning immune system is crucial for protecting an organism from infections and other threats, and therefore, may contribute to increased longevity (Xia *et al.* 2019). Furthermore, chronic inflammation and overactivation of the immune system have been linked to aging and age-related diseases, which can shorten lifespan (Rea *et al.* 2018). AD is defined as an immune complex disease

and can cause persistent and chronic infection in mink (Porter & Cho 1980; Stolze & Kaaden 1987). Thus, the detection of the longevity regulation pathway may be related to chronic infection and autoimmune disorders caused by AD.

5.4.2 General Resilience

Since the general response trait used in this study was a combination of three AD resilient traits, which include growth, feeding efficiency, and pelt quality, we focused on genomic regions containing genes related to these traits. A total of 1,933 genes were detected to be related to the general resilience trait (Supplementary dataset 3). Among them, several annotated genes were related to body growth. For example, *PRKAG3* (chr3: 29,115,382-29,120,999 bp), a regulatory subunit of the AMP-activated protein kinase, was detected in this study, and found to be related to body growth in several livestock species including swine (Ryan *et al.* 2012), sheep (Ibrahim 2015), and beef cattle (Li *et al.* 2012). The *PLAG1* (chr1: 58,588,578-58,696,784 bp) gene was also detected in this study. This gene is a positive regulator of insulin-like growth factor 2 (Voz *et al.* 2000; Van Dyck *et al.* 2007) that is known to affect body weight in both livestock (e.g., swine (Van Laere *et al.* 2003) and beef cattle (Huang *et al.* 2013)) and humans (Sandhu *et al.* 2003). The *TMEM18* (chr1: 8,940,691-9,011,524 bp) gene detected in this study has been reported to be associated with growth traits and obesity in rats (Rask-Andersen *et al.* 2012), cattle (Ma *et al.* 2012), and humans (Almén *et al.* 2010; Haupt *et al.* 2010). In the meantime, three genes, *TPRA1* (chr6: 165,580,535-165,594,267 bp), *MCM2* (chr6: 165,600,097-165,621,492 bp), and *Tbx18* (chr1: 44,894,084-44,922,875 bp), which were all found to be related to embryo development in mice (Aki *et al.* 2008; Wehn & Chapman 2010; Xu *et al.* 2022), were also detected in this study indicating that AD may influence the early stages of mink

development, and therefore, influence growth. Meanwhile, several genes related to feed efficiency were also detected, for example, *MRAP2* (chr1: 45,464,087-45,513,205 bp) and *GLPIR* (chr1: 85,852,947-85,884,385 bp). *MRAP2* (Berruën & Smith 2020) and *GLPIR* (Dailey & Moran 2013) were found to play important roles in regulating appetite, and AD has been reported to cause adverse influences on the appetite of infected mink (Jensen *et al.* 2016b). The annotated gene, *HCRTR2* (chr1: 101,039,715-101,147,858 bp), is an orexin receptor and plays an important role in feeding behaviour and balance of energy metabolism (Spinazzi *et al.* 2006; Belkina & Denis 2012). In addition, several annotated genes, including *ESRRG* (chr10: 14,353,012-14,953,383 bp), *LZTFL1* (chr6: 208,512,050-208,525,767 bp), and *ELOVL4* (chr1: 49,176,236-49,208,238 bp), were reported to have key roles in regulating metabolism processes (Zhang *et al.* 2001; Alaynick *et al.* 2007; Wei *et al.* 2018). Besides the genes related to growth and feed efficiency, *DCT* gene (chr5: 151,495,518-151,529,776 bp), related to pigmentation (Guyonneau *et al.* 2004) was also detected in this study, and this might be related to the hair depigmentation, which causes single white hairs in the fur (sprinklers) impacting the pelt quality of infected mink (Farid & Ferns 2011).

5.4.3 Female Reproductive Performance

A total of 1,538 genes were detected to be found to female reproductive performance (Figure 5.7, Table 5.6). Among them, several genes, including *SLX4* (chr14: 18,318,274-18,338,014 bp), *TDRD6* (chr1: 92,984,166-92,997,290 bp), *TACR3* (chr11: 104,943,216-105,013,153 bp), *SHOC1* (chr9: 21,365,597-21,443,498 bp), *FBXW11* (chr1: 255,864,225-255,951,567 bp), *EPC2* (chr3: 82,648,215- 82,734,211 bp), *GSC* (chr13: 10,120,630-10,122,701 bp), and *DICER1* (chr3: 9,803,946-9,876,750 bp) were found to be related to

reproduction. *SLX4* (Hamer & de Rooij 2018), *TDRD6* (Vasileva *et al.* 2009), *SHOC1* (Zhang *et al.* 2019b), and *FBXW11* (O’Doherty *et al.* 2018) play important roles in the development of germ cells. The gene *TACR3* has a key role in reproductive functions, and loss-of-function mutations in this gene can lead to hypogonadotropic hypogonadism and infertility in humans (Guran *et al.* 2009; Topaloglu *et al.* 2009; Young *et al.* 2010). *EPC2*, *GSC*, and *DICER1* genes are all important for development of early embryos in animals and have been related to the reproduction traits (e.g., litter size) in swine and cattle (Kaczmarek *et al.* 2020; Chen *et al.* 2022a; Chen *et al.* 2022b; Wang *et al.* 2022). The reproduction-related genes detected in this study were different from the genes detected in the signatures selection study for response to Aleutian disease by Karimi *et al.* (2021a). In that study, the genes *FBXO5*, *CATSPER4*, *GOT2*, and *CatSper β* were annotated from the candidate selection regions and related to reproductive performance, which were not detected in our study. The different genomic data, grouping methods, and population structures could be the potential reasons that lead to the differences between these studies. The KEGG pathway analyses of annotated genes detected only one significant ($q < 0.05$) pathway, the MAPK signaling pathway. The MAPK signaling pathway is involved in female reproductive performance by regulating the proliferation, differentiation, and apoptosis of granulosa cells in the follicle, ultimately affecting folliculogenesis and oocyte maturation (Zhang & Liu 2002; Sun *et al.* 2016; Huang *et al.* 2022). The MAPK pathway also plays a role in regulating luteinizing hormone secretion, which stimulates ovulation and formation of the corpus luteum (Kahnamouyi *et al.* 2018). Additionally, MAPK signaling has been implicated in regulating the menstrual cycle and endometrial function (Zhou *et al.* 2010; Makieva *et al.* 2018). In the meantime, previous studies found that

abnormal MAPK signaling can cause reproductive disorders (e.g., infertility and embryonic death) in swine (Prochazka *et al.* 2012; Prochazka & Nemcova 2019) and cattle (Sigdel *et al.* 2021; Tahir *et al.* 2021). The detection of the MAPK signaling pathway in this study may indicate that AD infection may lead to the disorder of the MAPK signaling pathway, therefore influencing female reproductive performance.

5.4.4 Common Genes and Ontology Terms Among All Three Traits

A total of 16 genes, *ARHGAP19*, *COL14A1*, *DEPTOR*, *EXOSC1*, *FAM135B*, *FRAT1*, *FRAT2*, *LOC122905718*, *MMS19*, *MRPL13*, *PGAM1*, *PTCHD4*, *RRP12*, *TBX18*, *UBTD1*, and *ZDHHC16*, were common to all three studied traits. Among them, five genes were found to be related to growth in livestock species in previous studies. For example, the gene *ARHGAP19* was found to be related to body weight in yak (Jiang *et al.* 2022), the gene *FAM135B* was related to body weight growth in cattle (Serão *et al.* 2013; Seabury *et al.* 2017), the genes *COL14A1* (Cardoso *et al.* 2018) and *PTCHD4* (Doyle *et al.* 2020) were found to play important roles in muscle development in cattle, in swine the gene *EXOSC1* (Ropka-Molik *et al.* 2018; Dall'Olio *et al.* 2020) has been related to muscle growth, and *PGAM1* was found to relate to the development of adipose tissue (Xing *et al.* 2019). Meanwhile, two genes, *FAM135B* (Serão *et al.* 2013; Seabury *et al.* 2017) and *COL14A1* (de Lima *et al.* 2020), were also found to be related to feed efficiency in cattle. In addition, several genes were found to be related to reproduction in previous studies. *UBTD1* (Kongmanas *et al.* 2015), *ZDHHC16* (Uzbekova *et al.* 2021; Caetano *et al.* 2023), *RRP12* (Tiensuu *et al.* 2019), *MMS19* (Tsai *et al.* 2017), and *PGAM1* (Zhang *et al.* 2015) genes were found to be associated with the development of germ cells. The genes *FAM135B* and *FRAT1* were detected to be associated with the reproductive performance in swine (Zhang

et al. 2019c) and cows (Melo *et al.* 2017), respectively. The *Tbx18* gene was related to mice embryo development (Wehn & Chapman 2010).

Two GO terms, olfactory receptor activity (GO:0004984) and detection of chemical stimulus involved in sensory perception of smell (GO:0050911), were significant ($q < 0.05$) among all three studied traits. This may indicate that AD may influence sense of smell in mink although the relationship between AD and smell has not been reported in the literature. However, reduced appetite of infected mink seems to corroborate the loss of their sense of smell because the smell is vital for mink feeding behavior (Saunders 1988). In American mink, Adney *et al.* (Adney *et al.* 2022) speculated that individuals experimentally infected with SARS-CoV-2 may have altered sense of smell because they observed neutrophilic infiltrate in the olfactory epithelium. Thus, future studies could assess the condition of the olfactory epithelium of AD-infected mink to determine if infection could influence their sense of smell.

5.5 Conclusion

The detection of potential signatures of selection related to the response of American mink to AD using three common approaches (Fst, $\theta\pi$, and XP-EHH) provides valuable insights into the genetic factors associated with the mink's immune response. The genes annotated from the candidate selection signatures were involved in immune system process, growth, reproduction, and pigmentation, all of which were associated with previously reported traits influenced by AD, including body weight, female reproductive performance, and pelt quality. In addition, the two significant olfactory-related GO terms indicated that the AD infection might cause loss of smell in mink, but a future study is encouraged to validate this conjecture by assessing the sense of smell of AD-infected individuals. Mink of

different color types were found to have different immune responses to AD infection based on the genes detected between them. In the meantime, mink of pastel color type seemed to have unique immune responses to AD infection compared with the minks of other three darker color types based on the common genes among all of the color types studied; however, future studies with more equal sample size in each color type and wider ranges of color types are needed to further investigate the potential different immune responses among mink of different color types.

The detection of numerous potential loci underlying the selection for responses to AD infection in this thesis chapter indicated that genomic selection could be a feasible approach to reduce the formation of infectious immune complexes and the adverse influence caused by AD on growth, reproduction, and pelt quality. By incorporating the detected loci with the availability of the first Axiom Affymetrix Mink 70K panel, the mink industry could eradicate the adverse influences caused by AD by increasing the resilience of American mink to AD infection through genomic selection.

Table 5.1 The number of individuals from different color types of each subgroup in different Aleutian disease tests and the final dataset for detecting selection signatures for immune response to Aleutian mink disease virus infection in American mink.

Color types	ELISA-G ¹ (0-7)		CIEP ²		Immune response ³	
	Negative (0)	Positive (5-7)	Negative	Positive	Low	High
Black	67	23	12	78	10	19
Demi	264	57	87	329	70	51
Mahogany	244	40	50	258	39	37
Pastel	42	31	14	70	11	25
Stardust	5	3	1	8	1*	1*
All	622	154	164	743	131	133

¹ELISA-G = AMDV-G based enzyme-linked immunosorbent assay test; ²CIEP = Counterimmunoelectrophoresis test; ³The individuals were used in the final dataset for detecting selection signatures for immune response to Aleutian mink disease virus infection.

* No independent analysis was conducted for stardust color type individuals due to the small sample size.

Table 5.2 The number of individuals with positive counterimmunoelectrophoresis test results in each subgroup of feed conversion ratio, Kleiber ratio, live pelt quality, general resilience performance, and female reproductive performance traits.

Feed conversion ratio		Kleiber ratio		Pelt quality		General resilience performance ¹		Female reproductive performance ²	
Bottom 20% (14.38-22.49)	Top 20% (41.46-72.28)	Bottom 20% (2.19-4.41)	Top 20% (7.14-9.17)	Score 1	Score 3	Resilient	Susceptible	Low litter size (1-4)	High litter size (9-11)
78	78	78	78	83	120	19	11	20	16

¹ The evaluation of individual general resilience performance based on feed conversion ratio, Kleiber ratio, and pelt quality.

² The measurement of female reproduction performance resilience (dams with positive counterimmunoelectrophoresis test only) based on the number of kits alive 24h after birth.

Table 5.3 Immune response related genes annotated from the selection signatures detected from different color types.

Color type	Genes
Black	<i>ANKRD17, CEBPA, CTSH, CXCL6, CXCL8, FYB1, GAL, HAVCRI, IL1A, IL1F10, IL1RN, IL36RN, ITK, MARCHF1, MTURN, PATZ1, SIGLEC15, TMEM178A, TNFRSF1B, UBASH3A</i>
Demi	<i>C4A, CACTIN, CCL26, CCR9, CEBPA, CGAS, CTLA4, CXCR6, DEF6, FYN, HIC2, HSPD1, MPIG6B, NFAM1, RUNX1, RUNX2, SH2B2, SHFL, TNFRSF21, TRAF3IP2, TYK2, VEGFA, XCRI, YES1, ZBTB12, ZBTB37</i>
Mahogany	<i>ANKRD17, C4A, CASP3, CXCL6, CXCL8, EPOR, FYB2, HSPD1, MEIS1, MPIG6B, NFAM1, PLA2G2D, PLA2G2F, PLA2G5, RAG2, REL, TNFRSF11A, TNFRSF13C, ZBTB12</i>
Pastel	<i>AKIRINI, BANK1, BCL10, UBASH3A, FGR, LPXN, SEC14L1, THEMIS2, TNFRSF1B</i>

Table 5.4 Significant (q-value<0.05) biological processes detected from overrepresentation tests of candidate genes from the whole studied population and different color types of mink for immune response trait.

Biological process (GO ID)	All	Black	Demi	Mahogany	Pastel
Adaptive immune response (GO:0002250)	*	-	-	-	-
Anatomical structure development (GO:0048856)	*	-	*	*	*
Anatomical structure morphogenesis (GO:0009653)	*	-	-	*	-
Bicellular tight junction assembly (GO:0070830)	-	-	*	-	-
Cell development (GO:0048468)	*	-	*	*	-
Cell differentiation (GO:0030154)	*	-	*	*	-
Cellular aromatic compound metabolic process (GO:0006725)	-	-	*	-	-
Cellular component morphogenesis (GO:0032989)	-	-	-	*	-
Cellular component organization (GO:0016043)	-	-	*	*	-
Cellular component organization or biogenesis (GO:0071840)	-	-	*	*	-
Cellular developmental process (GO:0048869)	*	-	*	*	-
Cellular metabolic process (GO:0044237)	-	-	*	-	-
Cellular nitrogen compound metabolic process (GO:0034641)	-	-	*	-	-
Detection of chemical stimulus (GO:0009593)	*	*	*	-	*
Detection of chemical stimulus involved in sensory perception (GO:0050907)	*	*	*	-	*
Detection of chemical stimulus involved in sensory perception of smell (GO:0050911)	*	*	*	*	*
Detection of stimulus (GO:0051606)	*	-	-	-	-
Detection of stimulus involved in sensory perception (GO:0050906)	*	*	-	-	-
Developmental process (GO:0032502)	*	-	*	*	-
Heterocycle metabolic process (GO:0046483)	-	-	*	-	-
Macromolecule metabolic process (GO:0043170)	-	-	*	-	-
Metabolic process (GO:0008152)	-	-	*	-	-
Mitochondrial gene expression (GO:0140053)	-	-	*	-	-

Table 5.4 Continuous.

Biological process (GO ID)	All	Black	Demi	Mahogany	Pastel
Multicellular organism development (GO:0007275)	*	-	-	*	*
Multicellular organismal process (GO:0032501)	*	-	-	-	-
Nitrogen compound metabolic process (GO:0006807)	-	-	*	-	-
Nucleobase-containing compound metabolic process (GO:0006139)	-	-	*	-	-
Organelle organization (GO:0006996)	-	-	-	*	-
Organic substance metabolic process (GO:0071704)	-	-	*	*	-
Positive regulation of multicellular organismal process (GO:0051240)	-	-	-	-	*
Primary metabolic process (GO:0044238)	-	-	*	*	-
Regulation of multicellular organismal process (GO:0051239)	-	-	-	-	*
Sensory perception of chemical stimulus (GO:0007606)	*	*	*	-	*
Sensory perception of smell (GO:0007608)	*	*	*	*	*
Small molecule catabolic process (GO:0044282)	-	*	-	-	-
System development (GO:0048731)	*	-	-	-	-
Tight junction organization (GO:0120193)	-	-	*	-	-

* The biological process was detected in this color type/population.

- The biological process was not detected in this color type/population.

Table 5.5 Significant (q-value<0.05) cellular components and molecular functions detected from overrepresentation tests of candidate genes from the whole studied population and different color types of mink for immune response trait.

Functional enrichment items	All	Black	Demi	Mahogany	Pastel
Cellular component (GO ID)					
Bicellular tight junction (GO:0005923)	-	-	*	-	-
Cell junction (GO:0030054)	*	-	*	-	-
Cellular anatomical entity (GO:0110165)	-	*	*	-	*
Collagen type IV trimer (GO:0005587)	-	-	-	-	*
Cytoplasm (GO:0005737)	*	*	*	*	*
Cytosol (GO:0005829)	-	*	*	-	-
Endomembrane system (GO:0012505)	-	-	-	-	*
Envelope (GO:0031975)	-	-	*	-	-
Intracellular anatomical structure (GO:0005622)	*	*	*	*	*
Intracellular membrane-bounded organelle (GO:0043231)	-	*	*	*	-
Intracellular organelle (GO:0043229)	-	*	*	*	*
Intracellular organelle lumen (GO:0070013)	-	-	*	-	-
Membrane-bounded organelle (GO:0043227)	-	*	*	*	*
Membrane-enclosed lumen (GO:0031974)	-	-	*	-	-
Mitochondrial matrix (GO:0005759)	-	-	*	-	-
Mitochondrion (GO:0005739)	-	-	*	-	-
Organelle (GO:0043226)	*	*	*	*	*
Organelle envelope (GO:0031967)	-	-	*	-	-
Organelle lumen (GO:0043233)	-	-	*	-	-
Protein-containing complex (GO:0032991)	-	-	*	-	-
Synapse (GO:0045202)	-	-	*	-	-

Table 5.5 Continuous.

Functional enrichment items	All	Black	Demi	Mahogany	Pastel
Tight junction (GO:0070160)	-	-	*	-	-
Molecular function (GO ID)					
Actin binding (GO:0003779)	*	-	-	-	-
Binding (GO:0005488)	*	*	*	*	-
Catalytic activity (GO:0003824)	-	-	-	*	-
Hydrolase activity (GO:0016787)	-	-	-	*	-
Identical protein binding (GO:0042802)	-	-	*	-	-
Olfactory receptor activity (GO:0004984)	*	*	*	*	*
Protein binding (GO:0005515)	*	*	*	*	-
Protein-containing complex binding (GO:0044877)	*	-	-	-	-
RNA binding (GO:0003723)	-	-	*	-	-
RNA polymerase II-specific DNA-binding transcription factor binding (GO:0061629)	*	-	-	-	-

* The cellular component or molecular function was detected in this color type/population.

- The cellular component or molecular function was not detected in this color type/population

Table 5.6 Significant (q-value<0.05) biological processes, cellular components, and molecular functions detected from overrepresentation tests of candidate genes for general resilience and female reproductive performance traits.

Trait	Term (GO ID)	Annotation set	
General resilience	Anatomical structure morphogenesis (GO:0009653)	Biological process	
	Cell migration (GO:0016477)	Biological process	
	Cell motility (GO:0048870)	Biological process	
	Cellular process (GO:0009987)	Biological process	
	Chemotaxis (GO:0006935)	Biological process	
	Detection of chemical stimulus involved in sensory perception of smell (GO:0050911)	Biological process	
	Locomotion (GO:0040011)	Biological process	
	Sensory perception of smell (GO:0007608)	Biological process	
	Taxis (GO:0042330)	Biological process	
	Cell projection (GO:0042995)	Cellular component	
	Cellular anatomical entity (GO:0110165)	Cellular component	
	Cytoplasm (GO:0005737)	Cellular component	
	Intracellular anatomical structure (GO:0005622)	Cellular component	
	Intracellular membrane-bounded organelle (GO:0043231)	Cellular component	
	Intracellular organelle (GO:0043229)	Cellular component	
	Membrane-bounded organelle (GO:0043227)	Cellular component	
	Organelle (GO:0043226)	Cellular component	
	Plasma membrane bounded cell projection (GO:0120025)	Cellular component	
	Binding (GO:0005488)	Molecular function	
	Olfactory receptor activity (GO:0004984)	Molecular function	
	Protein binding (GO:0005515)	Molecular function	
	Female reproductive performance	Adaptive immune response (GO:0002250)	Biological process
		Anatomical structure development (GO:0048856)	Biological process
Cellular process (GO:0009987)		Biological process	
	Detection of chemical stimulus (GO:0009593)	Biological process	

Table 5.6 Continuous.

Trait	Term (GO ID)	Annotation set
Female reproductive performance	Detection of chemical stimulus involved in sensory perception (GO:0050907)	Biological process
	Detection of chemical stimulus involved in sensory perception of smell (GO:0050911)	Biological process
	Developmental process (GO:0032502)	Biological process
	Protein metabolic process (GO:0019538)	Biological process
	Sensory perception of chemical stimulus (GO:0007606)	Biological process
	Sensory perception of smell (GO:0007608)	Biological process
	Cellular anatomical entity (GO:0110165)	Cellular component
	Cytoplasm (GO:0005737)	Cellular component
	Intracellular anatomical structure (GO:0005622)	Cellular component
	Intracellular membrane-bounded organelle (GO:0043231)	Cellular component
	Membrane-bounded organelle (GO:0043227)	Cellular component
	Organelle (GO:0043226)	Cellular component
	Binding (GO:0005488)	Molecular function
	Olfactory receptor activity (GO:0004984)	Molecular function
	Protein binding (GO:0005515)	Molecular function
Protein-arginine deiminase activity (GO:0004668)	Molecular function	

Table 5.7 Significantly (q-value<0.05) presented Kyoto Encyclopaedia of Genes and Genomes (KEGG) pathways of genes detected from signatures selection analyses of the immune response, general resilience, and female reproductive performance traits.

Trait	Pathway	Genes	q-value
Immune response (Mahogany color type mink only)	Longevity regulating pathway	<i>AKT3, ATF6B, CAMK4, CAT, CREB5, EHMT2, IGF1R, IRS1, PRKAA1, PRKAA2, RPTOR, SOD2</i>	0.049
Female reproductive performance	MAPK signaling pathway	<i>AKT3, ATF2, BRAF, CACNB1, CACNB4, CASP3, DUSP3, DUSP6, EGF, ERBB4, FGF17, FGF18, FGFR2, FLNB, IKBKB, KIT, KITLG, MAP2K5, MAP3K11, MAP3K2, MYC, NFKB1, PDGFRA, PPP3CA, PPP3CC, RELA, STK3</i>	0.015

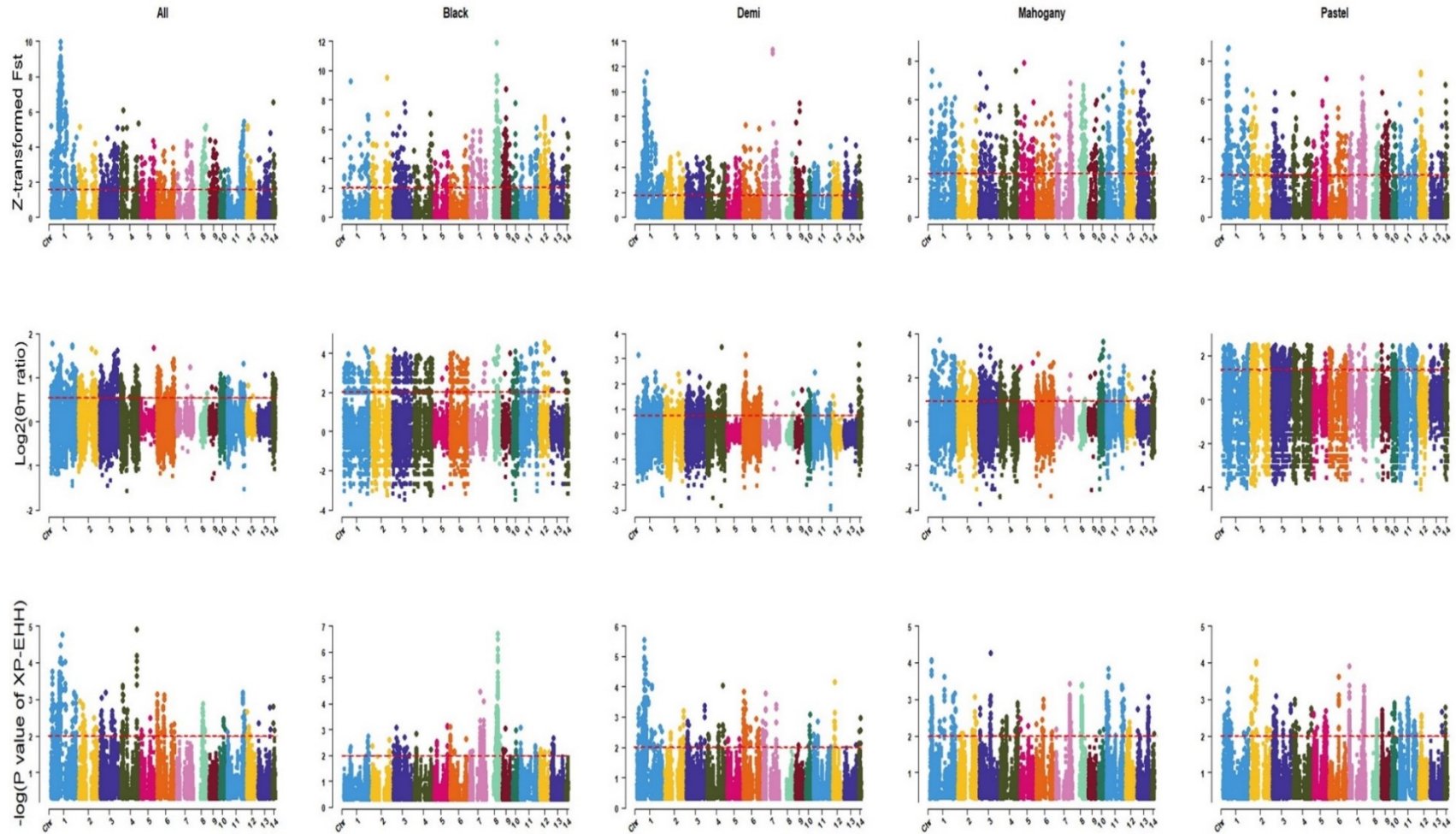


Figure 5.1 Genome-wide distribution of selection signatures for immune response trait detected by Fst (Z-transformed), nucleotide diversity ($\theta\pi$ ratio), and XP-EHH across all autosomes in the whole population (All) and different color types (Black, Demi, Mahogany, and Pastel) individuals. The red lines of Z-transformed Fst and $\log_2(\theta\pi$ ratio) plots display the threshold levels of 5%. The red lines of XP-EHH plots display the threshold levels of $-\log(p\text{-value}) > 2$.

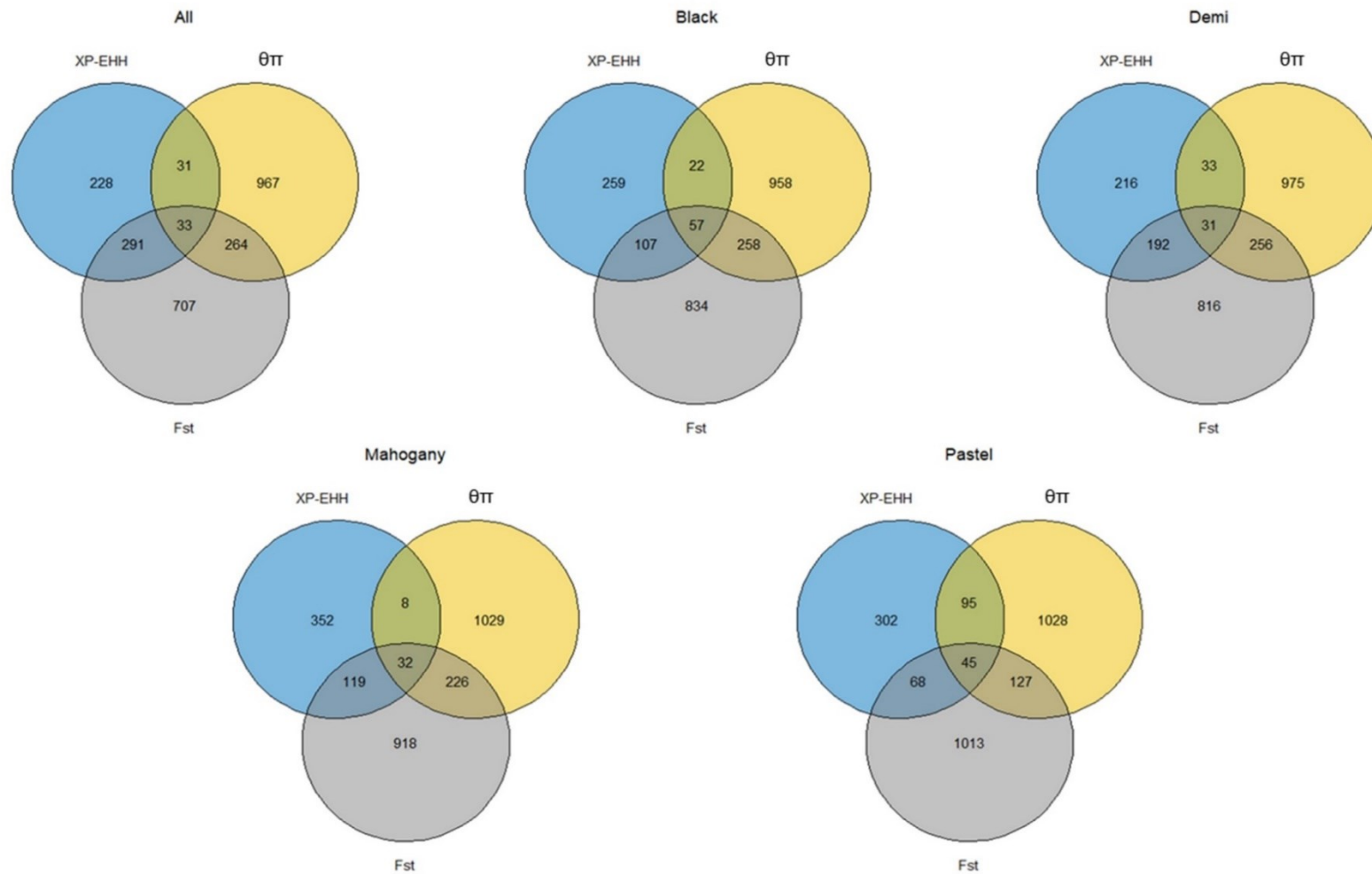


Figure 5.2 The overlapped selection signatures detected in the whole population (All) and different color types (Black, Demi, Mahogany, and Pastel) individuals among pairwise fixation index (Fst, top 5%), nucleotide diversity ($\theta\pi$, top 5%), and cross-population extended haplotype homozygosity (XP-EHH, $-\log(p\text{-value}) > 2$) tests for immune response trait.

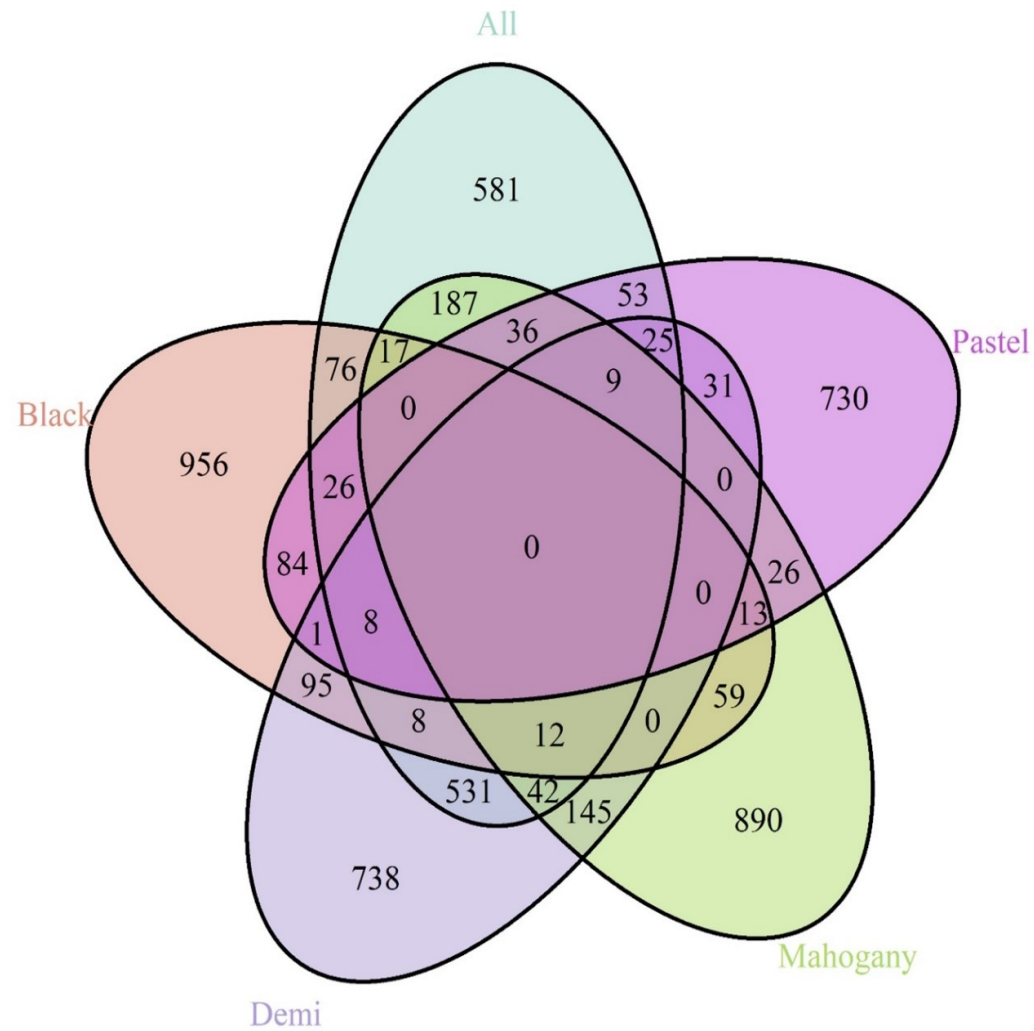


Figure 5.3 The Venn diagram shows the genes overlapping among the whole population (All) and different color types (Black, Demi, Mahogany, and Pastel) for immune response trait.

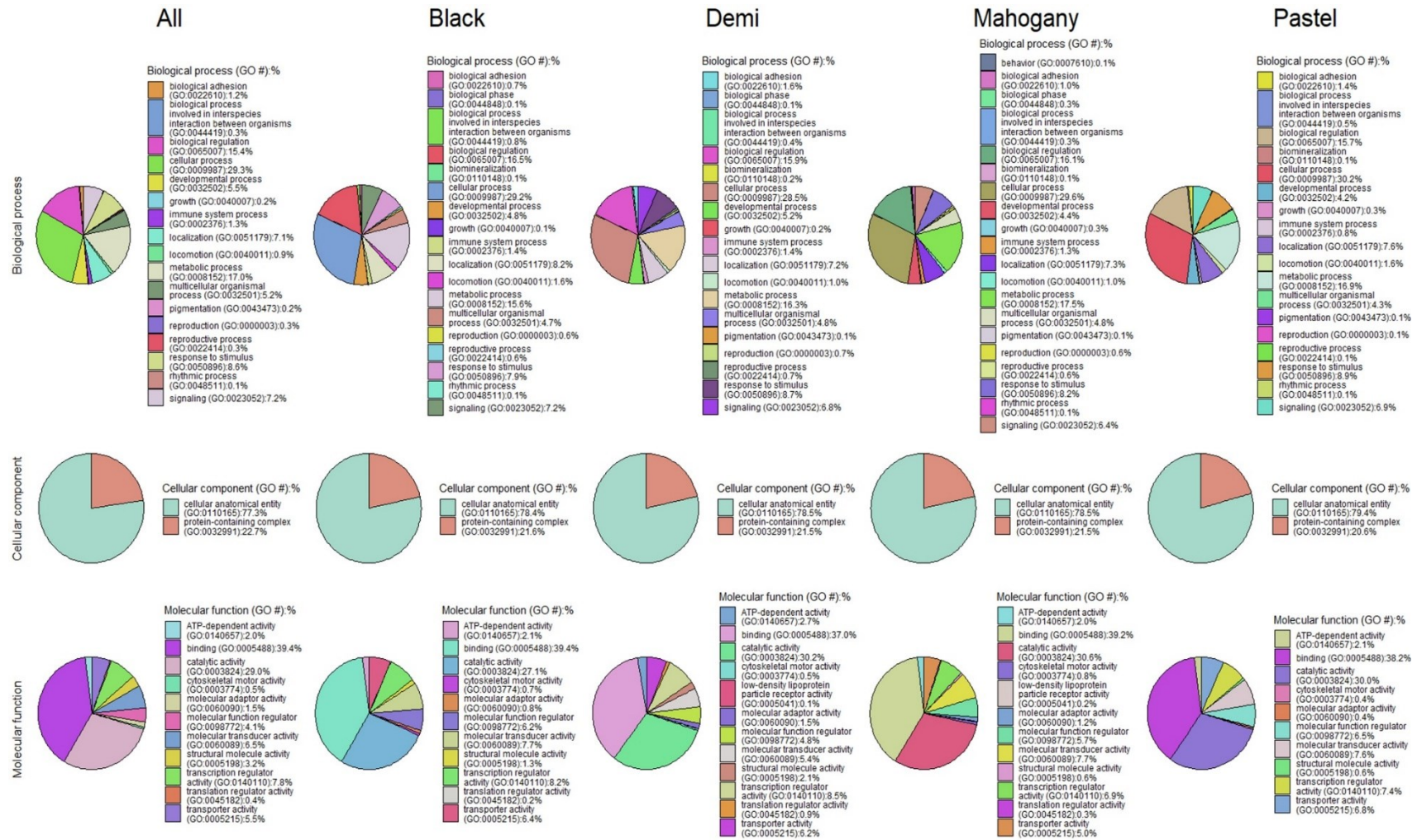


Figure 5.4 The pie charts of functional classifications (including biology process, cellular component, and molecular function) of candidate genes under selection pressure in the whole population (All) and different color types (Black, Demi, Mahogany, and Pastel) individuals for immune response trait.

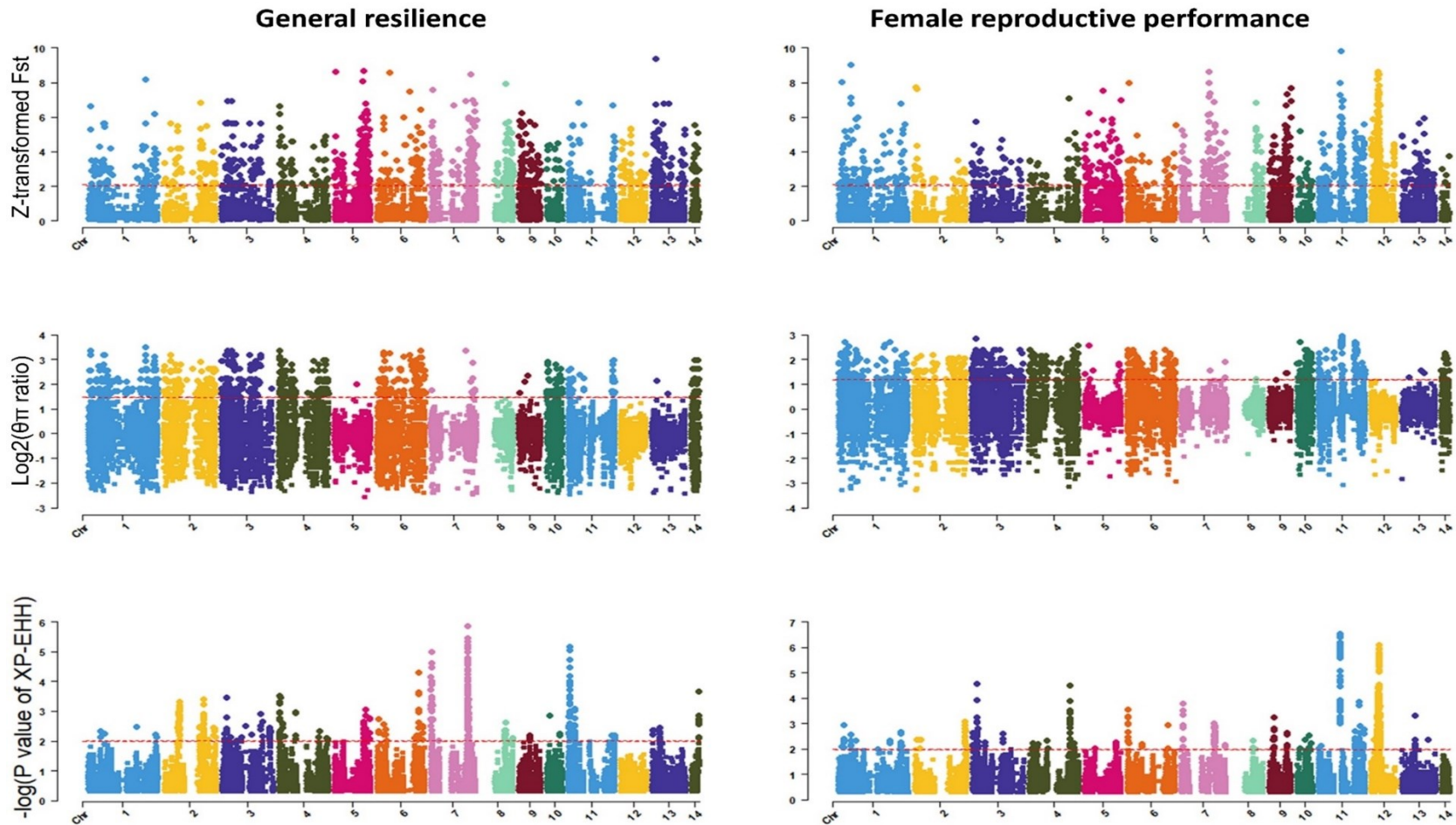


Figure 5.5 Genome-wide distribution of selection signatures for general resilience and female reproductive performance traits detected by F_{st} (Z-transformed), nucleotide diversity ($\theta\pi$ ratio), and XP-EHH across all autosomes from the whole population. The red lines of Z-transformed F_{st} and $\log_2(\theta\pi$ ratio) plots display the threshold levels of 5%. The red lines of XP-EHH plots display the threshold levels of $-\log(p\text{-value}) > 2$.

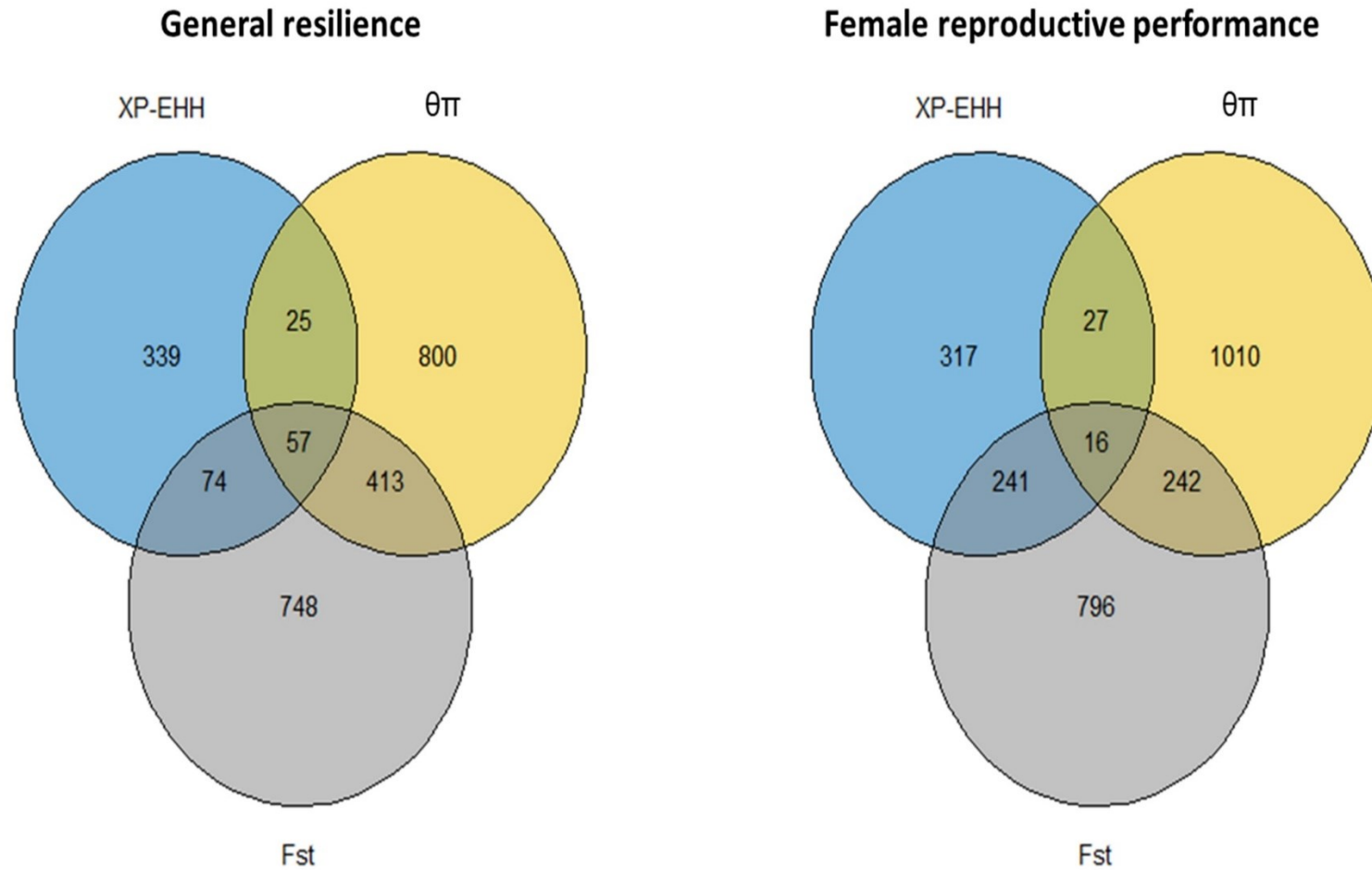


Figure 5.6 The overlapped selection signatures detected from the whole population individuals among pairwise fixation index (F_{st} , top 5%), nucleotide diversity ($\theta\pi$, top 5%), and cross-population extended haplotype homozygosity (XP-EHH, $-\log(p\text{-value}) > 2$) tests for general resilience and female reproductive performance traits.

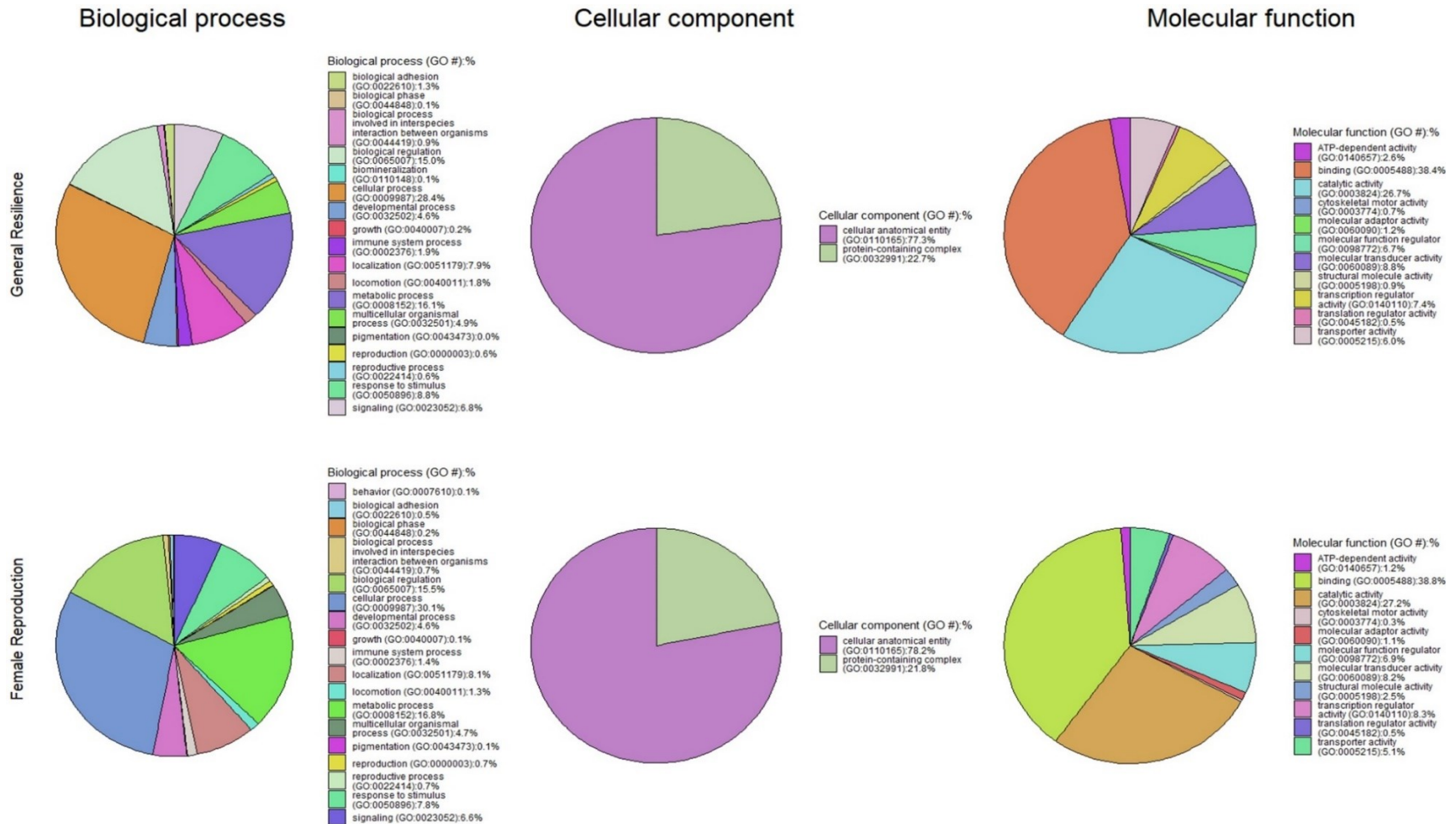


Figure 5.7 The pie charts of functional classifications (including biology process, cellular component, and molecular function) of candidate genes under selection pressure in the whole population individuals for general resilience and female reproductive performance traits.

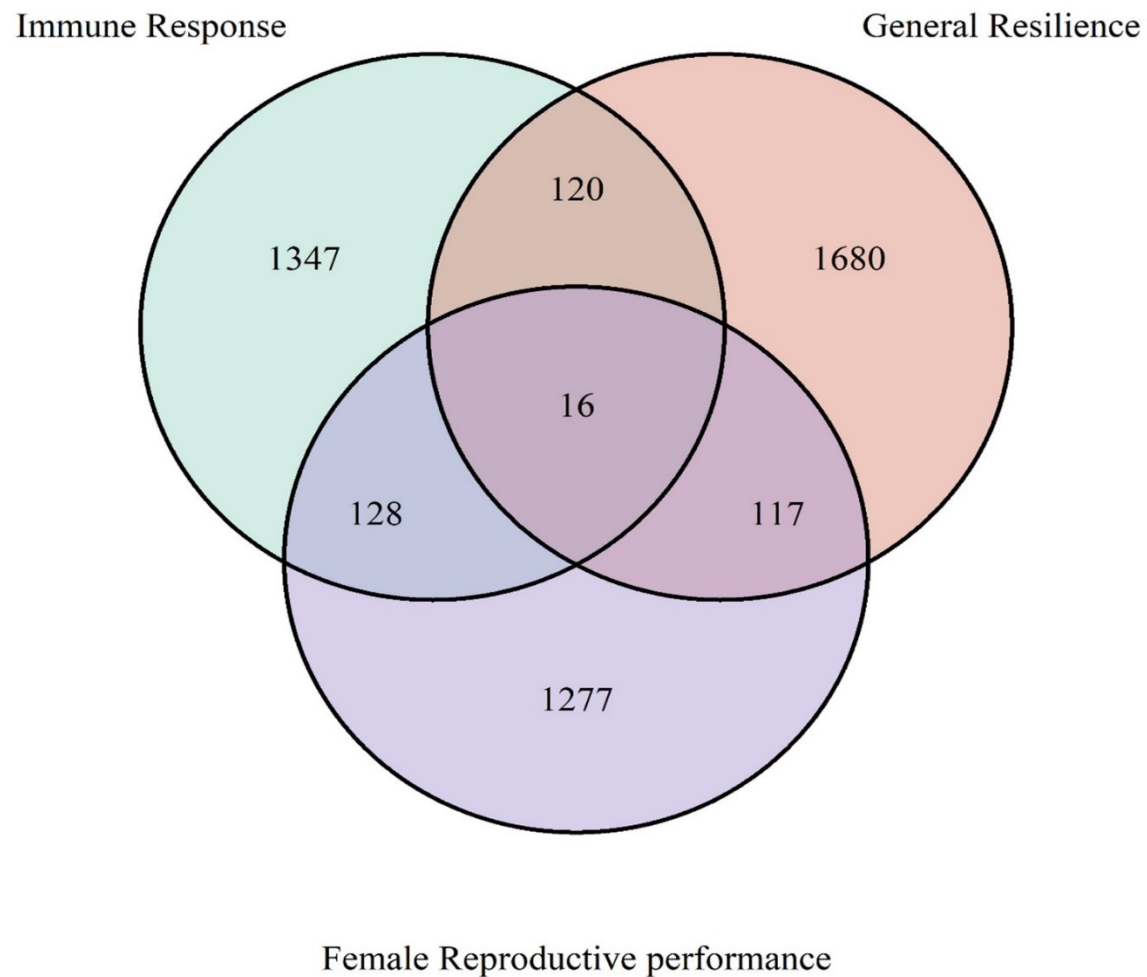


Figure 5.8 The overlapped genes among immune response, general resilience, and female reproductive performance traits. The common 16 genes among all traits were *ARHGAP19*, *COL14A1*, *DEPTOR*, *EXOSC1*, *FAM135B*, *FRAT1*, *FRAT2*, *LOC122905718*, *MMS19*, *MRPL13*, *PGAM1*, *PTCHD4*, *RRP12*, *TBX18*, *UBTD1*, *ZDHHC16*.

CHAPTER 6. Genome-wide Association Studies for Immune Response and Resilience to Aleutian Disease in Mink¹

6.1 Introduction

Aleutian disease (AD) is one of the most challenging mink diseases causing high mortality and affects several economically important traits, including body weight growth (Porter *et al.* 1982), feed intake (Elzhov *et al.* 2016; Jensen *et al.* 2016b), pelt quality (Farid & Ferns 2011), and female reproductive performance (Henson *et al.* 1962; Reichert & Kostro 2014). The Aleutian mink disease virus (AMDV) was identified as the causative agent of AD, which has been characterized as an immune complex disease due to the inability of the antibodies against AMDV to neutralize the virus effectively. As a result, the antibodies form complexes with the virus, leading to glomerular and arterial damage in mink (Porter *et al.* 1969; Cho & Ingram 1973; Porter *et al.* 1973; Stolze & Kaaden 1987). Thus, the higher the levels of anti-AMDV antibodies produced, the more severe the infection caused by AD (Porter *et al.* 1972; Kanno *et al.* 1993; Bloom *et al.* 1994; Aasted *et al.* 1998; Bloom *et al.* 2001). The inability of vaccination, medication, and culling tactics to control AD has compelled mink farmers to manage the disease by selecting AD-resistant mink based on

¹ A version of this Chapter will be submitted to the BMC Genomics by Hu *et al.* 2024. Genome-wide Association Studies for Immune Response and Resilience to Aleutian Disease in Mink.

immune response, which is measured by AD tests, and/or some AD-resilience indicator traits.

Disease resilience is an ability of an animal to mitigate the effects of disruptions and to maintain its performance under pathogen exposure (Albers *et al.* 1987; Bisset & Morris 1996). Immune response, growth, feed intake, and female reproductive performance were suggested as AD-resilience indicator traits (Hu *et al.* 2021; Hu *et al.* 2022). Several mink farms in the Canadian province of Nova Scotia select AD-resilient mink based on the productive performance and the iodine agglutination test (IAT), which measures the level of gamma globulin (Farid & Ferns 2017). More recently, some AD-positive mink farms in North America and Europe utilized enzyme-linked immunosorbent assay tests (ELISA), which quantify the antibody levels against AMDV, to select AD-resilient mink (Knuuttila *et al.* 2009; Farid & Rupasinghe 2016; Farid *et al.* 2018). Although the phenotypic selection of AD-resilient mink is conducted by some mink farms, the genetic architecture of AD resilience has not been widely explored.

Immune response and disease resilience traits are usually quantitative traits with complex genetic architectures (VanRaden 2008; Leach *et al.* 2010; Thompson-Crispi *et al.* 2014; Hu *et al.* 2020; Doeschl-Wilson *et al.* 2021). In recent years, with the development of next-generation sequencing technologies, high-density SNP arrays, and bioinformatic tools, genome-wide association studies (GWAS) have become increasingly popular for detecting genetic variants and genes associated with immune response and disease resilience traits in livestock. For example, in swine, several SNPs and genes were found to be related to the resilience to porcine reproductive and respiratory syndrome (Boddicker *et al.* 2014; Yang *et al.* 2016; Hickmann *et al.* 2021), *Mycoplasma hyopneumoniae* (Uemoto *et al.*

2021), and polymicrobial disease (Cheng *et al.* 2022) using GWAS. In cattle, several studies conducted GWAS and found several SNPs and genes associated with resilience to paratuberculosis (Alonso-Hearn *et al.* 2022). In poultry, Psifidi *et al.* (Psifidi *et al.* 2016) conducted GWAS to find the SNPs and genes associated with the immune response to four infectious diseases (infectious bursal disease, Marek's disease, fowl typhoid, and fowl cholera) and resistance to *Eimeria* and cestode parasitism. However, no GWAS on mink immune response to AD and AD-resilience indicator traits has been conducted using genotype data. Therefore, the objective of this thesis chapter was to conduct GWAS to identify genomic regions and genes associated with immune response and feed-intake-related resilience to AD in mink.

6.2 Materials and Methods

6.2.1 Ethics approval

This study was approved by the Dalhousie University Animal Care and Use Committee. All mink used in this study were farmed following the Code of Practice for the Care and Handling of Farmed Mink guidelines from the Canada Mink Breeders Association (Turner P *et al.* 2013).

6.2.2 Animals and Phenotypes

In total, 1,411 mink from the Canadian Centre for Fur Animal Research (CCFAR) at Dalhousie University, Faculty of Agriculture (Truro, Nova Scotia, Canada) from 2015 to 2020 were used. No persistent breeding program was employed in CCFAR during the study years (2013 to 2021). In 2013, an AD epidemic occurred at CCFAR whose exact origin could not be determined with certainty. However, the contamination of feed with AMDV

and contact with wild animals carrying AMDV were speculated to be the most probable reasons for the outbreak.

The immune response of the studied mink to AD virus exposure was evaluated using two types of tests: antigen-based ELISA (ELISA-G) and IAT. These tests were performed according to established protocols described by Hu et al. (2021). Blood samples from the mink were annually collected in mid-November prior to selecting breeders and in mid-February before mating from 2015 to 2020. The blood samples were sent to Middleton Veterinary Services (Nova Scotia, Canada) for ELISA-G testing. The ELISA-G tests measured antibody levels against AMDV through optical density, with results falling into eight categories scored in 1-point increments from 0 (none or extremely low) to 7 (extremely high). The IAT tests were performed at CCFAR to evaluate the serum gamma globulin level in the serum, and the results were classified into four categories ranging from 0 (low) to 4 (high).

This study utilized established procedures outlined by Davoudi et al. (2022) to obtain data on feed intake of the examined mink. Specifically, individuals were reared in separate cages, and feed was distributed daily to cages. The daily feed intake (DFI) was determined by subtracting the amount of feed remaining from the total provided. Two measures of feed intake, namely day-to-day variation in feed intake (Varf) and proportion of off-feed days (DOF), were computed using the DFI data for each mink according to the methodology detailed by Putz et al. (2019). The Varf was quantified by taking the root mean square error of within-individual regression of DFI on day via ordinary least squares linear regression. The off-feed days were identified by utilizing a 5% quantile regression of DFI on age (in days) for all mink, and negative residuals below the regression line were deemed off-feed

days for each mink. Finally, the DOF was determined as the proportion of off-feed days to the total number of days on which DFI was recorded.

6.2.3 Sample Collection and Genotyping

Tongue tissue samples were obtained from the studied animals prior to pelting. The DNA from the tongue tissue was extracted using the DNeasy Blood and Tissue Kit (Qiagen, Hilden, Germany) in accordance with the manufacturer's instructions. The quality and quantity of the extracted DNA were evaluated using a NanoDrop ND-1000 spectrophotometer (NanoDrop Technologies Inc., Wilmington, DE). The 260/280 nm readings for all samples were between 1.7 and 2.0. The final concentration of all samples was 20 ng, and genotyping was performed using the Axiom Affymetrix Mink 70K panel (Neogen, Lincoln, Nebraska, USA) (Do *et al.* 2024).

6.2.4 Estimation of Breeding Values and De-regressed Breeding Values

The estimated breeding values (EBV) for ELISA-G, IAT, DOF, and Varf traits were obtained from the study by Hu *et al.* (2022). The study employed a univariate animal model utilizing ASReml 4.1 software (Gilmour *et al.* 2018) to estimate the variance components of individual traits attributable to random additive genetic effects, permanent environmental effects, and maternal genetic effects. The model was as follows:

$$\mathbf{y} = \mathbf{X}\mathbf{b} + \mathbf{Z}\mathbf{a} + \mathbf{W}\mathbf{pe} + \mathbf{G}\mathbf{m} + \mathbf{e},$$

where \mathbf{y} is the vector of phenotypes; \mathbf{X} , \mathbf{Z} , \mathbf{W} , and \mathbf{G} are the incidence matrices relating phenotypes to fixed, random additive genetic, random permanent environmental, and random maternal genetic effects, respectively; \mathbf{b} is the vector of fixed effects; \mathbf{a} is the vector of random additive genetic effects, with $\mathbf{a} \sim N(0, \mathbf{A}\sigma_a^2)$, where \mathbf{A} is the numerator relationship matrix, and σ_a^2 is the additive genetic variance; \mathbf{pe} is the vector of random

permanent environmental effects, with $\mathbf{pe} \sim N(0, \mathbf{I}\sigma_{pe}^2)$, where \mathbf{I} is an identity matrix, and σ_{pe}^2 is the permanent environmental variance; \mathbf{m} is the vector of random maternal genetic effects, with $\mathbf{m} \sim N(0, \mathbf{A}\sigma_m^2)$, where σ_m^2 is the maternal genetic variance; and \mathbf{e} is the vector of residual effects, with $\mathbf{e} \sim N(0, \mathbf{I}\sigma_e^2)$, where σ_e^2 is the residual variance. Subsequently, the de-regressed EBVs (dEBVs) were obtained with the formula:

$$dEBV = \frac{g_i}{r_i^2},$$

where g_i is the EBV of the i^{th} individual and r_i^2 is the square of estimated accuracies for the i^{th} individual (Garrick *et al.* 2009), which were calculated using the DEBV calculator software (Salek Ardestani 2020, https://github.com/Siavash-cloud/DEBV_calculator). Only the individuals, which had a reliability of dEBV more than 0.1 for at least one studied trait, were kept in the dataset for the following analyses. The derived dEBVs for each trait were utilized as pseudo-phenotypes to perform the following GWAS analyses.

6.2.5 Animals and SNP Quality Control

The animals (n=1,356), which had reliability of dEBV more than 0.1 for at least one studied trait, and SNP data were filtered using PLINK (Purcell *et al.* 2007) before conducting analyses. The SNPs, which had minor allele frequencies lower than 5%, call rates lower than 90%, excess of heterozygosities higher than 15%, and Mendelian error frequencies larger than 5% and were out of Hardy-Weinberg equilibrium with very low probability (1×10^{-6}), and the mink, which had call rates lower than 90%, were excluded from the dataset.

6.2.6 Genome-Wide Association Studies

A single SNP univariate mixed linear animal model was used to perform the GWAS using the snp1101 software (Sargolzaei 2014). The model is described as follows:

$$\mathbf{y} = \boldsymbol{\mu} + \mathbf{X}\mathbf{m} + \mathbf{W}\mathbf{a} + \mathbf{e},$$

where \mathbf{y} is the vector of the dependent variable (dEBV); $\boldsymbol{\mu}$ is the population mean, \mathbf{m} is the vector of the SNP marker effects; \mathbf{a} is the vector of the residual polygenic effects with a normal distribution $\mathbf{a} \sim N(0, \mathbf{G}\sigma_a^2)$, where \mathbf{G} is the realized relationship matrix constructed with markers (VanRaden 2008), and σ_a^2 is the additive genetic variance; \mathbf{e} is the vector of residual errors with a normal distribution $\mathbf{e} \sim N(0, \mathbf{I}\sigma_e^2)$, where \mathbf{I} is an identity matrix, and σ_e^2 is the residual variance; and \mathbf{X} and \mathbf{W} are the incidence matrices of \mathbf{y} and are related to \mathbf{m} and \mathbf{a} , respectively.

The false-discovery rate (FDR) was employed as a correction to define the significant threshold (Glickman *et al.* 2014). The threshold p-value was calculated as $\mathbf{p} = \mathbf{FDR} * \frac{N}{M}$; the **FDR** was set to 0.01, N is the number of SNPs with p-value less than 0.01, and M refers to the total number of SNPs after quality control. The proportion of dEBV variance explained by significant SNPs was calculated according to the method proposed by Shim *et al.* (Shim *et al.* 2015). Quantile-quantile (Q-Q) plots and genomic inflation factor (Devlin & Roeder 1999) were applied to compare observed distributions of $-\log(\text{p-values})$ to its expected distributions under the no association model for each trait.

6.2.7 Gene Annotation, Gene Ontology, and Functional Analysis

The positional candidate genes within the range of the significant SNPs ± 350 kb region were annotated using the Bedtools software (Quinlan 2014) referring to the genome assembly of *Neogale vison* (Karimi *et al.* 2022). The delimitation of the regions was based on a previous investigation that indicated that linkage disequilibrium ($r^2 < 0.2$) within the present American mink population under study did not surpass 350 kb (Hu *et al.* 2023). The process of assigning gene ontology (GO) terms, which includes biological process (GO:BP), cellular component (GO:CC), and molecular function (GO:MF), to annotated

genes was carried out using PANTHER 14.1 (Thomas *et al.* 2003). The evaluation of the overrepresentation of annotated genes was performed through Fisher's exact test, and the FDR correction was used for adjustment. The terms with FDR-adjusted p-value (q) < 0.05 were considered significantly overrepresented. Additionally, the metabolic pathway analyses were conducted using the Kyoto Encyclopedia of Genes and Genomes (KEGG) database and utilizing the clusterProfiler package (Yu *et al.* 2012) in the R program with a significant threshold of $q < 0.05$.

6.3 Results

6.3.1 Summary Information of Phenotype Data and Genotype Data

Descriptive statistics of the dEBVs for four studied traits are presented in Table 6.1. A total of 1,057, 1,319, 1,269, and 996 animals were used in the final GWAS for ELISA-G, IAT, DOF, and Varf, respectively. The coefficient of variation (CV) of studied traits ranged from 4.4 to 93.5%, where IAT had the lowest CV, and Varf had the highest CV (Table 6.1). The distributions of the dEBVs for all studied traits are shown in Figure 6.1.

Among the 62,375 SNPs, 3,180 SNPs are located on sex chromosomes and thus were removed from the analysis. A total of 4,396 SNPs were removed due to genotype rate < 0.1 ; 26,387 SNPs due to minor allele frequency < 0.05 ; and 2,223 SNPs due to Hardy-Weinberg equilibrium with very low probability (1×10^{-6}). No individual was excluded due to a low ($< 90\%$) call rate. Finally, 26,189 SNPs and 1,356 animals remained and were used for further analyses. The density distributions of the filtered SNPs across the genome are shown in Figure 6.2.

6.3.2 Genome-wide Association Studies

The Q-Q plots of all studied traits were drawn, and the genomic inflation factors of all studied traits were calculated since population stratification could have an impact on GWAS. The Q-Q plot of each trait was shown following the Manhattan plot of the corresponding trait (Figure 6.3). For all studied traits, the observed $-\log(p\text{-values})$ were fairly close to the expected $-\log(p\text{-values})$ (Figure 6.3). In the meantime, the genomic inflation factors for all studied traits were close to 1 (ranging from 0.95 to 0.98). The Q-Q plots and genomic inflation factors results indicated that the influence of population stratification was negligible, and there were little or no residual population structure effects on the test statistic inflation in this study.

The significant ($q < 0.01$) SNPs for each studied trait are illustrated in Figure 6.3, and their chromosomes, physical positions, $-\log(p\text{-values})$, frequencies, substitution effects, and percentage of dEBV variance explained are provided in Table 6.2. For ELISA-G, 17 SNPs, which were distributed on chromosomes 1, 4, 6, and 13, were detected to be significant (threshold $p\text{-value} = 1.76 \times 10^{-4}$) with substitution effects ranging from -1.523 to 1.723 (Figure 6.3 and Table 6.2). These significant SNPs individually explained 0.048% to 0.094% of the dEBV variance of ELISA-G, and together they explained 1.252% of the dEBV variance of ELISA-G (Table 6.2). Eight genome-wide SNPs with substitution effects ranging from -0.313 to 0.366 were detected to be significant (threshold $p\text{-value} = 1.13 \times 10^{-4}$) for IAT, and these eight SNPs were distributed on chromosomes 2, 3, and 6 (Figure 6.3 and Table 6.2). These eight significant SNPs explained 0.799% of the dEBV variance of IAT, and a single SNP could explain 0.084 to 0.115% of the dEBV variance of IAT (Table 6.2). For DOF, seven SNPs, which were distributed on chromosomes 1, 4, 5, 11, and 14,

were detected to be significant (threshold p-value = 9.13×10^{-4}). These significant SNPs had substitution effects ranging from 0.006 to 0.100 and could explain 0.029 to 0.084% of the dEBV variance of DOF individually. Together, these significant SNPs accounted for a total of 0.405% of the dEBV variance of DOF. No significant ($q > 0.01$, threshold p-value = 1.07×10^{-4}) SNP was detected for Varf (Figure 6.3).

6.3.3 Gene Annotation and Gene Ontology of Significant SNPs

The candidate genes annotated from the significant SNPs for ELISA-G, IAT, and DOF are listed in Supplementary dataset 4. A total of 141, 44, and 42 unique candidate genes were annotated from the significant SNPs for ELISA-G, IAT, and DOF, respectively (Supplementary dataset 4). The annotated genes, which have available information in the existing literature, are listed in Table 6.3. For ELISA-G, 67, three, and five unique genes were detected on chromosomes 1, 6, and 13, respectively. For IAT, 20 and seven unique genes were annotated on chromosomes 1 and 3, respectively. Regarding DOF, the annotated genes were distributed on chromosomes 1, 3, 7, 10, and 11, where one, five, six, seven, and two unique genes were detected, respectively.

The functional classifications of candidate genes are shown in Figure 6.4. The cellular anatomical entity and protein-containing complex were the two GO:CCs detected for all three traits, and the cellular anatomical entity was the major one (occupied more than 72% of the detected cellular components) in all the cases (Figure 6.4). For ELISA-G, the annotated genes were classified into 13 GO:BPs and eight GO:MFs. Among the 13 GO:BPs, cellular process, metabolic process, and biological regulation were the top three BPs, and growth, immune system process, and reproduction, which are related to AD resilience indicator traits, were also included but with smaller proportions. The genes

annotated from IAT were classified into 11 GO:BPs, and again cellular process, metabolic process, and biological regulation were the top three BPs, and seven GO:MFs of binding, catalytic activity, and transporter activity were the top three MFs. The growth, immune system process, and reproduction were also included in the detected GO:BPs, but they occupied smaller proportions. Regarding DOF, the annotated genes were classified into eight GO:BPs, and cellular process, metabolic process, and biological regulation were also the top three BPs, and five GO:MFs, with binding, catalytic activity, and transporter activity were the top three MFs.

The overrepresentation tests of annotated genes were conducted for ELISA-G, IAT, and DOF, but significant ($q < 0.05$) overrepresentations were only detected in ELISA-G. The overrepresentations of candidate genes related to ELISA-G are presented in Table 6.4. In total, five significant ($q\text{-value} < 0.05$) overrepresented GO enrichment terms, including four GO:CCs (TAP complex, Classical-complement-pathway C3/C5 convertase complex, MHC class I peptide loading complex, and Extracellular region) and one GO:MF (ABC-type peptide transporter activity), were detected for ELISA-G (Table 6.4). No significant ($q < 0.05$) KEGG pathways of candidate genes were detected for all studied traits.

6.4 Discussion

Immune response and disease resilience are usually quantitative traits with complex genetic architectures (VanRaden 2008; Leach *et al.* 2010; Thompson-Crispi *et al.* 2014; Hu *et al.* 2020; Doeschl-Wilson *et al.* 2021). Therefore, identifying the candidate genes underlying immune response and disease resilience would be helpful for unlocking the genetic architectures and biological processes related to these traits. With the development of high-density SNP panels for multiple livestock species, GWAS has become one of the most

popular methods for identifying candidate genes underlying target traits in livestock research (Zhang *et al.* 2012; Sharma *et al.* 2015; Schmid & Bennewitz 2017; Mkize *et al.* 2021). In this study, the dEBVs of four phenotypes, including ELISA-G, IAT, DOF, and Varf, and genotypes from 1,411 mink raised at an AD-positive facility were used to conduct GWAS in order to identify SNPs and genes associated with immune response and resilience of mink to AD. In brief, 17, eight, and seven significant ($q < 0.01$) SNPs were detected for ELISA-G, IAT, and DOF, respectively and could explain 1.252, 0.779, and 0.405% of the dEBV variance of the corresponding trait. A total of 141, 44, and 42 unique candidate genes were annotated from the significant SNPs for ELISA-G, IAT, and DOF, respectively. Several of the annotated genes, such as *LOC122904531*, *LOC122911143*, and *LOC122898320*, were novel genes of unknown function in mink; thus, the discussion is focused on the genes for which information is available in the existing literature. In the meantime, the results associated with Varf were not further discussed in the discussion section as no significant ($q > 0.01$, threshold p -value = 1.07×10^{-4}) SNP was detected for Varf (Figure 6.3).

6.4.1 Candidate Genes for ELISA-G

A total of 141 genes were found to be related with immune response measured by ELISA-G. Among them, three genes, including *MPIG6B*, *RUNX2*, and *C4A*, were found to be related to the immune system process and might have important roles in immune-mediated responses to AMDV infection (Figure 6.4 and Table 6.3). The *MPIG6B* gene, also known as *G6B* or *C6orf25*, is localized in the class III region of the MHC, which is a region known to contain many genes associated with the immune system (de Vet *et al.* 2001; Geer *et al.* 2018). The *MPIG6B* gene plays a critical role in regulating megakaryocytic function and

platelet production (Ribas *et al.* 1999; de Vet *et al.* 2001), and loss-of-function of *MPIG6B* can cause severe thrombocytopenia, myelofibrosis, and anemia in both humans and mice (Mazharian *et al.* 2012; Morowski *et al.* 2013; Melhem *et al.* 2017; Geer *et al.* 2018; Nagy *et al.* 2018; Chen *et al.* 2019). The detection of *MPIG6B* gene in this study may be related to the severe platelet decrease (Eklund *et al.* 1968) and anemia (McGuire *et al.* 1979) caused by AD. The *RUNX2* gene is well-known as an important regulator of bone development, where it acts as an activator in the generation of osteoblasts and chondrocyte differentiation (Long 2012), but it also plays an important role in the immune system process. The *RUNX2* gene was found to regulate the development and homeostasis of plasmacytoid dendritic cells (Sawai *et al.* 2013; Chopin *et al.* 2016), which play a crucial role in antiviral immunity and may implicate initiating and developing immune-mediated diseases (Ye *et al.* 2020; Kerdidani *et al.* 2022). In the meantime, the *RUNX2* gene was found to play an important role in early T cell development (Vaillant *et al.* 2002) and the long-term maintenance of antiviral memory CD8⁺ T cells (Olesin *et al.* 2018). The identification of *RUNX2* may be related to the immune-mediated nature of AD and the proliferation of CD8⁺ T cells after AD infection (Aasted 1989). The *C4A* is one of the two genes (*C4A* and *C4B*) that encode for the complement component C4, which is a key protein involved in the classical pathway of the complement system (Wang & Liu 2021). The complement system is involved in several immune functions, including the recognition and elimination of pathogens, the clearance of damaged cells, and the modulation of inflammatory responses (Dunkelberger & Song 2010). The *C4A* shows preferential binding to the targets containing free amino groups, such as immune complex (Schifferli *et al.* 1985), with a role in the clearance of the immune complex (Dodds *et al.* 1996). The

deficiency of *C4A* has been found to cause less effective immune complex processing, resulting in the deposition of these complexes in tissues and subsequent damage (Pickering *et al.* 2001). AD has been defined as an immune complex disease (Stolze & Kaaden 1987); thus, the detection of the *C4A* gene in this study may relate to the characteristics of AD. These three genes were also detected by the selection signatures study related to immune response of mink to AD (Hu *et al.* 2024), which indicated these genes may play critical roles in the immune response of mink to AD.

6.4.2 Candidate Genes for IAT

A total of 44 genes were annotated from the significant ($q < 0.01$) SNPs associated with IAT in this study. Among them, two genes, *TNFRSF11A* and *C4A*, were related to the immune system process (Figure 6.4 and Table 6.3). The *TNFRSF11A* gene, which is also known as the nuclear factor- κ B receptor activator (Yang *et al.* 2004), was identified in both immune system and skeletal system (Anderson *et al.* 1997; Lacey *et al.* 1998). This gene was found to be related to the production of immunoglobulin in humans (Guerrini *et al.* 2008). Hypergammaglobulinemia is one of the typical symptoms of AD (Henson *et al.* 1962; Williams *et al.* 1965), and thus may explain the detection of *TNFRSF11A* gene in this study. The *TNFRSF11A* gene has been determined as the cause of autosomal recessive osteopetrosis in humans (Guerrini *et al.* 2008; Palagano *et al.* 2018); however, whether AD could cause skeletal-related issues is unknown, which is worth further investigation in the future. The *C4A* was found to have a greater affinity for the immunoglobulin molecules in immune complexes (Law *et al.* 1984; Schifferli *et al.* 1985; Kishore *et al.* 1988); thus, the hypergammaglobulinemia caused by AD, which is the overproduction of more than one

class of immunoglobulins by plasma cells, could be the reason *C4A* gene was detected for IAT.

6.4.3 Candidate Genes for DOF

A total of 42 genes were found to be related to DOF in this study. Among them, two genes, *ADCY7* and *CNDP2*, were found to be associated with feed intake in livestock or appetite in humans. The *ADCY7* gene was found to be associated with appetite in swine in previous studies (Barb *et al.* 2010; Miao *et al.* 2021). In the meantime, *ADCY7* was associated with depression in mice and humans (Lisa *et al.* 2006; Joeyen-Waldorf *et al.* 2012), which indicates the lower appetite of mink in AD-positive farms may be caused by a severe mood disorder. However, the relationship between AD and depression was not identified yet, which is worth further investigation. The *CNDP2* gene was found to be involved in the production of N-lactoyl-phenylalanine (Jansen *et al.* 2015), which has been thought to suppress feeding in mice (Li *et al.* 2022). In addition, several annotated genes, including *BRD7*, *FBXO25*, *ITPKB*, *LIN9*, *MIXL1*, and *TENT4B*, were related to metabolic processes (Figure 6.4 and Table 6.3). Feed intake is influenced by multiple dynamic physiological signals that are regulated by the metabolic and physiological conditions of animals (Woods & Ramsay 2011; Allen 2014; Albornoz *et al.* 2023). Thus, AD may affect the feed intake frequency or appetite of mink by affecting the metabolism, which needs further studies to explore.

6.4.4 Overrepresentations of Candidate Genes for ELISA-G

A total of five significant ($q\text{-value} < 0.05$) overrepresented GO enrichment terms, including four cellular components (TAP complex, Classical-complement-pathway C3/C5 convertase complex, MHC class I peptide loading complex, and Extracellular region) and

one molecular function (ABC-type peptide transporter activity), were detected for ELISA-G (Table 6.4). Among them, TAP (transporter associated with antigen processing) complex, MHC (major histocompatibility complex) class I peptide loading complex, and ABC-type (ATP-binding cassette) peptide transporter activity are closely correlated and play important roles in the adaptive immune response against virally or malignantly transformed cells. The TAP complex is a superfamily of ABC transporters and plays a crucial role in the processing and presentation of the MHC class I restricted antigens, which present their antigenic peptides to CD8⁺ cytotoxic T-lymphocytes and eventually induce the elimination of virally or malignantly transformed cells (Abele & Tampé 1999; Ritz & Seliger 2001; Lehnert & Tampé 2017; Reeves & James 2017). The cellular immune response of mink to AMDV infection has not been properly defined so far, and the detection of these GO terms may help further research into the cellular immune response to AD. The C3/C5 convertase is an essential component of the complement system, which is an immune defense mechanism present in the blood plasma to combat pathogens (Dunkelberger & Song 2010; Okroj *et al.* 2012). The classical-complement-pathway C3/C5 convertase complex pathway activates the proteases C3 and C5 convertase, thereby cleaving the proteins C3 and C5. The cleaved fragments can attract phagocytes to the site of infection and label target cells for elimination by phagocytosis (Dunkelberger & Song 2010; Okroj *et al.* 2012). The presence of immune complexes could activate the complement system, which plays an important role in clearing immune complexes (Sarma & Ward 2011; Marshall *et al.* 2018; Jia *et al.* 2022). The detection of the classical-complement-pathway C3/C5 convertase complex pathway may be related to the responses of the complement system to the

formation of immune complexes caused by AD, as the deposition C3 was detected in AD-infected mink (Cheema *et al.* 1972; Porter & Cho 1980).

6.5 Conclusion

In this thesis chapter, 1,411 mink raised in an AD-positive facility were utilized to perform GWAS to detect potential SNPs and genes related to immune response and resilience of mink to AD. A total of 17, eight, and seven significant ($q < 0.01$) SNPs were found to be associated with ELISA-G, IAT, and DOF, respectively. Among the 141 unique candidate genes annotated from the significant SNPs for ELISA-G, three genes, including *MPIG6B*, *RUNX2*, and *C4A*, might have important roles in immune-mediated responses to AMDV infection. Two (*TNFRSF11A* and *C4A*) of the 44 candidate genes annotated in IAT were also found to be involved in the immune system process. In addition, 42 candidate genes were annotated in DOF, and two of them, *ADCY7* and *CNDP2*, were related to feed intake or appetite. The newly detected significant SNPs and identified candidate genes in this thesis chapter would provide a better understanding of the genetic architecture and biological mechanisms underlying AD resilience in mink, which offers an opportunity for increasing resilience of mink to AD using marker-assisted/genomic selection in mink.

Table 6.1 Descriptive statistics of four studied traits.

Traits ¹	Number of records	Mean	SD	Range	CV
ELISA-G	1,057	-0.167	2.296	-4.951 to 6.814	13.749
IAT	1,319	0.122	0.532	-1.496 to 1.991	4.361
DOF	1,269	0.002	0.018	-0.054 to 0.064	9.000
Varf	996	-0.067	6.264	-20.26 to 19.797	93.493

¹ELISA-G = AMDV-G based enzyme-linked immunosorbent assay test; IAT = Iodine agglutination test; DOF = Proportion of off-feed days; Varf = Variation in daily feed intake; SD = Standard deviation; CV= Coefficient of variation.

Table 6.2 Summary information of significant ($q < 0.01$) SNPs for enzyme-linked immunosorbent assay test, iodine agglutination test, and off-feed days traits.

Traits ¹	Chr ²	Physical position (bp)	$-\log_{10}$ (p-value)	Allele frequency	Allele substitution effect	% dEBV ³
ELISA-G	1	91,348,258	3.772	0.695	1.309	0.048
	1	91,563,695	4.068	0.708	1.400	0.055
	1	119,668,108	4.112	0.683	1.552	0.068
	1	121,737,422	3.817	0.692	1.685	0.080
	1	121,755,885	3.961	0.691	1.711	0.083
	1	121,873,249	4.045	0.683	1.658	0.078
	1	121,899,199	3.916	0.692	1.702	0.082
	1	121,970,625	3.862	0.691	1.693	0.081
	1	121,976,198	3.862	0.691	1.693	0.081
	1	122,009,542	3.983	0.693	1.723	0.084
	1	122,459,883	3.928	0.692	1.710	0.083
	4	5,758,929	4.664	0.917	-1.685	0.080
	6	39,873,751	3.895	0.914	-1.584	0.071
	6	39,952,440	3.823	0.887	-1.348	0.051
	6	39,973,150	5.030	0.912	-1.819	0.094
	6	39,976,387	5.000	0.913	-1.823	0.094
	13	149,480,595	5.670	0.733	-1.166	0.038
IAT	2	13,247,909	4.316	0.935	0.359	0.111
	3	133,845,792	4.612	0.924	0.366	0.115
	3	133,851,626	4.563	0.924	0.363	0.113
	3	137,464,576	5.179	0.906	0.339	0.099
	3	142,608,584	4.386	0.906	0.318	0.087
	3	142,738,773	5.677	0.898	0.352	0.106
	3	142,775,506	4.348	0.906	0.316	0.086
	6	185,881,210	4.026	0.914	-0.313	0.084
DOF	1	296,396,353	5.640	0.876	0.010	0.082
	1	296,406,380	5.722	0.878	0.010	0.084
	4	223,648,486	4.213	0.908	0.009	0.067
	5	155,691,399	4.141	0.517	0.006	0.029
	11	201,098,313	4.194	0.853	0.008	0.048
	11	201,105,005	4.223	0.835	0.007	0.044
	14	38,377,828	4.284	0.893	0.008	0.052

¹ELISA-G = AMDV-G based enzyme-linked immunosorbent assay test; IAT = Iodine agglutination test; DOF = Proportion of off-feed days.

² Chromosome.

³ The percentage of dEBV variance explained by the SNP.

Table 6.3 Significant ($q < 0.01$) SNPs and genes annotated from the significant SNPs for enzyme-linked immunosorbent assay test, iodine agglutination test, and off-feed days traits.

Traits ¹	Chr ²	Physical position (bp)	Start	End	Annotated genes
ELISA-G	1	91,348,258	90,998,258	91,698,258	<i>SUPT3H</i>
	1	91,563,695	91,213,695	91,913,695	<i>RUNX2, SUPT3H</i>
	1	119,668,108	119,318,108	120,018,108	<i>BRD2, COL11A2, PSMB8, PSMB9, TAP1, TAP2</i>
	1	121,737,422	121,387,422	122,087,422	<i>ABHD16A, AGPAT1, AIF1, APOM, ATF6B, ATP6V1G2, BAG6, C1H6orf47, C2, C4A, CFB, CLIC1, CSNK2B, DDAH2, DDX39B, DXO, EGFL8, EHMT2, FKBPL, GPANK1, LSM2, LST1, LTA, LTB, LY6G5B, LY6G5C, LY6G6C, LY6G6D, LY6G6F, MCCD1, MPIG6B, MSH5, NCR3, NELFE, NEU1, NFKBIL1, PPT2, PRRC2A, PRRT1, SAPCD1, SKIV2L, SLC44A4, STK19, TNF, TNXB, VARS1, VWA7, ZBTB12</i>
	1	121,755,885	121,405,885	122,105,885	<i>ABHD16A, AIF1, APOM, ATF6B, ATP6V1G2, BAG6, C1H6orf47, C2, C4A, CFB, CLIC1, CSNK2B, DDAH2, DDX39B, DXO, EHMT2, FKBPL, GPANK1, LSM2, LST1, LTA, LTB, LY6G5B, LY6G5C, LY6G6C, LY6G6D, LY6G6F, MCCD1, MPIG6B, MSH5, NCR3, NELFE, NEU1, NFKBIL1, PRRC2A, PRRT1, SAPCD1, SKIV2L, SLC44A4, STK19, TNF, TNXB, VARS1, VWA7, ZBTB12</i>
	1	121,873,249	121,523,249	122,223,249	<i>ABHD16A, AIF1, APOM, ATP6V1G2, BAG6, C1H6orf47, C2, CFB, CLIC1, CSNK2B, DDAH2, DDX39B, EHMT2, GPANK1, LSM2, LST1, LTA, LTB, LY6G5B, LY6G5C, LY6G6C, LY6G6D, LY6G6F, MCCD1, MPIG6B, MSH5, NCR3, NELFE, NEU1, NFKBIL1, PRRC2A, SAPCD1, SKIV2L, SLC44A4, TNF, VARS1, VWA7, ZBTB12</i>
	1	121,899,199	121,549,199	122,249,199	<i>ABHD16A, AIF1, APOM, ATP6V1G2, BAG6, C1H6orf47, C2, CLIC1, CSNK2B, DDAH2, DDX39B, EHMT2, GPANK1, LSM2, LST1, LTA, LTB, LY6G5B, LY6G5C, LY6G6C, LY6G6D, LY6G6F, MCCD1, MPIG6B, MSH5, NCR3, NEU1, NFKBIL1, PRRC2A, SAPCD1, SLC44A4, TNF, VARS1, VWA7, ZBTB12</i>
	1	121,970,625	121,620,625	122,320,625	<i>ABHD16A, AIF1, APOM, ATP6V1G2, BAG6, C1H6orf47, CLIC1, CSNK2B, DDAH2, DDX39B, GPANK1, LSM2, LST1, LTA, LTB, LY6G5B, LY6G5C, LY6G6C, LY6G6D, LY6G6F, MCCD1, MPIG6B, MSH5, NCR3, NEU1, NFKBIL1, PRRC2A, SAPCD1, SLC44A4, TNF, VARS1, VWA7</i>
	1	121,976,198	121,626,198	122,326,198	<i>ABHD16A, AIF1, APOM, ATP6V1G2, BAG6, C1H6orf47, CLIC1, CSNK2B, DDAH2, DDX39B, GPANK1, LSM2, LST1, LTA, LTB, LY6G5B, LY6G5C, LY6G6C, LY6G6D, LY6G6F, MCCD1, MPIG6B, MSH5, NCR3, NEU1, NFKBIL1, PRRC2A, SAPCD1, TNF, VARS1, VWA7</i>
	1	122,009,542	121,659,542	122,359,542	<i>ABHD16A, AIF1, APOM, ATP6V1G2, BAG6, C1H6orf47, CLIC1, CSNK2B, DDAH2, DDX39B, GPANK1, LSM2, LST1, LTA, LTB, LY6G5B, LY6G5C, LY6G6C, LY6G6D, LY6G6F, MCCD1, MPIG6B, MSH5, NCR3, NFKBIL1, PRRC2A, SAPCD1, TNF, VARS1, VWA7</i>

Table 6.3. Continuous.

Traits ¹	Chr ²	Physical position (bp)	Start	End	Genes
ELISA-G	1	122,459,883	122,109,883	122,809,883	<i>CIH6orf15, CCHCR1, CDSN, DDR1, GTF2H4, MUC21, POU5F1, PSORS1C2, SFTA2, TCF19, VARS2</i>
	6	39,873,751	39,523,751	40,223,751	<i>CHMP2B, POU1F1, VGLL3</i>
	6	39,952,440	39,602,440	40,302,440	<i>CHMP2B, POU1F1, VGLL3</i>
	6	39,973,150	39,623,150	40,323,150	<i>CHMP2B, POU1F1, VGLL3</i>
	6	39,976,387	39,626,387	40,326,387	<i>CHMP2B, POU1F1, VGLL3</i>
	13	149,480,595	149,130,595	149,830,595	<i>ADAMTSL3, EFL1, MEX3B, SAXO2, SH3GL3</i>
IAT	1	102,821,396	102,471,396	103,171,396	<i>BAG2, BEND6, DST, PRIM2, RAB23, ZNF451</i>
	1	162,209,141	161,859,141	162,559,141	<i>ARF1, CIH1orf35, GJC2, GUK1, IBA57, JMJD4, MRPL55, OBSCN, PRSS38, SNAP47, TRIM11, TRIM17, WNT3A, WNT9A</i>
	3	133,845,792	133,495,792	134,195,792	<i>CDH19</i>
	3	133,851,626	133,501,626	134,201,626	<i>CDH19, PHLPP1, PIGN, RELCH, TCF4, TNFRSF11A, ZCCHC2</i>
	3	137,464,576	137,114,576	137,814,576	<i>PHLPP1, PIGN, RELCH, TNFRSF11A, ZCCHC2</i>
	3	142,738,773	142,388,773	143,088,773	<i>TCF4</i>
DOF	1	272,488,827	272,138,827	272,838,827	<i>GRIA1</i>
	3	128,189,409	127,839,409	128,539,409	<i>C3H18orf63, CNDP2, DIPK1C, FBXO15, TIMM21</i>
	7	32,578,011	32,228,011	32,928,011	<i>ADCY7, BRD7, CNEP1R1, HEATR3, NKD1, TENT4B</i>
	10	59,705,959	59,355,959	60,055,959	<i>ACBD3, ITPKB, LIN9, MIXL1, PARP1, SDE2, STUM</i>
	11	207,436,868	207,086,868	207,786,868	<i>ERICH1, FBXO25</i>

¹ELISA-G = AMDV-G based enzyme-linked immunosorbent assay test; IAT = Iodine agglutination test; DOF = Proportion of off-feed days.

² Chromosome.

Table 6.4 Significant (false discovery rate adjusted p-value<0.05) functional enrichment of candidate genes detected from enzyme-linked immunosorbent assay test trait.

Gene ontology term	GO ID	Annotation set	q-value
TAP complex	0042825	Cellular component	0.002
Classical-complement-pathway C3/C5 convertase complex	0005601	Cellular component	0.002
MHC class I peptide loading complex	0042824	Cellular component	0.006
Extracellular region	0005576	Cellular component	0.007
ABC-type peptide transporter activity	0015440	Molecular function	0.014

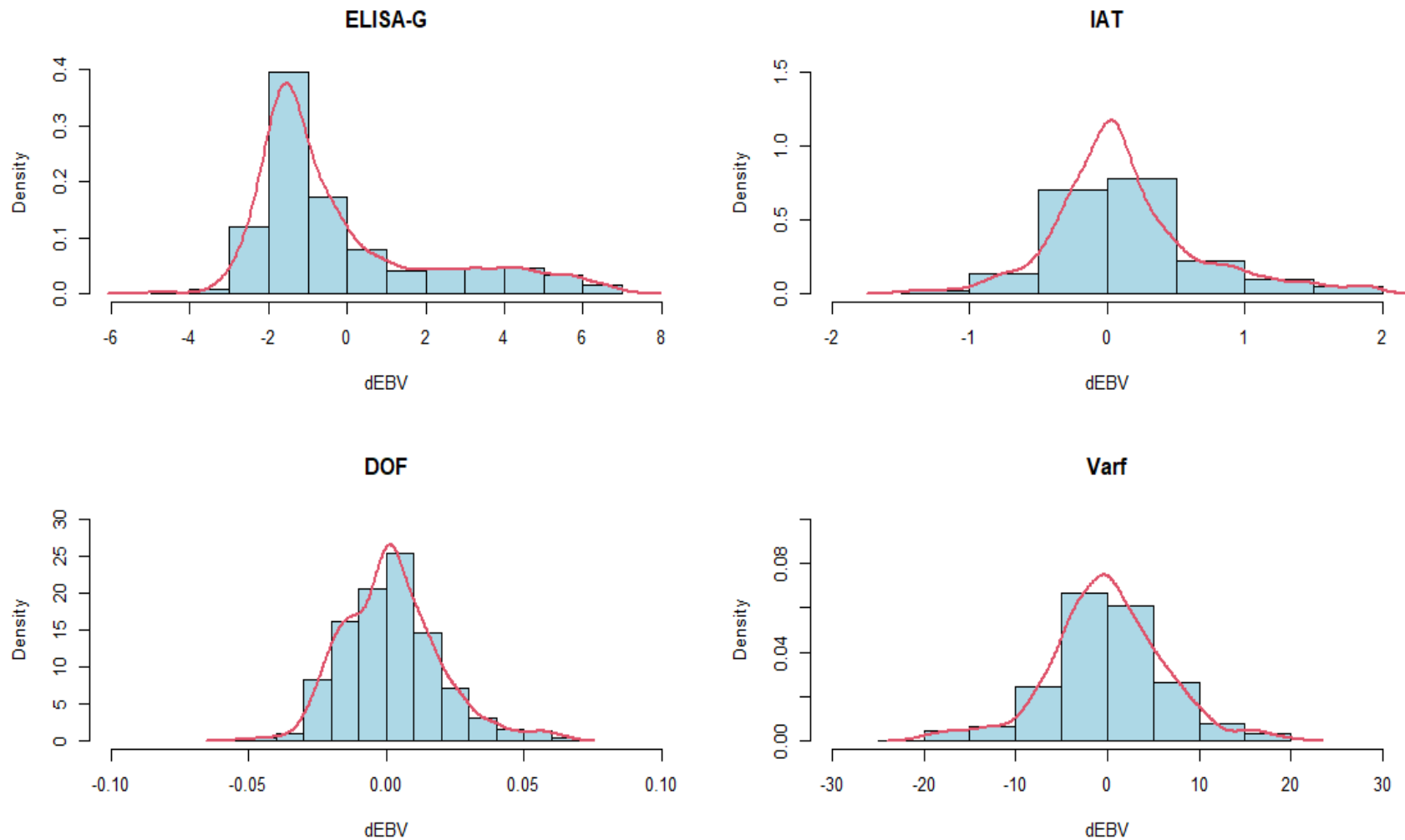


Figure 6.1 Frequency distribution histogram for AMDV-G based enzyme-linked immunosorbent assay test (ELISA-G), Iodine agglutination test (IAT), proportion of off-feed days (DOF), and Variation in daily feed intake (Varf).

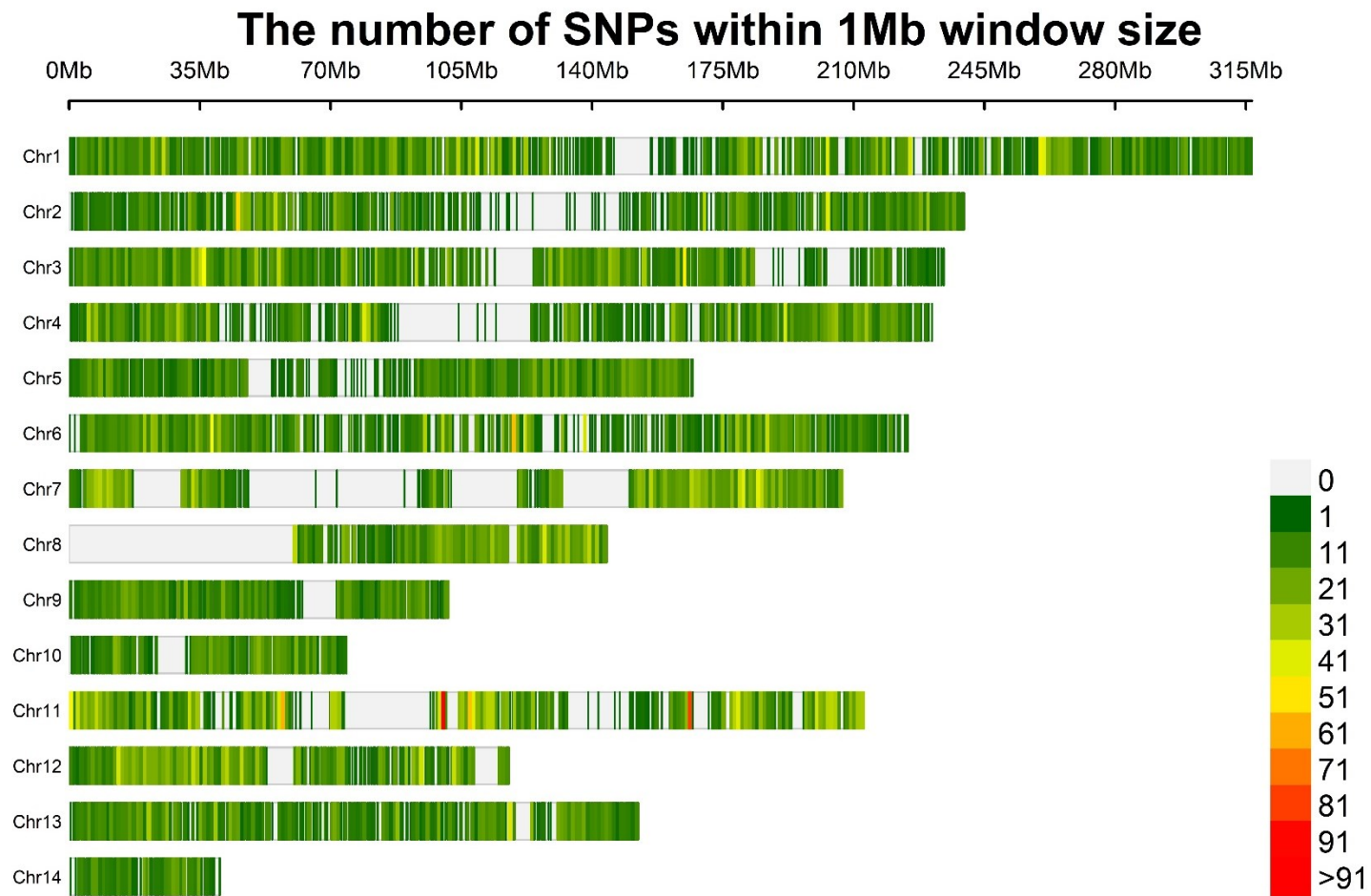


Figure 6.2 The filtered SNP density distributions on Nvison chromosomes. The horizontal axis (x-axis) shows the chromosome length (Mb). Color index indicates the number of labels.

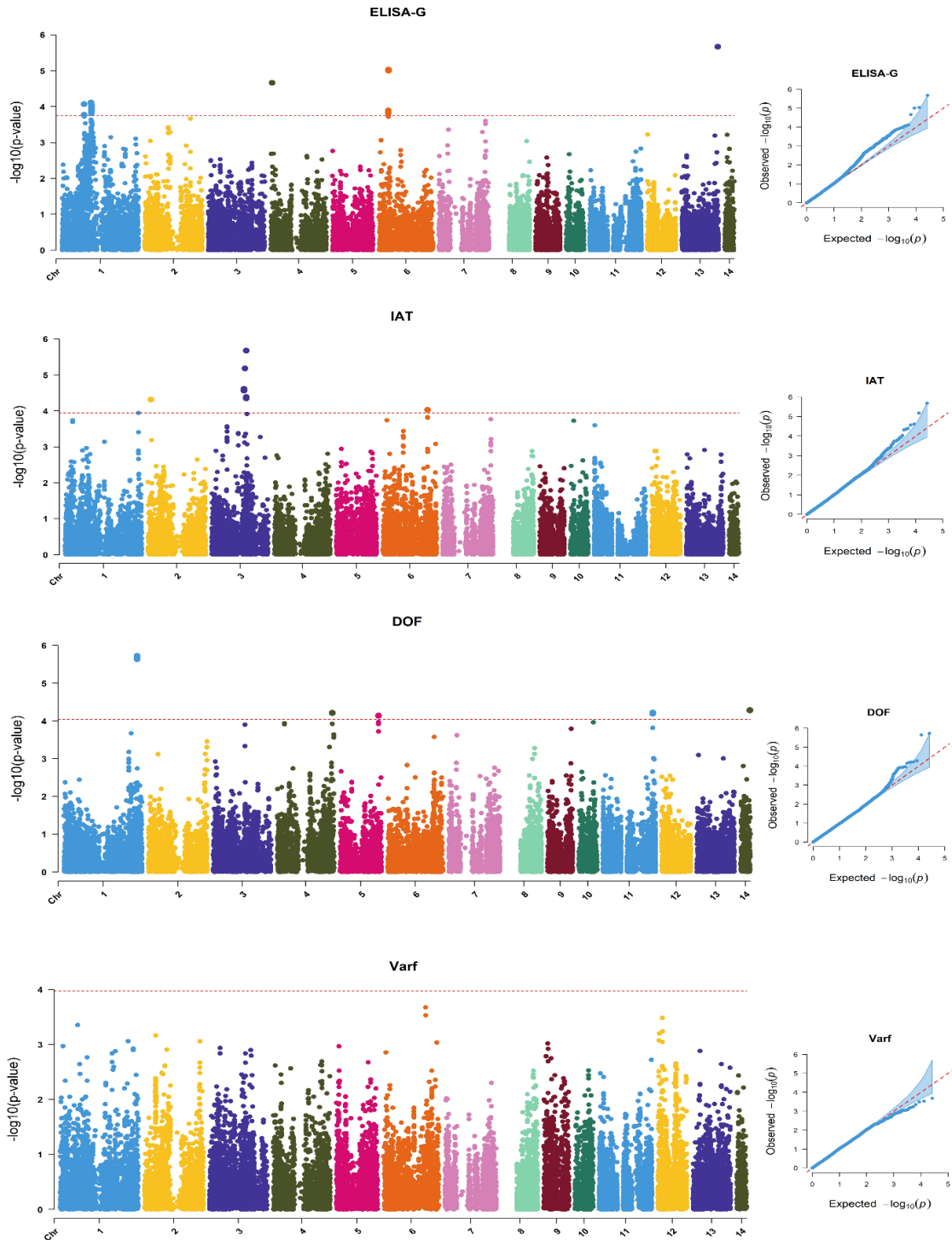


Figure 6.3 Manhattan plots and Quantile-Quantile plots for four studied traits. The X-axis is the position of SNP on each chromosome, and the Y-axis is the significant level ($-\log_{10}$ p value). The red lines indicate significant thresholds. There were 17, eight, seven, and zero SNPs that passed the significant thresholds for enzyme-linked immunosorbent assay test (ELISA-G), Iodine agglutination test (IAT), proportion of off-feed days (DOF), and Variation in daily feed intake (Varf) trait, respectively.

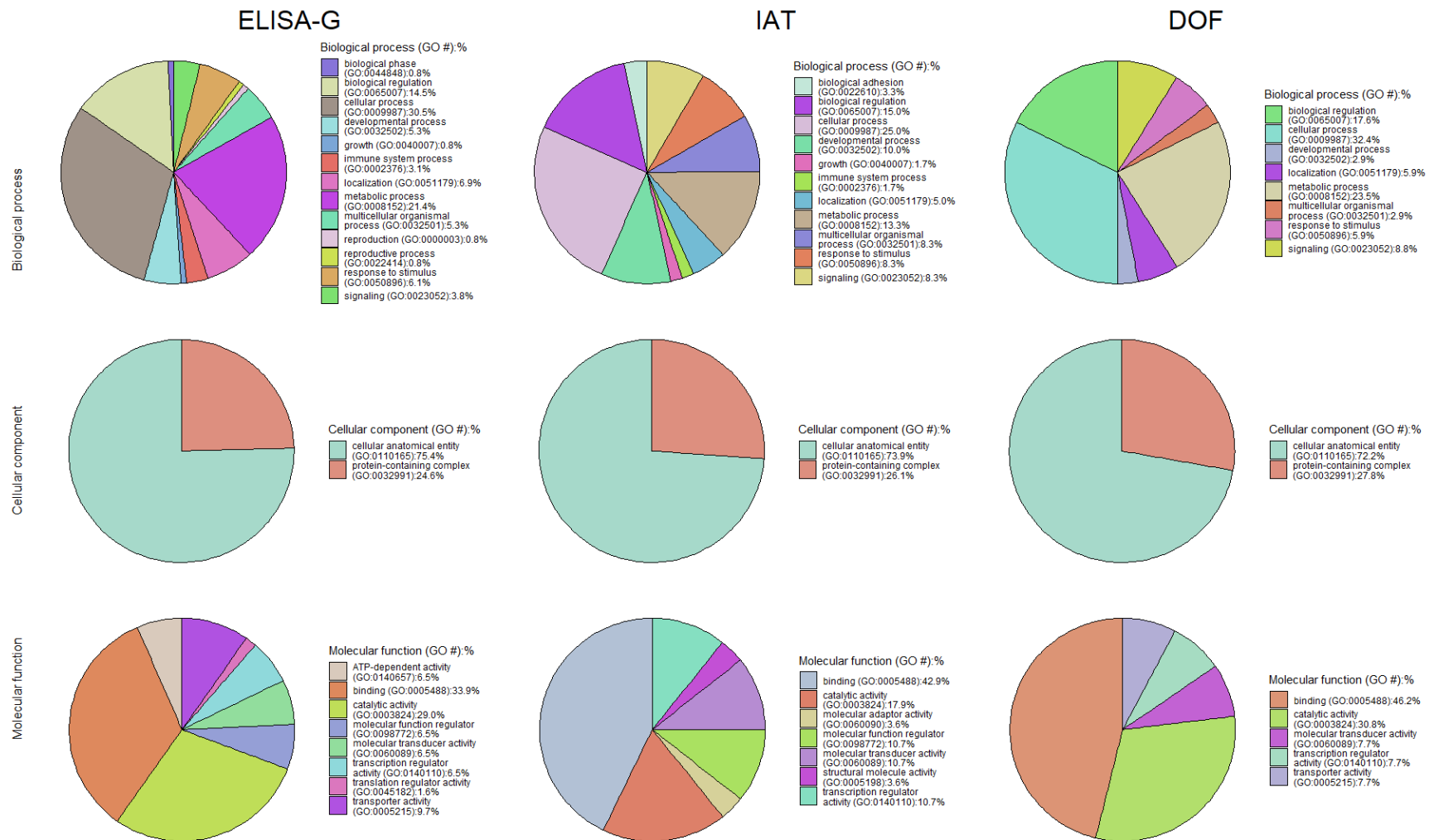


Figure 6.4 The pie charts of functional classifications (molecular function, cellular component, and biology process) of candidate genes related to significant ($q < 0.05$) SNPs for AMDV-G based enzyme-linked immunosorbent assay test (ELISA-G), iodine agglutination test (IAT), and the proportion of off-feed days (IAT).

CHAPTER 7. Genomic Prediction of Immune Response and Resilience to Aleutian Disease in Mink¹

7.1 Introduction

Aleutian disease (AD), caused by the Aleutian mink disease virus (AMDV), is one of the most severe health issues for mink farming and brings huge financial losses to the mink industry (Henson *et al.* 1962; Porter *et al.* 1982; Farid & Ferns 2011; Reichert & Kostro 2014; Wiggans *et al.* 2017). Several methods, including vaccination, medicine, and culling strategy, have been attempted to control AD but ended with failure. Thus, mink farmers attempt to control AD by phenotypically selecting AD-resilient mink based on AD tests and/or AD-resilient indicator traits, such as feed intake, pelt quality, and reproductive performance (Knuuttila *et al.* 2009; Farid & Ferns 2011; Farid & Rupasinghe 2016; Farid & Ferns 2017; Farid *et al.* 2018). Phenotypic selection is the simplest form of selection, and it is not efficient especially for low heritable traits (Falconer & Mackay 1996; Calus *et al.* 2008; Villumsen *et al.* 2009). On the other hand, genomic selection has the potential to improve the AD resilience in mink since the AD resilience traits are difficult and expensive to measure and have low-to-moderate heritability (Hu *et al.* 2021; Hu *et al.* 2022).

Genomic selection aims to estimate the breeding values using the genomic diversity captured by extensive markers distributed across the genome without knowing the

¹ A version of this chapter will be submitted to PLOS One by Hu *et al.* 2024. Genomic Prediction of Immune Response and Resilience to Aleutian Disease in Mink.

locations of specific genes (Goddard & Hayes 2007). With the development of dense panels of single nucleotide polymorphism (SNP) markers, genomic selection is now implemented in several livestock species (Misztal *et al.* 2021). Genomic selection accelerates genetic progress by increasing the accuracy of selection and reducing the generation intervals. The increase in selection accuracy is particularly important for traits with low heritabilities where the progress made by traditional pedigree-based selection is slow (Misztal *et al.* 2021). The heritabilities of disease-related traits are usually low-to-moderate. Therefore, genomic selection is suggested to improve disease-related traits (Bishop & Woolliams 2014; Iheshiulor *et al.* 2017). For example, genomic selection studies have been conducted for swine resistance to porcine reproductive and respiratory syndrome (Serão *et al.* 2016; Waide *et al.* 2018), and moderate genomic prediction accuracies were observed. The common methods used to conduct genomic prediction studies are genomic best linear unbiased prediction (GBLUP) and single-step GBLUP (ssGBLUP) approaches. The GBLUP is a multi-step method using genomic information to predict genomic breeding values (VanRaden 2008; Hayes *et al.* 2009). For this purpose, a genomic relationship matrix, which is created using DNA marker information instead of pedigree, is applied and expected to provide more accurate predictions of genetic merit than the traditional pedigree-based best linear unbiased prediction (BLUP) method (Clark & van der Werf 2013). Compared with GBLUP, ssGBLUP is a single-step methodology that combines pedigree, phenotypic and genomic information of all breeding individuals for genetic evaluation in one model (Misztal *et al.* 2013). Meanwhile, the ssGBLUP was generally found to be simpler, faster, and more accurate than multistep methods (Misztal *et al.* 2013; Cardoso *et al.* 2015; Miar *et al.* 2015; Silva *et al.* 2016).

With the development of dense panels of SNP markers, genomic selection is now implemented in all major farm animal species (Misztal *et al.* 2021). The chromosome-level genome assembly by Karimi *et al.* (2022) and the development of the first Axiom Affymetrix Mink 70K SNP panel for American mink (Do *et al.* 2024) have made the genomic prediction for AD resilience in mink feasible. However, no genomic prediction studies have been conducted for AD resilience in mink. Thus, this thesis chapter aimed to evaluate the accuracy of genomic prediction of AD resilience traits (three AD tests and two feed-intake-related resilience traits) in mink using the genomic information obtained from a 70K SNP panel. Three methods, including traditional pedigree-based BLUP, GBLUP, and ssGBLUP, were compared to determine the best method for each trait. Possible factors that influence the accuracy of genomic prediction were also discussed. The ultimate aim was to investigate the feasibility and optimal approach for using genomic information to increase genetic gain for AD resilience in mink.

7.2 Materials and Methods

7.2.1 Ethics Approval

This study was approved by the Dalhousie University Animal Care and Use Committee (certification#: 2018-009 and 2019-012). All mink used in this study were farmed following the Code of Practice for the Care and Handling of Farmed Mink guidelines from the Canada Mink Breeders Association (Turner P *et al.* 2013).

7.2.2 Animals and Phenotypes

Mink (n=1,411) raised at the Canadian Centre for Fur Animal Research (CCFAR), which is located at Dalhousie University, Faculty of Agriculture (Truro, Nova Scotia, Canada), from 2015 to 2020, were used in this study. A persistent breeding program was not

conducted in CCFAR during the study years from 2013 to 2021. AD was initially detected at CCFAR in 2013, and the exact origin was not determined with certainty, where the consumption of AMDV-contaminated feed and unperceived contact with wild animals carrying AMDV were speculated to be the most possible causes for the AD outbreak.

The phenotypes related to the immune response of the studied individuals to AMDV exposure were collected based on the established protocols described by Hu et al. (2021). The individual blood samples were annually collected in mid-November before the selection of breeders and mid-February prior to mating, from 2015 to 2020. Three types of tests, including antigen-based enzyme-linked immunosorbent assay (ELISA-G), counterimmunoelectrophoresis (CIEP), and iodine agglutination test (IAT), were applied to measure the individual level of immune response to AMDV exposure. The ELISA-G tests were conducted in the Middleton Veterinary Services (Nova Scotia, Canada) to evaluate anti-AMDV antibody levels through optical density, and the outcomes were grouped into eight categories with 1-point increments from 0 (none or extremely low level of antibody) to 7 (extremely high antibody level). The CIEP tests were performed at the Animal Health Laboratory (University of Guelph, Ontario, Canada) to detect the existence of anti-AMDV antibodies, and the results were recorded as 0, which indicated none or extremely low antibody level, or 1, which indicated detectable anti-AMDV antibody level. The IAT tests were conducted at CCFAR to measure the gamma globulin level in the serum, and the results were classified into four categories with 1-point increments ranging from 0 (none or low serum gamma globulin level) to 4 (extremely high gamma globulin level).

The feed-intake-related phenotypes were collected utilizing the established procedures outlined by Davoudi et al. (2022). Studied individuals were raised in separate cages, and

the daily feed was distributed to each individual separately. The daily feed intake (DFI) for each individual was calculated as:

$$\text{DFI} = \text{the total amount of feed distributed} - \text{the amount of feed leftover}$$

The feed-intake-related resilience of studied individuals to AMDV exposure was measured by two parameters, including day-to-day variation in feed intake (Varf) and proportion of off-feed days (DOF). The individual Varf and DOF were computed using all the available DFI data for each mink based on the methodology described by Putz et al. (2019). The Varf was measured through the calculation of the root mean square error from within-individual regression analysis, utilizing ordinary least squares linear regression, applied to DFI regressed on day. Identification of off-feed days involved a 5% quantile regression of DFI against age (in days) for all studied individuals, with off-feed days for each mink being those exhibiting negative residuals below the regression line. Ultimately, the proportion of off-feed days to the total recorded days of DFI determined the DOF.

7.2.3 Tongue Sample Collection and Genotyping

Prior to pelting, the tongue tissues were collected from the studied animals for DNA extraction. The DNA extractions of collected tongue tissue samples were conducted using the DNeasy Blood and Tissue Kit (Qiagen, Hilden, Germany) in accordance with the instructions provided by the manufacturer. The NanoDrop ND-1000 spectrophotometer (NanoDrop Technologies Inc., Wilmington, DE) was employed to evaluate the quality and quantity of the extracted DNA. The 260/280 nm readings for all samples were between 1.7 and 2.0, and the final concentrations of all samples were 20 ng. The extracted DNA samples were genotyped using the Axiom Affymetrix Mink 70K panel (Neogen, Lincoln, Nebraska, USA) (Do *et al.* 2024).

7.2.4 Animals and SNP Quality Control

The animals and SNPs data were filtered using PLINK (Purcell *et al.* 2007) before conducting analyses. The SNPs, which had a minor allele frequency lower than 5%, a call rate lower than 90%, an excess of heterozygosity higher than 15%, and a Mendelian error frequency larger than 5% and were out of Hardy-Weinberg equilibrium with very low probability (1×10^{-6}), were excluded. In the meantime, the mink, which had a call rate lower than 90%, was removed from the dataset as well. Finally, 26,189 SNPs and 1,356 animals remained and were used for further analyses.

7.2.5 Statistical Methods for Genetic and Genomic Predictions

Traditional BLUP

Model 1 was applied to estimate the breeding values of each animal utilizing ASReml 4.1 software (Gilmour *et al.* 2018). The model was as follows:

$$\text{Model 1. } \mathbf{y} = \mathbf{1}\mu + \mathbf{X}\mathbf{b} + \mathbf{Z}\mathbf{a} + \mathbf{W}\mathbf{pe} + \mathbf{D}\mathbf{m} + \mathbf{e},$$

where \mathbf{y} is the vector of phenotypes; μ is the overall mean; \mathbf{X} , \mathbf{Z} , \mathbf{W} , and \mathbf{D} are the incidence matrices relating phenotypes to fixed, random additive genetic, random permanent environmental, and random maternal genetic effects, respectively; \mathbf{b} is the vector of fixed effects (year, sex, age, color types, and cage location in the farm); \mathbf{a} is the vector of random additive genetic effects, with $\mathbf{a} \sim N(0, \mathbf{A}\sigma_a^2)$, where \mathbf{A} is the numerator relationship matrix, and σ_a^2 is the additive genetic variance; \mathbf{pe} is the vector of random permanent environmental effects, with $\mathbf{pe} \sim N(0, \mathbf{I}\sigma_{pe}^2)$, where \mathbf{I} is an identity matrix, and σ_{pe}^2 is the permanent environmental variance; \mathbf{m} is the vector of random maternal genetic effects, with $\mathbf{m} \sim N(0, \mathbf{A}\sigma_m^2)$, where σ_m^2 is the maternal genetic variance; and \mathbf{e} is the vector of residual effects, with $\mathbf{e} \sim N(0, \mathbf{I}\sigma_e^2)$, where σ_e^2 is the residual variance. The variance

components of each trait (full dataset and cross-validation datasets) were estimated using ASReml 4.1 software (Gilmour *et al.* 2018) in BLUP model (**Model 1**).

Phenotypic variances were calculated $\sigma_p^2 = \sigma_a^2 + \sigma_{pe}^2 + \sigma_m^2 + \sigma_e^2$ for ELISA-G, as $\sigma_p^2 = \sigma_a^2 + \sigma_m^2 + \sigma_e^2$ for CIEP, as $\sigma_p^2 = \sigma_a^2 + \sigma_{pe}^2 + \sigma_e^2$ for IAT, and as $\sigma_p^2 = \sigma_a^2 + \sigma_e^2$ for DOF and Varf. Heritability (h^2) was defined as follows:

$$h^2 = \frac{\sigma_a^2}{\sigma_p^2}$$

Subsequently, the de-regressed EBVs (dEBVs) were obtained with the formula:

$$dEBV = \frac{g_i}{r_i^2},$$

where g_i is the EBV of the i^{th} individual and r_i^2 is the square of estimated accuracies for the i^{th} individual (Garrick *et al.* 2009), which were calculated using the DEBV_calculator software (Salek Ardestani 2020, https://github.com/Siavash-cloud/DEBV_calculator). Only the individuals with a reliability of dEBV more than 0.1 for at least one studied trait, were kept in the dataset for the following analyses. The dEBVs were used for the following genomic BLUP analyses.

Genomic BLUP

The computed dEBVs were used as pseudo-phenotypes in GBLUP analyses, and the GBLUP method was performed using **Model 2** implemented in SNP1101 software (Sargolzaei 2014). The model was as follows:

$$\mathbf{Model\ 2.}\ y_c = \mathbf{1}\mu + \mathbf{Z}\mathbf{g} + \mathbf{e},$$

where y_c is the vector of dEBVs (training population) as pseudo-phenotypes; μ is the overall mean; \mathbf{Z} is the incidence matrix relating pseudo-phenotypes (dEBVs) to GEBVs; \mathbf{g} is the vector of GEBVs, with $\mathbf{g} \sim N(0, \mathbf{G}\sigma_g^2)$, where \mathbf{G} is the genomic relationship matrix

and σ_g^2 is the genomic variance; and \mathbf{e} is the vector of random residual effects, with $\mathbf{e} \sim N(0, \mathbf{W}\sigma_e^2)$, where \mathbf{W} is a diagonal matrix of residual weights and σ_e^2 is the residual variance. The residual weights were calculated based on the reliability of dEBVs (r_i^2) using the approach described by Garrick et al. (2009) as follows:

$$\mathbf{w} = \frac{1 - r_i^2}{r_i^2}$$

The \mathbf{G} matrix was computed based on the method proposed by VanRaden (VanRaden 2008) as follows:

$$\mathbf{G} = \frac{\mathbf{Z}\mathbf{Z}'}{2 \sum \mathbf{p}_i(1 - \mathbf{p}_i)},$$

where \mathbf{Z} is a matrix of the centered SNP genotypes; \mathbf{Z}' is a transpose matrix of \mathbf{Z} ; and \mathbf{p}_i is the minor allele frequency of the i^{th} SNP.

The variance components of each trait were obtained by applying the “aireml” procedure of SNP1101 software in GBLUP model (*Model 2*).

Single-Step Genomic BLUP

The ssGBLUP analysis (Legarra *et al.* 2009; Christensen & Lund 2010) was carried out using the program BLUPF90 (Aguilar *et al.* 2018). *Model 3* was used for the single-step genomic evaluation of each animal:

$$\mathbf{Model 3. } \mathbf{y} = \mathbf{X}\mathbf{b} + \mathbf{Z}\mathbf{g} + \mathbf{W}\mathbf{pe} + \mathbf{D}\mathbf{m} + \mathbf{e},$$

where \mathbf{y} , $\boldsymbol{\mu}$, \mathbf{X} , \mathbf{b} , \mathbf{W} , \mathbf{pe} , \mathbf{D} , \mathbf{m} , and \mathbf{e} were the same as parameters described in *Model 1*. \mathbf{Z} is the incidence matrix relating phenotypes to GEBVs, and \mathbf{g} is the vector of GEBVs, with $\mathbf{g} \sim N(0, \mathbf{H}\sigma_g^2)$, where \mathbf{H} is the relationship matrix, and σ_g^2 is the variance of genomic effects. The matrix \mathbf{H} is a combination of relationship matrices using both marker

genotypes (\mathbf{G} matrix) and pedigree information (\mathbf{A} matrix). The inverse of \mathbf{H} matrix was obtained using the default option in BLUPF90 (Aguilar *et al.* 2018) as follows:

$$\mathbf{H}^{-1} = \mathbf{A}^{-1} + \begin{bmatrix} \mathbf{0} & \mathbf{0} \\ \mathbf{0} & \tau(\alpha\mathbf{G} + \beta\mathbf{A}_{22})^{-1} - \omega\mathbf{A}_{22}^{-1} \end{bmatrix},$$

where \mathbf{A}_{22} is the pedigree-based relationship matrix of genotyped animals, τ and ω are the scaling factors, and α and β are blending factors of \mathbf{G} and \mathbf{A} matrices, respectively. The τ and ω were both set equal to one as the default option in BLUPF90 software (Aguilar *et al.* 2018). The blending factors α and β were set equal to 0.95 and 0.05 as the default option in BLUPF90 software (Aguilar *et al.* 2018), respectively. The variance components of each trait were estimated from ssGBLUP model (**Model 3**) using the program BLUPF90 (Aguilar *et al.* 2018).

7.2.6 Cross-Validation and Model Comparison

The 5-fold cross-validation strategy was applied to different prediction models. The whole dataset was randomly partitioned into five subsets (folds), and each subset had approximately equal sample sizes (Table 7.1). Then, four subsets were used as training population to train the prediction model, and the remaining one subset was used for validation. At each repetition, cross-validation was performed in the group, which was not used in the training set. This scheme was repeated until each of the five subsets were used as the validation set. To account for sampling variation, splitting was repeated ten times.

To evaluate the prediction accuracy obtained with different models, Pearson's correlations between the EBVs/GEBVs and the phenotypes adjusted for the fixed effects (\mathbf{aY}) were used (Legarra *et al.* 2008). The phenotype adjustment was performed using the *lm* function in R (Team 2022) and the complete dataset, which contained all phenotypic and genotypic information was available for both validation and training subsets. This correlation is

known as the prediction ability (r_{yy}) of the genomic selection to estimate phenotypes; therefore, the prediction accuracy (acc) is given by:

$$acc = \frac{r_{yy}}{h}$$

where r_{yy} is Pearson's correlation between the EBV/GEBV and aY (prediction ability), and h is the square root of the heritability of the trait.

To evaluate the extent of prediction bias of models, the regression of aY on the predicted breeding values (EBV or GEBV) was computed using simple linear regression of the adjusted phenotype on EBV/GEBV with an expected value of 1 for each trait.

7.3 Results

7.3.1 Descriptive Statistics

The number of records, mean, standard deviation (SD), range, and coefficient of variation (CV) for each trait are presented in Table 7.2. Among all studied traits, ELISA-G (n=1,421) and IAT (n=1,409) had the most phenotypes recorded because CCFAR started recording these two traits in 2013, while CIEP (n=960), DOF (n=890), and Varf (n=890) were recorded after 2018. The CVs of ELISA-G (157%), IAT (148%), and DOF (153%) were all higher than 100%, while CIEP (45%) and Varf (25%) had CVs less than 50%.

7.3.2 Estimation of Genetic Parameters

The variance components (SE) and heritabilities of studied traits, which were estimated by using traditional BLUP model (*Model 1*) and full dataset (all available phenotypes), are presented in Table 7.3. The heritabilities of the five studied traits were low to moderate, where ELISA-G had the highest heritability (0.31) and CIEP showed the lowest heritability (0.08). The heritabilities of IAT, DOF, and Varf were 0.18, 0.09, and 0.16, respectively.

The estimations of variance components (SE) and heritabilities for all studied traits from three different prediction models (BLUP, GBLUP, and ssGBLUP) using the validation dataset are shown in Table 7.4. For ELISA-G, the BLUP model showed the highest estimated heritability (0.31), while the GBLUP model showed the lowest estimated heritability (0.17), which was lower than the heritability estimated by the ssGBLUP model (0.20). For CIEP, all three prediction models gave the same heritability of 0.07. For IAT, both BLUP and ssGBLUP models showed heritability of 0.16, which were slightly lower than the heritability estimated by the GBLUP model (0.15). For DOF, the estimated heritabilities were 0.09 for the BLUP and GBLUP models, while the ssGBLUP model showed a slightly lower estimation of 0.08. For Varf, the BLUP model estimated a heritability of 0.11, which was slightly lower than the value estimated by GBLUP (0.12) but higher than the value estimated by ssGBLUP (0.08).

7.3.3 Prediction Abilities, Accuracies, and Bias

The prediction abilities and accuracies (SE) of three different prediction models (BLUP, GBLUP, and ssGBLUP) for all studied traits are present in Table 7.5. For ELISA-G, the BLUP model showed the highest prediction ability (0.39) and accuracy (0.71), while GBLUP and ssGBLUP models showed slightly lower prediction abilities (0.37 and 0.38, respectively) and accuracies (0.66 and 0.68, respectively). For CIEP, GBLUP and ssGBLUP models showed the same prediction ability (0.12) and accuracy (0.40), which were lower than the prediction ability (0.17) and accuracy (0.58) of BLUP models. For IAT, ssGBLUP showed the highest prediction ability (0.22) and accuracy (0.53), while GBLUP model showed the lowest prediction ability (0.15) and accuracy (0.34), which was also lower than the prediction ability (0.18) and accuracy (0.41) of BLUP model. For DOF,

the ssGBLUP model showed a prediction ability of 0.05 and an accuracy of 0.17, which were lower than the BLUP model (0.07 and 0.22, respectively) but higher than the GBLUP model (0.03 and 0.11, respectively). For Varf, the ssGBLUP models showed the highest prediction ability of 0.11 and accuracy of 0.32, which were similar to the GBLUP model (0.10 and 0.30, respectively) but higher than the BLUP model (0.08 and 0.23, respectively). The prediction biases of all prediction models for each trait, which were measured by the regression of adjusted phenotypes on the predicted breeding values, are shown in Table 7.6. For ELISA-G, the ssGBLUP and GBLUP models showed similar prediction bias (1.34 and 1.35, respectively), which were smaller than the BLUP model (1.55). For CIEP, the BLUP model had the largest prediction bias (1.79), while the ssGBLUP model showed the smallest prediction bias (1.05), and the GBLUP model showed the second smallest prediction bias (1.11). For IAT, the BLUP model showed the smallest prediction bias (1.09), while the GBLUP model showed the largest (1.67). The ssGBLUP model was the only model with a prediction bias of less than one (0.84) among all prediction models for IAT. For DOF, the BLUP and GBLUP models had prediction biases (0.80 and 0.65, respectively) larger than the ssGBLUP model (1.05). For Varf, the GBLUP model had a prediction bias of 1.33, which was smaller than the prediction bias of the ssGBLUP model (1.66) but larger than the prediction bias of the BLUP model (1.07).

7.4 Discussions

This thesis chapter compared prediction abilities, accuracies, and biases of traditional BLUP, GBLUP, and ssGBLUP for three AD tests and two feed-intake-related AD resilience traits. Except for GBLUP model in Varf, where the estimated heritability from GBLUP was slightly higher than the BLUP model, all the estimated heritabilities of studied traits from

GBLUP and ssGBLUP models were lower or equal to the heritabilities estimated by the BLUP model (Table 7.4). When the estimated heritabilities from GBLUP or ssGBLUP model were much lower than the BLUP model (in the case of ELISA-G trait) or the heritability of the traits itself was very low (less than 0.1, in the cases of CIEP and DOF traits), the BLUP model provided the best prediction ability and accuracy among all three prediction models (Table 7.5). However, when the ssGBLUP model had the similar (in the case of IAT trait) or close (in the case of Varf trait) heritability as the BLUP model, the ssGBLUP model showed the highest prediction ability and accuracy (Table 7.5). The ssGBLUP showed higher prediction ability and accuracy than the GBLUP model for all traits except for CIEP, where ssGBLUP model had the same prediction ability and accuracy as the GBLUP model (Table 7.5). Among all prediction models, the BLUP model provided the most unbiased prediction for the IAT and Varf traits, the ssGBLUP model showed the smallest biases for the CIEP and DOF traits, and the GBLUP model had the smallest bias for ELISA-G (Table 7.6).

The advantage of using genomic information (GBLUP and ssGBLUP methods) for breeding value prediction over using pedigree information (BLUP method) was not consistent across the studied traits. Compared to traditional BLUP method, using genomic information increased the prediction ability and accuracy for the IAT and Varf traits but not for the ELISA-G, CIEP, and DOF traits. The genomic predictions for all studied traits in the current study have not been conducted in the previous studies. Thus, no previous estimates are available for comparison. However, similar results were also reported in swine (Zhang *et al.* 2018), cattle (Silva *et al.* 2016), and sheep (Daetwyler *et al.* 2012) for the feed efficiency and growth traits and in chicken (Zhang *et al.* 2020) for immune

response traits, where the use of genomic data for genomic prediction was not beneficial for all traits. The usage of genomic information is generally expected to provide better prediction accuracy because genomic data could consider the Mendelian sampling terms better than pedigree information, therefore producing more accurate genetic relationships among animals (Christensen *et al.* 2012; Meuwissen *et al.* 2013; Knol *et al.* 2016). However, this is not always the case, as mentioned above. Several factors could affect the genomic prediction ability and accuracy, including the ability of markers to capture the total genetic variance of the traits (Goddard 2009), the accuracy of the estimates of marker effects (Goddard 2009), the density of markers used (Zhang *et al.* 2018; Zhang *et al.* 2019a), the heritability of the studied trait (Goddard 2009; Zhang *et al.* 2019a; Budhlakoti *et al.* 2022), and the population size (Guarini *et al.* 2018; Hidalgo *et al.* 2021; Budhlakoti *et al.* 2022).

The traditional BLUP model showed higher prediction ability and accuracy than GBLUP and ssGBLUP models for ELISA-G, which indicated the advantage of using genomic information for breeding value prediction over using pedigree information was not present for ELISA-G. The missing heritability was considered to be one of the main reasons leading to these results. In the case of ELISA-G trait, the heritabilities estimated by using genomic information were lower than the estimates obtained from pedigree-based BLUP model (Table 7.4), which indicated the existence of missing heritability. Missing heritability has been considered an issue in both human (Yang *et al.* 2010; Yang *et al.* 2015) and livestock genetics (Silva *et al.* 2016; Zhang *et al.* 2018; Zhang *et al.* 2020). Missing heritability could be caused by several reasons, including the incomplete linkage disequilibrium between causal genomic variants and genotyped SNPs (Yang *et al.* 2010;

Yang *et al.* 2015), the genetic architecture of the studied trait, epistatic effects, and genotype-by-environment interactions (Makowsky *et al.* 2011). For instance, if the genotyped SNPs are located closely to causal variants for the traits or the SNPs themselves are actually the causal variants for the traits, the SNPs could capture a large proportion of the genetic variance and provide high genomic prediction ability and accuracy. In another way, if the genotyped SNPs are not able to capture an adequate proportion of the genetic variation for the trait, the prediction accuracy could be limited. In the case of ELISA-G trait, the genotyped SNPs in our study could only catch 55 to 65% of the genetic variance based on the pedigree-based estimate of heritability (Table 7.4). Thus, missing heritability could be one of the main reasons for the lower prediction ability and accuracy in the GBLUP and ssGBLUP models compared to the BLUP model for ELISA-G.

Besides ELISA-G, the traditional BLUP model also showed higher prediction ability and accuracy than GBLUP and ssGBLUP models for the CIEP and DOF traits. Different from the case of ELISA-G trait, where the missing heritability issue existed, the estimated heritabilities from using genomic information were equal to or very close to the estimates from pedigree-based BLUP model (Table 7.4). However, the low level of heritability of these two traits themselves, small training population size, and insufficient SNP marker density could be the reasons leading to these results. The accuracy of genomic prediction could be affected by trait heritability, especially for the traits with low heritability (lower than 0.4) (Hayes *et al.* 2009). Many studies showed that the heritability of studied traits could strongly influence the accuracy of genomic selection because locus identification and effect estimation are difficult to predict in the case of low heritability quantitative traits (Goddard 2009; Hayes *et al.* 2009; Guarini *et al.* 2018; Zhang *et al.* 2018; Zhang *et al.*

2019a; Budhlakoti *et al.* 2022). Generally, it is assumed that the target trait with high heritability has good prediction accuracies and vice versa. For low heritable and complex traits, many previous studies showed that the performance of the traditional pedigree-based BLUP model seems to provide better prediction ability and accuracy compared to the prediction models (GBLUP and ssGBLUP) using genomic information (Silva *et al.* 2016; Guarini *et al.* 2018; Zhang *et al.* 2018; Zhang *et al.* 2020). The accuracy of genomic selection is also affected by the size of the training population because the small training population size could cause the model to estimate the marker effects poorly and hence the prediction accuracy (Budhlakoti *et al.* 2022). Vanraden *et al.* (VanRaden *et al.* 2009) found that the correlation between accuracy and the size of training population was nearly linear. In other words, the smaller that the training population size is, the lower accuracy of genomic selection could be observed (Goddard 2009; Budhlakoti *et al.* 2022; Gizachew Haile 2022). Marker density is another factor that influences the accuracy of genomic selection. The complete genome could be covered by a minimum number of markers based on the decay of linkage disequilibrium (LD), where at least one marker is expected in LD with each genomic region. The increase in marker density has the potential to improve the accuracy of genomic prediction, as more causative mutations are expected to be included in the increased genotype data (Meuwissen & Goddard 2010; Hayes *et al.* 2014). It requires a larger training population, a larger number of phenotypes, and a higher density of markers for traits with low heritability to attain a similar level of accuracy and persistence of accuracy as the traits with high heritability (Daetwyler *et al.* 2008; Hayes *et al.* 2009; Atefi *et al.* 2018; Hidalgo *et al.* 2021). However, in the cases of CIEP and DOF traits, where the heritabilities were lower than 0.1 (Table 7.3), the size of the training population (less than

750), the number of phenotypes records (less than 1,000), and marker density (around 26K after quality control) may not be sufficient to provide satisfactory prediction accuracy in genomic selection methods.

The ssGBLUP had higher or the same prediction ability and accuracy compared to the GBLUP model in all scenarios (Table 7.5). The ssGBLUP model has the advantage of simultaneously using the phenotypes of genotyped and non-genotyped animals, pedigrees, and genotypes. Compared with GBLUP model, ssGBLUP model predicts how non-genotyped individuals can benefit from genomic information by applying a blended genetic relationship matrix, which is computed using both genomic and pedigree relationship matrices (Legarra *et al.* 2009). The use of ssGBLUP model increased the accuracy of genomic selection in many contexts and species compared with GBLUP model (Chen *et al.* 2011; Carillier *et al.* 2014; Onogi *et al.* 2015; Matilainen *et al.* 2016). However, the increases in prediction accuracy from using ssGBLUP over GBLUP were not consistent among studied traits (Table 7.5). The inconsistency could be caused by several factors, including the size of the training population (Lourenco *et al.* 2014; Andonov *et al.* 2017), the relationship between the training and validation population (Meuwissen & Goddard 2010; Teissier *et al.* 2019), the extent of LD (Zhou *et al.* 2018), or the genetic architecture of the studied trait (Goddard 2009; Carillier-Jacquin *et al.* 2016; Zhou *et al.* 2018).

Based on the results of this study, different prediction models were suggested for different studied traits. Although the BLUP model showed slightly higher accuracy than the GBLUP and ssGBLUP models (Table 7.5) for ELISA-G, the noticeable higher prediction bias of the BLUP model over the GBLUP and ssGBLUP models (Table 7.6) cannot be ignored. In the case of ELISA-G, where the differences in prediction accuracy among different models

were slight, ssGBLUP, which showed the lowest prediction bias, would be the most appropriate prediction model for the selection of ELISA-G. For the CIEP and DOF traits, which had low heritabilities, although ssGBLUP showed the lowest prediction bias (Table 7.6), the BLUP model provided the best prediction accuracy for these two traits (Table 7.5). This may indicate that the BLUP model would be the better prediction model for the EBV prediction for the CIEP and DOF traits. However, genomic prediction models have the potential to increase the ability and accuracy of prediction if larger training population size and marker density could be applied in future studies. The ssGBLUP model seemed more suitable to obtain genomic predictions for IAT and Varf traits on an experimental population as the highest prediction ability and accuracy were observed on the ssGBLUP model in the predictions for these two traits (Table 7.5).

7.5 Conclusion

This thesis chapter examined the efficiency of BLUP, GBLUP, and ssGBLUP models in the EBV prediction on immune response and feed-intake-related resilience to AD in mink. The ssGBLUP resulted in higher prediction accuracy than the other methods tested for IAT and Varf traits. The pedigree-based traditional BLUP outperformed all genomic methods and produced the highest prediction accuracies for ELISA-G, CIEP, and DOF, likely because the SNPs captured less genetic variance for these traits than pedigree data (ELISA-G) or insufficient training population size and marker density for traits with low heritability (CIEP and DOF). In the future, as genotyping or sequencing becomes more affordable, people gain a deeper comprehension of genome and variant functional annotations (Andersson *et al.* 2015), along with the utilization of larger training population sizes,

ssGBLUP has the potential to emerge as the most effective approach for the selection of AD resilient mink.

Table 7.1 Number of animals in the training and validation populations.

Traits ¹	Total animals	Training animals	Validation animals
ELISA-G	1,120	896	224
CIEP	934	747	187
IAT	1,114	891	223
DOF	890	713	177
Varf	890	713	177

¹ELISA-G=Aleutian mink disease virus antigen-based enzyme-linked immunosorbent assay test; CIEP=Counterimmunoelectrophoresis test; IAT=Iodine agglutination test; DOF=the proportion of off-feed days; Varf=Variation in daily feed intake.

Table 7.2 Descriptive statistics of five studied traits.

Traits ¹	Phenotype records	Mean	SD ²	Range	CV ³ (%)
ELISA-G	1,421	1.40	2.20	0 to 7	157%
CIEP	960	0.83	0.38	0 to 1	45%
IAT	1,409	0.68	1.01	0 to 4	148%
DOF	890	5.42	8.30	0 to 65.45	153%
Varf	890	48.31	12.06	27.37 to 136.68	25%

¹ELISA-G=Aleutian mink disease virus antigen-based enzyme-linked immunosorbent assay test; CIEP=Counterimmunoelectrophoresis test; IAT=Iodine agglutination test; DOF=the proportion of off-feed days; Varf=Variation in daily feed intake; ²SD=Standard deviation; ³CV=Coefficient of variation.

Table 7.3 Estimates of variance components and heritabilities with their standard errors (SE) for all studied traits using traditional best linear unbiased prediction model and full dataset.

Traits ¹	Variance components				Heritabilities
	$\sigma_a^2 \pm SE^2$	$\sigma_m^2 \pm SE^3$	$\sigma_{pe}^2 \pm SE^4$	$\sigma_e^2 \pm SE^5$	h^2 ⁶
ELISA-G	1.49±0.43	0.87±0.25	1.16±0.26	1.31±0.11	0.31
CIEP	0.01±0.02	0.02±0.01	NA	0.10±0.01	0.08
IAT	0.18±0.05	NA ⁷	0.18±0.06	0.63±0.05	0.18
DOF	5.79±3.58	NA	NA	60.59±4.11	0.09
VarF	19.58±9.89	NA	NA	104.50±9.54	0.16

¹ELISA-G=Aleutian mink disease virus antigen-based enzyme-linked immunosorbent assay test; CIEP=Counterimmunoelectrophoresis test; IAT=Iodine agglutination test; DOF=the proportion of off-feed days; VarF=Variation in daily feed intake.

² σ_a^2 = additive genetic variance; ³ σ_m^2 = maternal genetic variance; ⁴ σ_{pe}^2 = permanent environmental variance; ⁵ σ_e^2 = residual variance; ⁶ h^2 = heritability.

⁷NA = not applicable.

Table 7.4 Estimates of variance components and heritabilities with their standard errors (SE) for all studied traits from three different prediction models using validation dataset.

Traits ⁴	BLUP ¹					GBLUP ²			ssGBLUP ³				
	$\sigma_a^2 \pm \text{SE}^5$	$\sigma_m^2 \pm \text{SE}^6$	$\sigma_{pe}^2 \pm \text{SE}^7$	$\sigma_e^2 \pm \text{SE}^8$	h^2 ⁹	$\sigma_a^2 \pm \text{SE}$	$\sigma_e^2 \pm \text{SE}$	h^2	$\sigma_a^2 \pm \text{SE}$	$\sigma_m^2 \pm \text{SE}$	$\sigma_{pe}^2 \pm \text{SE}$	$\sigma_e^2 \pm \text{SE}$	h^2
ELISA-G	1.50±0.48	0.80±0.27	1.21±0.30	1.30±0.12	0.31	0.91±0.10	4.41±0.36	0.17	0.97±0.28	1.09±0.27	1.47±0.22	1.29±0.12	0.20
CIEP	0.01±0.01	0.01±0.01	NA ¹⁰	0.12±0.01	0.07	0.01±0.01	0.14±0.04	0.07	0.02±0.01	0.01±0.01	NA	0.11±0.01	0.07
IAT	0.16±0.06	NA	0.19±0.07	0.63±0.06	0.16	0.04±0.04	0.22±0.07	0.15	0.16±0.05	NA	0.18±0.06	0.63±0.06	0.16
DOF	6.26±4.21	NA	NA	59.95±4.75	0.09	5.03±1.31	50.53±3.07	0.09	4.51±3.12	NA	NA	55.52±4.16	0.08
Varf	12.87±8.04	NA	NA	106.82±8.72	0.11	10.59±6.77	90.65±15.27	0.12	9.98±3.88	NA	NA	101.04±7.64	0.08

¹BLUP = traditional best linear unbiased prediction; ²GBLUP = multi-steps genomic best linear unbiased prediction; ³ssGBLUP = single-step genomic best linear unbiased prediction.

⁴ELISA-G = antigen-based enzyme-linked immunosorbent assay test; CIEP = Counterimmunoelectrophoresis test; IAT = Iodine agglutination test; DOF = the proportion of off-feed days; VarF = Variation in daily feed intake.

⁵ σ_a^2 = additive genetic variance; ⁶ σ_m^2 = maternal genetic variance; ⁷ σ_{pe}^2 = permanent environmental variance; ⁸ σ_e^2 = residual variance; ⁹ h^2 = heritability.

¹⁰NA = not applicable.

Table 7.5 The prediction abilities and accuracies and their SE for all studied traits from three different prediction models using validation dataset.

Trait ⁴	BLUP ¹		GBLUP ²		ssGBLUP ³	
	Prediction ability	Prediction accuracy	Prediction ability	Prediction accuracy	Prediction ability	Prediction accuracy
ELISA-G	0.39 (0.03)	0.71 (0.05)	0.37 (0.02)	0.66 (0.04)	0.38 (0.02)	0.68 (0.04)
CIEP	0.17 (0.02)	0.58 (0.07)	0.12 (0.02)	0.40 (0.06)	0.12 (0.03)	0.40 (0.09)
IAT	0.18 (0.02)	0.41 (0.05)	0.15 (0.04)	0.34 (0.09)	0.22 (0.05)	0.53 (0.11)
DOF	0.07 (0.03)	0.22 (0.11)	0.03 (0.01)	0.11 (0.03)	0.05 (0.02)	0.17 (0.09)
Varf	0.08 (0.02)	0.23 (0.06)	0.10 (0.02)	0.30 (0.04)	0.11 (0.06)	0.32 (0.05)

¹BLUP = traditional best linear unbiased prediction; ²GBLUP = multi-steps genomic best linear unbiased prediction; ³ssGBLUP = single-step genomic best linear unbiased prediction; ⁴ELISA-G = antigen-based enzyme-linked immunosorbent assay test; CIEP = Counterimmunoelectrophoresis test; IAT = Iodine agglutination test; DOF = the proportion of off-feed days; VarF = Variation in daily feed intake.

Table 7.6 Regression coefficient and their standard errors of adjusted phenotypes on the predicted breeding value (EBV or GEBV) from three different prediction models using validation dataset for all studied traits.

Trait ¹	BLUP ²	GBLUP ³	ssGBLUP ⁴
ELISA-G	1.55 (0.22)	1.35 (0.21)	1.34 (0.22)
CIEP	1.79 (0.62)	1.11 (0.75)	1.05 (0.47)
IAT	1.09 (0.54)	1.67 (0.60)	0.84 (0.27)
DOF	0.80 (0.53)	0.65 (0.30)	1.05 (0.75)
Varf	1.07 (0.76)	1.33 (0.61)	1.66 (0.65)

¹ELISA-G = antigen-based enzyme-linked immunosorbent assay test; IAT = Iodine agglutination test; CIEP = Counterimmunoelectrophoresis test; DOF = the proportion of off-feed days; VarF = Variation in daily feed intake.

²BLUP = traditional best linear unbiased prediction; ³GBLUP = multi-steps genomic best linear unbiased prediction; ⁴ssGBLUP = single-step genomic best linear unbiased prediction.

CHAPTER 8. General Discussion and Conclusion

8.1 Summary and general discussion

Aleutian disease (AD) brings severe health issues and results in substantial economic setbacks for the mink industry. The inefficacy of vaccination, medicine, and culling strategy in managing AD has prompted mink farmers to select AD-resilient mink. However, as the literature review in this thesis (Chapter 2) discussed, the lack of comprehensive knowledge of the genetic/genomic architecture of AD resilience prevents breeders from integrating this novel trait into their breeding programs. Thus, this thesis aimed to provide a comprehensive view of the genetic and genomic architecture of AD resilience and assess the potential of genomic prediction methods in the selection process for AD resilience. The genetic parameters estimated from Chapter 3 revealed the genetic correlations among the studied AD-resilient traits, and the results further illustrated the antigen-based enzyme-linked immunosorbent assay test (ELISA-G) was the most reliable and practical indicator trait to select AD-resilient mink among all AD tests. In Chapter 4, the genetic structure of farmed mink was investigated using genotypic information from the first Axiom Affymetrix Mink 70K single nucleotide polymorphism (SNP) panel to update the population genomics information of farmed mink in Canada. Selection signatures (Chapter 5) and genome-wide association studies (GWAS, Chapter 6) were performed to explore the genomic architecture of AD resilience, and several genes and biological pathways related to the studied AD-resilient traits were detected in these studies. The outcomes from selection signatures and GWAS studies not only contributed to a better

understanding of the genomic architecture underlying the immune response and resilience of mink to AD but also provided an opportunity for improving the resilience of mink to AD using marker-assisted/genomic selection in mink. In Chapter 7, different genomic prediction methods were assessed to investigate the viability and optimal strategy for leveraging genomic information to enhance genetic gains for AD resilience in mink. Based on the prediction accuracies and biases of different prediction methods for each trait, the most suitable prediction approach was suggested for each AD-resilient trait

8.1.1 Genetic Parameters

Chapter 3 assessed the genetic and phenotypic correlations among four AD tests, seven body weight (BW) traits, six growth parameters derived from the Richards growth model, and eight feed-related traits. Notably, both the ELISA-G and virus capsid protein-based enzyme-linked immunosorbent assay tests (ELISA-P) demonstrated significant ($p < 0.05$) moderate positive genetic correlations with maturation rate (0.36 and 0.38, respectively). ELISA-G exhibited a significant negative genetic correlation with average daily gain (ADG, -0.37), while ELISA-P displayed a significant positive moderate genetic correlation with off-feed days (DOF, 0.42). These results imply that selection for low ELISA scores could decrease the maturation rate, enhance ADG (as indicated by ELISA-G), and minimize DOF (as suggested by ELISA-P). Furthermore, the iodine agglutination test (IAT) demonstrated significant genetic correlations with DOF (0.73), BW at 16 weeks of age (BW16, 0.45), and BW at harvest (HW, 0.47). Consequently, selecting for lower IAT scores would likely result in reduced DOF and BW16, along with increased HW. The estimated genetic correlations collectively suggest that choosing specific AD tests would not adversely affect the growth, feed efficiency, and feed intake of mink. Specifically,

selecting mink with low ELISA-G scores could improve average daily gain and contribute to mature weight without detrimental effects on body weight, feed efficiency, off-feed days, and feed intake consistency.

Our previous study (Hu *et al.* 2021) indicated that ELISA-G had the potential to be applied as an indicator trait for genetic selection of AD-resilient mink in AD endemic ranches because ELISA-G had moderate heritability (0.39) and repeatability (0.58) and selecting for low ELISA-G test results could also enhance female reproductive performance traits and harvest length while decreasing anemia extent without compromising pelt quality. The findings from Chapter 3 further support the notion that ELISA-G could serve as a reliable and practical indicator trait in the genetic selection of AD-resilient mink within AD-positive farms.

8.1.2 Population Genomics

Clarifying the genetic structure of the target populations is critically important for the development of efficient genomic selection programs in domestic animals. Thus, Chapter 4 in this thesis aimed to compute a series of parameters, including linkage disequilibrium (LD), effective population size (N_e), genetic diversity, genetic distances, and population differentiation and admixture, using the genotypic data from the first SNP panel for American mink with a larger sample size to reveal the genetic structure of studied population (Canadian Centre for Fur Animal Research (CCFAR), Truro, NS and Millbank Fur Farm (MFF), Rockwood, ON). Based on the estimated LD patterns, the minimum marker densities to obtain adequate accuracy for genomic selection programs in CCFAR and MFF were suggested (7,700 and 4,200, respectively). The genetic distance and diversity analyses showed that American mink of the various color types had a close

genetic relationship and low genetic diversity, with most genetic variation occurring within rather than between color types. The results indicated that the color types of mink might not be a reliable indicator to differentiate American mink. The admixture analysis showed the genetic structure of the studied populations was composed of three ancestral genetic clusters, where black (in both CCFAR and MFF) and pastel color types had their own ancestral clusters, while demi, mahogany, and stardust color types were admixed with the three ancestral genetic clusters. This thesis chapter provided essential information to utilize the first SNP panel for American mink in genomic selection, as well as other genomic studies, such as quantitative trait locus mapping, identification of signatures of selection, and GWAS.

8.1.3 Selection Signatures

Many mink farms have employed phenotypic selections of AD-resilient mink based on AD tests and/or AD resilience indicator traits to reduce the adverse influence caused by AD. The utilization of these indicator traits in the selection process may have influenced the genetic variation patterns, potentially revealing genes subjected to selection pressures. Therefore, Chapter 5 in this thesis aimed to identify signatures of selection associated with various AD-resilient traits, such as immune response (IRE), general resilience (GRP), and female reproductive performance (FRP) to AD. A total of 619, 569, and 526 SNPs were identified as potential selection signatures for IRE, GRP, and FRP traits, respectively. The genes annotated from these signatures were implicated in processes like the immune system, growth, reproduction, and pigmentation. These annotated genes may help in better understanding the mechanism of AD in influencing immune response, body weight growth, female reproductive performance, and pelt quality. Notably, two olfactory-related gene

ontology (GO) terms were consistently significant across all traits, suggesting a potential impact of AD on the sense of smell in infected mink. This finding may explain the reduced feed intake observed in AD-infected mink. Variations in detected genes and GO terms among different color types for IRE indicated diverse immune responses to AD among mink of varying color types. The Kyoto Encyclopedia of Genes and Genomes pathway analyses for FRP highlighted the significance of the mitogen-activated protein kinase (MAPK) signalling pathway, implying that AD infection might disrupt MAPK signalling, affecting FRP. Overall, the findings from Chapter 5 advanced our understanding of the genomic architecture of AD resilience, shedding light on the underlying biological mechanisms associated with AD resilience.

8.1.4 Genome-wide Association Studies

In recent years, advancements in next-generation sequencing technologies, high-density SNP arrays, and bioinformatics tools have led to the increased popularity of GWAS for identifying genetic variants and genes associated with immune response and disease resilience traits in livestock. The introduction of the Axiom Affymetrix Mink 70K SNP panel has enabled GWAS investigations into the genomic architecture of resilience to AD using genotypic information. Chapter 6 of this thesis focuses on conducting GWAS to pinpoint genomic regions and genes linked to immune response and resilience to AD. The GWAS analysis identified 17, eight, and seven SNPs associated with ELISA-G, IAT, and the proportion of off-feed days (DOF), respectively. From these SNPs, 141 genes were annotated for ELISA-G, with *MPIG6B*, *RUNX2*, and *C4A* emerging as potential key genes in regulating immune-mediated responses to AD. Among the 44 genes annotated from SNPs associated with IAT, *TNFRSF11A* and *C4A* were found to be involved in the immune

system process. Additionally, 42 genes were annotated from SNPs associated with DOF, including *ADCY7* and *CNDP2*, which are relevant to feed intake or appetite. The study identified five significant ($q < 0.05$) overrepresented GO enrichment terms for ELISA-G, and these five GO terms play crucial roles in adaptive immune response or complement system. The significant SNPs, genes, and GO terms uncovered in this investigation enhance our understanding of the genomic basis of mink resilience to AD. This knowledge opens avenues for improving mink resilience to AD through marker-assisted or genomic selection strategies.

8.1.5 Genomic Prediction

The introduction of dense panels of SNP markers has greatly facilitated the widespread adoption of genomic selection in major farm animal species. This implementation expedites genetic trends by improving selection accuracy and reducing generation intervals. The heightened accuracy in selection is particularly important for traits with low heritabilities, which is often the case for traits associated with diseases that typically exhibit a low-to-moderate heritability range. Therefore, employing genomic selection is recommended to enhance disease-related traits. Chapter 7 of this thesis aimed to investigate the efficiency of genomic selection approaches on resilience traits related to AD. This investigation involved assessing the effectiveness of traditional pedigree-based Best Linear Unbiased Prediction (BLUP), Genomic BLUP (GBLUP), and Single-Step Genomic BLUP (ssGBLUP) models in predicting the estimated breeding values for immune response and feed-intake-related resilience to AD in mink. ssGBLUP demonstrated the highest prediction accuracy among all tested methods for IAT (0.53) and day-to-day variation in feed intake (Varf, 0.32). In comparison to genomic prediction methods, the pedigree-based

traditional BLUP yielded higher prediction accuracies for ELISA-G, counterimmunoelectrophoresis (CIEP), and DOF. This could be attributed to SNPs capturing less genetic variance for these traits than pedigree data (ELISA-G) or limitations in the training population size and marker density for traits with low heritability (CIEP and DOF).

This thesis chapter suggested different prediction models for different traits. Despite slightly lower prediction accuracy than the BLUP model, ssGBLUP could be considered the most appropriate prediction model for ELISA-G due to its lower prediction bias. For CIEP and DOF, the BLUP model provided the best prediction accuracy, indicating its suitability for breeding values estimation for these traits. However, genomic prediction models have the potential to enhance prediction ability and accuracy with larger training populations and marker density in future studies. The ssGBLUP model appears more suitable for obtaining genomic predictions for IAT and Varf, showing the highest prediction ability and accuracy. As genotyping or sequencing costs decrease and our understanding of genome and variant functional annotations improves, coupled with larger training populations, ssGBLUP may emerge as the most effective approach for genomic prediction of AD resilience in mink.

8.1.6 Conclusion

In conclusion, the studies conducted in this thesis not only provide practical information and suggestions for future implementation of genetic/genomic selection on AD resilience, but also enhance our understanding of the genomic architecture and biological pathways underlying mink's resilience to AD. The estimates of genetic parameters in Chapter 3 further support the practicability and reliability of ELISA-G as an indicator trait of AD

resilience in the genetic selection of AD-resilient mink. The updated population genomics information obtained from Chapter 4 would direct the utilization of the first SNP panel for American mink in their genomic studies and help to better understand the genetic structure of mink populations. The genes and GO terms, which were estimated to be related to AD resilience, from Chapters 5 and 6 advanced our knowledge of the genomic architecture and biological pathways associated with AD resilience. Chapter 7 suggested the most suitable prediction model for each AD-resilient trait based on the performances of different methods in the prediction of EBV, which provided helpful information for future genomic selection of AD resilience in mink. To the best of our knowledge, this thesis offered the first comprehensive genomic analyses to identify genetic variants and biological mechanisms underlying AD resilience traits in mink. This would contribute to understanding the biological foundation of AD resilience in mink and directing the future breeding program for AD-resilient mink.

8.1.7 General Recommendations and Future Directions

Given the insights derived from this thesis, several enhancements and strategies could be implemented in subsequent studies to advance the resilience of mink to AD:

- a) Future investigations on genetic parameters of AD resilience in mink could benefit from the inclusion of diverse mink populations sourced from various farms and larger sample sizes, therefore increasing the accuracy of genetic evaluation.
- b) Using a larger sample size with whole-genome sequencing data or imputing the current genotypic data to the whole-genome level may help in addressing the limitations of SNP arrays, such as the limitation in capturing a significant portion of heritability (missing heritability issue), in future genomic studies of AD resilience.

- c) The detected genomic regions and candidate genes associated with AD resilience traits in this thesis should be validated through various methods, such as web laboratory validation and fine mapping, thereby confirming the impact of these genes on AD resilience traits in mink.
- d) To identify more biomarkers associated with AD-resilient traits in mink, future research could include more omics approaches, such as transcriptomics, metabolomics, and microbiomics.
- e) Applying machine learning and deep learning approaches may significantly contribute to the future genetic and genomic studies of AD resilience by providing more robust statistical models for analyzing and interpreting phenotypic and genomic data.

REFERENCES

Aasted B. (1989) Mink infected with Aleutian disease virus have an elevated level of CD8-positive T-lymphocytes. *Vet. Immunol. Immunopathol.* **20**, 375-85.

Aasted B., Alexandersen S. & Christensen J. (1998) Vaccination with Aleutian mink disease parvovirus (AMDV) capsid proteins enhances disease, while vaccination with the major non-structural AMDV protein causes partial protection from disease. *Vaccine* **16**, 1158-65.

Aasted B. & Bloom M.E. (1983) Sensitive radioimmune assay for measuring Aleutian disease virus antigen and antibody. *J. Clin. Microbiol.* **18**, 637-44.

Aasted B. & Cohn A. (1982) INHIBITION OF PRECIPITATION IN COUNTER CURRENT ELECTROPHORESIS. A SENSITIVE METHOD FOR DETECTION OF MINK ANTIBODIES TO ALEUTIAN DISEASE VIRUS. **90C**, 15-9.

Abele R. & Tampé R. (1999) Function of the transport complex TAP in cellular immune recognition. *Biochim. Biophys. Acta. -Biomembr* **1461**, 405-19.

Adney D.R., Lovaglio J., Schulz J.E., Yinda C.K., Avanzato V.A., Haddock E., Port J.R., Holbrook M.G., Hanley P.W., Saturday G., Scott D., Shaia C., Nelson A.M., Spengler J.R., Tansey C., Cossaboom C.M., Wendling N.M., Martens C., Easley J., Yap S.W., Seifert S.N. & Munster V.J. (2022) Severe acute respiratory disease in American mink experimentally infected with SARS-CoV-2. *JCI Insight* **7**, e159573.

Agriculture_and_Marketing_of_Nova_Scotia_Government (1998) Agriculture and Marketing of Nova Scotia Government, Testing for Aleutian Disease in Minks, 1998. URL <https://novascotia.ca/news/release/?id=19980120008>.

Aguilar I., Tsuruta S., Masuda Y., Lourenco D.A.L., A. Legarra A. & Misztal I. (2018) BLUPF90 suite of programs for animal breeding with focus on genomics. No. 11.751. *The 11th World Congress of Genetics Applied to Livestock Production, Auckland, New Zealand*.

Aichele P., Neumann-Haefelin C., Ehl S., Thimme R., Cathomen T., Boerries M. & Hofmann M. (2022) Immunopathology caused by impaired CD8+ T-cell responses. *Eur. J. Immunol.* **52**, 1390-5.

Aki T., Funakoshi T., Nishida-Kitayama J. & Mizukami Y. (2008) TPRA40/GPR175 regulates early mouse embryogenesis through functional membrane transport by Sjögren's syndrome-associated protein NA14. *J. Cell. Physiol.* **217**, 194-206.

Alaynick W.A., Kondo R.P., Xie W., He W., Dufour C.R., Downes M., Jonker Johan W., Giles W., Naviaux R.K., Giguère V. & Evans R.M. (2007) ERR γ Directs and Maintains the Transition to Oxidative Metabolism in the Postnatal Heart. *Cell Metab.* **6**, 13-24.

Albers G.A., Gray G.D., Piper L.R., Barker J.S., Le Jambre L.F. & Barger I.A. (1987) The genetics of resistance and resilience to *Haemonchus contortus* infection in young merino sheep. *Int. J. Parasitol.* **17**, 1355-63.

Albornoz R.I., Kennedy K.M. & Bradford B.J. (2023) Symposium review: Fueling appetite: Nutrient metabolism and the control of feed intake. *J. Dairy Sci.* **106**, 2161-6.

Alexander D.H. & Lange K. (2011) Enhancements to the ADMIXTURE algorithm for individual ancestry estimation. *BMC Bioinform.* **12**, 246.

Alexander D.H., Novembre J. & Lange K. (2009) Fast model-based estimation of ancestry in unrelated individuals. *Genome Res.* **19**, 1655-64.

Allen M.S. (2014) Drives and limits to feed intake in ruminants. *Anim. Prod. Sci.* **54**, 1513-24.

Almén M.S., Jacobsson J.A., Shaik J.H.A., Olszewski P.K., Cedernaes J., Alsiö J., Sreedharan S., Levine A.S., Fredriksson R., Marcus C. & Schiöth H.B. (2010) The obesity gene, TMEM18, is of ancient origin, found in majority of neuronal cells in all major brain regions and associated with obesity in severely obese children. *BMC Med. Genet.* **11**, 58.

Alonso-Hearn M., Badia-Bringué G. & Canive M. (2022) Genome-wide association studies for the identification of cattle susceptible and resilient to paratuberculosis. *Front. vet. sci.* **9**, 935133.

Alpay F., Zare Y., Kamalludin M.H., Huang X., Shi X., Shook G.E., Collins M.T. & Kirkpatrick B.W. (2014) Genome-wide association study of susceptibility to infection by *Mycobacterium avium* subspecies paratuberculosis in Holstein cattle. *PLoS One* **9**, e111704.

An B., Liang M., Chang T., Duan X., Du L., Xu L., Zhang L., Gao X., Li J. & Gao H. (2021) KCRR: a nonlinear machine learning with a modified genomic similarity matrix improved the genomic prediction efficiency. *Brief. Bioinform.*

Anderson D.M., Maraskovsky E., Billingsley W.L., Dougall W.C., Tometsko M.E., Roux E.R., Teepe M.C., DuBose R.F., Cosman D. & Galibert L. (1997) A homologue of the TNF receptor and its ligand enhance T-cell growth and dendritic-cell function. *Nature* **390**, 175-9.

Andersson A.-M. & Wallgren P. (2013) Evaluation of two enzyme-linked immunosorbent assays for serodiagnosis of Aleutian mink disease virus infection in mink. *Acta Vet. Scand.* **55**, 86.

Andersson L., Archibald A.L., Bottema C.D., Brauning R., Burgess S.C., Burt D.W., Casas E., Cheng H.H., Clarke L., Couldrey C., Dalrymple B.P., Elsik C.G., Foissac S., Giuffra E., Groenen M.A., Hayes B.J., Huang L.S., Khatib H., Kijas J.W., Kim H., Lunney J.K., McCarthy F.M., McEwan J.C., Moore S., Nanduri B., Notredame C., Palti Y., Plastow G.S., Reecy J.M., Rohrer G.A., Sarropoulou E., Schmidt C.J., Silverstein J., Tellam R.L., Tixier-Boichard M., Tosser-Klopp G., Tuggle C.K., Vilkki J., White S.N., Zhao S. & Zhou H. (2015) Coordinated international action to accelerate genome-to-phenome with FAANG, the Functional Annotation of Animal Genomes project. *Genome Biol.* **16**, 57.

Andonov S., Lourenco D.A.L., Fragomeni B.O., Masuda Y., Pocrnic I., Tsuruta S. & Misztal I. (2017) Accuracy of breeding values in small genotyped populations using different sources of external information-A simulation study. *J. Dairy Sci.* **100**, 395-401.

Anistoroaei R., Ansari S., Farid A., Benkel B., Karlskov-Mortensen P. & Christensen K. (2009) An extended anchored linkage map and virtual mapping for the American mink genome based on homology to human and dog. *Genomics* **94**, 204-10.

Ardlie K.G., Kruglyak L. & Seielstad M. (2002) Patterns of linkage disequilibrium in the human genome. *Nat. Rev. Genet.* **3**, 299-309.

Atefi A., Shadparvar A.A. & Ghavi Hossein-Zadeh N. (2018) Accuracy of Genomic Prediction under Different Genetic Architectures and Estimation Methods. *Iran. J. Appl. Anim. Sci.* **8**, 43-52.

Badke Y.M., Bates R.O., Ernst C.W., Schwab C. & Steibel J.P. (2012) Estimation of linkage disequilibrium in four US pig breeds. *BMC genomics* **13**, 24.

Barb C.R., Hausman G.J., Rekaya R., Lents C.A., Lkhagvadorj S., Qu L., Cai W., Couture O.P., Anderson L.L., Dekkers J.C. & Tuggle C.K. (2010) Gene expression in hypothalamus, liver, and adipose tissues and food intake response to melanocortin-4 receptor agonist in pigs expressing melanocortin-4 receptor mutations. *Physiol Genomics* **41**, 254-68.

Bashalkhanov S., Pandey M. & Rajora O.P. (2009) A simple method for estimating genetic diversity in large populations from finite sample sizes. *BMC Genet.* **10**, 84.

Bateman K.G., Martin S.W., Shewen P.E. & Menzies P.I. (1990) An evaluation of antimicrobial therapy for undifferentiated bovine respiratory disease. *Can. Vet. J.* **31**, 689.

Belkina A.C. & Denis G.V. (2012) BET domain co-regulators in obesity, inflammation and cancer. *Nat. Rev. Cancer* **12**, 465-77.

Berg P. & Lohi O. (1992) Feed consumption and efficiency in paternal progeny groups in mink. *Acta. Agric. Scand. A Anim. Sci.* **42**, 27-33.

Berghof T.V., Poppe M. & Mulder H.A. (2019a) Opportunities to improve resilience in animal breeding programs. *Front. Genet.* **9**, 692.

Berghof T.V.L., Bovenhuis H. & Mulder H.A. (2019b) Body Weight Deviations as Indicator for Resilience in Layer Chickens. *Front. Genet.* **10**, 1216.

Berruén N.N.A. & Smith C.L. (2020) Emerging roles of melanocortin receptor accessory proteins (MRAP and MRAP2) in physiology and pathophysiology. *Gene* **757**, 144949.

Berry D. & Crowley J. (2012) Residual intake and body weight gain: a new measure of efficiency in growing cattle. *J. Anim. Sci.* **90**, 109-15.

Bertolini F., Servin B., Talenti A., Rochat E., Kim E.S., Oget C., Palhière I., Crisà A., Catillo G. & Steri R. (2018) Signatures of selection and environmental adaptation across the goat genome post-domestication. *Genet. Sel. Evol.* **50**, 1-24.

Best S.M. & Bloom M.E. (2006) *Aleutian mink disease parvovirus*. London. Hodder Arnold Publication, Chap. 32, 457-471.

Best S.M., Shelton J.F., Pompey J.M., Wolfinbarger J.B. & Bloom M.E. (2003) Caspase cleavage of the nonstructural protein NS1 mediates replication of Aleutian mink disease parvovirus. *J. Virol.* **77**, 5305-12.

Biegelmeyer P., Nizoli L.Q., da Silva S.S., dos Santos T.R.B., Dionello N.J.L., Gullias-Gomes C.C. & Cardoso F.F. (2015) Bovine genetic resistance effects on biological traits of *Rhipicephalus (Boophilus) microplus*. *Vet. Parasitol.* **208**, 231-7.

Bishop S.C. & Woolliams J.A. (2014) Genomics and disease resistance studies in livestock. *Livest. Sci.* **166**, 190-8.

Bisset S.A. & Morris C.A. (1996) Feasibility and implications of breeding sheep for resilience to nematode challenge. *Int. J. Parasitol.* **26**, 857-68.

Black W.C., Baer C.F., Antolin M.F. & DuTeau N.M. (2001) Population genomics: genome-wide sampling of insect populations. *Annu. Rev. Entomol.* **46**, 441-69.

Bloom M.E., Alexandersen S., Perryman S., Lechner D. & Wolfinbarger J.B. (1988) Nucleotide sequence and genomic organization of Aleutian mink disease parvovirus (ADV): sequence comparisons between a nonpathogenic and a pathogenic strain of ADV. *Journal of Virology* **62**, 2903-15.

Bloom M.E., Best S.M., Hayes S.F., Wells R.D., Wolfinbarger J.B., McKenna R. & Agbandje-McKenna M. (2001) Identification of Aleutian mink disease parvovirus capsid sequences mediating antibody-dependent enhancement of infection, virus neutralization, and immune complex formation. *J. Virol.* **75**, 11116-27.

Bloom M.E., Kanno H., Mori S. & Wolfinbarger J.B. (1994) Aleutian mink disease: puzzles and paradigms. *Infect. Agents Dis.* **3**, 279-301.

Boddicker N.J., Bjorkquist A., Rowland R.R.R., Lunney J.K., Reecy J.M. & Dekkers J.C.M. (2014) Genome-wide association and genomic prediction for host response to porcine reproductive and respiratory syndrome virus infection. *Genet. Sel. Evol.* **46**, 18.

Bouix J., Krupinski J., Rzepecki R., Nowosad B., Skrzyzala I., Roberzynski M., Fudalewicz-Niemczyk W., Skalska M., Malczewski A. & Gruner L. (1998) Genetic resistance to gastrointestinal nematode parasites in Polish long-wool sheep. *Int. J. Parasitol.* **28**, 1797-804.

Brito L.F., Jafarikia M., Grossi D.A., Kijas J.W., Porto-Neto L.R., Ventura R.V., Salgorzaei M. & Schenkel F.S. (2015) Characterization of linkage disequilibrium, consistency of gametic phase and admixture in Australian and Canadian goats. *BMC Genet.* **16**, 67.

Brito L.F., Kijas J.W., Ventura R.V., Sargolzaei M., Porto-Neto L.R., Cánovas A., Feng Z., Jafarikia M. & Schenkel F.S. (2017) Genetic diversity and signatures of selection in various goat breeds revealed by genome-wide SNP markers. *BMC genomics* **18**, 229.

Broll S. & Alexandersen S. (1996) Investigation of the pathogenesis of transplacental transmission of Aleutian mink disease parvovirus in experimentally infected mink. *J. Virol.* **70**, 1455-66.

Browning B.L., Zhou Y. & Browning S.R. (2018) A One-Penny Imputed Genome from Next-Generation Reference Panels. *Am. J. Hum. Genet.* **103**, 338-48.

Budhlakoti N., Kushwaha A.K., Rai A., Chaturvedi K.K., Kumar A., Pradhan A.K., Kumar U., Kumar R.R., Juliana P., Mishra D.C. & Kumar S. (2022) Genomic Selection: A Tool for Accelerating the Efficiency of Molecular Breeding for Development of Climate-Resilient Crops. *Front. Genet.* **13**, 832153.

Bush W.S. & Moore J.H. (2012) Chapter 11: Genome-Wide Association Studies. *PLoS Comput. Biol.* **8**, e1002822.

Caetano L.C., Verruma C.G., Pinaffi F.L.V., Jardim I.B., Furtado G.P., Silva L.A., Furtado C.L.M. & Rosa-e-Silva A.C.J.d.S. (2023) In vivo and in vitro matured bovine oocytes present a distinct pattern of single-cell gene expression. *Zygote* **31**, 31-43.

Calus M.P., Meuwissen T.H., de Roos A.P. & Veerkamp R.F. (2008) Accuracy of genomic selection using different methods to define haplotypes. *Genetics* **178**, 553-61.

Cardoso D.F., de Albuquerque L.G., Reimer C., Qanbari S., Erbe M., do Nascimento A.V., Venturini G.C., Scalez D.C.B., Baldi F., de Camargo G.M.F., Mercadante M.E.Z., do Santos Gonçalves Cyrillo J.N., Simianer H. & Tonhati H. (2018) Genome-wide scan reveals population stratification and footprints of recent selection in Nelore cattle. *Genet. Sel. Evol.* **50**, 22.

Cardoso F., Gomes C., Sollero B., Oliveira M., Roso V., Piccoli M., Higa R., Yokoo M., Caetano A. & Aguilar I. (2015) Genomic prediction for tick resistance in Braford and Hereford cattle. *J. Anim. Sci.* **93**, 2693-705.

Carillier-Jacquin C., Larroque H. & Robert-Granié C. (2016) Including α s1 casein gene information in genomic evaluations of French dairy goats. *Genet. Sel. Evol.* **48**, 54.

Carillier C., Larroque H. & Robert-Granié C. (2014) Comparison of joint versus purebred genomic evaluation in the French multi-breed dairy goat population. *Genet. Sel. Evol.* **46**, 67.

Castelruiz Y., Blixenkron-Møller M. & Aasted B. (2005) DNA vaccination with the Aleutian mink disease virus NS1 gene confers partial protection against disease. *Vaccine* **23**, 1225-31.

Charlesworth B. (2009) Effective population size and patterns of molecular evolution and variation. *Nat Rev Genet* **10**, 195-205.

Cheema A., Henson J.B. & Gorham J.R. (1972) Aleutian disease of mink. Prevention of lesions by immunosuppression. *Am. J. Pathol.* **66**, 543-56.

Chen C.Y., Misztal I., Aguilar I., Tsuruta S., Meuwissen T.H.E., Aggrey S.E., Wing T. & Muir W.M. (2011) Genome-wide marker-assisted selection combining all pedigree phenotypic information with genotypic data in one step: An example using broiler chickens. *J. Anim. Sci.* **89**, 23-8.

Chen H., Zheng J., Chen Z., Ma H., Zhang R. & Wu R. (2019) Case report of a novel MPIG6B gene mutation in a Chinese boy with pancytopenia and splenomegaly. *Gene* **715**, 143957.

Chen J., Wu Z., Chen R., Huang Z., Han X., Qiao R., Wang K., Yang F., Li X.-J. & Li X.-L. (2022a) Identification of Genomic Regions and Candidate Genes for Litter Traits in French Large White Pigs Using Genome-Wide Association Studies. *animals* **12**, 1584.

Chen Z., Zhang Z., Wang Z., Zhang Z., Wang Q. & Pan Y. (2022b) Heterozygosity and homozygosity regions affect reproductive success and the loss of reproduction: A case study with litter traits in pigs. *Comput. Struct. Biotechnol. J.* **20**, 4060-71.

Cheng J., Fernando R., Cheng H., Kachman S.D., Lim K., Harding J.C.S., Dyck M.K., Fortin F., Plastow G.S., Canada P. & Dekkers J.C.M. (2022) Genome-wide association study of disease resilience traits from a natural polymicrobial disease challenge model in pigs identifies the importance of the major histocompatibility complex region. *G3 (Bethesda, Md.)* **12**.

Cheng J., Putz A.M., Harding J.C., Dyck M.K., Fortin F., Plastow G.S., Canada P. & Dekkers J.C. (2020) Genetic analysis of disease resilience in wean-to-finish pigs from a natural disease challenge model. *J. Anim. Sci.* **98**, skaa244.

Cheng J., Putz A.M., Harding J.C.S., Dyck M.K., Fortin F., Plastow G.S., Canada P.G. & Dekkers J.C.M. (2021) Genetic parameters of drinking and feeding traits of wean-to-finish pigs under a polymicrobial natural disease challenge. *J. Anim. Sci. Biotechnol.* **12**, 105.

Cho H.J. & Greenfield J. (1978) Eradication of Aleutian disease of mink by eliminating positive counterimmunoelectrophoresis test reactors. *J. Clin. Microbiol.* **7**, 18.

Cho H.J. & Ingram D.G. (1972) Antigen and antibody in Aleutian disease in mink. I. Precipitation reaction by agar-gel electrophoresis. *J. Immunol.* **108**, 555-7.

Cho H.J. & Ingram D.G. (1973) Pathogenesis of Aleutian Disease of Mink: Nature of the Antiglobulin Reaction and Elution of Antibody from Erythrocytes and Glomeruli of Infected Mink. *Infect. Immun.* **8**, 264.

Chopin M., Preston Simon P., Lun Aaron T.L., Tellier J., Smyth Gordon K., Pellegrini M., Belz Gabrielle T., Corcoran Lynn M., Visvader Jane E., Wu L. & Nutt Stephen L. (2016) RUNX2 Mediates Plasmacytoid Dendritic Cell Egress from the Bone Marrow and Controls Viral Immunity. *Cell Rep.* **15**, 866-78.

Christensen L.S., Gram-Hansen L., Chriél M. & Jensen T.H. (2011) Diversity and stability of Aleutian mink disease virus during bottleneck transitions resulting from eradication in domestic mink in Denmark. *Vet. Microbiol.* **149**, 64-71.

Christensen O.F. & Lund M.S. (2010) Genomic prediction when some animals are not genotyped. *Genet. Sel. Evol.* **42**, 2.

Christensen O.F., Madsen P., Nielsen B., Ostersen T. & Su G. (2012) Single-step methods for genomic evaluation in pigs. *Animal* **6**, 1565-71.

Clark S.A. & van der Werf J. (2013) Genomic best linear unbiased prediction (gBLUP) for the estimation of genomic breeding values. *Methods. Mol. Biol.* **1019**, 321-30.

Colditz I.G. & Hine B.C. (2016) Resilience in farm animals: biology, management, breeding and implications for animal welfare. *Anim. Prod. Sci.* **56**, 1961-83.

Daetwyler H.D., Kemper K.E., van der Werf J.H. & Hayes B.J. (2012) Components of the accuracy of genomic prediction in a multi-breed sheep population. *J. Anim. Sci.* **90**, 3375-84.

Daetwyler H.D., Villanueva B. & Woolliams J.A. (2008) Accuracy of Predicting the Genetic Risk of Disease Using a Genome-Wide Approach. *PLoS One* **3**, e3395.

Dailey M.J. & Moran T.H. (2013) Glucagon-like peptide 1 and appetite. *Trends Endocrinol. Metab.* **24**, 85-91.

Dall'Olio S., Schiavo G., Gallo M., Bovo S., Bertolini F., Buttazzoni L. & Fontanesi L. (2020) Candidate gene markers associated with production, carcass and meat quality traits in Italian Large White pigs identified using a selective genotyping approach. *Livest. Sci.* **240**, 104145.

Dam-Tuxen R., Dahl J., Jensen T.H., Dam-Tuxen T., Struve T. & Bruun L. (2014) Diagnosing Aleutian mink disease infection by a new fully automated ELISA or by counter current immunoelectrophoresis: A comparison of sensitivity and specificity. *J. Virol. Methods* **199**, 53-60.

Danecek P., Auton A., Abecasis G., Albers C., Banks E., DePristo M., Handsaker R., Lunter G., Marth G. & Sherry S. (2011) The variant call format and VCFtools. *Bioinformatics* **27**, 2156-8.

Davoudi P., Do D.N., Colombo S., Rathgeber B., Hu G., Sargolzaei M., Wang Z., Plastow G. & Miar Y. (2022) Genetic and phenotypic parameters for feed efficiency and component traits in American mink. *J. Anim. Sci.* **100**, skac216.

de Lima A.O., Koltés J.E., Diniz W.J.S., de Oliveira P.S.N., Cesar A.S.M., Tizioto P.C., Afonso J., de Souza M.M., Petrini J., Rocha M.I.P., Cardoso T.F., Neto A.Z., Coutinho L.L., Mourão G.B. & Regitano L.C.A. (2020) Potential Biomarkers for Feed Efficiency-Related Traits in Nelore Cattle Identified by Co-expression Network and Integrative Genomics Analyses. *Front. Genet.* **11**, 189.

de Vet E.C.J.M., Aguado B. & Campbell R.D. (2001) G6b, a Novel Immunoglobulin Superfamily Member Encoded in the Human Major Histocompatibility Complex, Interacts with SHP-1 and SHP-2 *. *J. Biol. Chem.* **276**, 42070-6.

Decout A., Katz J.D., Venkatraman S. & Ablasser A. (2021) The cGAS–STING pathway as a therapeutic target in inflammatory diseases. *Nat. Rev. Immunol.* **21**, 548-69.

Delves P.J. & Roitt I.M. (1998) *Encyclopedia of immunology*. Academic Press, New York.

Deperi S.I., Tagliotti M.E., Bedogni M.C., Manrique-Carpintero N.C., Coombs J., Zhang R., Douches D. & Huarte M.A. (2018) Discriminant analysis of principal components and pedigree assessment of genetic diversity and population structure in a tetraploid potato panel using SNPs. *PLoS One* **13**, e0194398.

Devlin B. & Roeder K. (1999) Genomic Control for Association Studies. *Biometrics* **55**, 997-1004.

Do D.N., Hu G., Salek Ardestani S. & Miar Y. (2021) Genetic and phenotypic parameters for body weights, harvest length, and growth curve parameters in American mink. *J. Anim. Sci.* **99**, 1-7.

Do D.N., Karimi K., Sargolzaei M., Plastow G., Wang Z. & Miar Y. (2024) Development of a 70K SNP genotyping array for American mink (*Neogale vison*). *Under preparation*.

Do D.N. & Miar Y. (2020) Evaluation of growth curve models for body weight in American mink. *animals* **10**, 22.

Dodds A.W., Ren X.-D., Willis A.C. & Law S.K.A. (1996) The reaction mechanism of the internal thioester in the human complement component C4. *Nature* **379**, 177-9.

Doeschl-Wilson A., Knap P.W., Opriessnig T. & More S.J. (2021) Review: Livestock disease resilience: from individual to herd level. *Animal* **15**, 100286.

Doeschl-Wilson A.B., Brindle W., Emmans G. & Kyriazakis I. (2009) Unravelling the Relationship between Animal Growth and Immune Response during Micro-Parasitic Infections. *PLoS One* **4**, e7508.

Doyle J.L., Berry D.P., Veerkamp R.F., Carthy T.R., Evans R.D., Walsh S.W. & Purfield D.C. (2020) Genomic regions associated with muscularity in beef cattle differ in five contrasting cattle breeds. *Genet. Sel. Evol.* **52**, 2.

Dunkelberger J.R. & Song W.-C. (2010) Complement and its role in innate and adaptive immune responses. *Cell Res.* **20**, 34-50.

Eady S., Woolaston R., Ponzoni R., Lewer R., Raadsma H. & Swan A. (1998) Resistance to nematode parasites in Merino sheep: correlation with production traits. *Aust. J. Agric. Res.* **49**, 1201-12.

Eklund C., Hadlow W., Kennedy R., Boyle C. & Jackson T. (1968) Aleutian disease of mink: properties of the etiologic agent and the host responses. *J. Infect. Dis.* **118**, 510-26.

Ellegren H. & Galtier N. (2016) Determinants of genetic diversity. *Nat. Rev. Genet.* **17**, 422-33.

Ellis L.C. (1996) Melatonin reduces mortality from Aleutian disease in mink (*Mustela vison*). *J. Pineal Res.* **21**, 214-7.

Elzhov T.V., Mullen K.M., Spiess A. & Bolker B. (2016) Package ‘minpack.lm’. Title R Interface to the Levenberg-Marquardt Nonlinear Least-Squares Algorithm Found in MINPACK. *Plus support for bounds*, 1.2-1.

Excoffier L., Smouse P.E. & Quattro J.M. (1992) Analysis of molecular variance inferred from metric distances among DNA haplotypes: application to human mitochondrial DNA restriction data. *Genetics* **131**, 479-91.

Falconer D. & Mackay T. (1996) *Introduction to quantitative genetics 4th edition*. Longmans, Harlow, UK.

Farid A., Daftarian P. & Fatehi J. (2018) Transmission dynamics of Aleutian mink disease virus on a farm under test and removal scheme. *J. Vet. Sci. Med. Diagn.* **7**.

Farid A. & Ferns L. (2011) Aleutian mink disease virus infection may cause hair depigmentation. *Scientifur* **35**, 55-9.

Farid A. & Ferns L. (2017) Reduced severity of histopathological lesions in mink selected for tolerance to Aleutian mink disease virus infection. *Res. Vet. Sci.* **111**, 127-34.

Farid A. & Rupasinghe P.P. (2016) Accuracy of enzyme-linked immunosorbent assays for quantification of antibodies against Aleutian mink disease virus. *J. Virol. Methods* **235**, 144-51.

Farid A., Zillig M., Finley G. & Smith G. (2012) Prevalence of the Aleutian mink disease virus infection in Nova Scotia, Canada. *Prev. Vet. Med.* **106**, 332-8.

Farid A.H. (2020) Response of American Mink to Selection for Tolerance to Aleutian Mink Disease Virus. *EC Microbiol.* **16.6**, 110-28.

Farid A.H., Hussain I. & Arju I. (2015) Detection of Aleutian mink disease virus DNA and antiviral antibodies in American mink (*Neovison vison*) 10 days postinoculation. *J. Vet. Diagn. Invest.* **27**, 287-94.

Farid A.H. & Segervall J. (2014) A comparison between ELISA and CIEP for measuring antibody titres against Aleutian mink disease virus. *Viol. Mycol.* **3**, 137.

Farid A.H., Smith N.J. & White M.B. (2020) Effects of dietary kelp (*Ascophylum nodosum*) supplementation on survival rate and reproductive performance of mink challenged with Aleutian mink disease virus. *Can. J. Anim. Sci.* **100**, 547-56.

Fitzpatrick B.M. (2009) Power and sample size for nested analysis of molecular variance. *Mol. Ecol.* **18**, 3961-6.

Frigo E., Dechow C.D., Pedron O. & Cassell B.G. (2010) The genetic relationship of body weight and early-lactation health disorders in two experimental herds. *J. Dairy Sci.* **93**, 1184-92.

Fu G., Vallée S., Rybakin V., McGuire M.V., Ampudia J., Brockmeyer C., Salek M., Fallen P.R., Hoerter J.A., Munshi A., Huang Y.H., Hu J., Fox H.S., Sauer K., Acuto O. & Gascoigne N.R. (2009) Themis controls thymocyte selection through regulation of T cell antigen receptor-mediated signaling. *Nat. Immunol.* **10**, 848-56.

García-Bermúdez M., López-Mejías R., Genre F., Castañeda S., Corrales A., Llorca J., González-Juanatey C., Ubilla B., Miranda-Fillooy J.A., Pina T., Gómez-Vaquero C., Rodríguez-Rodríguez L., Fernández-Gutiérrez B., Balsa A., Pascual-Salcedo D., López-Longo F.J., Carreira P., Blanco R., Martín J. & González-Gay M.A. (2015) Lack of association between JAK3 gene polymorphisms and cardiovascular disease in Spanish patients with rheumatoid arthritis. *Biomed. Res. Int.* **2015**, 318364.

García P., Arévalo V. & Lizana M. (2010) Characterisation of den sites of American mink *Neovison vison* in central Spain. *Wildlife Biol.* **16**, 276-82.

Gardner B., Dolezal H., Bryant L., Owens F. & Smith R. (1999) Health of finishing steers: Effects on performance, carcass traits, and meat tenderness. *J. Anim. Sci.* **77**, 3168-75.

Garrick D.J., Taylor J.F. & Fernando R.L. (2009) Deregressing estimated breeding values and weighting information for genomic regression analyses. *Genet. Sel. Evol.* **41**, 55.

Geer M.J., van Geffen J.P., Gopalasingam P., Vögtle T., Smith C.W., Heising S., Kuijpers M.J.E., Tullemans B.M.E., Jarvis G.E., Eble J.A., Jeeves M., Overduin M., Heemskerk J.W.M., Mazharian A. & Senis Y.A. (2018) Uncoupling ITIM receptor G6b-B from tyrosine phosphatases Shp1 and Shp2 disrupts murine platelet homeostasis. *Blood* **132**, 1413-25.

Getabalew M., Alemneh T. & Akeberegn D. (2019) Heritability and its use in animal breeding. *Int. J. Vet. Sci. Technol.* **4**, 1-5.

Gianola D. (1982) Theory and Analysis of Threshold Characters. *J. Anim. Sci.* **54**, 1079-96.

Gilmour A.R., Gogel B.J., Cullis B.R. & Thompson R. (2018) ASReml-R Reference Manual Version 4.

Gizachew Haile G. (2022) Genomic Selection: A Faster Strategy for Plant Breeding. In: *Breeding Strategies and Cases for Several Major Plants* (ed. by Haiping W). IntechOpen, Rijeka.

Glickman M.E., Rao S.R. & Schultz M.R. (2014) False discovery rate control is a recommended alternative to Bonferroni-type adjustments in health studies. *Journal of Clinical Epidemiology* **67**, 850-7.

Goddard M. (2009) Genomic selection: prediction of accuracy and maximisation of long term response. *Genetica* **136**, 245-57.

Goddard M.E. & Hayes B.J. (2007) Genomic selection. *J. Anim. Breed. Genet.* **124**, 323-30.

Goddard M.E. & Hayes B.J. (2009) Mapping genes for complex traits in domestic animals and their use in breeding programmes. *Nat. Rev. Genet.* **10**, 381-91.

Gordon D.A., Franklin A.E. & Karstad L. (1967) Viral plasmacytosis (Aleutian disease) of mink resembling human collagen disease. *Can. Med. Assoc. J.* **96**, 1245-51.

Gottschalck E., Alexandersen S., Storgaard T., Bloom M.E. & Aasted B. (1994) Sequence comparison of the non-structural genes of four different types of Aleutian mink disease parvovirus indicates an unusual degree of variability. *Arch. Virol.* **138**, 213-31.

Groeneveld L.F., Lenstra J.A., Eding H., Toro M.A., Scherf B., Pilling D., Negrini R., Finlay E.K., Jianlin H., Groeneveld E., Weigend S. & The G.C. (2010) Genetic diversity in farm animals – a review. *Anim. Genet.* **41**, 6-31.

Guarini A.R., Lourenco D.A.L., Brito L.F., Sargolzaei M., Baes C.F., Miglior F., Misztal I. & Schenkel F.S. (2018) Comparison of genomic predictions for lowly heritable traits using multi-step and single-step genomic best linear unbiased predictor in Holstein cattle. *J. Dairy Sci.* **101**, 8076-86.

Guerrini M.M., Sobacchi C., Cassani B., Abinun M., Kilic S.S., Pangrazio A., Moratto D., Mazzolari E., Clayton-Smith J., Orchard P., Coxon F.P., Helfrich M.H., Crockett J.C., Mellis D., Vellodi A., Tezcan I., Notarangelo L.D., Rogers M.J., Vezzoni P., Villa A. & Frattini A. (2008) Human Osteoclast-Poor Osteopetrosis with Hypogammaglobulinemia due to TNFRSF11A (RANK) Mutations. *Am. J. Hum. Genet.* **83**, 64-76.

Gunia M., David I., Hurtaud J., Maupin M., Gilbert H. & Garreau H. (2018) Genetic Parameters for Resistance to Non-specific Diseases and Production Traits Measured in Challenging and Selection Environments; Application to a Rabbit Case. *Front. Genet.* **9**, 467.

Gunnarsson E. (2001) Documenting Freedom From Disease And Re-Establishing a Free Status After a Breakdown Aleutian Disease (Plasmacytosis) in Farmed Mink in Iceland. *Acta Vet. Scand.* **42**, S87.

Guran T., Tolhurst G., Bereket A., Rocha N., Porter K., Turan S., Gribble F.M., Kotan L.D., Akcay T., Atay Z., Canan H., Serin A., O'Rahilly S., Reimann F., Semple R.K. & Topaloglu A.K. (2009) Hypogonadotropic hypogonadism due to a novel missense mutation in the first extracellular loop of the neurokinin B receptor. *J. Clin. Endocrinol. Metab.* **94**, 3633-9.

Guyonneau L., Murisier F., Rossier A., Moulin A. & Beermann F. (2004) Melanocytes and pigmentation are affected in dopachrome tautomerase knockout mice. *Mol. Cell Biol.* **24**, 3396-403.

Hamer G. & de Rooij D.G. (2018) Mutations causing specific arrests in the development of mouse primordial germ cells and gonocytes. *Biol. Reprod.* **99**, 75-86.

Harlizius B., Mathur P. & Knol E.F. (2020) Breeding for resilience: new opportunities in a modern pig breeding program. *J. Anim. Sci.* **98**, S150-S4.

Haupt A., Thamer C., Heni M., Machicao F., Machann J., Schick F., Stefan N., Fritsche A., Häring H.-U. & Staiger H. (2010) Novel Obesity Risk Loci Do Not Determine Distribution of Body Fat Depots: A Whole-body MRI/MRS study. *Obesity* **18**, 1212-7.

Hay E.H. & Rekaya R. (2018) Use of Observed Genomic Information to Infer Linkage Disequilibrium between Markers and QTLs *Agric. Sci.* **9**, 1470-8.

Hayes B., MacLeod I., Daetwyler H., Bowman J., Chamberlain A. & Vander Jagt C., et al. (2014) Genomic prediction from whole genome sequence in livestock: the 1000 bull genomes project. In: Proceedings of the 10th world congress on genetics applied to livestock production, Vancouver, 19–23 August 2014.

Hayes B.J., Bowman P.J., Chamberlain A.J. & Goddard M.E. (2009) Invited review: Genomic selection in dairy cattle: Progress and challenges. *J. Dairy Sci.* **92**, 433-43.

Hayes B.J., Visscher P.M., McPartlan H.C. & Goddard M.E. (2003) Novel multilocus measure of linkage disequilibrium to estimate past effective population size. *Genome Res.* **13**, 635-43.

Henson J., Gorham J. & Leader R. (1962) Field test for Aleutian disease. *National Fur News* **34**, 8-9.

Henson J.B., Gorham J.R., McGuire T.C. & Crawford T.B. (1976) Pathology and pathogenesis of Aleutian disease. *Front. Biol.* **44**, 175-205.

Hess A.S., Tribble B.R., Hess M.K., Rowland R.R., Lunney J.K., Plastow G.S. & Dekkers J.C.M. (2018) Genetic relationships of antibody response, viremia level, and weight gain in pigs experimentally infected with porcine reproductive and respiratory syndrome virus. *Sci. J. Anim. Sci.* **96**, 3565-81.

Hickmann F.M.W., Braccini Neto J., Kramer L.M., Huang Y., Gray K.A., Dekkers J.C.M., Sanglard L.P. & Serão N.V.L. (2021) Host Genetics of Response to Porcine Reproductive and Respiratory Syndrome in Sows: Reproductive Performance. *Front. Genet.* **12**.

Hidalgo J., Lourenco D., Tsuruta S., Masuda Y., Breen V., Hawken R., Bermann M. & Misztal I. (2021) Investigating the persistence of accuracy of genomic predictions over time in broilers. *J. Anim. Sci.* **99**, skab239.

Hill W.G. (1981) Estimation of effective population size from data on linkage disequilibrium. *Genet. Res.* **38**, 209-16.

Hill W.G. & Robertson A. (1968) Linkage disequilibrium in finite populations. *Theor. Appl. Genet.* **38**, 226-31.

Hirschhorn J.N. & Daly M.J. (2005) Genome-wide association studies for common diseases and complex traits. *Nat. Rev. Genet.* **6**, 95-108.

Hsu A.P., Dowdell K.C., Davis J., Niemela J.E., Anderson S.M., Shaw P.A., Rao V.K. & Puck J.M. (2012) Autoimmune lymphoproliferative syndrome due to FAS mutations outside the signal-transducing death domain: molecular mechanisms and clinical penetrance. *Genet. Med.* **14**, 81-9.

Hu G., Do D.N., Davoudi P., Manafiazar G., Kelvin A.A., Plastow G., Wang Z., Sargolzaei M. & Miar Y. (2022) Genetic and phenotypic correlations between Aleutian disease tests with body weight, growth, and feed efficiency traits in mink. *J. Anim. Sci.* **100**, skac346.

Hu G., Do D.N., Gray J. & Miar Y. (2020) Selection for Favorable Health Traits: A Potential Approach to Cope with Diseases in Farm Animals. *animals* **10**, 1717.

Hu G., Do D.N., Karimi K. & Miar Y. (2021) Genetic and phenotypic parameters for Aleutian disease tests and their correlations with pelt quality, reproductive performance, packed-cell volume, and harvest length in mink. *J. Anim. Sci.* **99**, 1-12.

Hu G., Do D.N., Manafiazar G., Kelvin A.A., Plastow G., Sargolzaei M., Wang Z. & Miar Y. (2024) Identifying Selection Signatures for Immune Response and Resilience to Aleutian Disease in Mink Using Genotypes Data. *Under preparation*.

Hu G., Do D.N., Manafiazar G., Kelvin A.A., Sargolzaei M., Plastow G., Wang Z. & Miar Y. (2023) Population Genomics of American Mink Using Genotype Data. *Front. Genet.* **14**, 1175408.

Huang Q., Luo Y., Cheng F., Best S.M., Bloom M.E. & Qiu J. (2014) Molecular characterization of the small nonstructural proteins of parvovirus Aleutian mink disease virus (AMDV) during infection. *Virology* **452-453**, 23-31.

Huang Y., Wang J., Zhan Z., Cao X., Sun Y., Lan X., Lei C., Zhang C. & Chen H. (2013) Assessment of association between variants and haplotypes of the IGF2 gene in beef cattle. *Gene* **528**, 139-45.

Huang Z., Tian Z., Zhao Y., Zhu F., Liu W. & Wang X. (2022) MAPK Signaling Pathway Is Essential for Female Reproductive Regulation in the Cabbage Beetle, *Colaphellus bowringi*. *Cells* **11**, 1602.

Hughes A.R., Inouye B.D., Johnson M.T.J., Underwood N. & Vellend M. (2008) Ecological consequences of genetic diversity. *Ecol. Lett.* **11**, 609-23.

Ibrahim A.H.M. (2015) The *prkag3* gene polymorphisms and their associations with growth performance and body indices in barki lambs. *Egyptian Journal of Sheep and Goat Sciences* **10**, 1-14.

Iheshiulor O.O., Woolliams J.A., Svendsen M., Solberg T. & Meuwissen T.H. (2017) Simultaneous fitting of genomic-BLUP and Bayes-C components in a genomic prediction model. *Genet. Sel. Evol.* **49**, 1-13.

Iung L.H.d.S., Carneiro R., Neves H.H.d.R. & Mulder H.A. (2020) Genetics and genomics of uniformity and resilience in livestock and aquaculture species: A review. *J. Anim. Breed. Genet.* **137**, 263-80.

Jansen R.S., Addie R., Merckx R., Fish A., Mahakena S., Bleijerveld O.B., Altelaar M., Ijlst L., Wanders R.J., Borst P. & van de Wetering K. (2015) N-lactoyl-amino acids are ubiquitous metabolites that originate from CNBP2-mediated reverse proteolysis of lactate and amino acids. *Proc. Natl. Acad. Sci.* **112**, 6601-6.

Jensen J.D., Foll M. & Bernatchez L. (2016a) The past, present and future of genomic scans for selection. *Mol. Ecol.* **25**, 1-4.

Jensen P.V., Castelruiz Y. & Aasted B. (2003) Cytokine Profiles in Adult Mink Infected with Aleutian Mink Disease Parvovirus. *J. Virol.* **77**, 7444-51.

Jensen T.H., Chriél M. & Hansen M.S. (2016b) Progression of experimental chronic Aleutian mink disease virus infection. *Acta Vet. Scand.* **58**, 35-.

Jepsen J.R., d'Amore F., Baandrup U., Clausen M.R., Gottschalck E. & Aasted B. (2009) Aleutian mink disease virus and humans. *Emerg. Infect. Dis.* **15**, 2040-2.

Jia C., Tan Y. & Zhao M. (2022) The complement system and autoimmune diseases. *Chronic Dis. Transl. Med.* **8**, 184-90.

Jiang H., Chai Z., Cao H., Zhang C., Zhu Y., Zhang Q. & Xin J. (2022) Genome-wide identification of SNPs associated with body weight in yak. *BMC Genom.* **23**, 833.

Joergensen G. (1985) Colour types and other qualitative characteristics in mink. In: *Mink Production* (pp. 106-8. Scientifur, Denmark.

Joeyen-Waldorf J., Nikolova Y.S., Edgar N., Walsh C., Kota R., Lewis D.A., Ferrell R., Manuck S.B., Hariri A.R. & Sibille E. (2012) Adenylate cyclase 7 is implicated in the biology of depression and modulation of affective neural circuitry. *Biol. Psychiatry.* **71**, 627-32.

Jombart T., Devillard S. & Balloux F. (2010) Discriminant analysis of principal components: a new method for the analysis of genetically structured populations. *BMC genetics* **11**, 94.

June C.H., Ledbetter J.A., Gillespie M.M., Lindsten T. & Thompson C.B. (1987) T-cell proliferation involving the CD28 pathway is associated with cyclosporine-resistant interleukin 2 gene expression. *Mol. Cell Biol.* **7**, 4472-81.

Kaczmarek M.M., Najmula J., Guzewska M.M. & Przygodzka E. (2020) MiRNAs in the Peri-Implantation Period: Contribution to Embryo-Maternal Communication in Pigs. *Int. J. Mol. Sci.* **21**, 2229.

Kadarmideen H.N., Schwörer D., Ilahi H., Malek M. & Hofer A. (2004) Genetics of osteochondral disease and its relationship with meat quality and quantity, growth, and feed conversion traits in pigs1. *J. Anim. Sci.* **82**, 3118-27.

Kahnamouyi S., Nouri M., Farzadi L., Darabi M., Hosseini V. & Mehdizadeh A. (2018) The role of mitogen-activated protein kinase-extracellular receptor kinase pathway in female fertility outcomes: a focus on pituitary gonadotropins regulation. *Ther. Adv. Endocrinol. Metab.* **9**, 209-15.

Kamvar Z.N., Tabima J.F. & Grünwald N. (2014) Poppr: an R package for genetic analysis of populations with clonal, partially clonal, and/or sexual reproduction. *PeerJ* **2**, e281.

Kanno H., Wolfenbarger J.B. & Bloom M.E. (1993) Aleutian mink disease parvovirus infection of mink macrophages and human macrophage cell line U937: demonstration of antibody-dependent enhancement of infection. *J. Virol.* **67**, 7017.

Karaman E., Su G., Croue I. & Lund M.S. (2021) Genomic prediction using a reference population of multiple pure breeds and admixed individuals. *Genet. Sel. Evol.* **53**, 46.

Karimi K., Do D.N., Wang J., Easley J., Borzouie S., Sargolzaei M., Plastow G., Wang Z. & Miar Y. (2022) A chromosome-level genome assembly reveals genomic characteristics of the American mink (*Neogale vison*). *Commun. Biol.* **5**, 1381.

Karimi K., Farid A.H., Myles S. & Miar Y. (2021a) Detection of selection signatures for response to Aleutian mink disease virus infection in American mink. *Sci. Rep.* **11**, 2944.

Karimi K., Farid A.H., Sargolzaei M., Myles S. & Miar Y. (2020) Linkage Disequilibrium, Effective Population Size and Genomic Inbreeding Rates in American Mink Using Genotyping-by-Sequencing Data. *Front. Genet.* **11**.

Karimi K., Ngoc Do D., Sargolzaei M. & Miar Y. (2021b) Population Genomics of American Mink Using Whole Genome Sequencing Data. In: *Genes*.

Karimi K., Sargolzaei M., Plastow G.S., Wang Z. & Miar Y. (2018) Genetic and phenotypic parameters for litter size, survival rate, gestation length, and litter weight traits in American mink1. *Sci. J. Anim. Sci.* **96**, 2596-606.

Kerdidani D., Papaioannou N.E., Nakou E. & Alissafi T. (2022) Rebooting Regulatory T Cell and Dendritic Cell Function in Immune-Mediated Inflammatory Diseases: Biomarker and Therapy Discovery under a Multi-Omics Lens. In: *Biomedicines*.

Kidd A.G., Bowman J., LesbarrÈRes D. & Schulte-Hostedde A.I. (2009) Hybridization between escaped domestic and wild American mink (*Neovison vison*). *Mol. Ecol.* **18**, 1175-86.

Kishore N., Shah D., Skanes V.M. & Levine R.P. (1988) The fluid-phase binding of human C4 and its genetic variants, C4A3 and C4B1, to immunoglobulins. *Mol. Immunol.* **25**, 811-9.

Klein R.J., Zeiss C., Chew E.Y., Tsai J.-Y., Sackler R.S., Haynes C., Henning A.K., SanGiovanni J.P., Mane S.M. & Mayne S.T. (2005) Complement factor H polymorphism in age-related macular degeneration. *Sci.* **308**, 385-9.

Knap P.W. & Doeschl-Wilson A. (2020) Why breed disease-resilient livestock, and how? *Genet. Sel. Evol.* **52**, 60.

Knol E.F., Nielsen B. & Knap P.W. (2016) Genomic selection in commercial pig breeding. *Anim. Front.* **6**, 15-22.

Knuuttila A., Aronen P., Saarinen A. & Vapalahti O. (2009) Development and Evaluation of an Enzyme-Linked Immunosorbent Assay Based on Recombinant VP2 Capsids for the Detection of Antibodies to Aleutian Mink Disease Virus. *Clin. Vaccine Immunol.* **16**, 1360.

Kongmanas K., Kruevaisayawan H., Saewu A., Sugeng C., Fernandes J., Souda P., Angel J.B., Faull K.F., Aitken R.J., Whitelegge J., Hardy D., Berger T., Baker M.A. & Tanphaichitr N. (2015) Proteomic Characterization of Pig Sperm Anterior Head Plasma Membrane Reveals Roles of Acrosomal Proteins in ZP3 Binding. *J. Cell. Physiol.* **230**, 449-63.

Kowalczyk M., Gąsiorek B., Kostro K., Borzym E. & Jakubczak A. (2019) Breeding parameters on a mink farm infected with Aleutian mink disease virus following the use of methisoprinol. *Arch. Virol.* **164**, 2691-8.

Kreitman M. (2000) Methods to detect selection in populations with applications to the human. *Annu. Rev. Genomics Hum. Genet.* **1**, 539-59.

Lacey D.L., Timms E., Tan H.L., Kelley M.J., Dunstan C.R., Burgess T., Elliott R., Colombero A., Elliott G., Scully S., Hsu H., Sullivan J., Hawkins N., Davy E., Capparelli C., Eli A., Qian Y.X., Kaufman S., Sarosi I., Shalhoub V., Senaldi G., Guo J., Delaney J. & Boyle W.J. (1998) Osteoprotegerin Ligand Is a Cytokine that Regulates Osteoclast Differentiation and Activation. *Cell* **93**, 165-76.

Lal M.M., Waqairatu S.S., Zenger K.R., Nayfa M.G., Pickering T.D., Singh A. & Southgate P.C. (2021) The GIFT that keeps on giving? A genetic audit of the Fijian Genetically Improved Farmed Tilapia (GIFT) broodstock nucleus 20 years after introduction. *Aquaculture* **537**, 736524.

Läubli H. & Varki A. (2020) Sialic acid-binding immunoglobulin-like lectins (Siglecs) detect self-associated molecular patterns to regulate immune responses. *Cell. Mol. Life Sci.* **77**, 593-605.

Law S.K., Dodds A.W. & Porter R.R. (1984) A comparison of the properties of two classes, C4A and C4B, of the human complement component C4. *EMBO J.* **3**, 1819-23.

Leach R.J., Craigmile S.C., Knott S.A., Williams J.L. & Glass E.J. (2010) Quantitative trait loci for variation in immune response to a Foot-and-Mouth Disease virus peptide. *BMC Genet.* **11**, 107.

Lecis R., Ferrando A., Ruiz-Olmo J., Mañas S. & Domingo-Roura X. (2008) Population genetic structure and distribution of introduced American mink (*Mustela vison*) in Spain, based on microsatellite variation. *Conserv. Genet.* **9**, 1149-61.

Legarra A., Aguilar I. & Misztal I. (2009) A relationship matrix including full pedigree and genomic information. *J. Dairy Sci.* **92**, 4656-63.

Legarra A., Robert-Granié C., Manfredi E. & Elsen J.M. (2008) Performance of genomic selection in mice. *Genetics* **180**, 611-8.

Lehnert E. & Tampé R. (2017) Structure and Dynamics of Antigenic Peptides in Complex with TAP. *Front. Immunol.* **8**, 10.

Levin C., Koren A., Pretorius E., Rosenberg N., Shenkman B., Hauschner H., Zalman L., Khayat M., Salama I., Elpeleg O. & Shalev S. (2015) Deleterious mutation in the FYB gene is associated with congenital autosomal recessive small-platelet thrombocytopenia. *J. Thromb. Haemost.* **13**, 1285-92.

Li B., Zhang N., Wang Y.-G., George A.W., Reverter A. & Li Y. (2018) Genomic prediction of breeding values using a subset of SNPs identified by three machine learning methods. *Front. Genet.* **9**, 237.

Li R., Li C., Chen H., Li R., Chong Q., Xiao H. & Chen S. (2020) Genome-wide scan of selection signatures in Dehong humped cattle for heat tolerance and disease resistance. *Anim. Genet.* **51**, 292-9.

Li V.L., He Y., Contrepolis K., Liu H., Kim J.T., Wiggenhorn A.L., Tanzo J.T., Tung A.S., Lyu X., Zushin P.H., Jansen R.S., Michael B., Loh K.Y., Yang A.C., Carl C.S., Voldstedlund C.T., Wei W., Terrell S.M., Moeller B.C., Arthur R.M., Wallis G.A., van de Wetering K., Stahl A., Kiens B., Richter E.A., Banik S.M., Snyder M.P., Xu Y. & Long J.Z. (2022) An exercise-inducible metabolite that suppresses feeding and obesity. *Nature* **606**, 785-90.

Li W., Li J., Gao X., Xu S. & Yue W. (2012) Association analysis of PRKAG3 gene variants with carcass and meat quality traits in beef cattle. *Afr. J. Biotechnol.* **11**, 1855-61.

Lisa M.H., Paula L.H., Sanjiv B., Laura S., Alan K., Larry S., Igor G., Lucie L., Maurice D., Bridget G., Sergey P., Larry M., Masami Y. & Boris T. (2006) A Sex-Specific Role of Type VII Adenylyl Cyclase in Depression. *J. Neurosci.* **26**, 12609.

Liu C.C., Shringarpure S., Lange K. & Novembre J. (2020a) Exploring Population Structure with Admixture Models and Principal Component Analysis. *Methods Mol. Biol.* **2090**, 67-86.

Liu D., Li J., Shi K., Zeng F., Zong Y., Leng X., Lu H. & Du R. (2017) Construction and Immunogenicity Analysis of Whole-Genome Mutation DNA Vaccine of Aleutian Mink Virus Isolated Virulent Strain. *Viral Immunol.* **31**, 69-77.

Liu W., Taso O., Wang R., Bayram S., Graham A.C., Garcia-Reitboeck P., Mallach A., Andrews W.D., Piers T.M., Botia J.A., Pocock J.M., Cummings D.M., Hardy J., Edwards F.A. & Salih D.A. (2020b) Trem2 promotes anti-inflammatory responses in microglia and is suppressed under pro-inflammatory conditions. *Hum. Mol. Genet.* **29**, 3224-48.

Liu Z., Du Z., Yang C., Fu J., Wang X., Bai X. & Ning F. (2011) Modelling growth of five different colour types of mink. *S. Afr. J. Anim. Sci.* **41**, 116-25.

Long F. (2012) Building strong bones: molecular regulation of the osteoblast lineage. *Nat. Rev. Mol. Cell Biol.* **13**, 27-38.

Long N., Gianola D., Rosa G. & Weigel K. (2011) Dimension reduction and variable selection for genomic selection: application to predicting milk yield in Holsteins. *J. Anim. Breed. Genet.* **128**, 247-57.

Lourenco D.A.L., Misztal I., Tsuruta S., Aguilar I., Ezra E., Ron M., Shirak A. & Weller J.I. (2014) Methods for genomic evaluation of a relatively small genotyped dairy population and effect of genotyped cow information in multiparity analyses. *J. Dairy Sci.* **97**, 1742-52.

Luikart G., England P.R., Tallmon D., Jordan S. & Taberlet P. (2003) The power and promise of population genomics: from genotyping to genome typing. *Nat. Rev. Genet.* **4**, 981-94.

Lwelamira J., Kifaro G.C. & Gwakisa P.S. (2009) Genetic parameters for body weights, egg traits and antibody response against Newcastle Disease Virus (NDV) vaccine among two Tanzania chicken ecotypes. *Trop. Anim. Health Prod.* **41**, 51-9.

Ma F., Zhang L., Wang Y., Lu R., Hu B., Lv S., Xue X., Li X., Ling M., Fan S., Zhang H. & Yan X. (2016) Development of a Peptide ELISA for the Diagnosis of Aleutian Mink Disease. *PLoS One* **11**, e0165793.

Ma W., Ma Y., Liu D., Gao Y., Sun X.m., Li A.M., Zhang C. & Chen H. (2012) Novel SNPs in the bovine Transmembrane protein 18 gene, their linkage and their associations with growth traits in Nanyang cattle. *Genes & Genomics* **34**, 591-7.

Ma Y., Ding X., Qanbari S., Weigend S., Zhang Q. & Simianer H. (2015) Properties of different selection signature statistics and a new strategy for combining them. *Heredity* **115**, 426-36.

Makieva S., Giacomini E., Ottolina J., Sanchez A.M., Papaleo E. & Viganò P. (2018) Inside the Endometrial Cell Signaling Subway: Mind the Gap(s). *Int. J. Mol. Sci.* **19**, 2477.

Makowsky R., Pajewski N.M., Klimentidis Y.C., Vazquez A.I., Duarte C.W., Allison D.B. & de los Campos G. (2011) Beyond missing heritability: prediction of complex traits. *PLoS Genet.* **7**, e1002051.

Mallikarjunappa S., Schenkel F.S., Brito L.F., Bissonnette N., Miglior F., Chesnais J., Lohuis M., Meade K.G. & Karrow N.A. (2020) Association of genetic polymorphisms related to Johne's disease with estimated breeding values of Holstein sires for milk ELISA test scores. *BMC Vet. Res.* **16**, 1-7.

Mancini G., Gargani M., Chillemi G., Nicolazzi E.L., Marsan P.A., Valentini A. & Pariset L. (2014) Signatures of selection in five Italian cattle breeds detected by a 54K SNP panel. *Mol. Biol. Rep.* **41**, 957-65.

Markarian N.M. & Abrahamyan L. (2021) AMDV Vaccine: Challenges and Perspectives. In: *Viruses*.

Marshall J.S., Warrington R., Watson W. & Kim H.L. (2018) An introduction to immunology and immunopathology. *Allergy Asthma Clin. Immunol.* **14**, 49.

Matilainen K., Koivula M., Strandén I., Aamand G.P. & Mäntysaari E.A. (2016) Managing genetic groups in single-step genomic evaluations applied on female fertility traits in Nordic Red Dairy cattle. *Interbull Bull.*, 71-5.

Mazharian A., Wang Y.-J., Mori J., Bem D., Finney B., Heising S., Gissen P., White J.G., Berndt M.C., Gardiner E.E., Nieswandt B., Douglas M.R., Campbell R.D., Watson S.P. & Senis Y.A. (2012) Mice Lacking the ITIM-Containing Receptor G6b-B Exhibit Macrothrombocytopenia and Aberrant Platelet Function. *Sci. Signal.* **5**, ra78-ra.

McGuire T.C., Perryman L.E. & Gorham J.R. (1979) Mechanisms of anemia in Aleutian disease viral infection of mink. *Vet. Microbiol.* **4**, 17-27.

Melhem M., Abu-Farha M., Antony D., Madhoun A.A., Bacchelli C., Alkayal F., AlKhairi I., John S., Alomari M., Beales P.L. & Alsmadi O. (2017) Novel G6B gene variant causes familial autosomal recessive thrombocytopenia and anemia. *Eur. J. Haematol.* **98**, 218-27.

Melo T.P.d., de Camargo G.M.F., de Albuquerque L.G. & Carneiro R. (2017) Genome-wide association study provides strong evidence of genes affecting the reproductive performance of Nelore beef cows. *PLoS One* **12**, e0178551.

Meuwissen T. & Goddard M. (2010) Accurate prediction of genetic values for complex traits by whole-genome resequencing. *Genetics* **185**, 623-31.

Meuwissen T., Hayes B. & Goddard M. (2013) Accelerating improvement of livestock with genomic selection. *Annu. Rev. Anim. Biosci.* **1**, 221-37.

Meuwissen T., Hayes B. & Goddard M. (2016) Genomic selection: A paradigm shift in animal breeding. *Anim. Front.* **6**, 6-14.

Meuwissen T.H.E., Hayes B.J. & Goddard M.E. (2001) Prediction of Total Genetic Value Using Genome-Wide Dense Marker Maps. *Genetics* **157**, 1819-29.

Miao Y., Mei Q., Fu C., Liao M., Liu Y., Xu X., Li X., Zhao S. & Xiang T. (2021) Genome-wide association and transcriptome studies identify candidate genes and pathways for feed conversion ratio in pigs. *BMC Genom.* **22**, 294.

Miar Y., Plastow G., Bruce H., Moore S., Durunna O., Nkrumah J. & Wang Z. (2014a) Estimation of genetic and phenotypic parameters for ultrasound and carcass merit traits in crossbred beef cattle. *Can. J. Anim. Sci.* **94**, 273-80.

Miar Y., Plastow G. & Wang Z. (2015) Genomic selection, a new era for pork quality Improvement. *Springer Sci. Rev.* **3**, 27-37.

Miar Y., Plastow G.S., Moore S.S., Manafiazar G., Charagu P., Kemp R.A., Van Haandel B., Huisman A.E., Zhang C.Y., McKay R.M., Bruce H.L. & Wang Z. (2014b) Genetic and phenotypic parameters for carcass and meat quality traits in commercial crossbred pigs1. *Sci. J. Anim. Sci.* **92**, 2869-84.

Minges Wols H.A. (2015) Plasma Cells. In: *Encyclopedia of Life Sciences* (pp. 1-11).

Misztal I., Aggrey S.E. & Muir W.M. (2013) Experiences with a single-step genome evaluation. *Poult. Sci.* **92**, 2530-4.

Misztal I., Aguilar I., Lourenco D., Ma L., Steibel J.P. & Toro M. (2021) Emerging issues in genomic selection. *J. Anim. Sci.* **99**.

Mkize N., Maiwashe A., Dzama K., Dube B. & Mapholi N. (2021) Suitability of GWAS as a Tool to Discover SNPs Associated with Tick Resistance in Cattle: A Review. *Pathogens* **10**.

Moller S. & Sorensen J. (2003) Management problems and tools for strictly synchronised animal production systems exemplified by mink production. *Scientifur* **27**, 85-96.

Mora M., Medina-Vogel G., Sepúlveda M.A., Noll D., Álvarez-Varas R. & Vianna J.A. (2018) Genetic structure of introduced American mink (Neovison vison) in Patagonia: colonisation insights and implications for control and management strategies. *Wildl. Res.* **45**, 344-56.

Morowski M., Vögtle T., Kraft P., Kleinschnitz C., Stoll G. & Nieswandt B. (2013) Only severe thrombocytopenia results in bleeding and defective thrombus formation in mice. *Blood* **121**, 4938-47.

Mujibi F.D., Okoth E., Cheruiyot E.K., Onzere C., Bishop R.P., Fèvre E.M., Thomas L., Masembe C., Plastow G. & Rothschild M. (2018) Genetic diversity, breed composition and admixture of Kenyan domestic pigs. *PLoS One* **13**, e0190080.

Mulder H.A. & Rashidi H. (2017) Selection on resilience improves disease resistance and tolerance to infections. *J. Anim. Sci.* **95**, 3346-58.

Nagy M., Mastebroek T.G., Mattheij N.J.A., de Witt S., Clemetson K.J., Kirschner J., Schulz A.S., Vraetz T., Speckmann C., Braun A., Cosemans J., Zieger B. & Heemskerk J.W.M. (2018) Variable impairment of platelet functions in patients with severe, genetically linked immune deficiencies. *Haematologica* **103**, 540-9.

Nei M. (1972) Genetic distance between populations. *The American Naturalist* **106**, 283-92.

Nei M. & Li W. (1979) Mathematical model for studying genetic variation in terms of restriction endonucleases. *Proc. Natl. Acad. Sci.* **76**, 5269-73.

Nes N., Einarsson J., Lohi O., Jarosz S. & Scheelje R. (1988) MINK Mustela vison. In: *Beautiful Fur Animals and Their Color Genetics* (pp. 153-98. Scientifur, Denmark.

Nielsen R. (2005) Molecular signatures of natural selection. *Annu. Rev. Genet.* **39**, 197-218.

Notter D.R. (1999) The importance of genetic diversity in livestock populations of the future1. *J. Anim. Sci.* **77**, 61-9.

O'Doherty A.M., O'Brien Y.M., Browne J.A., Wingfield M. & O'Shea L.C. (2018) Expression of granulosa cell microRNAs, AVEN and ATRX are associated with human blastocyst development. *Mol. Reprod. Dev.* **85**, 836-48.

Oaten M. (2021) MARKET UPTURN: STRONG DEMAND AND RISING FUR PRICES. URL <https://www.wearefur.com/market-upturn-strong-demand-and-rising-fur-prices/>.

Okada M., Sakano T., Senna K., Maruyama T., Murofushi J., Okonogi H. & Sato S. (1999) Evaluation of Mycoplasma hyopneumoniae inactivated vaccine in pigs under field conditions. *J. Vet. Med. Sci.* **61**, 1131-5.

Okamura T., Maeda K., Onodera W., Kadowaki H., Kojima-Shibata C., Suzuki E., Uenishi H., Satoh M. & Suzuki K. (2016) Correlated responses of respiratory disease and immune capacity traits of Landrace pigs selected for Mycoplasmal pneumonia of swine (MPS) lesion. *Anim. Sci. J.* **87**, 1099-105.

Okroj M., Holmquist E., King B.C. & Blom A.M. (2012) Functional Analyses of Complement Convertases Using C3 and C5-Depleted Sera. *PLoS One* **7**, e47245.

Olesin E., Nayar R., Saikumar-Lakshmi P. & Berg L.J. (2018) The Transcription Factor Runx2 Is Required for Long-Term Persistence of Antiviral CD8+ Memory T Cells. *ImmunoHorizons* **2**, 251-61.

Ollivier L. (2009) European pig genetic diversity: a minireview. *Animal* **3**, 915-24.

Onogi A., Ogino A., Komatsu T., Shoji N., Shimizu K., Kurogi K., Yasumori T., Togashi K. & Iwata H. (2015) Whole-genome prediction of fatty acid composition in meat of Japanese Black cattle. *Anim. Genet.* **46**, 557-9.

Pakdel A., Arendonk J.V., Vereijken A. & Bovenhuis H. (2005) Genetic parameters of ascites-related traits in broilers: correlations with feed efficiency and carcass traits. *Br. Poult. Sci.* **46**, 43-53.

Palagano E., Menale C., Sobacchi C. & Villa A. (2018) Genetics of Osteopetrosis. *Curr. Osteoporos Rep.* **16**, 13-25.

Parker H.G., Dreger D.L., Rimbault M., Davis B.W., Mullen A.B., Carpintero-Ramirez G. & Ostrander E.A. (2017) Genomic Analyses Reveal the Influence of Geographic Origin, Migration, and Hybridization on Modern Dog Breed Development. *Cell Rep.* **19**, 697-708.

Patterson N., Price A.L. & Reich D. (2006) Population Structure and Eigenanalysis. *PLoS Genet.* **2**, e190.

Pembleton L.W., Cogan N.O.I. & Forster J.W. (2013) StAMPP: an R package for calculation of genetic differentiation and structure of mixed-ploidy level populations. *Molecular Ecology Resources* **13**, 946-52.

Persichilli C., Senczuk G., Mastrangelo S., Marusi M., van Kaam J.T., Finocchiaro R., Di Civita M., Cassandro M. & Pilla F. (2023) Exploring genome-wide differentiation and signatures of selection in Italian and North American Holstein populations. *J. Dairy. Sci.* **106**, 5537-53.

Pfaff C.L., Parra E.J., Bonilla C., Hiester K., McKeigue P.M., Kamboh M.I., Hutchinson R.G., Ferrell R.E., Boerwinkle E. & Shriver M.D. (2001) Population Structure in Admixed Populations: Effect of Admixture Dynamics on the Pattern of Linkage Disequilibrium. *Am. J. Hum. Genet.* **68**, 198-207.

Pickering M.C., Botto M., Taylor P.R., Lachmann P.J. & Walport M.J. (2001) Systemic Lupus Erythematosus, Complement Deficiency, and Apoptosis. In: *Adv. Immunol.* (ed. by Dixon FJ), pp. 227-324. Academic Press.

Porter D.D. & Cho H.J. (1980) Aleutian Disease of Mink: A Model for Persistent Infection. In: *Comprehensive Virology: Vol. 16: Virus-Host Interactions: Viral Invasion, Persistence, and Disease* (eds. by Fraenkael-Conrat H & Wagner RR), pp. 233-56. Springer US, Boston, MA.

Porter D.D., Larsen A.E. & Porter H.G. (1969) The pathogenesis of Aleutian disease of mink: I. In vivo viral replication and the host antibody response to viral antigen. *J. Exp. Med.* **130**, 575-93.

Porter D.D., Larsen A.E. & Porter H.G. (1972) The Pathogenesis of Aleutian Disease of Mink. *J. Immunol.* **109**, 1.

Porter D.D., Larsen A.E. & Porter H.G. (1973) The pathogenesis of Aleutian disease of mink. 3. Immune complex arteritis. *Am. J. Pathol.* **71**, 331-44.

Porter H.G., Porter D.D. & Larsen A.E. (1982) Aleutian disease in ferrets. *Infect. Immun.* **36**, 379-86.

Prochazka R., Blaha M. & Nemcova L. (2012) Signaling pathways regulating FSH- and amphiregulin-induced meiotic resumption and cumulus cell expansion in the pig. *REPRODUCTION* **144**, 535-46.

Prochazka R. & Nemcova L. (2019) Mechanisms of FSH- and Amphiregulin-Induced MAP Kinase 3/1 Activation in Pig Cumulus-Oocyte Complexes During Maturation In Vitro. *Int. J. Mol. Sci.* **20**, 1179.

Psifidi A., Banos G., Matika O., Desta T.T., Bettridge J., Hume D.A., Dessie T., Christley R., Wigley P., Hanotte O. & Kaiser P. (2016) Genome-wide association studies of immune, disease and production traits in indigenous chicken ecotypes. *Genet. Sel. Evol.* **48**, 74.

Purcell S., Neale B., Todd-Brown K., Thomas L., Ferreira M.A.R., Bender D., Maller J., Sklar P., de Bakker P.I.W., Daly M.J. & Sham P.C. (2007) PLINK: a tool set for whole-genome association and population-based linkage analyses. *Am. J. Hum. Genet.* **81**, 559-75.

Putz A.M., Harding J., Dyck M.K., Fortin F., Plastow G.S. & Dekkers J. (2019) Novel resilience phenotypes using feed intake data from a natural disease challenge model in wean-to-finish pigs. *Front. Genet.* **9**, 660.

Qanbari S. (2020) On the Extent of Linkage Disequilibrium in the Genome of Farm Animals. *Front. Genet.* **10**.

Qanbari S. & Simianer H. (2014) Mapping signatures of positive selection in the genome of livestock. *Livest. Sci.* **166**, 133-43.

Quinlan A.R. (2014) BEDTools: The Swiss-Army Tool for Genome Feature Analysis. *Curr. Protoc. Bioinform.* **47**, 11-2.

R Development Core Team R. (2011) R: a language and environment for statistical computing. Vienna, Austria: R Foundation for Statistical Computing.

Rask-Andersen M., Jacobsson J.A., Moschonis G., Chavan R.A., Sikder M.A.N., Allzén E., Alsiö J., Chrousos G.P., Manios Y., Fredriksson R. & Schiöth H.B. (2012) Association of TMEM18 variants with BMI and waist circumference in children and correlation of mRNA expression in the PFC with body weight in rats. *Eur. J. Hum. Genet.* **20**, 192-7.

Rea I.M., Gibson D.S., McGilligan V., McNerlan S.E., Alexander H.D. & Ross O.A. (2018) Age and Age-Related Diseases: Role of Inflammation Triggers and Cytokines. *Front. Immunol.* **9**, 586.

Reeves E. & James E. (2017) Antigen processing and immune regulation in the response to tumours. *Immunology* **150**, 16-24.

Reichert M. & Kostro K. (2014) Effect of persistent infection of mink with Aleutian mink disease virus on reproductive failure. *Bull. Vet. Inst. Pulawy.* **58**, 369-73.

Ribas G., Neville M., Wixon J.L., Cheng J. & Campbell R.D. (1999) Genes Encoding Three New Members of the Leukocyte Antigen 6 Superfamily and a Novel Member of Ig Superfamily, Together with Genes Encoding the Regulatory Nuclear Chloride Ion Channel Protein (hRNCC) and a N ω -N ω -Dimethylarginine Dimethylaminohydrolase Homologue, Are Found in a 30-kb Segment of the MHC Class III Region1 2. *J. Immunol.* **163**, 278-87.

Ribeiro V.M.P., Gouveia G.C., Moraes M.M.d., Araújo A.E.M.d., Raidan F.S.S., Fonseca P.A.d.S., Cardoso E.P., Silva M.V.G.B.d. & Toral F.L.B. (2021) Genes underlying genetic correlation between growth, reproductive and parasite burden traits in beef cattle. *Livest. Sci.* **244**, 104332.

Richards O. & Kavanagh A. (1945) The analysis of growing form. In essays on growth and form. *Oxford Univ. Press.*, 188.

Ritz U. & Seliger B. (2001) The Transporter Associated With Antigen Processing (TAP): Structural Integrity, Expression, Function, and Its Clinical Relevance. *Mol. Med.* **7**, 149-58.

Ropka-Molik K., Bereta A., Żukowski K., Tyra M., Piórkowska K., Żak G. & Oczkiewicz M. (2018) Screening for candidate genes related with histological microstructure, meat quality and carcass characteristic in pig based on RNA-seq data. *Asian-Australas J. Anim. Sci.* **31**, 1565-74.

Rupasinghe P.P. & Farid A. (2017) A new look at an old virus: Phylogenetic relationship between an Aleutian mink disease virus from Nova Scotia and global strains. In: *International Virology Conference*, Toronto, Canada.

Ryan M.T., Hamill R.M., O'Halloran A.M., Davey G.C., McBryan J., Mullen A.M., McGee C., Gispert M., Southwood O.I. & Sweeney T. (2012) SNP variation in the promoter of the PRKAG3 gene and association with meat quality traits in pig. *BMC Genet.* **13**, 66.

Ryman N., Laikre L. & Hössjer O. (2019) Do estimates of contemporary effective population size tell us what we want to know? *Mol. Ecol.* **28**, 1904-18.

Sabeti P.C., Varilly P., Fry B., Lohmueller J., Hostetter E., Cotsapas C., Xie X., Byrne E.H., McCarroll S.A. & Gaudet R. (2007) Genome-wide detection and characterization of positive selection in human populations. *Nature* **449**, 913-8.

sagafurs (2022) Saga Furs September auction, reports and stock exchange releases. URL <https://www.sagafurs.com/corporate/news/saga-furs-september-auction-reports-and-stock-exchange-releases/>.

Salek Ardestani S. (2020, https://github.com/Siavash-cloud/DEBV_calculator) DEBV_calculator.

Samorè A.B. & Fontanesi L. (2016) Genomic selection in pigs: state of the art and perspectives. *Ital. J. Anim. Sci.* **15**, 211-32.

Sandhu M.S., Gibson J.M., Heald A.H., Dunger D.B. & Wareham N.J. (2003) Low Circulating IGF-II Concentrations Predict Weight Gain and Obesity in Humans. *Diabetes* **52**, 1403-8.

Santer D.M., Wiedeman A.E., Teal T.H., Ghosh P. & Elkon K.B. (2012) Plasmacytoid Dendritic Cells and C1q Differentially Regulate Inflammatory Gene Induction by Lupus Immune Complexes. *J. Immunol.* **188**, 902-15.

Saravanan K.A., Panigrahi M., Kumar H., Bhushan B., Dutt T. & Mishra B.P. (2020) Selection signatures in livestock genome: A review of concepts, approaches and applications. *Livest. Sci.* **241**, 104257.

Saravanan K.A., Panigrahi M., Kumar H., Parida S., Bhushan B., Gaur G.K., Dutt T., Mishra B.P. & Singh R.K. (2021) Genomic scans for selection signatures revealed candidate genes for adaptation and production traits in a variety of cattle breeds. *Genomics* **113**, 955-63.

Sargolzaei M. (2014) *snpl101 User's Guide. Version 1.0*, University of Guelph, Guelph, ON, Canada.

Sarma J.V. & Ward P.A. (2011) The complement system. *Cell Tissue Res.* **343**, 227-35.

Sarviaho K., Uimari P. & Martikainen K. (2024) Signatures of positive selection after the introduction of genomic selection in the Finnish Ayrshire population. *J. Dairy. Sci.*

Saunders D.A. (1988) *Adirondack mammals*, State University of New York, College of Environmental Science and Forestry.

Sawai C.M., Sisirak V., Ghosh H.S., Hou E.Z., Ceribelli M., Staudt L.M. & Reizis B. (2013) Transcription factor Runx2 controls the development and migration of plasmacytoid dendritic cells. *J. Exp. Med.* **210**, 2151-9.

Schäfer S. & Zerneck A. (2020) CD8(+) T Cells in Atherosclerosis. *Cells* **10**, 37.

Schifferli J.A., Steiger G., Hauptmann G., Spaeth P. & Sjöholm A. (1985) Formation of soluble immune complexes by complement in sera of patients with various hypocomplementemic states. Difference between inhibition of immune precipitation and solubilization. *J. Clin. Invest.* **76**, 2127-33.

Schmid M. & Bennewitz J. (2017) Invited review: Genome-wide association analysis for quantitative traits in livestock – a selective review of statistical models and experimental designs. *Arch. Anim. Breed.* **60**, 335-46.

Seabury C.M., Oldeschulte D.L., Saatchi M., Beever J.E., Decker J.E., Halley Y.A., Bhattarai E.K., Molaei M., Freetly H.C., Hansen S.L., Yampara-Iquise H., Johnson K.A., Kerley M.S., Kim J., Loy D.D., Marques E., Neibergs H.L., Schnabel R.D., Shike D.W., Spangler M.L., Weaber R.L., Garrick D.J. & Taylor J.F. (2017) Genome-wide association study for feed efficiency and growth traits in U.S. beef cattle. *BMC Genom.* **18**, 386.

Searle S. (1961) Phenotypic, genetic and environmental correlations. *Biometrics* **17**, 474-80.

Seo H., Chen J., González-Avalos E., Samaniego-Castruita D., Das A., Wang Y.H., López-Moyado I.F., Georges R.O., Zhang W., Onodera A., Wu C.-J., Lu L.-F., Hogan P.G., Bhandoola A. & Rao A. (2019) TOX and TOX2 transcription factors cooperate with NR4A transcription factors to impose CD8⁺ T cell exhaustion. *Proc. Natl. Acad. Sci.* **116**, 12410-5.

Serão N.V., Kemp R.A., Mote B.E., Willson P., Harding J.C., Bishop S.C., Plastow G.S. & Dekkers J.C. (2016) Genetic and genomic basis of antibody response to porcine reproductive and respiratory syndrome (PRRS) in gilts and sows. *Genet. Sel. Evol.* **48**, 1-15.

Serão N.V.L., González-Peña D., Beever J.E., Faulkner D.B., Southey B.R. & Rodriguez-Zas S.L. (2013) Single nucleotide polymorphisms and haplotypes associated with feed efficiency in beef cattle. *BMC Genet.* **14**, 94.

Serwas N.K., Hoeger B., Ardy R.C., Stulz S.V., Sui Z., Memaran N., Meeths M., Krolo A., Yüce Petronczki Ö., Pfajfer L., Hou T.Z., Halliday N., Santos-Valente E., Kalinichenko A., Kennedy A., Mace E.M., Mukherjee M., Tesi B., Schrempf A., Pickl W.F., Loizou J.I., Kain R., Bidmon-Fliegenschnee B., Schickel J.-N., Glauzy S., Huemer J., Garncarz W., Salzer E., Pierides I., Bilic I., Thiel J., Priftakis P., Banerjee P.P., Förster-Waldl E., Medgyesi D., Huber W.-D., Orange J.S., Meffre E., Sansom D.M., Bryceson Y.T., Altman A. & Boztug K. (2019) Human DEF6 deficiency underlies an immunodeficiency syndrome with systemic autoimmunity and aberrant CTLA-4 homeostasis. *Nat. Commun.* **10**, 3106.

Shackelford R.M. (1948) The Nature of Coat Color Differences in Mink and Foxes. *Genetics* **33**, 311-36.

Sharma A., Lee J.S., Dang C.G., Sudrajad P., Kim H.C., Yeon S.H., Kang H.S. & Lee S.-H. (2015) Stories and challenges of genome wide association studies in livestock—a review. *Asian-australas. J. Anim. Sci.* **28**, 1371.

Shim H., Chasman D.I., Smith J.D., Mora S., Ridker P.M., Nickerson D.A., Krauss R.M. & Stephens M. (2015) A Multivariate Genome-Wide Association Analysis of 10 LDL Subfractions, and Their Response to Statin Treatment, in 1868 Caucasians. *PLoS One* **10**, e0120758.

Sigdel A., Bisinotto R.S. & Peñagaricano F. (2021) Genes and pathways associated with pregnancy loss in dairy cattle. *Sci. Rep.* **11**, 13329.

Silva R.M., Fragomeni B.O., Lourenco D.A., Magalhães A.F., Irano N., Carvalheiro R., Canesin R.C., Mercadante M.E., Boligon A.A., Baldi F.S., Misztal I. & Albuquerque L.G. (2016) Accuracies of genomic prediction of feed efficiency traits using different prediction and validation methods in an experimental Nelore cattle population. *J. Anim. Sci.* **94**, 3613-23.

Slatkin M. (2008) Linkage disequilibrium — understanding the evolutionary past and mapping the medical future. *Nat. Rev. Genet.* **9**, 477-85.

Snowder G., Van Vleck L.D., Cundiff L. & Bennett G. (2006) Bovine respiratory disease in feedlot cattle: environmental, genetic, and economic factors. *J. Anim. Sci.* **84**, 1999-2008.

Snowder G.D., Van Vleck L.D., Cundiff L.V., Bennett G.L., Koohmaraie M. & Dikeman M.E. (2007) Bovine respiratory disease in feedlot cattle: Phenotypic, environmental, and genetic correlations with growth, carcass, and longissimus muscle palatability traits 1. *J. Anim. Sci.* **85**, 1885-92.

Sørensen K., Grossman M. & Koops W. (2003) Multiphasic growth curves in mink (*Mustela vison*) selected for feed efficiency. *Acta. Agric. Scand. A Anim. Sci.* **53**, 41-50.

Southey B. & Gilmour A.R. (2021) Generalized models. URL <https://asreml.kb.vsnr.co.uk/knowledge-base/cookbook-generalized-models/>.

Spinazzi R., Andreis P.G., Rossi G.P. & Nussdorfer G.G. (2006) Orexins in the Regulation of the Hypothalamic-Pituitary-Adrenal Axis. *Pharmacol. Rev.* **58**, 46.

Statistics_Canada (2018a) Table 32-10-0115-01 Number and value of mink pelts sold, by colour type. URL <https://www150.statcan.gc.ca/t1/tbl1/en/tv.action?pid=3210011501>.

Statistics_Canada (2018b) Supply and disposition of mink and fox on fur farms. URL <https://www150.statcan.gc.ca/t1/tbl1/en/tv.action?pid=3210011601>.

Statistics_Canada (2022) Mink Statistical Briefer. URL <https://agriculture.canada.ca/en/canadas-agriculture-sectors/animal-industry/red-meat-and-livestock-market-information/mink-statistical-briefer>.

Stolze B. & Kaaden O. (1987) Apparent lack of neutralizing antibodies in aleutian disease is due to masking of antigenic sites by phospholipids. *Virology* **158**, 174-80.

Stubbs V.E., Power C. & Patel K.D. (2010) Regulation of eotaxin-3/CCL26 expression in human monocytic cells. *Immunology* **130**, 74-82.

Sun M.J., Zhu S., Li Y.W., Lin J., Gong S., Jiao G.Z., Chen F. & Tan J.H. (2016) An essential role for the intra-oocyte MAPK activity in the NSN-to-SN transition of germinal vesicle chromatin configuration in porcine oocytes. *Sci. Rep.* **6**, 23555.

Sved J.A. (1971) Linkage disequilibrium and homozygosity of chromosome segments in finite populations. *Theor. Popul. Biol.* **2**, 125-41.

Tabel H. & Ingram D.G. (1970) The immunoglobulins in Aleutian disease (viral plasmacytosis) of mink. Different types of hypergammaglobulinemias. *Can. J. Comp. Med.* **34**, 329-32.

Tahir M.S., Porto-Neto L.R., Gondro C., Shittu O.B., Wockner K., Tan A.W.L., Smith H.R., Gouveia G.C., Kour J. & Fortes M.R.S. (2021) Meta-Analysis of Heifer Traits Identified Reproductive Pathways in *Bos indicus* Cattle. *Genes (Basel)* **12**, 768.

Tam V., Patel N., Turcotte M., Bossé Y., Paré G. & Meyre D. (2019) Benefits and limitations of genome-wide association studies. *Nat. Rev. Genet.* **20**, 467-84.

Tamlin A., Bowman J., Hackett D. & Wildlife (2009) Separating Wild from Domestic American Mink *Neovison vison* Based on Skull Morphometries. *Wildl. Biol* **15**, 266-77.

Team R.C. (2022) R: A Language and Environment for Statistical Computing. . R Foundation for Statistical Computing, Vienna, Austria.

Teissier M., Larroque H. & Robert-Granie C. (2019) Accuracy of genomic evaluation with weighted single-step genomic best linear unbiased prediction for milk production traits, udder type traits, and somatic cell scores in French dairy goats. *J. Dairy. Sci.* **102**, 3142-54.

Themudo G.E., Østergaard J. & Ersbøll A.K. (2011) Persistent spatial clusters of plasmacytosis among Danish mink farms. *Prev. Vet. Med.* **102**, 75-82.

Thia J.A. (2022) Guidelines for standardizing the application of discriminant analysis of principal components to genotype data. *Mol. Ecol. Resour.*, 1-16.

Thirstrup J.P., Ruiz-Gonzalez A., Pujolar J.M., Larsen P.F., Jensen J., Randi E., Zalewski A. & Pertoldi C. (2015) Population genetic structure in farm and feral American mink (*Neovison vison*) inferred from RAD sequencing-generated single nucleotide polymorphisms. *J. Anim. Sci.* **93**, 3773-82.

Thomas P.D., Campbell M.J., Kejariwal A., Mi H., Karlak B., Daverman R., Diemer K., Muruganujan A. & Narechania A. (2003) PANTHER: a library of protein families and subfamilies indexed by function. *Genome. Res.* **13**, 2129-41.

Thomasen J.R., Sørensen A.C., Su G., Madsen P., Lund M.S. & Guldbrandtsen B. (2013) The admixed population structure in Danish Jersey dairy cattle challenges accurate genomic predictions. *J. Anim. Sci.* **91**, 3105-12.

Thompson-Crispi K.A., Sargolzaei M., Ventura R., Abo-Ismael M., Miglior F., Schenkel F. & Mallard B.A. (2014) A genome-wide association study of immune response traits in Canadian Holstein cattle. *BMC Genom.* **15**, 559.

Tiensuu H., Haapalainen A.M., Karjalainen M.K., Pasanen A., Huusko J.M., Marttila R., Ojaniemi M., Muglia L.J., Hallman M. & Rämetsä M. (2019) Risk of spontaneous preterm birth and fetal growth associates with fetal SLIT2. *PLoS Genet.* **15**, e1008107.

Toghiani S. (2012) Quantitative Genetic Application in the Selection Process for Livestock Production. In: *Livestock Production* (ed. by Javed K). IntechOpen, Rijeka, Croatia.

Toosi A., Fernando R.L. & Dekkers J.C.M. (2010) Genomic selection in admixed and crossbred populations I. *J. Anim. Sci.* **88**, 32-46.

Topaloglu A.K., Reimann F., Guclu M., Yalin A.S., Kotan L.D., Porter K.M., Serin A., Mungan N.O., Cook J.R., Imamoglu S., Akalin N.S., Yuksel B., O'Rahilly S. & Semple R.K. (2009) TAC3 and TACR3 mutations in familial hypogonadotropic hypogonadism reveal a key role for Neurokinin B in the central control of reproduction. *Nat. Genet.* **41**, 354-8.

Torres R., Szpiech Z.A. & Hernandez R.D. (2018) Human demographic history has amplified the effects of background selection across the genome. *PLoS Genet.* **14**, e1007387.

Tsai T.S., Johnson J., White Y. & John J.C. (2017) The molecular characterization of porcine egg precursor cells. *Oncotarget* **8**, 63484-505.

Turner P, Buijs S, Rommers JM & M T. (2013) The code of practice for the care and handling of farmed mink, vol. 58. Rexdale: The National Farm Animal Care Council.

Uemoto Y., Ichinoseki K., Matsumoto T., Oka N., Takamori H., Kadowaki H., Kojima-Shibata C., Suzuki E., Okamura T., Aso H., Kitazawa H., Satoh M., Uenishi H. & Suzuki K. (2021) Genome-wide association studies for production, respiratory disease, and immune-related traits in Landrace pigs. *Sci. Rep.* **11**, 15823.

Uffelmann E., Huang Q.Q., Munung N.S., de Vries J., Okada Y., Martin A.R., Martin H.C., Lappalainen T. & Posthuma D. (2021) Genome-wide association studies. *Nat. Rev. Methods Primers* **1**, 59.

Uzbekova S., Teixeira-Gomes A.-P., Marestaing A., Jarrier-Gaillard P., Papillier P., Shedova E.N., Singina G.N., Uzbekov R. & Labas V. (2021) Protein Palmitoylation in Bovine Ovarian Follicle. *Int. J. Mol. Sci.* **22**, 11757.

Vaillant F.o., Blyth K., Andrew L., Neil J.C. & Cameron E.R. (2002) Enforced Expression of Runx2 Perturbs T Cell Development at a Stage Coincident with β -Selection1. *J. Immunol.* **169**, 2866-74.

van der Most P.J., de Jong B., Parmentier H.K. & Verhulst S. (2011) Trade-off between growth and immune function: a meta-analysis of selection experiments. *Funct. Ecol.* **25**, 74-80.

Van Dyck F., Declercq J., Braem C.V. & Van de Ven W.J. (2007) PLAG1, the prototype of the PLAG gene family: versatility in tumour development (review). *Int. J. Oncol.* **30**, 765-74.

Van Laere A.S., Nguyen M., Braunschweig M., Nezer C., Collette C., Moreau L., Archibald A.L., Haley C.S., Buys N., Tally M., Andersson G., Georges M. & Andersson L. (2003) A regulatory mutation in IGF2 causes a major QTL effect on muscle growth in the pig. *Nature* **425**, 832-6.

VanRaden P.M. (2008) Efficient methods to compute genomic predictions. *J. Dairy Sci.* **91**, 4414-23.

VanRaden P.M., Van Tassell C.P., Wiggans G.R., Sonstegard T.S., Schnabel R.D., Taylor J.F. & Schenkel F.S. (2009) Invited review: reliability of genomic predictions for North American Holstein bulls. *J. Dairy. Sci.* **92**, 16-24.

Vasileva A., Tiedau D., Firooznia A., Müller-Reichert T. & Jessberger R. (2009) Tdrd6 is required for spermiogenesis, chromatoid body architecture, and regulation of miRNA expression. *Curr. Biol.* **19**, 630-9.

Verhoeven K.J.F., Macel M., Wolfe L.M. & Biere A. (2011) Population admixture, biological invasions and the balance between local adaptation and inbreeding depression. *Proc. R. Soc. B.* **278**, 2-8.

Villumsen T.M., Janss L. & Lund M.S. (2009) The importance of haplotype length and heritability using genomic selection in dairy cattle. *J. Anim. Breed. Genet.* **126**, 3-13.

Visscher P.M., Hill W.G. & Wray N.R. (2008) Heritability in the genomics era—concepts and misconceptions. *Nat. Rev. Genet.* **9**, 255-66.

Voz M.L., Agten N.S., Van de Ven W.J. & Kas K. (2000) PLAG1, the main translocation target in pleomorphic adenoma of the salivary glands, is a positive regulator of IGF-II. *Cancer Res.* **60**, 106-13.

Waide E.H., Tuggle C.K., Serão N.V., Schroyen M., Hess A., Rowland R.R., Lunney J.K., Plastow G. & Dekkers J.C. (2018) Genomic prediction of piglet response to infection with one of two porcine reproductive and respiratory syndrome virus isolates. *Genet. Sel. Evol.* **50**, 1-12.

Wang H. & Liu M. (2021) Complement C4, Infections, and Autoimmune Diseases. *Front. Immunol.* **12**, 694928.

Wang X., Wang L., Shi L., Zhang P., Li Y., Li M., Tian J., Wang L. & Zhao F. (2022) GWAS of Reproductive Traits in Large White Pigs on Chip and Imputed Whole-Genome Sequencing Data. *Int. J. Mol. Sci.* **23**, 13338.

Wang Y., Ding X., Tan Z., Xing K., Yang T., Wang Y., Sun D. & Wang C. (2018) Genome-wide association study for reproductive traits in a Large White pig population. *Anim. Genet.* **49**, 127-31.

Wang Y., Ning X., Gao P., Wu S., Sha M., Lv M., Zhou X., Gao J., Fang R., Meng G., Su X. & Jiang Z. (2017) Inflammasome Activation Triggers Caspase-1-Mediated Cleavage of cGAS to Regulate Responses to DNA Virus Infection. *Immunity* **46**, 393-404.

Waples R.S. & Do C. (2010) Linkage disequilibrium estimates of contemporary Ne using highly variable genetic markers: a largely untapped resource for applied conservation and evolution. *Evol. Appl.* **3**, 244-62.

Wassmuth R., Madsen D., Jensen P. & Jensen P. (2000) Genetic parameters of disease incidence, fertility and milk yield of first parity cows and the relation to feed intake of growing bulls. *Acta Agric. Scand. A Anim. Sci.* **50**, 93-102.

Wehn A.K. & Chapman D.L. (2010) Tbx18 and Tbx15 null-like phenotypes in mouse embryos expressing Tbx6 in somitic and lateral plate mesoderm. *Dev. Biol.* **347**, 404-13.

Wei Q., Gu Y.F., Zhang Q.J., Yu H., Peng Y., Williams K.W., Wang R., Yu K., Liu T. & Liu Z.P. (2018) Lztfl1/BBS17 controls energy homeostasis by regulating the leptin signaling in the hypothalamic neurons. *J. Mol. Cell Biol.* **10**, 402-10.

Weir B.S. & Cockerham C.C. (1984) Estimating F-statistics for the analysis of population structure. *Evolution* **38**, 1358-70.

Wellmann R. & Bennewitz J. (2019) Key Genetic Parameters for Population Management. *Front. Genet.* **10**.

Wiggans G.R., Cole J.B., Hubbard S.M. & Sonstegard T.S. (2017) Genomic Selection in Dairy Cattle: The USDA Experience. *Annu. Rev. Anim. Biosci.* **5**, 309-27.

Williams R.C., Jr., Williams L.P., Jr. & Wollheim F.A. (1965) Immunoglobulins in Mink Ranchers Associated With Aleutian Disease. *JAMA* **194**, 605-8.

Wilson K.C., Center D.M. & Cruikshank W.W. (2004) The effect of interleukin-16 and its precursor on T lymphocyte activation and growth. *Growth Factors* **22**, 97-104.

Wilson S., Van Brussel L., Saunders G., Taylor L., Zimmermann L., Heinritzi K., Ritzmann M., Banholzer E. & Eddicks M. (2012) Vaccination of piglets at 1 week of age with an inactivated *Mycoplasma hyopneumoniae* vaccine reduces lung lesions and improves average daily gain in body weight. *Vaccine* **30**, 7625-9.

Wolc A., Kranis A., Arango J., Settar P., Fulton J.E., O'Sullivan N.P., Avendano A., Watson K.A., Hickey J.M., de los Campos G., Fernando R.L., Garrick D.J. & Dekkers J.C.M. (2016) Implementation of genomic selection in the poultry industry. *Anim. Front.* **6**, 23-31.

Woods S.C. & Ramsay D.S. (2011) Food intake, metabolism and homeostasis. *Physiol. Behav.* **104**, 4-7.

Wu P., Wang K., Zhou J., Chen D., Yang Q., Yang X., Liu Y., Feng B., Jiang A., Shen L., Xiao W., Jiang Y., Zhu L., Zeng Y., Xu X., Li X. & Tang G. (2019) GWAS on Imputed Whole-Genome Resequencing From Genotyping-by-Sequencing Data for Farrowing Interval of Different Parities in Pigs. *Front. Genet.* **10**, 1012.

Xia J., Gravato-Nobre M. & Ligoxygakis P. (2019) Convergence of longevity and immunity: lessons from animal models. *Biogerontology* **20**, 271-8.

Xing K., Wang K., Ao H., Chen S., Tan Z., Wang Y., Xitong Z., Yang T., Zhang F., Liu Y., Ni H., Sheng X., Qi X., Wang X., Guo Y. & Wang C. (2019) Comparative adipose transcriptome analysis digs out genes related to fat deposition in two pig breeds. *Sci. Rep.* **9**, 12925.

Xu X., Hua X., Brown K., Ren X. & Zhang Z. (2022) Mcm2 promotes stem cell differentiation via its ability to bind H3-H4. *eLife* **11**, e80917.

Xu Z., Sun H., Zhang Z., Zhang C.Y., Zhao Q.B., Xiao Q., Olasege B.S., Ma P.P., Zhang X.Z., Wang Q.S. & Pan Y.C. (2020) Selection signature reveals genes associated with susceptibility loci affecting respiratory disease due to pleiotropic and hitchhiking effect in Chinese indigenous pigs. *Asian-Australas J. Anim. Sci.* **33**, 187-96.

Yang C.R., Wang J.H., Hsieh S.L., Wang S.M., Hsu T.L. & Lin W.W. (2004) Decoy receptor 3 (DcR3) induces osteoclast formation from monocyte/macrophage lineage precursor cells. *Cell Death Differ.* **11**, S97-S107.

Yang J., Bakshi A., Zhu Z., Hemani G., Vinkhuyzen A.A., Lee S.H., Robinson M.R., Perry J.R., Nolte I.M., van Vliet-Ostaptchouk J.V., Snieder H., Esko T., Milani L., Mägi R., Metspalu A., Hamsten A., Magnusson P.K., Pedersen N.L., Ingelsson E., Soranzo N., Keller M.C., Wray N.R., Goddard M.E. & Visscher P.M. (2015) Genetic variance estimation with imputed variants finds negligible missing heritability for human height and body mass index. *Nat. Genet.* **47**, 1114-20.

Yang J., Benyamin B., McEvoy B.P., Gordon S., Henders A.K., Nyholt D.R., Madden P.A., Heath A.C., Martin N.G., Montgomery G.W., Goddard M.E. & Visscher P.M. (2010) Common SNPs explain a large proportion of the heritability for human height. *Nat. Genet.* **42**, 565-9.

Yang T., Wilkinson J., Wang Z., Ladinig A., Harding J. & Plastow G. (2016) A genome-wide association study of fetal response to type 2 porcine reproductive and respiratory syndrome virus challenge. *Sci. Rep.* **6**, 20305.

Ye Y., Gaugler B., Mohty M. & Malard F. (2020) Plasmacytoid dendritic cell biology and its role in immune-mediated diseases. *Clin. Transl. Immunol.* **9**, e1139.

Young J., Bouligand J., Francou B., Raffin-Sanson M.L., Gaillez S., Jeanpierre M., Grynberg M., Kamenicky P., Chanson P., Brailly-Tabard S. & Guiochon-Mantel A. (2010) TAC3 and TACR3 defects cause hypothalamic congenital hypogonadotropic hypogonadism in humans. *J. Clin. Endocrinol. Metab.* **95**, 2287-95.

Yu G., Wang L.-G., Han Y. & He Q.-Y. (2012) clusterProfiler: an R Package for Comparing Biological Themes Among Gene Clusters. *OMICS J. Integr. Biol.* **16**, 284-7.

Yukari S., Yuko F., Ryosuke K. & Ryuichi M. (2010) Genetic Variation and Population Structure of the Feral American Mink (*Neovison vison*) in Nagano, Japan, Revealed by Microsatellite Analysis. *Mammal Study* **35**, 1-7.

Zalewski A., Zalewska H., Lunneryd S.-G., André C. & Mikusiński G. (2016) Reduced Genetic Diversity and Increased Structure in American Mink on the Swedish Coast following Invasive Species Control. *PLoS One* **11**, e0157972.

Zhang C., Kemp R.A., Stothard P., Wang Z., Boddicker N., Krivushin K., Dekkers J. & Plastow G. (2018) Genomic evaluation of feed efficiency component traits in Duroc pigs using 80K, 650K and whole-genome sequence variants. *Genet. Sel. Evol.* **50**, 14.

Zhang H., Wang Z., Wang S. & Li H. (2012) Progress of genome wide association study in domestic animals. *J. Anim. Sci. Biotechnol.* **3**, 26.

Zhang H., Yin L., Wang M., Yuan X. & Liu X. (2019a) Factors Affecting the Accuracy of Genomic Selection for Agricultural Economic Traits in Maize, Cattle, and Pig Populations. *Front. Genet.* **10**, 00189.

Zhang J., Wang J., Li Q., Wang Q., Wen J. & Zhao G. (2020) Comparison of the Efficiency of BLUP and GBLUP in Genomic Prediction of Immune Traits in Chickens. *animals* **10**, 419.

Zhang K., Kniazeva M., Han M., Li W., Yu Z., Yang Z., Li Y., Metzker M.L., Allikmets R., Zack D.J., Kakuk L.E., Lagali P.S., Wong P.W., MacDonald I.M., Sieving P.A., Figueroa D.J., Austin C.P., Gould R.J., Ayyagari R. & Petrukhin K. (2001) A 5-bp deletion in ELOVL4 is associated with two related forms of autosomal dominant macular dystrophy. *Nat. Genet.* **27**, 89-93.

Zhang L., Hua Y. & Wei S. (2021a) High Genetic Diversity of an Invasive Alien Species: Comparison between Fur-Farmed and Feral American Mink (*Neovison vison*) in China. In: *animals*.

Zhang Q., Ji S., Busayavalasa K. & Yu C. (2019b) SPO16 binds SHOC1 to promote homologous recombination and crossing-over in meiotic prophase I. *Sci. Adv.* **5**, eaau9780.

Zhang S., Zhao Y., Lei B., Li C. & Mao X. (2015) PGAM1 is Involved in Spermatogenic Dysfunction and Affects Cell Proliferation, Apoptosis, and Migration. *Reprod. Sci.* **22**, 1236-42.

Zhang W. & Liu H.T. (2002) MAPK signal pathways in the regulation of cell proliferation in mammalian cells. *Cell Res.* **12**, 9-18.

Zhang Y., Wang Y., Li Y., Wu J., Wang X., Bian C., Tian Y., Sun G., Han R., Liu X., Jiang R., Wang Y., Li G., Li W., Hu X. & Kang X. (2021b) Genome-wide association study reveals the genetic determinism of growth traits in a Gushi-Anka F2 chicken population. *Heredity* **126**, 293-307.

Zhang Z., Chen Z., Ye S., He Y., Huang S., Yuan X., Chen Z., Zhang H. & Li J. (2019c) Genome-Wide Association Study for Reproductive Traits in a Duroc Pig Population. *animals* **9**, 732.

Zhao F., McParland S., Kearney F., Du L. & Berry D.P. (2015) Detection of selection signatures in dairy and beef cattle using high-density genomic information. *Genet. Sel. Evol.* **47**, 1-12.

Zhou L., Mrode R., Zhang S., Zhang Q., Li B. & Liu J.F. (2018) Factors affecting GEBV accuracy with single-step Bayesian models. *Heredity* **120**, 100-9.

Zhou W.D., Chen Q.H. & Chen Q.X. (2010) The action of p38 MAP kinase and its inhibitors on endometriosis. *Yao xue xue bao = Acta pharmaceutica Sinica* **45**, 548-54.

APPENDIX 1. List of Publications and Conference Presentations (as of March 1, 2024)

1. Based on chapter 3:

Hu, G, Do, D.N, Davoudi, P, Manafiazar, G., Kelvin, A.A., Sargolzaei, M., Wang, Z, W., Plastow, G., & Miar, Y. Genetic and phenotypic correlations between Aleutian disease tests with body weight, growth, and feed efficiency traits in mink. **Journal of Animal Science**, 100(12), skac346.

2. Based on chapter 4:

Hu, G, Do, D.N, Davoudi, P, Manafiazar, G., Kelvin, A.A., Sargolzaei, M., Wang, Z, W., Plastow, G., & Miar, Y. Population Genomics of American Mink Using Genotypes Data. **Frontiers in Genetics**, 2023, 14, 1175408.

3. Based on chapter 5:

Hu, G, Do, D.N, Davoudi, P, Manafiazar, G., Kelvin, A.A., Sargolzaei, M., Wang, Z, W., Plastow, G., & Miar, Y. Identifying Selection Signatures for Immune Response and Resilience to Aleutian Disease in Mink Using Genotypes Data. **Submitted to Frontiers in Genetics**

AND

Hu, G, Do, D.N, Davoudi, P, Manafiazar, G., Kelvin, A.A., Sargolzaei, M., Wang, Z, W., Plastow, G., & Miar, Y. Identifying selection signatures for immune response and resilience to Aleutian disease in mink using genotype data. 2023 ASAS-CSAS-WSASAS Annual Meeting, Albuquerque, New Mexico, USA.

4. Based on chapter 6:

Hu, G, Do, D.N, Davoudi, P, Manafiazar, G., Kelvin, A.A., Sargolzaei, M., Wang, Z, Plastow, G, & Miar, Y. Genome-wide Association Study for Immune Response and Resilience to Aleutian Disease in Mink. **Submitted to BMC Genomics**.

5. Based on chapter 7:

Hu, G, Do, D.N, Davoudi, P, Manafiazar, G., Kelvin, A.A., Sargolzaei, M., Wang, Z, Plastow, G., & Miar, Y. Genomic Prediction of Immune Response and Resilience to Aleutian Disease in Mink. **Will BE SUBMITTED to PLOS One.**

APPENDIX 2. Description of Electronic Supplements

Supplementary dataset 1

The dataset includes 1) significant SNPs detected from different methods, 2) SNPs detected as candidate selection signatures by at least two methods, and 3) the genes annotated from the candidate selection signatures for immune response trait from Chapter 5.

Supplementary dataset 2

The dataset includes 1) The genes annotated from the detected significant SNPs for immune response, general resilience, and female reproductive performance traits, and 2) the common genes among the three studied traits from Chapter 5.

Supplementary dataset 3

The dataset includes 1) significant SNPs detected from different methods, 2) SNPs detected as candidate selection signatures by at least two methods, and 3) the genes annotated from the candidate selection signatures for general resilience and female reproductive performance trait from Chapter 5.

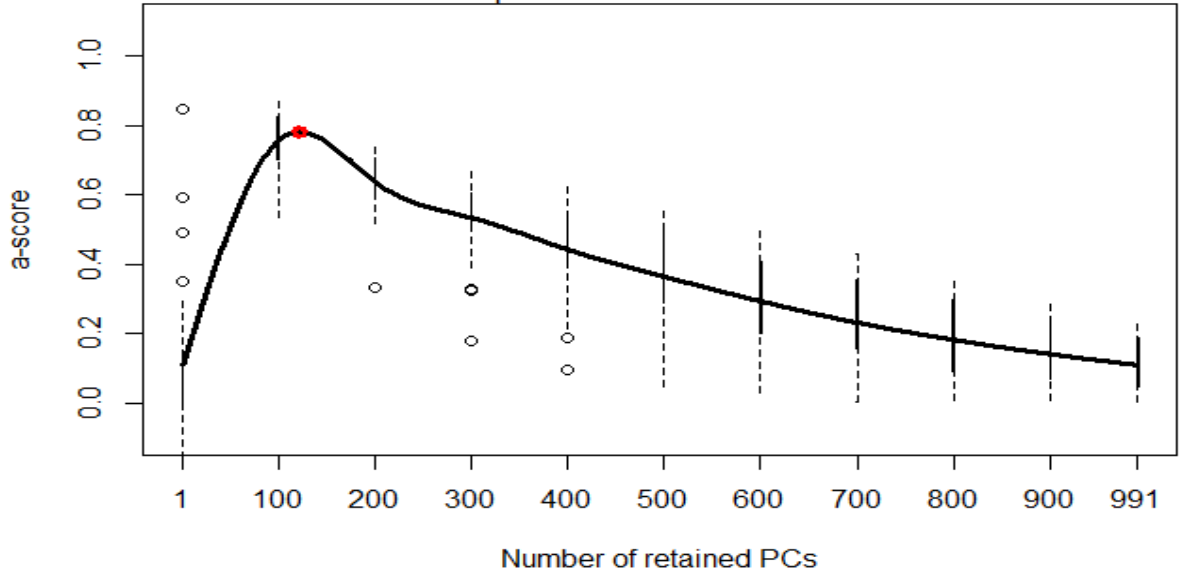
Supplementary dataset 4

The dataset of significant SNPs detected from the GWAS analyses, and the genes annotated from these significant SNPs for all three studied traits in Chapter 6.

SUPPLEMENTARY MATERIAL

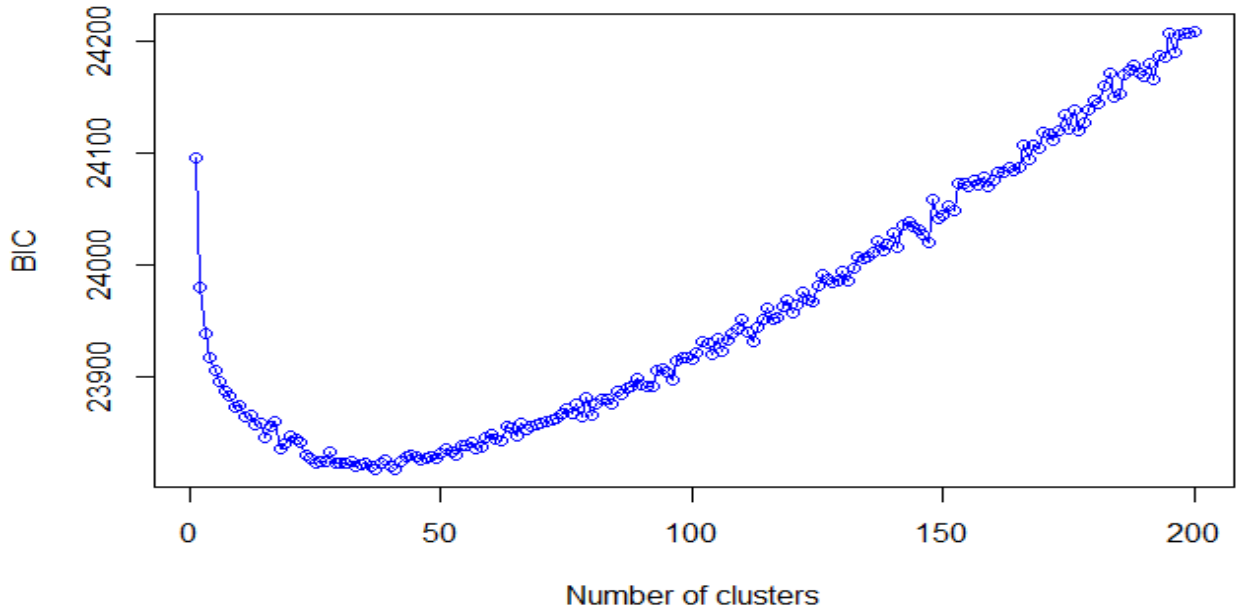
a-score optimisation - spline interpolation

Optimal number of PCs: 123



Supplementary Figure 1. Optimization α -score graph.

Value of BIC versus number of clusters



Supplementary Figure 2. Population genetic clustering results based on the Bayesian Information Criterion (BIC) in relation to the number of clusters identified by the find.cluster function in DAPC analysis.

Supplementary dataset 1. Significant SNPs detected as candidate selection signatures for immune response trait by each method, and the genes annotated from these candidate selection signatures from Chapter 5.

Supplementary dataset 2. The genes annotated from the detected significant SNPs for immune response, general resilience, and female reproductive performance traits, and the common genes among the three studied traits from Chapter 5.

Supplementary dataset 3. The significant SNPs detected as candidate selection signatures for general resilience and female reproductive performance trait by each method, and the genes annotated from these candidate selection signatures from Chapter 5.

Supplementary dataset 4. The dataset of significant SNPs detected from the GWAS analyses, and the genes annotated from these significant SNPs for all three studied traits in Chapter 6.